Downstream Processing of Influenza Whole-Virions for Vaccine Production

Dissertation zur Erlangung des akademischen Grades

Doktoringenieur (Dr.-Ing.)

von Dipl.-Ing. (FH) Bernd Kalbfuß-Zimmermann

geb. am 17.04.1978 in Mannheim

genehmigt durch die Fakultät für Verfahrens- und Systemtechnik

der Otto-von-Guericke-Universität Magdeburg

Gutachter:

Prof. Dr.-Ing. Udo Reichl

Prof. Dr.-Ing. Andreas Seidel-Morgenstern

Promotionskolloquium am 11.08.2009

Zusammenfassung

Die durch Influenzaviren verursachte Grippe ist ein Atemwegsinfekt, an dem jährlich bis zu 10% der Weltbevölkerung erkranken. Zusätzlich besteht das unkalkulierbare Risiko einer Pandemie, welches erst kürzlich durch die Übertragung von Vogelgrippeviren auf den Menschen in das Bewusstsein der Öffentlichkeit gerückt ist. Vorbeugende Impfung ist gegenwärtig die einzige wirkungsvolle Maßnahme zum Schutz gegen Influenzaviren. Die Herstellung von sicheren Influenzaimpfstoffen in ausreichenden Mengen ist daher von großer Bedeutung für die öffentliche Gesundheitsversorgung. Herkömmlich werden Influenzaviren in befruchteten Hühnereiern kultiviert. Seit etwa 15 Jahren gewinnt jedoch die Vermehrung in tierischer Zellkultur immer mehr an Bedeutung. Die Aufreinung von Influenzaviren aus tierischer Zellkultur für die Herstellung von inaktivierten Ganzvirion-Impfstoffen ist das Thema dieser Arbeit.

Die humanen Influenzaviren A/PR/8/34 (H1N1), A/Wis/67/2005 (H3N2) und B/Mal/2506/2005 wurden in MDCK-Zellen als Wirt gezogen. Ihre Kultivierung in Rollerflaschen wurde hinsichtlich der Freisetzung der Virionen sowie von Verunreinigungen charakterisiert. Die Bestimmung eines geeigneten Erntezeitpunkts auf der Basis von statistischen Quantilen der HA-Aktivität, welche sich durch Interpretation des Freisetzungsprofils als Summenverteilung bestimmen lassen, wird beschrieben. Die Trübung des Kulturüberstandes, welche die Ablösung der Zellen und deren Lyse widerspiegelt, wird als ein Marker zur Überwachung des Infektionsfortschrittes vorgeschlagen. In Abhängigkeit vom Virusstamm und Kulturmedium ergaben sich in Rollerflaschen mittlere HA-Aktivitäten zwischen 130 und 450 HAU $(0.1\ ml)^{-1}$. Ausgehend von theoretischen Betrachtungen wurde ein Hemagglutinin-Antigenhalt zwischen 0.42 und 1.5 $\mu g\ ml^{-1}$ auf der Basis der gemessenen HA-Aktivitäten geschätzt. Die mittleren Konzentrationen an Wirtszell-DNA waren mit Werten zwischen 5.9 und 8.9 $\mu g\ ml^{-1}$ vergleichsweise einheitlich. Die Gesamtproteinkonzentration (34 $\mu g\ ml^{-1}$ mit GMEM-basiertem bzw. 62 $\mu g\ ml^{-1}$ mit Ex-Cell MDCK-Medium) hingegen schien überwiegend vom Kulturmedium abzuhängen bzw. der Durchführung eines Mediumwechsels vor der Infektion, welche bei GMEM-basiertem Medium notwendig war. Ausgehend von den Spezifikationen des europäischen Arzneimittelbuches (EA) und den mittleren Resultaten aus der Viruskultur wurde die Notwendigkeit einer 20 000-fachen Abreicherung des virusspezifischen DNA-Gehaltes sowie einer 10-fachen Abreicherung des Proteingehaltes berechnet.

Es wurden zwei Aufarbeitungsschemata hinsichtlich ihrer Eignung und Einhaltung der zuvor beschriebenen Anforderungen untersucht. Im ersten Schema wurde der virushaltige Kulturüberstand mittels zweifacher Normalfluss-Filtration (NFF) geklärt und die Viren im Anschluss durch Zugabe von β-Propiolakton chemisch inaktiviert. Die inaktivierten Viren wurden mittels Tangentialfluss-Ultrafiltration (TFUF) aufkonzentriert und die Abtrennung des verbleibenden Wirtszellproteins durch Gelfiltration (GF) erreicht. Die noch enthaltene Wirtszell-DNA wurde durch Anionenaustausch-Chromatographie (AIEC) im Durchflussverfahren weiter abgereichert. Die Adsorption der Virionen an die stationäre Phase wurde durch Konditionierung der virushaltigen Eluatfraktion auf hohe Salzkonzentrationen während der GF erreicht. Die Gesamtvirusausbeute nach der AIEC betrug 53% basierend auf der HA-Aktivität. Der virusspezifische Gehalt an Wirtszell-DNA wurde etwa 270-fach, der Gehalt an Gesamtprotein etwa 15-fach reduziert. Die Abreicherung der Wirtszell-DNA war folglich unzureichend bezüglich der Forderungen des EA. Die Optimierung der Betriebsbedingungen während der GF wurde retrospektiv in einer Modellierungsstudie adressiert. Präparationen unter den abgeleiteten Bedingungen stehen jedoch noch aus.

Im zweiten Schema wurde die Zentrifugation als Alternative zur NFF untersucht. Ihre Leistungsfähigkeit wurde auf Basis der Sigma-Theorie charakterisiert. Zusätzlich wurde ein weiterer DNA-Abreicherungsschritt, realisiert durch die selektive Fällung von DNA mittels Polyethylenimin, in den Prozess aufgenommen. Die Selektivität des Verfahrens konnte durch Ausführung und Auswertung eines faktoriellen statistischen Versuchsplans („Factorial Design“) verbessert werden. Der pH-Wert und die Ionenstärke wurden hierbei als kritische Faktoren identifiziert. Die gefällte DNA wurde durch eine Kombination aus Zentrifugation und Membranmikrofiltration abgetrennt. Nach Inaktivierung wurde der Virus wieder mittels TFUF aufkonzentriert; gefolgt von einem Diafiltrationsschritt bei konstantem Volumen zwecks Abreicherung von Wirtszell-Proteinen und zur Vorbereitung auf die nachfolgende chromatographische Feinreinigung („Polishing“). Abschließend wurde der Versuch der adsorptiven Feinreinigung mittels Monolithen und gepackten Betten unternommen. Geeignete Liganden waren zuvor in Vorversuchen mit Membranadsorbern ermittelt worden. Die Machbarkeit einer direkten Anreicherung („Capture“) von Influenzaviren aus Kulturüberstand mittels Anionenaustausch-Membranchromatographie wurde in einem Nebenprojekt belegt. Obwohl die Charakterisierung des zweiten Schemas noch nicht abgeschlossen ist, kann bereits von einer zusätzlichen Abreicherung der Wirtszell-DNA um den Faktor 6.5 durch die selektive

Fällung ausgegangen werden. Die Gesamtabreicherung der Wirtszell-DNA nach Diafiltration erreichte den Faktor 500, während die Abreicherung nach TFUF im ersten Prozess lediglich den Faktor 3 beziehungsweise nach GF den Faktor 8 erreichte. Die Gesamtausbeute an Virus war hingegen, auf Grund der hohen Verluste während der Diafiltration, mit weniger als 50% vergleichsweise gering. Die mittlere Gesamtausbeute im ersten Prozess betrug 77% nach TFUF beziehungsweise 65% nach GF. Erste Ergebnisse bezüglich der adsorptiven AIEC mit Monolithen und gepackten Betten lassen auf die Erreichbarkeit einer endgültigen DNA-Belastung in der Größenordnung von 10 ng pro Dosis schließen, welche vom EA gefordert wird.

Trotz dieser viel versprechenden Ergebnisse bleibt die Robustheit der adsorptiven AIEC hinsichtlich weiterer Virusstämme zu überprüfen. Weiterhin ist es wichtig, die Virusausbeuten nach der Diafiltration zu verbessern. Darüber hinaus verbleibt der mögliche Einfluss verschiedener Kultivierungssysteme auf die Aufreinigung zu überpüfen und die Charakterisierung der Virusernten auf Systeme mit Mikroträgern auszudehnen. Abschließend sollte der Gehalt an Hämagglutinin-Antigen in den aufgereinigten Virussuspensionen mittels Antikörperpräzipitationstest („SRID assay“) entsprechend den Forderungen des EA bestimmt sowie die gemessenen DNA-Konzentrationen durch einen zweiten Nachweis überprüft werden, um die Richtigkeit der präsentierten Werte zu gewährleisten.

Abstract

Influenza disease caused by influenza viruses is a respiratory disease affecting up to 10% of the world's population every year. Besides, there is an unforeseeable risk of pandemic influenza, which has gained public awareness only recently due to infection of human individuals by avian influenza viruses. Immune-prophylaxis by vaccination currently provides the only effective means for protection against influenza disease. The preparation of safe influenza vaccines in quantity, hence, is of eminent importance to public health care. Traditionally, influenza viruses have been cultivated in fertilized chicken eggs. Since about 15 years, propagation in mammalian cell culture has been gaining more and more importance. It is the purification of influenza viruses propagated in cell culture for use in inactivated whole-virion vaccines, which has been investigated in this work.

Human influenza viruses A/PR/8/34 (H1N1), A/Wis/67/2005 (H3N2) and B/Mal/2506/2005 were propagated in mammalian cell culture using MDCK cells as a host. Virus propagation in roller bottles was characterized with respect to the release of virions but also impurities. An appropriate time for harvesting is suggested based on statistical quantiles of the HA activity by interpreting release profiles as cumulative distributions. The turbidity of supernatant, reflecting cell detachment and lysis, is proposed as a maker for monitoring the progress of infection. Depending on the virus strain and culture medium, average HA activities between 130 and 450 HAU $(0.1\ ml)^{-1}$ were determined in roller bottles. Based on theoretical considerations, an approximate hemagglutinin antigen content between 0.42 and 1.5 $\mu g\ ml^{-1}$ was estimated from measured HA activities. Average concentrations of host-cell DNA, in contrast, were rather consistent with 5.9 to 8.9 $\mu g\ ml^{-1}$. The concentration of total protein (34 $\mu g\ ml^{-1}$ with GMEM-based or 62 $\mu g\ ml^{-1}$ with Ex-Cell MDCK medium) appeared to depend on the virus propagation medium or more likely the presence of a medium exchange step prior to infection, which was necessary in the case of GMEM-based medium. Based on specifications by the European Pharmacopoeia (EP) and average cultivation outcome, the requirement of 20 000 and 10-fold reduction in the virus-specific content of host-cell DNA and total protein, respectively, was deduced from these values.

Two downstream processing schemes were investigated with respect to their suitability of meeting above-mentioned requirements. In the first scheme, virus-containing supernatant was clarified by sequential normal-flow filtration (NFF), followed by chemical inactivation of virions with

β-propiolactone. Inactivated virions were concentrated by tangential-flow ultrafiltration (TFUF) afterwards. Separation from remaining host-cell proteins was realized by size-exclusion chromatography (SEC). Residual host-cell DNA was eliminated by flowthrough anion-exchange chromatography (AIEC). Adsorption of virions to AIEC resins was prevented by pre-conditioning of virus-containing eluate fractions to high salt concentrations in SEC. The overall virus yield after AIEC was 53% based on HA activity in product fractions. The virus-specific content of host-cell DNA and total protein were reduced about 270 and 15-fold, respectively. Reduction of host-cell DNA was hence insufficient with respect to specifications of the EP. Optimization of operating conditions in SEC was addressed retrospectively in a modeling study. Preparations under the conditions derived, however, remain to be conducted.

In the second scheme, centrifugation was investigated as an alternative to NFF. Performance was characterized on the basis of Sigma theory. Moreover, an additional DNA-clearance step, rendered by the selective precipitation of DNA with polyethylenimine, was introduced due to insufficient reduction in the first scheme. Selectivity of the operation was enhanced by execution of a factorial experimental design. Ionic strength and pH were identified as the critical parameters. Precipitated DNA was separated by a combination of centrifugation and membrane microfiltration. After inactivation, virus was again concentrated by TFUF followed by constant-volume diafiltration for the separation of host-cell proteins and conditioning prior to chromatographic polishing. Finally, adsorptive polishing on monoliths and high-performance packed-beds was attempted. Suitable ligands had been identified before in scouting experiments with membrane adsorbers. The feasibility of direct capture of influenza virions from clarified supernatant by anion-exchange membrane chromatography was demonstrated in a side study. While characterization of the second scheme remains to be completed, an additional reduction in host-cell DNA by a factor of 6.5 can already be assumed due to the selective precipitation step. Overall reduction of host-cell DNA after diafiltration was 500-fold compared to 3-fold after TFUF or 8-fold after SEC in the first scheme. Overall virus yields below 50% were, however, comparatively low due to the high losses during diafiltration. For comparison, overall yields after TFUF or SEC in the first scheme were 77% or 65%, respectively. Preliminary results for adsorptive AIEC with monoliths and packed-beds indicate that a final DNA burden near the limit of 10 ng per dose can be achieved, which is requested by the EP.

Despite these promising first results, robustness of adsorptive AIEC with respect to additional virus strains remains to be confirmed. Moreover, the low virus yield after diafiltration has to be

overcome. Besides, the influence of cultivation systems on downstream processing remains to be investigated and characterization of viral harvests should be extended to microcarrier cultivations. Finally, determination of the final hemagglutinin antigen content in purified virus bulk by SRID assay, as is requested by the EP, and verification of DNA levels by a second assay should be conducted, in order to assure accuracy of reported results

Danksagung

Meinem Doktorvater, Herrn **Prof. Udo Reichl,** möchte ich dafür danken, dass er mir als FH-Absolvent die Möglichkeit gegeben hat, an der Otto-von-Guericke Universität zu promovieren. Wer selbst an einer Fachhochschule studiert hat, der weiß, dass dies bei Weitem keine Selbstverständlichkeit ist. Besonders schätzen gelernt habe ich während meiner Zeit am MPI die große Freiheit, die er mir bei der Bearbeitung meines Themas zugestanden hat. Herrn **Prof. Andreas Seidel-Morgenstern** gilt mein Dank dafür, dass er sich bereit erklärt hat, als Gutachter zur Verfügung zu stehen. Angesichts der Tatsache, dass die Verfassung eines Gutachtens vor allem eine Menge Arbeit bedeutet, betrachte ich dies als eine besondere Auszeichnung. Als drittem Professor in der Runde möchte ich mich bei Herrn **Prof. Dietrich Flockerzi** für seine Hilfe beim Verfassen unseres gemeinsamen Artikels bedanken. Die mathematischen Lektionen waren äußerst hilfreich und stets interessant – auch wenn ich befürchte, bis heute nur einen kleinen Teil davon verstanden zu haben.

Mein ganz besonderer Dank gilt den von mir betreuten Diplomandinnen bzw. Master-Studentinnen **Tina Kröber**, **Anne Knöchlein** und **Katrin Eisold**. Ihrem Einsatz ist es zu zuzuschreiben, dass die Charakterisierung eines zweiten Prozessschemas überhaupt erst möglich wurde. Anne Knöchlein war es, die mit ihrer detaillierten Charakterisierung der Viruskultur in Rollerflaschen, der Zentrifugation auf Basis der Sigma-Theorie und Vorversuchen zur selektiven DNA-Fällung den Anfang machte. Ihre Ergebnisse wurden von Tina Kröber aufgegriffen und das Verfahren der selektiven Fällung in der Folge weiterentwickelt. In ihrer Arbeit wurde außerdem die Diafiltration der vorbehandelten Virussuspension mittels Tangentialfluss-Ultrafiltration beschrieben. Darüber hinaus führte sie die ersten Experimente zur adsorptiven chromatographischen Reinigung der Influenzaviren durch. In der abschließenden Arbeit von Katrin Eisold wurde erneut die Diafiltration adressiert, die sich auf Grund chronisch schlechter Ausbeuten als Sorgenkind herauskristallisiert hatte. Außerdem führte sie weitere Virusstämme in die Prozesscharakterisierung ein und zeigte auf, dass die hydrophobe Interaktionschromatographie möglicherweise eine Alternative zur Ionenaustauschchromatographie in der Feinreinigung darstellt.

Ebenfalls nicht aussparen möchte ich an dieser Stelle Herrn **Dr. Robert Morenweiser** von der Firma GE Healthcare. Das von ihm initiierte Projekt zum Beginn meiner Doktorarbeit hat mir rückblickend Halt gegeben und mich auf die richtigen Bahnen gelenkt. Anfänglich Flüche auf

Grund meiner beschnittenen Freiheit sind recht schnell der Erkenntnis gewichen, dass ohne die Erfahrungen dieses Projektes viele Folgearbeiten wahrscheinlich weniger erfolgreich ausgefallen wären.

Natürlich möchte ich an dieser Stelle auch meine **Weggefährten** und die **Angehörigen der AG Bioverfahrenstechnik** erwähnen. Die lockere Atmosphäre und das gute Klima am MPI waren eine permanente Unterstützung und haben mir dabei geholfen, mich immer wieder aufs Neue anzutreiben. Die häufig bissigen, von Sarkasmus, Zynismus und zuweilen Verzweiflung geprägten Diskussionen in unserem Büro waren mir außerdem oft eine willkommene Ablenkung. Unvergessen sind natürlich auch die vielen schönen Momente auf Feiern, bei gemeinsamen Frühstücken, abendlichen Sitzungen, Umzügen und allem was sonst noch so dazu gehört. Ich wünsche euch allen viel Glück und Erfolg bei eurem weiteren Werdegang. Dem ein oder anderen werde ich mit Sicherheit auch in Zukunft noch über den Weg laufen.

Abschließend, aber bestimmt nicht mit geringerer Wertschätzung, möchte ich meiner Frau **Anke** dafür danken, dass sie bereit war, mir für einen Zeitraum von fünf Jahren nach Magdeburg zu folgen und so überhaupt erst meine Promotion ermöglichte. Die anfänglichen Bedenken auf Grund unserer gemeinsamen Arbeit am MPI haben sich schnell als unbegründet erwiesen. Die gemeinsamen Mittagspausen und der Weg zur Arbeit waren eine Quelle der Ruhe und Entspannung im manchmal hektischen Arbeitsalltag.

Abbreviations

AIEC	Anion-exchange chromatography
β-PL	β-propiolactone
BEI	Binary ethylenimine
CDC	Center for Disease Control and Prevention of the United States
CI	Confidence Interval
CIEC	Cation-exchange chromatography
DF	Diafiltration
ECACC	European collection of cell cultures
EP	European Pharmacopoeia
FA	Formaldehyde
GMEM	Glasgow minimum essential medium
HA	Hemagglutinin or hemagglutinating
HETP	Height of equivalent theoretical plate
IDA	Iminodiacetic acid
IEC	Ion-exchange chromatography
MDCK	Madin-Darby canine kidney
m.o.i.	Multiplicity of infection
NA	Neuraminidase
NIBSC	National Institute for Biological Standards and Control
NFF	Normal-flow filtration
ODE	Ordinary differential equation
PBS	Phosphate-buffered saline
PEI	Polyethylenimine
PET	Poylyethylene terephtalate
PES	Polyethersulfone
PS	Polysulfone
RSD	Relative standard deviation
UV	Ultraviolet
VLP	Virus-like particle
SEC	Size-exclusion chromatography
TFUF	Tangential-flow ultrafiltration
TMP	Trans-membrane pressure
WHO	World Health Organization

Symbols

A list of symbols including units and a brief description is given in the following. Note that some of the symbols are not unique but their meaning depends on the context. Most symbols will be also introduced in the text when they appear for the first time.

Symbol	Units	Description
A	cm^{-2}	Membrane area
a	-	Parameter in growth functions (related to the initial value)
a^*	-	Non-dimensional parameter a
Abs_{280}	a.u., au, mAU[1]	Absorbance of light at 280 nm
A_{HA}	HAU, kHAU[2]	HA activity
a_{HA}	HAU $(0.1\ ml)^{-1}$	Volumetric HA activity
a_{NA}	$\mu M\ min^{-1}$	Volumetric NA activity
b	-	Parameter in growth functions (related to the growth rate)
b^*	-	Non-dimensional parameter b
b_i	-	Weight in linear combination
c	various	General concentration
c_0	various	General initial concentration
c_0	$mol\ L^{-1}$	Initial molar concentration of β-PL
c_b	$mol\ L^{-1}$, $g\ L^{-1}$	Molar or mass concentration in the mobile phase
c_{DNA}	$\mu g\ ml^{-1}$	Mass concentration of host-cell DNA
c_{NaCl}	M, mM	Molar concentration of sodium chloride
c_p	$mol\ L^{-1}$, $g\ L^{-1}$	Molar or mass concentration in the stationary phase
c_{PEI}	% (m/v)	Mass per volume concentration of PEI
c_{prot}	$\mu g\ ml^{-1}$	Mass concentration of total protein
D	-	Discrepancy functional
d	m^{-1}	Diameter of fibers
E	-	Clarification efficiency
Ext_{700}	O.D.	Extinction of light at 700 nm
g	$m\ s^{-2}$	Gravitational acceleration
$g(t)$	-	Input signal or forcing function
H	cm, mm	Height
$h(t)$	-	Output signal
$h_\delta(t)$	-	Impulse-Response

1 au = 10^3 mAU

2 kHAU = 10^3 HAU

Symbol	Units	Description
J	L m^{-2} h^{-1}	Flux
J_{crit}	L m^{-2} h^{-1}	Critical Flux
J_{lim}	L m^{-2} h^{-1}	Limiting Flix
K	-	Distribution coefficient
K	various	Supremum or upper asymptote of growth functions
k_1	min^{-1}	Kinetic rate constant for decay of β-PL
k_2	L mol^{-1} min^{-1}	Kinetic rate constant for inactivation of infectious virions
K_{av}	-	Approximated distribution coefficient based on total column volume
L	m	Length of fibers
m_{DNA}	mg	Mass of DNA
m_{prot}	mg	Mass of protein
MW	kDa	Molecular Weight
N	-	Number of experiments or batches
p_{in}	Pa	Pressure at module inlet (retentate side)
p_{out}	Pa	Pressure at module outlet (retentate side)
p_{perm}	Pa	Average pressure on the permeate side
Q	m^3 s^{-1}	Volumetric flow rate
R	%	Recovery
r	m	Radius
r_1	mm	Inner radius
r_2	mm	Outer radius
R_f	m	Overall filtration resistance
R_λ^{pen}	-	Penality-based reconstruction operator
R_ε^{tol}	-	Tolerance-based reconstruction operator
S	-	Degree of inactivation
S_{max}	-	Maximum degree of inactivation
$\mathbf{T}$	-	LTI transformation operator
t	h, min	Time
$t.p.i.$	h	Time post-infection
$\mathbf{T'}$	-	Related LTI transformation operator
t^*	-	Non-dimensional time
t_0	min, h	Point in time
$t_{0.1}'$	h	Centered 10% quantile
$t_{0.9}'$	h	Centered 90% quantile
t_c'	h	Centered locus of the inflection point
t_p	h	Quantile of the population

Symbol	Units	Description
u	cm h^{-1}	Superficial mobile phase velocity
u	m s^{-1}	Flow velocity
V	m^3, L	Volume
V_0	ml	Void volume of chromatography column
V_{col}	ml	Column volume
V_{dia}	L	Exchanged volume
V_e	cv	Elution volume
V_{inj}	cv	Injection volume
V_l	cv	Left fractionation limit
V_p	L	Permeate volume
V_r	cv	Right fractionation limit
V_t	ml	Total liquid volume of chromatography column
V_t	L	Total retentate volume
x	-	Fraction of centrifugation time required for acceleration
x	various	Population
x^*	-	Non-dimensional population
$x_{-\infty}$	various	Infimum or lower asymptote of growth function
x_c	-	Locus of the inflection point
Y	%	Yield
y	-	Fraction of centrifugation time required for deceleration
α	-	Sieving coefficient
Δp_{dyn}	Pa	Dynamic pressure drop
Δp_{tm}	Pa	Trans-membrane pressure difference
ε	-	Porosity
ε	-	Regularization parameter
η	Pa s	Dynamic viscosity
$\dot{\gamma}_0$	s^{-1}	Wall shear rate
λ	-	Regularization parameter
μ	-	Correction factor
Σ	m^3	Equivalent settling tank area
Ω	-	Desirability functional (negated information entropy)
ω	rad s^{-1}	Angular velocity

Table of Contents

1 Introduction

1.1 Influenza Disease

Influenza disease (shortly the “flu”) caused by influenza viruses is a respiratory disease affecting up to 10% of the world's population every year [Gerdil, 2003]. Most relevant are viruses of type A and B, which are wide-spread and can cause serious illness in humans [Wilschut et al., 2005]. Symptoms of the flu include fever, headache, extreme tiredness, dry cough, sore throat, runny or stuffy nose, and muscle aches. Children can have additional gastrointestinal symptoms, such as nausea, vomiting, and diarrhea, but these symptoms are uncommon in adults. Infection usually persists over a period of one up to two weeks. The virus is spread in respiratory droplets of coughs and sneezes. Infected individuals may be contagious even before the first symptoms of infection become apparent. More information on influenza disease can be obtained through the web pages of the Center for Disease Control and Prevention of the United States (CDC) or the Robert-Koch-Institute in Germany [CDC, 2008; RKI, 2008].

Annually re-occurring influenza epidemics during fall and winter time are referred to as “seasonal influenza”. Particularly, in the case of elderly and children, infection is often serious and can be fatal. The precise number of influenza-related fatalities, however, is difficult to determine and subject to debate. This is partially due to a lack of diagnosis but also due to the fact that death may occur only after secondary infection. According to statistics of the CDC, fatalities in the category “pneumonia and influenza” have risen from 20 to 31.8 deaths per 100 000 inhabitants per year during the period from 1979 to 1994 [CDC, 1995]. In the season of 2007/2008 the percentage of “pneumonia and influenza”-related fatalities among all recorded deaths in the United States was as high as 7.6% [CDC, 2008]. Seasonal influenza is therefore antagonized by means of immune-prophylaxis through annual vaccination programs [Nicholson, 1998; Wilschut et al., 2005]. Risk groups are vaccinated either with killed influenza vaccines (“flu shot”) or more recently also live-attenuated vaccines (nasal spray).

In addition to seasonal influenza, there is an unforeseeable risk of pandemic flu whenever genetic shift of surface antigens occurs. At least 10 influenza pandemics are known to have occurred in the period from the late 12th century up to now [Potter, 1998]. The most devastating pandemic in history took place in the years from 1918 to 1920. This pandemic, later referred to as the “Spanish flu”, was caused by an influenza A virus of subtype H1N1. It demanded for the lives of an

estimated 20 to 50 million people world wide [Johnson et al., 2002]. Two other pandemics in the 20th century were caused by influenza A viruses of subtypes H2N2 and H3N2 known as the "Asian flu" from 1957 to 1958 and "Hong Kong flu" from 1968 to 1969 [Kilbourne, 2006]. Fortunately, neither of them was as devastating as the pandemic from 1918 to 1920. The precise origin of pandemics remains mostly unclear. However, it is widely agreed on, that pandemics are triggered by the formation of new subtypes, e.g. after transmittal from animals to humans (zoonosis). Hence, the reports of lethal infection of humans with bird influenza virus of subtype H5N1 led to world wide concern about a new influenza pandemic approaching [Cinatl et al., 2007; Keitel et al., 2007].

1.2 Influenza Viruses

Influenza viruses are enveloped viruses which belong to the family of Orthomyxoviridae [Lamb et al., 2001; Wilschut et al., 2005]. They split into the three types (or genera) of influenza A, B and C viruses. Of these, influenza A viruses are known to infect swines, horses, humans and birds while influenza B and C viruses are mostly restricted to humans [Webster, 1998]. Influenza A viruses are further categorized into sub- or serotypes based on the nature of their hemagglutinin and neuraminidase antigens. Up to now, 16 different hemagglutinin and 9 different neuraminidase antigens have been identified in wild-type isolates giving rise to a large number of possible combinations. However, not all of these combinations seem to occur in nature. With respect to influenza B and C viruses there are no known subtypes. However, a vast number of strains exist within each type or subtype having slight variations in their genome and protein structure. New subtypes come into existence by a process known as antigenic shift [Wilschut et al., 2005], which refers to significant changes in the viral genome. Subtypes are generally demarcated by the lack of immunological cross-reactivity towards their surface antigens. This means that even individuals that have survived infection by influenza virus are mostly naive with respect to a newly occurring subtype. New strains, in contrast, evolve by subtle changes in the genome leading only to slight variations in surface antigens or other components. This process is referred to as antigenic drift. Cross-reactivity of antibodies is generally observed to a certain degree. Nomenclature of influenza viruses has been standardized and is based on the type, origin, an isolate number and the year of isolation (Figure 1-2). For influenza A viruses the subtype is appended in addition. Outbreaks of influenza disease and related viruses are surveyed world-wide by the Global Influenza

Surveillance Network [WHO, 2008] of the World Health Organization (WHO). This network was established in 1952 and comprises of four collaborating and many national influenza centers. Their task is the collection of specimens, primary virus isolation and antigenic characterization. An overview of strains that have been isolated up to now is given by the taxonomy browser of the National Center for Biotechnology Information (Bethesda, United States) [NCBI, 2008].

Influenza virions are commonly described as nearly spherical particles with a mean diameter of 100 nm (Figure 1-3a). In principle, however, viruses are pleomorph and their appearance depends on the actual strain and host. The structure of all types is very similar but influenza B virions may be somewhat more regular [Hay, 1998]. The virion core consists of the nucleocapsid (8 fragments of RNA associated with NP and and polymerases) surrounded by a shell of M1 protein. The envelope-forming lipid bilayer is wrapped around this core, carrying HA and NA surface antigens as well as M2 membrane protein. Carbohydrates are present as glycosylations of HA and NA proteins but possibly also in the form of glycolipids. In influenza B viruses, M2 is substituted for the NB protein. Influenza C viruses only have a single surface glycoprotein [Hay, 1998; Wilschut et al., 2005]. A cartoon of virion ultrastructure is given in Figure 1-3b. Biochemically, virions are approximately composed of 70% protein, 20% lipid, 5–8% carbohydrates and only 1% RNA [Lamb et al., 2001]. The genomes of influenza A and B viruses code for a total of 11 proteins. Of these, eight can be found in virions. Approximate protein composition of influenza A virions is given in Table 1-1. The majority of viral protein (about 95%) is composed by surface antigens HA and NA, structural protein M1 and nucleic acid-associated NP. About 40% of protein (or 30% of total mass) can be ascribed to surface antigens HA and NA alone.

Replication of influenza viruses has been throughly investigated by many groups. Like all viruses, they are dependent on a host for replication. The underlying mechanism is complex and includes a large number of steps. Fortunately, several excellent books and reviews do exist summarizing the available information [Lamb et al., 2001; Hay, 1998; Enquist et al., 1999; Nayak et al., 2004]. For a more compact overview, readers are referred to the introduction by Sidorenko and Reichl [2004] or the influenza book by Wilschut and McElhaney [2005]. A cartoon of the different stages, which are briefly summarized in the following, is given in Figure 1-1.

Table 1-1. Protein composition of influenza A virions

Protein	MW	No. per Virion	Mass per Virion	Mass Fraction
	10^4 g mol^{-1}		ag	%
PB2	8.57	30..60	6	1.5
PB1	8.65	30..60	6	1.5
PA	8.42	30..60	6	1.4
HA	6.15[d]	1500[a]	153	35
NP	5.61	1000	93	21
NA	5.01[d]	400[b]	32	7.6
M1	2.78	3000	138	32
M2	1.10	20..60	1	0.2
NS1[c]	2.68	-	-	-
NS2[c]	1.42	-	-	-
Sum			311	100

a: number of trimers, b: number of tetramers, c: non-structural proteins, d: molecular weight of monomers

Note: Protein composition was calculated from data for A/PR/8/34 (H1N1) by Lamb and Krug [2001].

Naturally, influenza viruses are taken up via the mucosa of the respiratory tract. Transmittal typically occurs via droplets spread by infected individuals. With the help of HA protein, inhaled virions are capable of attaching to the surface of epithelial cells. Eventually, attached virions are taken up by cells in endosomes as part of their endocytotic activity. Upon maturation of endosomes to lysosomes, which is accompanied by a drop in pH, a membrane fusion and uncoating mechanism is triggered, which leads to release of nucleocapsids into the cytosol. In the following, NP-associated RNA and polymerases (vRNPs) are imported into the nucleus where transcription and replication of the viral genome takes place. Translation of viral proteins occurs in the cytosol after splicing and export of viral messenger RNA. Whereas the viral proteins M1, NP, polymerases and non-structural proteins NS1/NS2 accumulate in the cytosol, membrane proteins HA, NA and M2 are directly synthesized into the membrane of the endoplasmatic reticulum. From there, they are exported to the apical cell membrane via the Golgi apparatus. NP and polymerases, in contrast, are re-imported into the nucleus where they are packaged into vRNPs together with genomic viral RNA. Association of M1 protein to vRNPs results in transfer out of the nucleus back to the cytosol. Finally, interaction of vRNP-M1 complexes with viral

membrane proteins is believed to induce budding of new virus particles. After release from the host-cell, newly formed virus particles are ready to spread and infect further cells in the host organism.

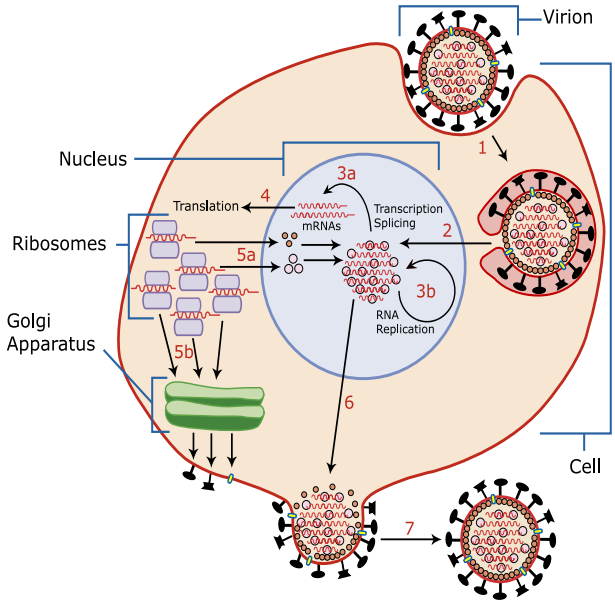

Figure 1-1. Replication of influenza virus.
The complex replication cycle is usually divided into virus entry, membrane fusion, uncoating, transcription, translation, packaging and budding. Newly budded virions are released from the host-cell and ready to infect other cells in the organism. Picture from Wiki Commons [Times, 2007]

1.3 Influenza Vaccines

Immune-prophylaxis by vaccination provides an effective means for the protection of human and animal beings against a number of severe and often fatal diseases - many of them being caused by viral pathogens. In contrast to therapeutic approaches, disease is prevented from the very beginning or the course of disease is alleviated at least. Accordingly, vaccination does not only lead to an overall gain in life time but also in the quality of life. Vaccination further belongs to the group of healthcare interventions that are not only considered cost-effective but can be even cost-saving [Chabot et al., 2004; Drummond et al., 2007; Armstrong, 2007]. The success story of vaccination against smallpox with vaccinia virus, which finally led to the eradication of smallpox worldwide (as proclaimed in 1979), but also other examples like vaccination against poliomyelitis and rabies virus clearly demonstrate the value of immune-prophylaxis in human medicine. Veterinary vaccines, in addition, have helped to secure the food supply from live stock farming

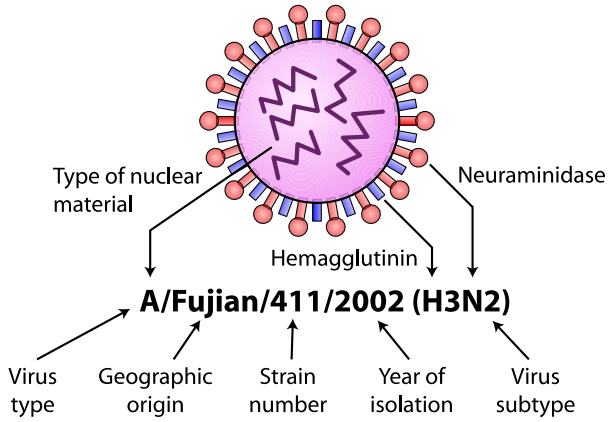

Figure 1-2. Nomenclature of influenza viruses.

The nomenclature of newly isolated virus strains has been standardized. Names are derived from the virus type, geographic origin, an isolate number and the year of isolation. For influenza A viruses the subtype is appended. Picture from Wiki Commons [Vickers, 2007].

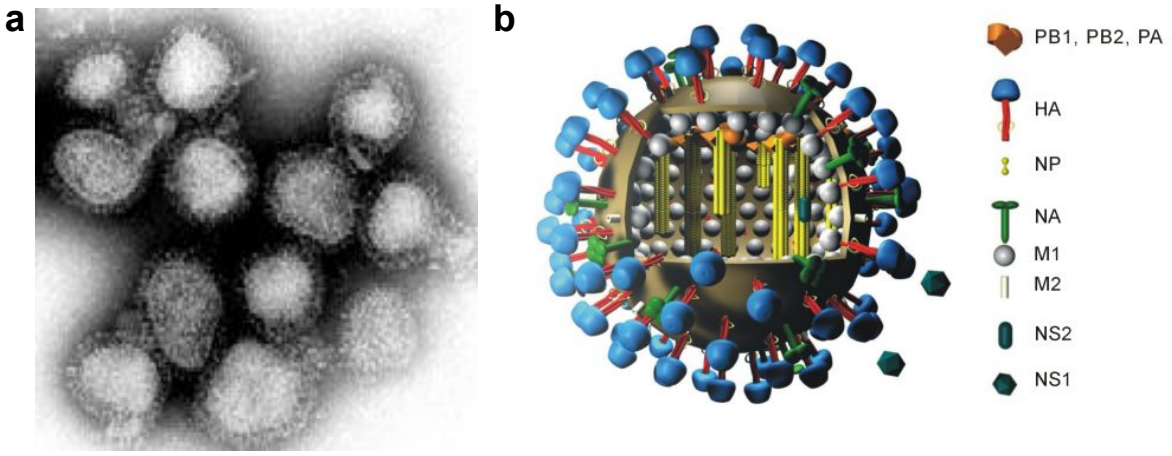

Figure 1-3. Ultrastructure of influenza viruses

Electron micrograph of influenza virus A/Hong Kong/1/68 (H3N2) (a). Negatively stained virions show surface projections, which contain the receptors (HA protein) by which the virus attaches to host respiratory tract epithelial cells. Picture from Wiki Commons [Murphy, 2005]. Cartoon of the ultrastructure of influenza A virions (b). The nucleocapsid (8 fragments of RNA associated with NP and polymerases) is protected by a shell of M1 protein. Viral core particles are surrounded by a lipid bilayer carrying surface antigens HA, NA and M2 protein. Influenza B virions are similar but have NB protein instead of M2. Picture from Wiki Commons [Eickmann, 2006].

and reduce the risk of zoonoses [Lombard et al., 2007]. Today a multitude of viral vaccines have become available many of them being used in routine vaccination (e.g. vaccines against

poliovirus, hepatitis A, mumps, measles and rubella virus in childhood vaccination [Baker et al., 2004]).

The development of viral vaccines has gone a long way since the invention of Jenner's smallpox vaccine. First immunizations were still accomplished by deliberate infection of healthy individuals with attenuated pathogens - often directly extracted from sick people or from related disease. Later, attenuation of pathogens was striven for in a directed fashion by propagation in foreign hosts, chemical attenuation or – as is still being done today – propagation in tissue culture. A different approach is the use of whole inactivated organisms (or certain antigen carrying parts) for vaccination. More recently, with the advent of genetic engineering technology further options like recombinant expression of antigens or DNA vaccines have become available [Plotkin, 2005; Ada, 2005; McCullers, 2007].

Viral vaccines are typically categorized into live (attenuated) and dead vaccines. While the first group comprises all vaccines containing infectious, replicating virus, vaccines of the second group only contain virus that has been rendered replication-deficient or viral components. Accordingly, dead vaccines can be further divided into whole-virion, split virion and subvirion vaccines corresponding to complete inactivated virions purified from viral culture, chemically or physically disrupted virions or viral components only. Of these, the latter may be either extracted from naturally occurring virions or nowadays produced recombinantly.

While live vaccines are usually given orally or nasally mimicking the natural route of infection, inactivated or dead vaccines are either applied subcutaneously or intramuscularly. Typically, much lower doses of virus are required for live vaccination, since the virus is able to replicate to some extent. Another consequence of oral or nasal application is that live vaccines do not have to be purified to the same extent as dead vaccines, since the mucosa poses an effective barrier against residues from viral culture. Dead vaccines, in contrast, need to be highly purified in particular to avoid anaphylaxis, inflammation and intrusion of host-cell DNA, which can potentially code for harmful oncogenes.

Live human influenza vaccines containing cold-adapted influenza viruses were developed more than three decades ago and have a long tradition in countries of the former U.S.S.R. [Kendal, 1997; Wareing et al., 2001]. However, most influenza vaccines in use in western countries belong to the category of dead viral vaccines [Fukuda et al., 2004; Belsey et al., 2006]. In particular,

trivalent inactivated whole-virion and subunit vaccines have been applied massively in annual vaccination programs. Traditionally, influenza viruses for these vaccines are propagated in fertilized hens' eggs. Propagation in eggs is followed by crude purification and inactivation by chemical agents like formaldehyde (FA) or β-propiolactone (β-PL) [Bardiya et al., 2005]. Protection by inactivated vaccines is short-lasting and fairly specific to vaccine strains. Vaccination therefore has to be repeated in annual campaigns with the composition of vaccines being adjusted continuously [Fukuda et al., 2004]. Most vaccines are of trivalent type containing two influenza A and one influenza B strain. Seasonal strains are selected according to recommendations of the WHO, which are based on a global surveillance program [WHO, 2008].

About 15 years ago, a trend towards mammalian cell culture for the propagation of influenza virus was started [Kistner et al., 1998; Brands et al., 1999]. However, only in January 2008 the first killed human influenza vaccine derived from cell culture-grown virus was approved for seasonal vaccination (Optaflu® by Novartis-Behring [2008]). Other candidates appear to be at the late stage of development or approval and can be expected to come soon. The primary argument for establishment of cell culture-based processes is the improved flexibility and scalability compared to propagation in eggs. At least in theory, cell culture-based production should be capable of providing sufficient quantities of influenza vaccines in the case of a pandemic [WHO, 1995]. Moreover, the security of supply is enhanced by the use of both cultivation systems. This is particularly true since not all influenza strains grow equally well in one or the other system [Voeten et al., 1999; Tree et al., 2001]. Another aspect is that in the case of a bird flue pandemic the supply of hens' eggs would be equally affected.

1.4 Downstream Processing of Influenza Virus

Before influenza virions, either propagated in hens' eggs or mammalian cell culture, can be used in inactivated whole-virion vaccines, purification is necessary due to the high level of impurities present after virus propagation. In fact, strict regulations with respect to antigen purity exist in most countries. As an example, recommendations by the WHO and specifications by the European Medicines Agency (EMEA) have been summarized in Table 1-2. It can be seen that a hemagglutinin antigen content of at least 15 µg per strain is demanded in all three cases. In addition, limits for the final content of host-cell DNA, total protein and endotoxins are typically stated. Moreover, some specific thresholds depending on the inactivation method or cultivation

system may be given. Beyond purification, the fairly low concentrations of virions usually obtained after virus propagation requires the concentration of virions. Low initial concentrations further put a burden on the purification process due to an unfavorable ratio of product and impurities.

Table 1-2. Specifications for inactivated whole-virion influenza vaccines.

Characteristic	WHO[1]	EP (egg-derived)[2]	EP (cell culture)[3]
HA antigen	> 15 µg per strain	15 µg per strain[a]	15 µg per strain[a]
DNA	< 10 ng[b]	-	< 10 ng
Protein	< 100 µg per strain < 300 µg per dose	< 6 x Ha antigen content < 100 µg per strain	< 6 x Ha antigen content < 100 µg per strain
Endotoxins	to be tested	< 100 IU	< 25 IU
Sterility	to be tested	to be tested	to be tested
Formaldehyde	< 0.1%[c]	< 0.2 g l^{-1} [c]	< 0.2 g L^{-1}
β-Propiolactone	< 0.1%[c]	< 0.1 %[c]	-
Ovalbumin	< 5 µg	< 1 µg	-
BSA (from serum)	-	-	< 50 ng
Residual Infectivity	to be tested in fertilized eggs or cell culture, respectively	amplification test in fertilized eggs over two passages	amplification test in cell culture over two passages

1: [WHO Technical Report Series, 1998, 2005], 2: [European Pharmacopoeia Commission, 2005], 3: [European Pharmacopoeia Commission, 2007], a: unless clinical evidence supports the use of a different amount, b: for virus grown in cell culture, c: at any time during inactivation

Regarding process design, current Good Manufacturing Practice (cGMP), guidelines of the International Standardization Organization (ISO) and International Conference on Harmonization (ICH), basic guides of the International Society of Pharmaceutical Engineers (ISPE) and legal aspects have to be taken into account. Of particular importance are the respective documents of the WHO and regional pharmacopoeias published by regulatory bodies, which give detailed recommendations for manufacturing, production controls and final lot testing. The particular choice of unit operations and their consecutive order mostly depends on the source of virus crude (fertilized eggs vs. cell culture). Once the upstream process has been characterized, requirements on the downstream process can be derived from specifications by regulatory bodies. Importantly, safety margins have to be chosen such that the process is robust with respect to variations in titers for different virus strains. Applying specifications of the EMEA (Table 1-2), requirements for the purification of A/PR/8/34 (H1N1) NIBSC propagated in MDCK cells have been calculated and

results are given in Table 1-3. Characteristics for the cultivation outcome were taken from the first column of Table 4-20. Disregarding safety margins, the virus antigen concentration has to be increased about 40-fold. At the same time, the burden by host-cell DNA and total protein needs to be reduced by a factor of 20 000 and 10, respectively. The initial content of endotoxins has not been quantitated. Still, a limit of 6.7 IU (µg HA)$^{-1}$ for the final level can be stated.

Table 1-3. Downstream requirements for the purification of an inactivated whole-virion influenza vaccine

	Supernatant		Requirement[1]		Factor
HA[2]	1.3	µg ml^{-1}	> 50	µg ml^{-1}	40 ▲
DNA	4.4	µg / µg HA	< 0.22	ng (µg HA)$^{-1}$	20000 ▼
Protein	55	µg / µg HA	< 6.6	µg (µg HA)$^{-1}$	10 ▼
Endotoxins		n.a.	< 6.7	IU (µg HA)$^{-1}$	n.a.

1: Requirements were calculated according to the EP [European Pharmacopoeia Commission, 2007] assuming a final volume of 0.3 ml per strain and 15 µg of hemagglutinin antigen per dose. Characteristic data for supernatant was taken from the campaign with A/PR/8/34 (H1N1) NIBSC propagated in Ex-Cell MDCK medium (Table 4-20), 2: Content of hemagglutinin antigen was estimated from HA activity [Kalbfuss et al., 2008].

Noteworthy, human influenza vaccines have been available for many decades now. However despite the long development, little information has been published about the manufacturing of influenza vaccines. In particular the purification of virions or viral components of cell-culture derived influenza virus has been barely addressed in the scientific literature. It is this lack of knowledge which led to investigations described in this work. Albeit, experiments were exclusively conducted with cell culture-derived influenza virus, the methodology described is by no means restricted to purification of the latter. It should be rather considered universal for the purification of cell culture-derived enveloped virions but also virus-like particles (VLPs) [Chackerian, 2007; Ramqvist et al., 2007]. Last but not least, the closely related task of purifying virions as gene therapy vectors shall be pointed out [Braas et al., 1996; Morenweiser, 2005; Segura et al., 2006].

1.5 Purification Strategies

In principle, many combinations of unit operations can be considered for the purification of influenza virions. On a functional level, however, a number of tasks can be named that are more or less equivalent in all downstream processes – independently of the virus strain and upstream conditions. To begin with, cell debris and possibly microcarriersneed to be separated after propagation of the virus. Next, virions have to be concentrated, purified and inactivated whereby the actual order of unit operations depends on the overall strategy pursued. Finally, the vaccine is blended from purified virus bulk, adjuvanted and filled. These latter aspects, however, will not be covered here. Generally, all unit operations should be performed under sterile conditions whenever possible.

Similar to the production of other biologicals, separation of cell debris is commonly achieved by centrifugation or normal-flow filtration [Hagen et al., 2000; Peixoto et al., 2007; Montagnon et al., 1985; Wiktor et al., 1987; Brands et al., 1999]. Tangential-flow microfiltration is another technique that has been used for this purpose [Maiorella et al., 1991; van Reis et al., 1991; Berthold et al., 1994]. For the purification of virions a vast number of possibilities exists. Traditional processes often incorporated a selective virus precipitation step [Reimer, Baker, Newlin, Havens, van Frank, et al., 1966; Cox et al., 1946; Polson, 1974]. Density gradient centrifugation is another technique among the first to be described in literature [Reimer, Baker, Newlin, and Havens, 1966; Hilfenhaus et al., 1976]. More recently, tangential-flow ultrafiltration (TFUF) has evolved as a universal tool for the concentration of virions that can simultaneously be used for the conditioning of concentrates and separation of low molecular weight impurities [Valeri et al., 1977; Wickramasinghe et al., 2005; Peixoto et al., 2007]. Similarly, size-exclusion chromatography (SEC) has routinely been used for the separation of small impurities and buffer-exchange [Heyward et al., 1977; Valeri et al., 1981; Nayak et al., 2005]. Adsorptive chromatography, i.e. mainly ion-exchange [Muller et al., 1952; Hagen, Aboud, et al., 1996; Vicente et al., 2008] and affinity chromatography [Sweet et al., 1974; Opitz et al., 2007], which used to suffer from low capacity in the past, is gaining more and more importance. New materials like adsorptive membranes, monolithic supports and non-porous media have opened new possibilities making chromatography an attractive choice for the purification of virus particles in particular due to its high resolving power. Inactivation of infectious virions can either take place towards the end of a process or directly after clarification. In the latter case, handling of infectious

material is reduced to a minimum but inactivation conditions are less defined due variations in the composition of viral harvests. Common ways of inactivation are by chemical agents such as FA, β-PL or aziridines [Lauffer et al., 1949; Budowsky et al., 1991; Brown, 2002]. Moreover, UV irradiation has been proposed as a gentle method reducing incubation time and avoiding residues [Budowsky et al., 1981; Wang et al., 1995].

1.6 Overview of Investigated Processes

Over the course of this work, two process schemes of which the second can be thought of as an advancement of the first scheme have been investigated. In both cases, purification of whole influenza virions was intended. In addition, a platform approach was pursued, i.e. unit operations were chosen having universality in mind (independence from virus strains and ideally also virus type). Hence, influenza virus should be regarded a model system for the purification of cell-culture derived enveloped viruses - nevertheless, a model system of practical relevance. Highly specific unit operations making use of affinity ligands were generally avoided since these would have increased the risk of strain-specificity. Instead, purification was based on common principles like separation by size and ionic interaction. Albeit differences in these properties exist among strains, associated unit operations usually provide sufficient flexibility to allow for the necessary adaptation. In addition, wherever possible, impurities were targeted for separation instead of virions themselves.

Scalability and suitability for industrial manufacturing was the dominant criterion for the selection of unit operations. Expensive or only limitedly scalable operations were generally excluded from investigations. Consequently, the use of DNase for digestion of host-cell DNA and density-gradient centrifugation were not considered. In the first process, adsorption of virions was totally avoided due to generally low capacities of traditional sorbents for nanoparticles. In subsequent investigations, in contrast, adsorptive chromatography using membrane adsorbers, monoliths and high-performance bead-media was considered since these chromatography media have the potential of overcoming limitations of traditional sorbents. In both schemes infectious virus was inactivated directly after separation of cell debris. This was owed to safety concerns during processing since most experiments could not be conducted in a fully contained environment.

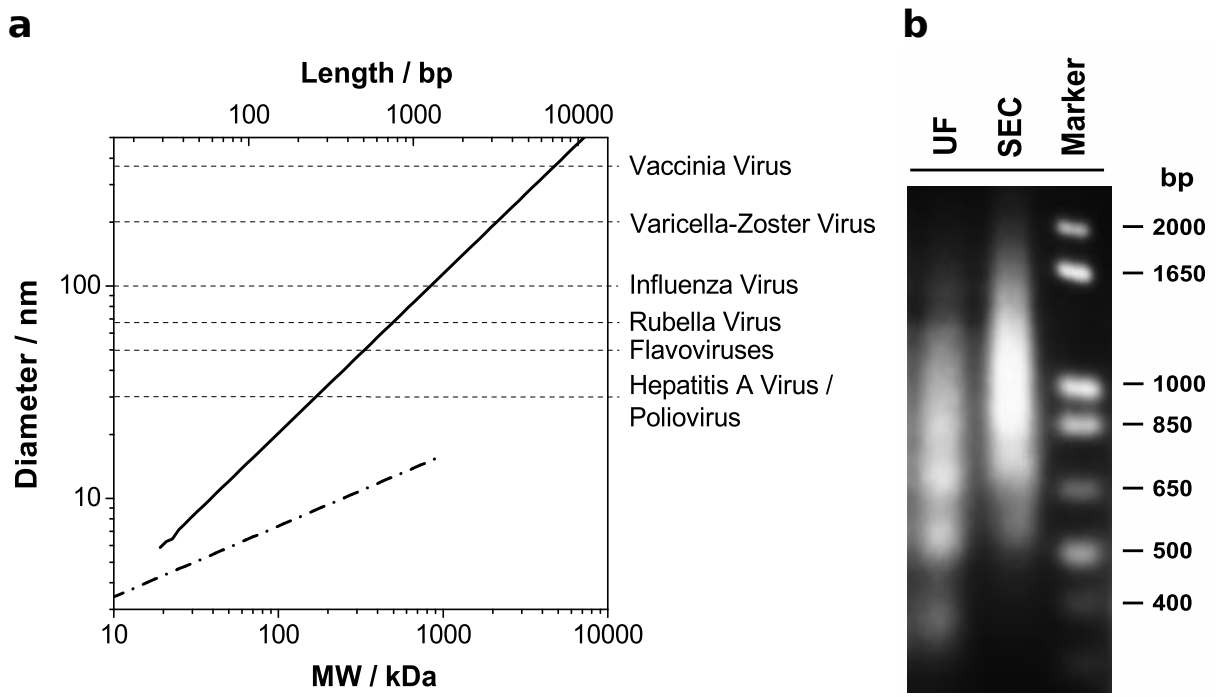

Figure 1-4. Size of virions and impurities.
Characteristic size of DNA (—), protein (- · -) and various viruses (a). The size of DNA (chromatographic diameter at 200 mM ionic strength and pH 6.85) was calculated from the size-length correlation reported by Potschka [1991]. Hydrodynamic diameters of proteins were derived from experimentally determined diffusion coefficients [Li et al., 1998]. Concerning viruses, the largest dimension is reported [Knipe et al., 2001]. Agarose gel electrophoresis of samples taken during downstream processing of cell culture derived influenza virus (b). The content of DNA in product fractions after TFUF and SEC was visualized by staining with propidium iodide.

Appropriate infrastructure presumed, however, inactivation post-purification may be advantageous due to better defined reaction conditions.

Separation by size was pursued as the primary strategy for the separation of proteins (and even smaller impurities) from virions. This can be readily achieved due to the large difference in dimensions by typically more than one order of magnitude (Figure 1-4a). Unit operations like TFUF or SEC seem most appropriate for this purpose. Genomic DNA fragments, in contrast, may reach dimensions similar to those of influenza virions. According to the length-size correlation for naked DNA by Potschka [1991], a DNA fragment of 1000 bp (approximately 1000 kDa molecular weight) already corresponds to a chromatographic diameter of 100 nm. And indeed, the presence of nucleic acids in the order of 1000 bp has been confirmed by agarose gel electrophoresis (Figure 1-4b). Host-cell DNA can thus not be fully separated by size-based fractionation alone. For the

complete separation of nucleic acids orthogonal methods have to applied. In this work, the separation of nucleic acids was specifically pursued by interaction with suitable counter-ions. These were either immobilized and used in the form of anion-exchange chromatography (AIEC). Alternatively, polyvalent cations were used for the selective precipitation of DNA.

An overview of process schemes investigated in this work, including all unit operations and their purpose, is given in Figure 1-5. In the first process, separation of cell debris is achieved by normal-flow microfiltration through mesh filters (4.2.1). Directly afterwards, virus is inactivated chemically by the addition of β-propiolactone (2.3). A second normal-flow filtration step follows for the removal of residual fines and virions are concentrated by TFUF (4.4.2). SEC is applied for the separation of proteins and smaller impurities (4.5.1). Simultaneously, the virus-containing fraction is conditioned for subsequent AIEC (4.5.2.2). The latter is operated in flowthrough mode such that virions do not adsorb to the column. Only DNA is adsorbed and thereby separated from virions. A putative diafiltration (DF) step after AIEC, necessary for the desalting of product bulk, is not included but assumed to behave similar to the first TFUF step.

Since investigations on the first process scheme revealed an insufficient reduction in DNA, a second process was designed including a dedicated unit operation. This unit operation, realized by the selective precipitation of DNA (4.3), was intentionally placed at the beginning of the process for early depletion. This is believed to reduce the formation of mixed virus-DNA aggregates, which can hamper complete separation later on. Moreover, centrifugation was investigated as an alternative to normal-flow filtration for the separation of cell debris (4.2.2). SEC was replaced by DF following concentration by TFUF (4.4.3). Finally, adsorptive AIEC was attempted with modern chromatography media such as monoliths and high-performance packed-beds (4.5.2.5). Opposed to AIEC in flowthrough mode, adsorption and elution of virions was explicitly intended in order to not only purify but also concentrate the virus.

In addition to process schemes described in Figure 1-5, direct capture of virions by anion-exchange membrane chromatography was investigated as an alternative (4.5.2.4). Although, general feasibility was confirmed, the approach was not further pursued due to the fairly low selectivity of anion-exchange membranes and the resulting weak purification efficiency at that stage.

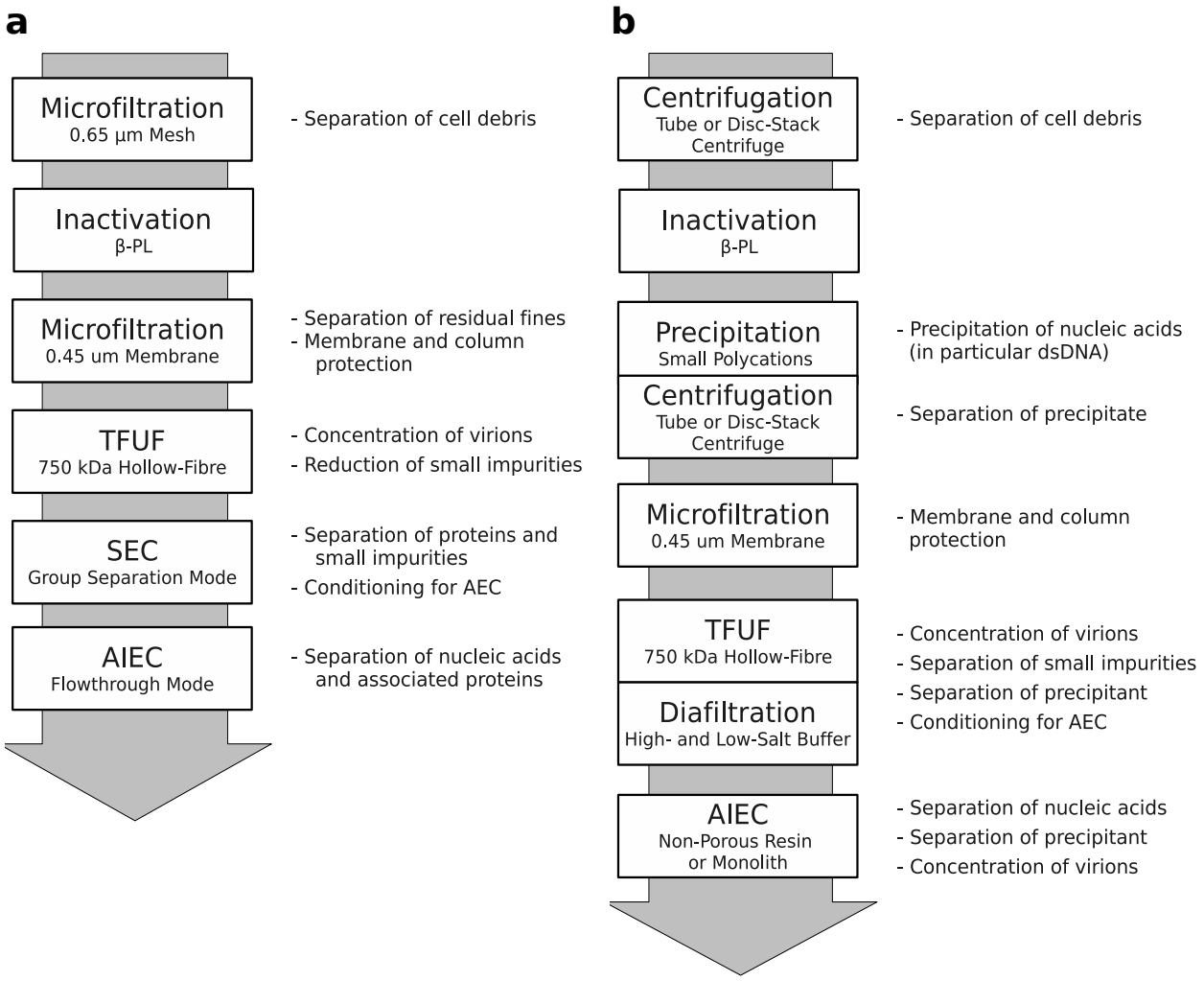

Figure 1-5. Investigated process schemes for the purification of influenza whole-virions from mammalian cell culture.

2 Background and Theory

2.1 Virus Cultivation

2.1.1 General Overview

Traditionally, influenza virus has been propagated in fertilized chicken eggs even at large-scale production [Bardiya et al., 2005]. Some years ago, mammalian cells were proposed as an alternative for virus replication either using MDCK [Tree et al., 2001], Vero [Kistner et al., 1998], or PER.C6 cells [Pau et al., 2001]. Similarly, the production of other vaccines in mammalian cells, for example, against rabies [Kumar et al., 2002] or Japanese encephalitis [Sugawara et al., 2002] has been reported. Viral vectors for gene therapy are routinely produced with mammalian packaging cell lines [Konz et al., 2005; Segura et al., 2005; Transfiguracion et al., 2003].

Cell substrates for the propagation of viruses can be divided into two categories: suspension or adherent cells. While the first are able to survive and divide in suspension, the latter need a surface substrate for attachment. Of the cell lines suitable for propagation of influenza virus, PER.C6 cells belong to the first category whereas MDCK and Vero cells belong to the second. Adherent cell lines, for instance, can be grown on the walls of poly(ethyleneterephtalate) or plasma-treated polysulfone vessels such as T-flasks or petri dishes (referred to as static cultures). These vessels are placed into incubators for providing the required environmental conditions (temperature and atmospheric composition). Mass-transfer exclusively occurs by diffusion, i.e. there is no active mixing involved. Alternatively, microcarriers such as functionalized gel beads can be added into vessels in order to provide the necessary surface [Genzel et al., 2004, 2006]. This technique is referred to as microcarrier cultivation and allows for the scale-up of culture volumes up to several cubic meters. Mixing is usually provided by some kind of stirrer (stirred-tank reactor) or by shaking of the whole reactor (wave bags). Again, environmental conditions are tightly controlled but this time directly in the reactor (temperature, pH and dissolved O_2 / CO_2 concentrations). Roller bottles provide an intermediate cultivation system were cells still grow on the wall of vessels but the culture volume is mixed by rotation of bottles in a special incubator. Opposed to static cultures roller bottles are completely sealed and only need to be tempered. For culture volumes beyond about 5 L, cascading cultivations including scale-up from step to step becomes necessary. At production-scale cells often go all the way from static cultures over roller bottles to microcarrier cultures of different scales. Common volume scale-up factors are in the

range from five to ten. An overview of cultivation systems available in the bioprocessing group at the Max Planck Institute for Dynamics of Complex Technical Systems including approximate amounts of HA antigen that can be produced is given in Table 2-4.

Although, cultivations are routinely conducted in static cultures at the laboratory-scale, at least roller bottles or microcarrier cultures are necessary for production-scale in order to obtain sufficient quantities of virus. While roller bottles may have their place in the manufacture of some vaccines, microcarrier cultivations in stirred-tanks or wave bags are usually required for the manufacture of influenza vaccines due to comparatively low virus yields. Still, roller bottles pose a valuable tool during process development due to their flexibility, low cost and ease of handling.

Another aspect is the type of growth medium used. Traditional cell culture media are complex media[3] containing fetal calf or a similar serum. A prominent example is the Glasgow Minimum Essential Medium (GMEM), which needs to be supplemented with up to 10% of serum for decent cell growth. Media supplemented with serum are rich in protein rendering product purification more difficult. In addition, serum is poorly defined, resulting in considerable lot-to-lot variations. Serum further involves the risk of contamination by viruses, mycoplasms or prions. Accordingly, the switch from serum-containing to serum-free media has been a major issue in vaccine production for many years [Merten, 2002]. Especially for virus propagation serum-free media do have several advantages [Genzel et al., 2006]. For the growth of Madine Darby Canine Cells (MDCK) used in this work Ex-Cell MDCK and Episerf media have been reported suitable. Both however, still contain complex plant components leaving the problem of lot-to-lot variation unsolved.

Once cells have grown to high density (typically late exponential or beginning of stationary phase), influenza virus and often trypsin are added for infection. Addition of trypsin is usually required for complete activation of viral hemagglutinin, which enhances infectivity of the virus. Moreover, a medium exchange may be necessary for replacement of nutrients and elimination of inhibiting catabolites. If serum-containing medium was used during cell cultivation, the medium further needs to be replaced by a serum-free medium to prevent inhibition of virus adsorption or trypsin activity [Genzel et al., 2004]. First virions can be observed approximately 4 to 6 hours post infection. Depending on the multiplicity of infection[4] (m.o.i.), infection occurs within one to three

3 i.e. of unknown composition

4 Ratio of infectious virus units over total number of living cells. Number of infectious units is determined either by

waves. Release of virions usually occurs over a period of 24 to 36 h before infected cells die [Gaush et al., 1968; Schulze-Horsel et al., 2008; Möhler et al., 2005]. According to estimates based on quantitative real-time PCR, each infected cell produces virions in the order of 1000 to 10 000 particles per cell. However, only a small fraction of these appears to be infectious as is indicated by the much lower infectious titer that can be determined by $TCID_{50}$ or plaque assays [Youil et al., 2004]. Another interpretation is that the infection process is highly ineffective and requires large numbers of intact virions. Eventually, infected cells die due to apoptosis triggered by virus infection or due to other environmental factors. The concentration of virus in the supernatant reaches a maximum and can be harvested for downstream processing.

Table 2-4. Overview of cultivation systems

	Area[1]	Volume	MC	HA Antigen[2]	
Static Cultures	10 – 175 cm^2	3 – 50 ml	-	4 – 70 µg	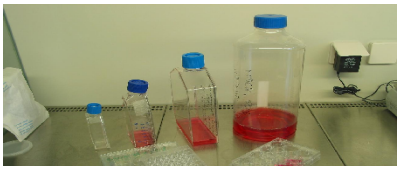
Roller Bottles	400 – 1600 cm^2	125 – 500 ml	-	160 – 650 µg	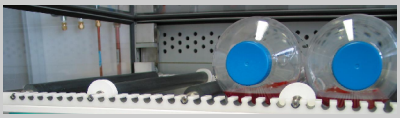
Wave Bags	1.2 – 14 m^2	1 – 15 L	√	1 – 20 mg	
Stirred Vessels	1.2 – 14 m^2	1 – 15 L	√	1 – 20 mg	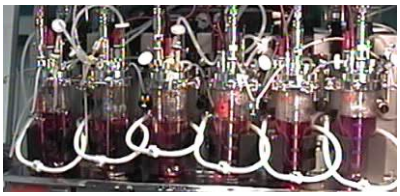

1: Surface area of microcarrier cultures based on standard conditions with 2 g L^{-1} Cytodex carriers, 2: Estimates based on an average HA activity of 400 HAU (0.1 ml)$^{-1}$ after propagation, MC: microcarrier culture

2.1.2 Growth Functions

The characterization of growth phenomena is of interest in many areas of biology and biochemical engineering. In most cases, systems of ordinary differential equations (ODEs) are used for the

pfu or $TCID_{50}$ assay.

mathematical description of investigated processes. Concerning the propagation of adherent mammalian cells on microcarriers and the propagation of influenza virus in mammalian cell culture, the publications of Möhler et al. [2005, 2008] and Sidorenko et. al. [2008, 2004] shall be mentioned here. Despite the undoubted value of their sophisticated approaches, resulting systems of ODEs usually contain a large number of parameters that have to be identified. Moreover, such nonlinear systems of ODEs can only be solved numerically. For a first quick and simple analysis, it is therefore sometimes advisable to rely on less complicated growth models.

Most biological growth processes feature an initial lag-phase followed by a more or less pronounced exponential growth phase. Due to limited resources, the growth rate eventually declines and the population asymptotically approaches a maximum. Corresponding graphs of populations over time are of sigmoid shape. Prominent examples for such growth models are the functions of Verhulst and Gompertz [Backman, 1938]. A side by side comparison including simple exponential growth is given in Table 2-5.

Table 2-5. Comparison of growth functions

Name	Function	Growth Rate	Initial $t=0$:	Supremum $t\to\infty$:	Max Rate $t_c=a/b$:
Exponential	$x(t)=a\cdot e^{bt}$	$\frac{1}{x}\frac{dx}{dt}=b$	$x=a$	-	-
Verhulst's	$x(t)=\frac{K}{1+e^{a-bt}}$	$\frac{1}{x}\frac{dx}{dt}=b-\frac{b}{K}\cdot x$	$x=\frac{K}{1+e^{a}}$	$x\to K$	$\frac{dx}{dt}=0.25\cdot Kb$
Gompertz'	$x(t)=K\cdot e^{-e^{a-bt}}$	$\frac{1}{x}\frac{dx}{dt}=b\cdot e^{a-bt}$	$x=K\cdot e^{-e^{a}}$	$x\to K$	$\frac{dx}{dt}=0.37\cdot Kb$

In all cases, the scaled growth rate $1/x\,(dx/dt)$ is a function of parameter *b*. Concerning exponential growth, the scaled growth rate is identical to *b* and therefore constant. While the population described by exponential growth diverges for $t\to\infty$, populations by Verhulst's and Gompertz' function are limited to values smaller than *K* (supremum or upper asymptote). Parameter *a* is an integration constant that needs to be filled in by some auxiliary condition. Typically, the size of the population at a certain time is given. Integrated Verhulst's and Gompertz' functions are both of sigmoid shape with maximum growth rates at their inflection points. These are located at $t_c=a/b$. All functions approach 0 for $t\to-\infty$ (infimum or lower asymptote).

Functions can, however, be extended by an additive constant $x_{-\infty}$, which allows to shift the lower and upper asymptote. The upper asymptote is then equal to $K + x_{-\infty}$.

In the following, the focus will be set on Gompertz' function which was used to describe experimental data from virus cultivations (4.1). A more illustrative representation of Gompertz' function is achieved by means of the locus t_c of the inflection point:

$$x(t) = K \cdot e^{-e^{-b(t-t_c)}} + x_{-\infty} \tag{2-1}$$

Note, that parameters a and t_c are interconvertible due to $t_c = a/b$. The shape of Gompertz' function, including its main features, is depicted in Figure 2-6.

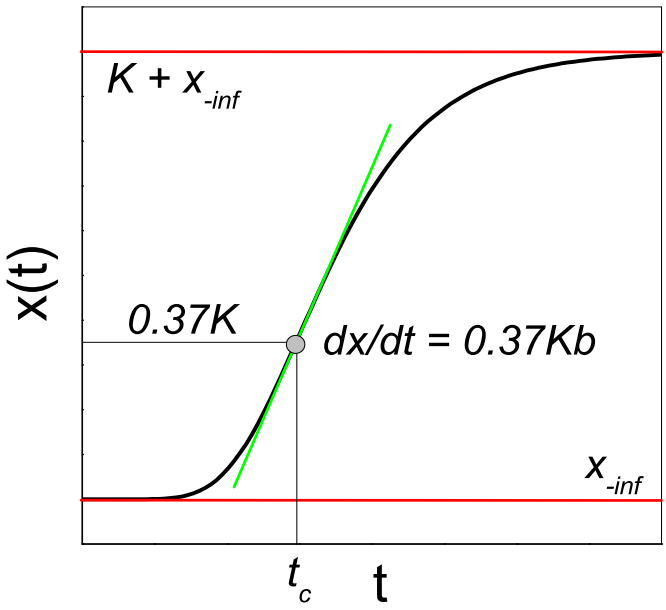

Figure 2-6. Shape and features of Gompertz' function.

Since Gompertz' function is monotonically increasing, it can be interpreted as a cumulative probability distribution after subtraction of $x_{-\infty}$ and division by K (equivalent to reduction of x; see below). After inversion, we obtain the relation

$$t_p = \frac{a - \ln(-\ln p)}{b} \tag{2-2}$$

for the calculation of quantiles t_p linked to probability p. With respect to virus propagation, quantiles t_p are to be interpreted as the time up to which a certain fraction p of the difference between upper and lower asymptote has been released into the supernatant.

For a non-dimensional representation of Gompertz' function, reduced variables $x^* \equiv (x - x_{-\infty})/K$ and $t^* \equiv tb - a$ have to be introduced. In the following, the representation of Gompertz' function simplifies to

$$x^*(t^*) = e^{-e^{-t^*}} \tag{2-3}$$

Since in a multivariate scenario a common time axis is shared, time can only be reduced with respect to one variable. The remaining variables x_i^* are represented by

$$x_i^*(t^*_0) = e^{-e^{a_i' - b_i^* t_0^*}} \tag{2-4}$$

with reduced parameters $b_i^* \equiv b_i/b_0$ and $a_i^* \equiv a_i - a_0(b_i/b_0)$. Variables and parameters with index 0 hereby refer to the reference variable which may be chosen arbitrarily (HA activity in this work). Representation (2-4) can be applied in order to check for self-similarity and in order to achieve a more universal description of data.

2.2 Centrifugation and Sigma Theory

Centrifugation in disc-stack or tubular bowl centrifuges is probably the most common method for the clarification of culture broth at large scales. In comparison to dead-end filtration, the cost of investment is fairly high and cleaning of rotors is often considered critical. However, significant savings in operating costs may be the benefit when centrifugation is used. Moreover, centrifugation can be operated as a continuous operation at a constant flow rate in contrast to the limited capacity of dead-end filters. Also, the risk of early filter blockage is eliminated. On the other hand, centrifugal clarification may be insufficient for the protection of chromatography operations and require additional clarification by microfiltration [Kempken et al., 1995; Berthold et al., 1994].

Opposed to filtration, separation in centrifuges is governed by the sedimentation velocity of particles (and not their size or adsorptive properties). According to Sigma theory, the cut-off sedimentation velocity is equivalent to $u_s = Q / 2\Sigma$ whereby Q is the volumetric flow rate and Σ the equivalent area of a settling tank. The ratio Q / Σ corresponds to the load of the centrifuge [Ambler, 1959] (Note that for non-continuous centrifuges the flow rate is replaced by the ratio of batch volume and centrifugation time V / t). By definition, in ideal systems half of the particle population having cut-off sedimentation velocity will be recovered after centrifugation. Various

expressions have been derived for the calculation of Σ including laboratory, bowl and disc stack centrifuges [Ambler, 1959]. Concerning scale-up in theory, the only criteria to be fulfilled is an equivalent load of centrifuges $Q_1 / \Sigma_1 = Q_2 / \Sigma_2$. In reality however, correction factors μ_i have to be introduced such that $Q_1 / \mu_1\Sigma_1 = Q_2 / \mu_2\Sigma_2$ with values ranging from 0.4 to 1 [Maybury et al., 2000]. The correction factor of laboratory centrifuges is typically assumed as unity.

Practically, the distribution of settling velocity is almost never available. It is thus necessary to characterize clarification efficiency as a function of centrifugal load. In these experiments, clarification efficiency is followed by measures for the content of solid in feed and supernatant. Often, the measurement of turbidity is used for this purpose. A possible definition for the clarification efficiency E is

$$E \equiv 1 - \frac{c_{super}}{c_{feed}} \tag{2-5}$$

with c_{super} and c_{feed} denoting concentrations in the supernatant and feed, respectively. Finally, a critical clarification efficiency has to be defined which is considered acceptable for the process. The corresponding load is then used for definition of appropriate operating conditions and scale-up.

Clarification efficiency can be either characterized directly on the system of interest (typically a bowl or disc-stack centrifuge) or by using scale-down models. While the first approach is less likely to fail, it is also very expensive requiring large volumes of feed material and a production-scale centrifuge at the stage of process development. Maybury et al. [1998] reported how to minimize the hold-up volume and separation area of a disc-stack centrifuge without affecting separation behavior. Even simpler, initial studies can be conducted in laboratory centrifuges, which require only a minimum amount of feed [Maybury et al., 2000]. As long as the time for acceleration and deceleration phases remains negligible, the equivalent settling tank area of a laboratory centrifuge can be be calculated according to

$$\Sigma_{lab} = \frac{V \omega^2}{2g \cdot \ln\left(\frac{2r_2}{r_2 + r_1}\right)} \tag{2-6}$$

with r_1 and r_2 denoting the inner and outer radius of the liquid volume V and angular velocity ω [Ambler, 1959]. For short centrifugation times, acceleration and deceleration phases have to be considered and the approach described by Maybury et al. [2000] is more appropriate:

$$\Sigma_{lab} = \frac{V\omega^2(3-2x-2y)}{6g\cdot\ln\left(\frac{2r_2}{r_2+r_1}\right)} \tag{2-7}$$

In this equation x and y correspond to the fractions of overall centrifugation time required for acceleration and deceleration. Linear acceleration / deceleration with respect to rotational velocity was assumed in derivations. Both, x and y depend on the centrifuge / rotor combination, angular velocity and overall centrifugation time. Normally, their values are not available a priori but have to determined experimentally.

Data obtained from scale-down centrifugation experiments usually suffers from significant scatter. Interpretation is therefore difficult without applying some kind of smoothing, for example, in the form of trend lines. In this work, it was found that experimentally determined clarification efficiency E could be well described by the modified Verhulst' function

$$E(x) = \left[1-e^{(x-x_c)/b}\right]^{-1}, \quad \text{with } x \equiv \log\left[\frac{V(\Sigma t)^{-1}}{m\,s^{-1}}\right] \tag{2-8}$$

Log-transformed centrifugal load $V / \Sigma t$ in units m s^{-1} was passed as the function argument. The locus of the inflection point is given by x_c, steepness of the sigmoid is determined by b. The function approaches zero for $V/\Sigma t \to \infty$ and one for $V/\Sigma t \to 0$. See also 2.1.2 for comparison.

2.3 Chemical Inactivation

Inactivation of infectious virus is a key process in the manufacture of inactivated whole-virion vaccines. Whereas for subunit vaccines inactivation usually occurs as part of the dismantling process, for inactivated whole-virion vaccines dedicated unit operations have to be integrated into the process. Inactivation has to be safe, complete and irreversible but potency of the vaccine should not be affected. Although a large number of inactivation methods exists (see e.g. [Benedictis et al., 2007]), the latter requirement dramatically reduces the number of viable options. Traditionally, vaccines have been inactivated by FA and still appear to be [Lauffer et al., 1949; Timm et al., 1956; Armstrong et al., 1993; Kistner et al., 1998]. However, FA inactivates

virions by reaction with amines showing only low specificity for nucleic acids [Deng et al., 1974]. In addition, there have been concerns about the safety of FA inactivation - possibly linked to only reversible modifications of viral genomes [Budowsky, 1991; King et al., 1981; Beck et al., 1987]. In a search for alternatives, new reagents like aziridines and β-PL have been suggested for inactivation, which are considered safer and more specific for nucleic acids. A list of selected inactivation studies including all three agents is given in Table 2-6.

Table 2-6.Studies on virus inactivation

Virus	Reagent	Reference
Hepatitis A virus	FA	Armstrong, 1993
HIV-1	β-PL, BEI	Race, 1995
Influenza virus	FA	Lauffer, 1949
	β-PL	Budowsky, Friedman, 1991 Budowksky, 1993
	BEI	King, 1991
Rabies virus	BEI	Larghi, 1980
Poliovirus	FA	Timm, 1956 Lycke, 1958
	BEI, AEI	Brown, 2002
Vaccinia virus (recombinant)	BEI	Hulskotte, 1997

BEI: binary ethyleneimine, AEI: N-acetyl-ethyleneimine

Both, aziridines and lactones are highly strained molecules that react with nucleophilic compounds by ring-opening [Vollhardt et al., 1999, 1999; Bartlett et al., 1950]. Whereas β-PL is available as a pure liquid, which can be stably stored at -20 °C, ethyleneimine in the form of BEI is usually synthesized from 2-bromo-ethylamine under alkaline conditions [Bahnemann, 1990]. Both reagents are extremely toxic [Bahnemann, 1990; Brusick, 1977] and need to be handled with special precaution. They are hydrolyzed in (acidic) aqueous solution [Vollhardt et al., 1999, 1999; Bartlett et al., 1950]. Thiosulfate may be equally used for neutralization [Bahnemann, 1990] but also titration of β-PL and ethyleneimine in analytical assays for the determination of residual concentration [Budowsky et al., 1991; Bartlett et al., 1950]. In addition, colorimetric quantitation by reaction with 4-(p-nitrobenzyl)pyridine has been described for aziridines [Tsvetkova et al., 2001; Epstein et al., 1955].

β-PL has been demonstrated to alkylate nucleic acids (RNA and DNA) both in vitro [Chen et al., 1981; Roberts et al., 1963; Morgeaux et al., 1993] and in vivo [Morgeaux et al., 1993; Boutwell et al., 1969]. At elevated concentrations it has been shown to induce nicks into DNA and lead to cross-linking between DNA and proteins as well as between DNA-strands in the double helix [Perrin et al., 1995]. Furthermore, β-PL is able to react with amino acids (cysteine and probably also methionine) [Dickens et al., 1961] and proteins [Boutwell et al., 1969]. Application of β-PL for inactivations of Newcastle disease virus and avian influenza virus, for example, led to partial inactivation of hemagglutination activity at doses higher than 0.1%, which corresponds to a molar concentration of 15.3 mM [King, 1991].

The degree of inactivation is commonly described by survival curves of type $S(t)=lg(x_0/x(t))$ whereby x either denotes the concentration or total amount of infectious virions. The shape of survival curves very much depends on the virus to be inactivated (very often the type of genome) and, obviously, the method of inactivation [Budowsky, 1991]. In the simplest case, an exponential decay (first order process) can be observed. The probability of finding a single infectious virion per dose is equal to $x(t)$ (denoting the total amount of virions) in the limit of $x(t) \rightarrow 0$ [Storhas, 1994]. Typically, inactivation of 15 to 20 orders of magnitude will be required for the probability of an infectious virus being present in any annual production of the vaccine not exceeding 10^{-1} to 10^{-2} [Budowsky, 1991]. Experimentally, however, reduction can only be controlled by 10 orders of magnitude at most. Safety of inactivation methods must hence be inferred from proper description of inactivation kinetics requiring a profound understanding of the inactivation mechanism. In addition, in-process safety testing of inactivation for every lot by inoccuity tests is usually required [WHO Technical Report Series, 2005; European Pharmacopoeia Commission, 2005, 2007]. However, such innocuity testing can only provide an additional level of safety. Especially, a low level of residual infectivity following inactivation is not necessarily detected due to limited sampling volumes. Finally, the risk of virus particles escaping the inactivation process has to be minimized. In particular dead ends in inactivation vessels (e.g. dip tubes, sampling ports and valves) have to be avoided. After addition of the inactivant, the virus-inactivant mixture should be transferred into a second vessel for completion of the inactivation process while inactivation conditions (pH and °C) need to be tightly controlled to guaranty safety of inactivated vaccines.

Despite the fact that inactivation kinetics of the experimentally controllable region often appear of first order, deviation from first order kinetics is to be expected whenever the inactivating agent is

consumed in the process [Budowsky et al., 1991]. Since conditions for safe inactivation have to be inferred from proper description of inactivation kinetics, it is dangerous to neglect consumption of the inactivating agent. An excellent example for adequate description of inactivation kinetics is given by Budowsky et al., who characterized the inactivation of bacterial phage MS2 [Budowsky et al., 1991] and egg derived influenza virus by β-PL [Budowsky et al., 1991, 1993]. Inactivation of infectious virions was found to follow second order kinetics while β-PL was consumed in a first order reaction. No lag time in the reduction of viral infectivity could be detected in either case indicating complete inactivation of virions after the first lesion [Budowsky, 1991]. But a heterogeneous population was observed for influenza virus A/WSN/33 (H1N1) such that analysis had to be restricted to the haploid[5] form of virions [Budowsky et al., 1993]. Inactivation kinetics could be appropriately described by the equation

$$S(t, c_0) = 0.434 \frac{c_0 \cdot k_2}{k_1} \cdot \left[1 - e^{-k_1 t}\right] \tag{2-9}$$

with the initial concentration of β-PL c_0, incubation time t, and rate constants k_1 for the first order decay of β-PL and k_2 for the second order inactivation of infectious virions. Additionally, in the case of phage MS2, the Arrhenius law was applied to describe temperature dependency of rate constants [Budowsky et al., 1991].

Parameters for different strains of influenza virus and rate constants for reaction of β-PL with water and thiosulfate have been summarized in Table 2-7. The degree of inactivation of influenza virus as a function of initial concentration of β-PL and incubation time (assuming the most unfavorable parameters $k_1 = 8 \cdot 10^{-3}$ min^{-1} and $k_2 = 50$ L mol^{-1} h^{-1}) is illustrated in Figure 2-7. As can be seen, the maximum degree of inactivation $S_{max} = 0.434 \cdot c_0 k_2 / k_1$ for $t \to \infty$ is almost reached after about 8 hours independently of the initial concentration. Based on this scenario, the inital β-PL concentration of 3 mM used as the default (see 3.4) corresponds to a maximum degree of inactivation of about 6 orders. The doubled concentration of 6 mM used for inactivation of A/Wis/67/2005 (H3N2) even corresponds to a degree of 15 orders.

5 containing a single genome copy per virion only

Table 2-7. Rate constants for the inactivation of influenza virus with β-PL

Virus or Reactant	Medium	pH	Temp. / °C	k_1 / 10^{-3} min^{-1}	k_2 / L mol^{-1} min^{-1}	Reference
B/Leningrad/489/80	allantoic fluid[a]	7.2 - 7.3	20	6.9	50	Budowsky, Friedman, 1991
	purified virus[b]	7.2 - 7.4	20	5.1	80	
A/Leningrad/385 (H3N2)	allantoic fluid[a]	7.2 - 7.3	20	8.0	50	
	purified virus[b]	7.2 - 7.4	20	5.1	120	
A/WSN/33 (H1N1)	allantoic fluid[a]		20	2.3	110	Budowksky, 1993
	purified virus[b]		20	1.3	250	
Water (acidic solution)	0.01 to 0.05 M perchloric acid	1.3 - 2.0	25	3.35[c]	-	Bartlett, 1950
Sodium thiosulfate	-	n.a.	25	-	11.2[d]	

a: 0.2 M phosphate buffer added, b: in 0.15 M NaCl + 0.2 M phosphate buffer, c: first order reaction, d: second order reaction

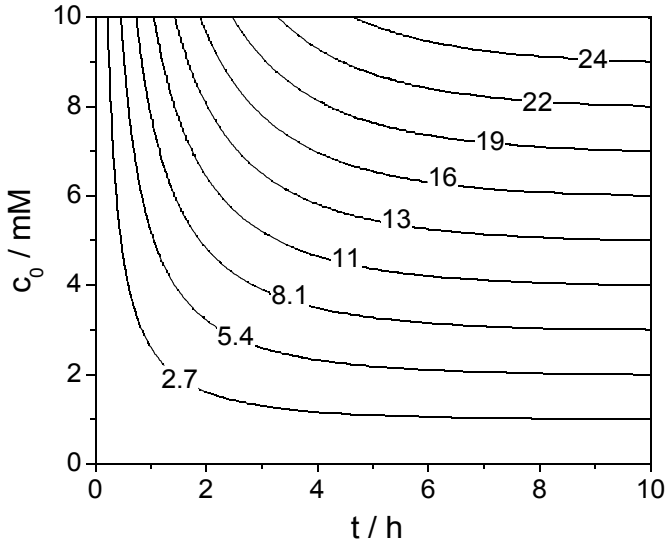

Figure 2-7. Inactivation of influenza virus with β-PL.
The degree of inactivation S (contour lines) is given as a function of the initial concentration of β-PL c_0 and incubation time. Most unfavorable parameters from literature have been assumed for calculation ($k_1 = 8 \cdot 10^{-3}$ min^{-1} and $k_2 = 50$ l mol^{-1} h^{-1}) [Budowsky et al., 1991].

2.4 Selective precipitation of DNA

Selective precipitation of DNA appears to be an attractive choice for the early depletion of host-cell DNA as it is simple to conduct and comparably inexpensive. It can either be implemented as an additional clearance step right after primary clarification or later in the process under more defined conditions. The principal prerequisite is the availability of a selective agent that allows for the quantitative precipitation of DNA while virions remain in the supernatant.

Precipitation of DNA has been achieved by salting-out (LiCl) [Wolf et al., 1977], addition of divalent ions (Ca^{2+}, Mg^{2+}) [de Frutos et al., 2001], alcohol (ethanol and isopropanol) [Moore et al., 2007; Eickbush et al., 1978], PEG [Lis, 1980], detergents (CTAB, CPC, DB) [Gustincich et al., 1991; Goerke et al., 2005], protamine sulfate [Amosenko et al., 1991], poly-L-lysine [Shapiro et al., 1969], cobalthexamide [Widom et al., 1980; Pelta et al., 1996] or polyamines like spermine or spermidine [Pelta et al., 1996; Hoopes et al., 1981; Raspaud et al., 1999] and polyethylenimine (PEI) [Cordes et al., 1990; Jendrisak, 1987]. Moreover, harsh methods like the precipitation of genomic DNA by boiling and acidification or alkalinization play a role in the purification of plasmid DNA [Babu et al., 1998]. Noteworthy, when interpreting the results of these studies, the specific type of DNA should be kept in mind since different behavior may be observable among different types of DNA. It needs to be distinguished between chromosomal DNA or nucleosomes, naked DNA, and supercoiled circular DNA (i.e. plasmid DNA). In the context of virus purification only the precipitation of chromosomal DNA is of practical interest. Basically by definition, such DNA incorporates structural proteins and may be decorated with other proteins in complex mixtures. Moreover, the size distribution of DNA fragments may play a role in the precipitation process.

Several examples for the selective precipitation of DNA have been reported in literature. Selective precipitation has been employed in the purification of poliovirus [Amosenko et al., 1991] and Japanese encephalitis virus (protamine sulphate) [Hong et al., 2001; Srivastava et al., 2001], adenovirus (detergents) [Goerke et al., 2005] and in the general clarification of microbial lysates (spermine and PEI) [DeWalt et al., 2003; Choe et al., 2001; Salt et al., 1995]. Another important application is the purification of plasmid DNA by selective precipitation of plasmids with isopropanol or ammonium sulphate [Freitas et al., 2006], poly(N,N'-dimethyldiallylammoium [Nicoletti et al., 1993], spermidine [Murphy et al., 1999] and PEG [Wahlund et al., 2004].

Crucial for the performance of DNA clearance operations is the selectivity of precipitating agents and operation under mild conditions that are compatible with the product. Methods like salting-out or solvent addition are usually fairly unspecific and have been described for the precipitation of viruses as well. The same applies for the precipitation with PEG (see e.g. [Polson, 1974, 1993; Kanarek et al., 1967]). Although acceptable selectivity may be achievable under appropriate conditions, method development can be rather tedious and robustness of the operation may be insufficient. Other methods like boiling or precipitation at extreme pH will most certainly damage

the product and can usually be excluded a priori for the purification of virions. Protamine sulphate on the other hand may be fairly selective but is of biological origin and should thus be avoided in production processes. Polyamines like spermidine, spermine and PEI, in contrast, are synthetic polymers that posses high affinity towards DNA and are effective even at low concentrations [Pelta et al., 1996; Raspaud et al., 1999]. However, when used as precipitating agents, some loss of protein and lipid is typically observed [Hoopes et al., 1981; Cordes et al., 1990; Salt et al., 1995]. In the case of PEI direct interaction with proteins has even been demonstrated by chromatography [Atkinson et al., 1973]. PEI further involves the risk of in vivo toxicity [Chollet et al.; Regnström et al., 2003; Moghimi et al., 2005] and therefore has to be removed in follow-up unit operations.

2.5 Tangential-Flow Filtration and Critical Flux

TFUF can nowadays probably be considered the default method for concentrating virions [Peixoto et al., 2007; Srivastava et al., 2001; Kim et al., 1999; Paul et al., 1993]. By the use of DF, which often follows the concentration step, its function can be further extended to purification and conditioning [Maranga et al., 2002; Cruz et al., 2000; Valeri et al., 1977]. Since viral harvests are typically dilute (concentrations in the range of a few µg per ml only), TFUF is often used as a first step to enrich the product [Peixoto et al., 2007; Srivastava et al., 2001; Kim et al., 1999; Hong et al., 2001; Montagnon et al., 1984; Frazatti-Gallina et al., 2004]. Volume reduction in the range of 20 to 50-fold can usually be achieved while more than 80% of the product is recovered [Peixoto et al., 2007; Hong et al., 2001; Trudel et al., 1983]. If higher volume reduction should be required TFUF operations can be cascaded using filtration rigs of different scale [Trudel et al., 1983]. Alternatively, devices optimized with respect to hold-up volume can be used [Schu et al., 2001].

DF may be employed to wash out small impurities and condition concentrates for subsequent unit operations (such as chromatography). If conducted at a constant volume (assuming an ideal system), the residual content of fully permeable impurities may be estimated according to

$$c(V_{dia}) = c_0 \cdot e^{-V_{dia}/V_t} \tag{2-10}$$

with V_{dia} / V_t denoting the number of buffer exchanges. Fully permeable means that the sieving coefficient (α) is equal to unity. It is defined as the ratio of concentrations in the initial feed (c_{feed}) and permeate (c_{perm}):

$$\alpha = \frac{c_{perm}}{c_{feed}} \tag{2-11}$$

The sieving coefficient is equivalent to the maximum depletion than can be achieved by DF or infinite concentration. Since most virions are comparatively large, values of sieving coefficients close to unity can typically be realized for small molecules and proteins while coefficients of large genomic DNA fragments are close to zero (see Figure 1-4 for comparison).

The choice of membrane cut-off obviously depends on the dimensions of the product. It should be maximized at early process stages for a maximum reduction of impurities. But a membrane with large pores close to the dimensions of the product may be more prone to fouling [Wu et al., 1999; Bacchin et al., 2006]. The material of the membrane should be chosen such that unspecific adsorption is minimized, which is particularly important during DF. Unspecific adsorption has been addressed in the context of concentrating viruses from ground and waste water [Winona et al., 2001; Divizia et al., 1989; Jansons et al., 1986]. In all cases, high recoveries were only achieved by the addition of blocking agents like beef extract thus stressing the importance of the membrane material but also composition of the DF buffer. In another report dealing with DF of hepatitis B surface antigen, pretreatment of the membrane with 0.1% Tween 20 solution was required [Schu et al., 2001]. But also chemical and physical stability (with respect to cleaning-in-place, steaming-in-place, storage, etc.) and cost usually play a role in the membrane selection process. The choice of module design (hollow-fibers, flat-sheet or spiral-wound membranes), in contrast, may be rather a question of philosophy or availability. Whereas hollow-fiber modules are probably best characterized [Belfort et al., 1994], flat-sheet and spiral-wound membrane modules may yield higher productivity and better fouling control [Schwinge et al., 2004]. When choosing the latter designs one should consider that filtration behavior is a lot more difficult to predict since it does not only depend on membrane characteristics and geometry but also on the type of spacers used, their orientation and the flow distribution in channels.

The final task of the process engineer remains to find appropriate operating conditions (i.e. the wall shear rate or Reynolds number on the retentate side; trans-membrane pressure (TMP) or flux on the permeate side) and configurations of filtration modules (serial, parallel or tapered array) [Schwinge et al., 2004]. A first estimate for the maximum productivity of hollow-fiber modules can be obtained by the limiting flux concept. The limiting flux is reached when flux becomes independent of driving force (Figure 2-8a). In the case of sub-micron sized particles like virions,

Brownian diffusion is th dominant driving force for back migration from the membrane [Belfort et al., 1994; Davis, 1992]. Hence, the similarity solution by Tretin and Doshi [1980] can be used for estimation of the limiting flux. Alternatively, prediction based on film theory can be used to obtain an estimate [Porter, 1972].

However, since the limiting flux concept exclusively considers hydrodynamic mechanisms it is only partially applicable to the filtration of viruses. In the sub-micron range, surface interactions usually play an additional role such [Bacchin et al., 2006]that the achievable productivity may differ significantly [Bacchin et al., 2006]. For such systems it has been observed that fouling often occurs if a certain flux is exceeded but remains negligible otherwise [Wu et al., 1999]. This led to the development of the critical flux concept defining a critical flux beyond which irreversible fouling occurs [Field et al., 1995; Bacchin et al., 2006] and that is distinct from the limiting flux (Figure 2-8a). In contrast to the limiting flux, it is a local concept characterized by a local critical Peclet number [Bacchin et al., 2002]. It has been further distinguished between the strong and weak form of the concept in the absence or the presence of flux-independent fouling [Field et al., 1995; Bacchin et al., 2006].

Although fouling should be in general avoided or at least minimized, this is particularly important for the concentration of virions. Due to the very low content of biomass in viral feed streams, flux-dependent fouling as caused by excessive TMP or forced flux very often coincides with a loss of product [Peixoto et al., 2007; Paul et al., 1993]. In addition, deposits on the membrane can alter rejection behavior (sieving effect of a gel layer or by pore constriction/blocking) such that impurities are no longer separable from the product.

Different approaches exist for the inclusion of surface interactions into filtration models [Baruah et al., 2005; Rabiller-Baudry et al., 2000; Bacchin et al., 2002; Harmant et al., 1998]. The history of development has been summarized by Bacchin et al. [2006]. However, all of them are fairly complex and difficult to apply since the required information on particle characteristics (size distribution, zeta or surface potential, electrophoretic mobility, etc.) is usually not available. Properties like the surface potential further depend on the environment (pH, ionic strength, temperature) [Lucas et al., 1998] and, in addition, specific adsorption of ions to the surface of colloids may play a role [Rabiller-Baudry et al., 2003]. Finally, none of these models is able to deal with the highly complex mixtures of particles that are typically found at the early stages of

purification processes. Experimental determination of filtration behavior (flux-pressure dependency, flux decline, concentration dependence, hysteresis behavior) therefore remains essential.

A safe but not necessarily the best strategy could be to operate filtration always just below the critical flux of the system, hence totally avoiding fouling. Determination of the critical flux by several methods has been reported in the past leading to different definitions of the latter [Schwinge et al., 2004]. Critical flux can be determined either by monitoring the TMP increase for a constant flux or monitoring flux decline at a constant pressure [Espinasse et al., 2002; Kwon et al., 2000], bymass balancing of particles [Kwon et al., 2000] or direct observation of particle deposition on the membrane [Li et al., 1998; Chen et al., 2004]. An example for the determination of critical flux based on the detection of flux decline is given in Figure 2-8b. Interestingly, values for the critical flux determined by different methods do not necessarily coincide. Deposition on the membrane seems to appear earlier than can be detected by a rise in TMP or flux decline [Kwon et al., 2000].

In this work the TMP method was used for approximate determination of critical flux. More precisely, the increase of overall filtration resistance was monitored, which has the advantage of being independent of viscosity and hence temperature of the filtered fluid. A basic description of flux is provided by the general membrane equation [Coulson et al., 1997, 1991]. In this equation, permeate flux (J) is a function of TMP (Δp_{tm}), dynamic viscosity (η) and an overall filtration resistance (R_f):

$$J = \frac{\Delta p_{tm}}{\eta \cdot R_f} \tag{2-12}$$

Noteworthy, the filtration resistance is an overall resistance including friction in membrane pores, resistance due to a polarization layer and - most importantly - deposits on the membrane (fouling layer). By monitoring filtration resistance fouling can be detected readily during filtration. TMP defined as the mean pressure difference between the retentate and permeate side of the module can be calculated according to

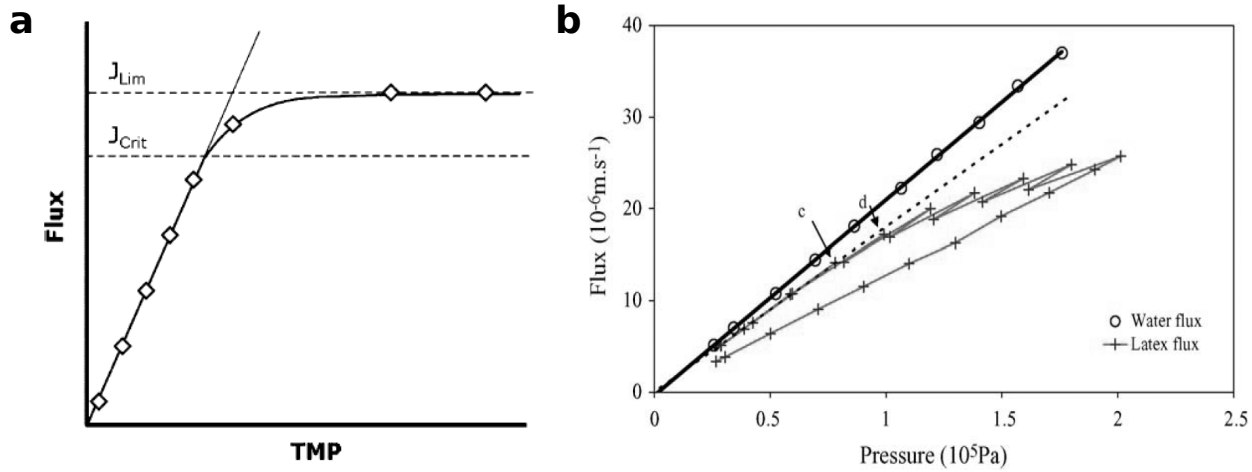

Figure 2-8. The critical flux concept in TFUF.

Critical and limiting flux in tangential-flow filtration (a). The critical flux J_{Crit} denotes the flux below which there is no increase in TMP with time or particle deposition on the membrane. The limiting flux J_{Lim} is the threshold beyond which flux becomes independent of driving force. Reproduced from Schwinge et al. [2004] with kind permission of Elsevier. Determination of the critical flux by flux cycling (b). Relationship between transmembrane pressure and flux for the filtration of water (o) and PVC latex (+) at 7.1 · 10^{-4} g l^{-1} without salt. The dotted line corresponds to the permeability measured on the first points of the filtration of latex. Points c and d correspond to the range of critical flux. Reproduced from Espinasse et al. [2002] with kind permission of Elsevier.

$$\Delta p_{tm} = \frac{p_{in} + p_{out}}{2} - p_{perm} \tag{2-13}$$

Mean pressure of the retentate side is calculated as the average of pressures measured at the retentate inlet (p_{in}) and outlet (p_{out}). In contrast, pressure of the permeate side (p_{perm}) is typically assumed constant due to comparatively low permeate flow rates. Applying the law of pressure drop for laminar flow in pipes (tube-like hollow-fibers only), dynamic viscosity can be calculated from dynamic pressure drop, dimensions of fibers (inner diameter *d,* length *L*) and the wall shear rate ($\dot{\gamma}_0$):

$$\eta = \frac{d \cdot \Delta p_{dyn}}{4L \cdot \dot{\gamma}_0} \tag{2-14}$$

For laminar flow of a Newtonian fluid the velocity profile in tube-like fibers is of parabolic shape. The shear rate at the wall can be calculated according to

$$\dot{\gamma}_0 = \frac{8u}{d} \tag{2-15}$$

The wall shear rate, hence, only is a function of mean flow velocity (u) and the inner diameter of fibers. The dynamic pressure drop (Δp_{dyn}) due to friction at the tube walls is calculated as the difference between pressure measured at the retentate inlet and outlet:

$$\Delta p_{dyn} = p_{in} - p_{out} \tag{2-16}$$

2.6 Size-Exclusion Chromatography

2.6.1 General Overview

SEC is a universal method for the separation of solutes by size. It dates back to the late 1950s when Porath and Flodin [1959] reported on the first chromatography media made from cross-linked dextran. Today, a variety of chemistries are in use including matrices from silica, agarose, polyacrylamide, polyacrylates and their co-polymers [Eriksson, 2002; Mori et al., 1999]. Historically, media made from controlled pore glass also played a role since they can be cast with narrow pore size distributions [Haller, 1965, 1965]. The surface of controlled pore glass, however, is barely inert and therefore not truly suited for SEC without surface modification [Mizutani, 1985; Schnabel et al., 1991]. Nowadays, SEC is a well established technique having its place in analytical and preparative applications [Janca, 1983; Eriksson, 2002; Mori et al., 1999]. Concerning the purification of viruses, SEC is probably the most widely used type of chromatography. Published records include the chromatography of influenza virus [Heyward et al., 1977; Abraham et al., 1984; Nayak et al., 2005], rubella virus [Trudel et al., 1981], tick-borne encephalitis virus [Crooks et al., 1990], rotavirus-like particles [Peixoto et al., 2007], coronavirus [Nagano et al., 1989; Loa et al., 2002], baculovirus [Transfiguracion et al., 2007], bacteriophages [Gschwender et al., 1969] and retroviral vectors [Transfiguracion et al., 2003; Segura et al., 2005]. SEC has been further mentioned in the context of industrial vaccine manufacturing [Hagen et al., 2000; Montagnon et al., 1985; Wiktor et al., 1987].

Preparative SEC is typically operated in group separation mode aiming at the separation of smaller colloids such as proteins from virions. Simultaneously, the product fraction can be conditioned for subsequent unit operations or desalted after ion-exchange and affinity

chromatography (see e.g. [Segura et al., 2005]). Noteworthy, it were already Porath and Flodin [1959] who introduced the term group separation within the context of preparative SEC. In this mode the chromatography medium is chosen such that virions are totally excluded from the stationary phase. Due to the absence of mass-transfer, virions and other excluded solutes elute in a narrow peak almost independently of flow rate (Figure 2-9a). High resolution and low dilution of the product are the result. The choice of chromatography media hence mostly depends on the size and geometry of the virus to be purified (Figure 1-4a). The selection will normally be based on experiments. Although, chromatography media with pores sufficiently large for the entry of virions may exist, theoretically allowing for the separation of larger impurities in addition, their operation would be restricted to very low flow rates in order to avoid excessive band broadening (Figure 2-9b). Another problem is the inherent mechanical instability of such media. Therefore, the latter mode of operation is usually not considered in preparative SEC of virions.

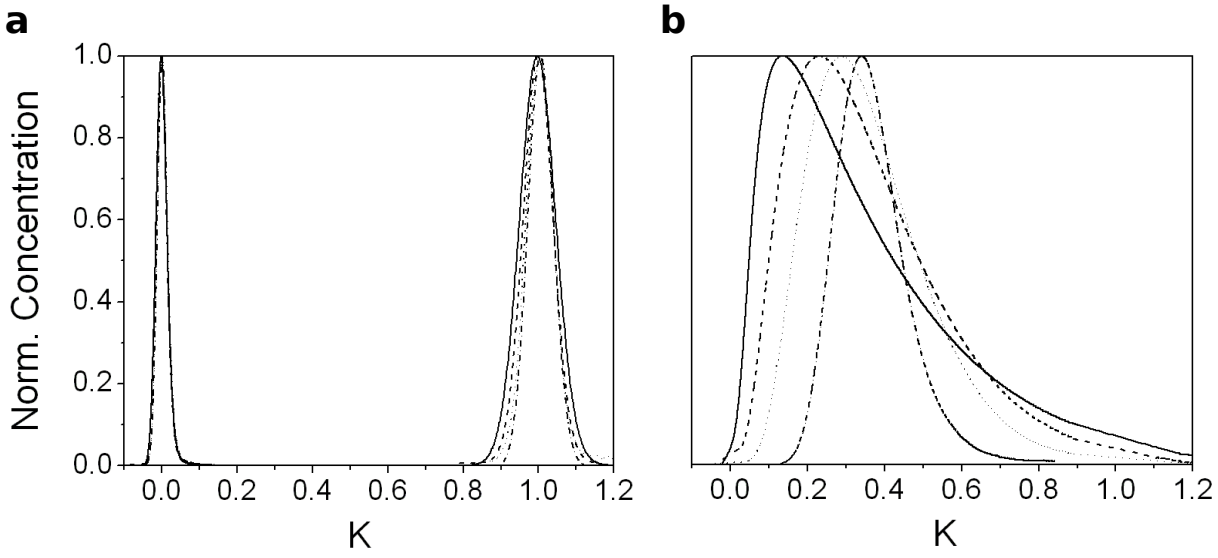

Figure 2-9. Band broadening in SEC.

100 nm BSA-coated polystyrene beads (a, left), acetone (a, right) and a 201 kDa polymethacrylic acid marker (b) were injected onto a 30 cm column packed with Sepharose 4 FF. Markers were eluted at linear flow rates of 120 (—), 60 (---), 30 (···) and 7.5 (–·–) cm h^{-1}. The injection volume was less than 0.1% of the column volume. Chromatograms were normalized to the maximum concentration.

SEC is operated strictly isocratically and hence a diluting chromatography operation. Concentration of the sample as in gradient chromatography is not possible due to the separation

principle (non-adsorptive, molecular sieving effect). But dilution can be minimized by minimizing axial dispersion (i.e. maximizing column efficiency) and choosing a sufficiently large injection volume. On the other hand, SEC does not suffer from a limited capacity for virus particles that is typical for most chromatography media but columns may be loaded with highly concentrated feed streams. In general, productivity and dilution have to be balanced with resolution and hence the degree of purification by selecting an appropriate injection volume, flow rate and column length. Although operation under analytical conditions (low injection volume, low flow rate and long column) will deliver the highest purity, it is typically economically unfeasible. But even after careful optimization of operating conditions, SEC may still pose a bottleneck in large-scale manufacturing of viral vaccines.

SEC at moderate concentrations belongs to the realm of linear chromatography. Moderate means that particle-particle interactions are still negligible with respect to mass-transfer. Historically, the propagation of band profiles has been described using plate models [Giddings et al., 1966; Yamamoto et al., 1990] and continuum approaches [Li et al., 1998; Zelic et al., 2006]. A more recent and distinct view is given by the stochastic theory of SEC, which builds upon the stochastic processes of single solutes (pore ingress and egress) [Dondi et al., 2002]. In the simplest case, attention is only payed to the location of peaks (i.e. mean elution volume or retention time) after short injections (less than 1% column volume) which can be predicted from the distribution coefficient K between phases [Eriksson, 2002; Mori et al., 1999]

$$K = c_p / c_b = (V_e - V_0)/(V_t - V_0) \tag{2-17}$$

The distribution coefficient is defined as the ratio of concentrations in the stationary (c_p) and mobile phase (c_b). It is related to the mean elution volume V_e of a solute and can be calculated once the column void volume V_0 and total liquid volume V_l have been determined. In general, the use of K is preferable over V_e since it is independent of column dimensions and can be directly used to compare the selectivity of chromatography media. For convenience, a similar definition of an apparent distribution coefficient K_{av} exists, which is based on the volume of the column and not the total liquid volume. It is used in cases where a total inclusion marker for the determination of V_l is not available or the volume fraction of the solid is negligible. Importantly, values of K in true SEC are always in the range from 0 (total exclusion) to 1 (total inclusion). Solutes therefore have to elute within one liquid volume of the column. Values of $K > 1$ indicate non-specific interaction

with the stationary phase. For colloids significantly larger than the largest pores, the stationary phase is practically non-porous and SEC passes over to the principle of hydrodynamic chromatography [Stegeman, Kraak, Poppe, and Tijssen, 1993; Stegeman, Kraak, and Poppe, 1993].

The description of peak broadening and finally the prediction of elution profiles is a much more delicate matter. On the one hand peak broadening is affected by axial dispersion and mass-transfer. On the other hand effects related to volume overloading have to be considered. As can be seen in Figure 2-9, peak broadening as a function of flow rate is closely related to the distribution coefficient. While the shape of peaks of totally excluded solutes is solely affected by axial dispersion, which is almost independently of flow rate, other solutes suffer from significant broadening of peaks due to limitations in mass-transfer. In particular solutes close to the exclusion limit are strongly affected and a shift of modal values towards earlier elution volumes can be observed together with an increase in peak asymmetry.

2.6.2 SEC as a Linear Time-Invariant Transfer System

Despite the fact that SEC is one of the best characterized principles in chromatography, development of an efficient SEC operation still constitutes a laborious task. A two-dimensional space is spanned by the parameters mobile phase velocity and injection volume alone, already requiring a large number of experiments for characterization. If column length was to be altered in addition, a three-dimensional parameter space would be obtained. Including further parameters like the choice of resin or eluent, a vast number of combinations arises that can be barely covered experimentally. Viable approaches are therefore needed to reduce the problem to manageable extend.

In an abstract manner, SEC can be regarded as a linear time-invariant (LTI) transfer system. In this approach, SEC is reduced to a single-input-single-output system with respect to each solute or class of solutes. The output signal $h(t)$ (solute concentration over time at the column outlet) is considered the response $\mathbf{T}\{g\}(t)$ to perturbation by a forcing function $g(t)$ (feed concentration over time at the column inlet). For SEC to be a true LTI system, it needs to obey the following equalities [Gajic, 2003]:

$$h(t-t_0)=\mathbf{T}\{g\}(t-t_0) \tag{2-18}$$

$$\sum_1^N b_i h_i(t)=\sum_1^N \mathbf{T}\{b_i g_i\}(t) \tag{2-19}$$

Transformation of signals due to chromatography is hereby presented in the form of an abstract operator **T**. The property of time-invariance is conveyed in (2-18), the property of linearity in (2-19). Time-invariance of SEC is an obvious property as chromatograms do not depend on the time of injection. They will be the same for runs under identical conditions as long as the column has been well equilibrated (i.e. the system is at rest). Linearity, in contrast, remains to be confirmed. It can be argued, however, that the principle of superposition will hold as long as inter-particle interactions remain negligible.

Response of LTI systems to perturbation by admissible forcing functions *g*(t) can be predicted once the response to an infinitely short pulse has been determined. This response is called the system impulse-response and its Laplace transform is referred to as the system transfer function [Gajic, 2003]. In general, the response $h(t)$ of an LTI system at rest can be obtained by convolution of the system impulse-response $h_\delta(t)$ with the forcing function $g(t)$:

$$\begin{aligned} h(t)&=\mathbf{T}\{g\}(t)=\int_{-\infty}^{+\infty} h_\delta(t-\tau)g(\tau)\,d\tau=h_\delta * g \\ &=\int_{-\infty}^{+\infty} g(t-\tau)h_\delta(\tau)\,d\tau=g*h_\delta=\mathbf{T'}\{h_\delta\}(t) \end{aligned} \tag{2-20}$$

In the particular case of SEC, this translates to a convolution of the injection profile g(t) with a characteristic function $h_\delta(t)$ of the system yet to be described.

If sample is, however, injected in overlapping cycles, as is done to enhance throughput, the assumption of a system at rest (i.e. a well equilibrated column) is no longer valid. In preparative chromatography, it is true that $g(t)\neq 0$ only within $t_1\leq t\leq T_1$ corresponding to a finite injection. If the impulse-response is assumed to be finite as well with $h_\delta(t)\neq 0$ only if $t_2\leq t\leq T_2$, it is true that $h(t)\neq 0$ only within $t_1+t_2\leq t\leq T_1+T_2$ [Gajic, 2003]. In other words, if elution occurs within different intervals of time (referred to as windows of elution in this article), the response derived remains valid within the interval $t_1+t_2\leq t\leq T_1+T_2$, which is ensured by the injection-elution strategy described in Figure 4-30 (page 114). Since we are dealing with a causal system it is further true that $t_2\geq t_1$ and $T_2\geq T_1$. Noteworthy, from a mathematical point of view, $h_\delta(t)$

generally approaches zero only in the limit of $t \to \infty$. Practically, however, the assumption of a limited impulse-response is reasonable since impulse-responses in chromatography approach zero sufficiently rapidly (see Figure 2-9 for an example).

Several methods exist to determine the system impulse-response of real columns. In the simplest case, it is approximated by the response to a finite short injection. Analytical problems may, however, arise due to the resulting very low outlet concentrations. An intuitive alternative would be to acquire the response to a finite injection of sufficient extent with a known temporal concentration profile. The impulse-response could then be determined by inversion of the convolution integral in (2-20). This type of problem is referred to as a deconvolution problem and is related to solving a Fredholm integral equation of the first kind. Unfortunately, the latter is known to be an ill-conditioned problem in the presence of experimental noise [Mohammad-Djafari et al., 2002; Bott, 1983].

In order to find meaningful solutions, regularization methods have to be applied. Variational regularization methods can be formulated as solving an optimization problem which is defined by a regularization functional $\Omega(h_\delta)$ and a data discrepancy functional $D(h_\delta,h)$ [Rullgard et al., 2007]. A common choice for the discrepancy functional is $D := \|T' h_\delta - h\|^2$ with $\| \ \|^2$ denoting the L^2 Hilbert norm. Note that the operator **T'** in this expression is identical to the integral operator defined in (2-20) which uses the forcing function $g(t)$ and not the system impulse-response as kernel. Applying a penalization-based regularization approach, a reconstruction operator $R_\lambda^{pen}(h)$ can be defined according to

$$R_\lambda^{pen}(h) := \underset{h_\delta}{\operatorname{argmin}} \left[\|\mathbf{T'} h_\delta - h\|^2 + \lambda \Omega(h_\delta) \right] \tag{2-21}$$

In this approach, the regularization functional $\Omega(h_\delta)$ has the form of a penalty function containing information on the desirability of a solution. It is weighted by a regularization parameter λ. One possible choice for the penalty function is

$$\Omega(h_\delta) = \int_0^\infty h_\delta(t) \ln h_\delta(t)\, dt \quad \text{with } h_\delta \geq 0 \text{ and } \int_0^\infty h_\delta(t)\, dt = 1 \tag{2-22}$$

leading to the concept of maximum entropy (MaxEnt) regularization [Shore et al., 1980]. Normalization and positivity of h_δ is thereby assumed such that it can be interpreted as a probability density function (in this case a residence time distribution). According to Rullgård et

al. [2007] the optimization problem in (2-21) can be restated as a tolerance-based reconstruction operator

$$R_{\varepsilon}^{tol}(h) := \underset{\|\mathbf{T}^{\cdot} h_{\delta} - h\| \le \varepsilon}{\operatorname{argmin}} \Omega(h_{\delta}) \tag{2-23}$$

if both optimization problems are strictly convex. In this case, there exists a correspondence between the regularization parameters λ and ε. The correspondence, however, depends on the data and is not straight forward to delineate. In the tolerance-based approach, the regularization parameter ε defines an upper bound for the data discrepancy functional D. It is equivalent to finding a solution for h_δ which maximizes information entropy defined as $S = -\Omega$ while some deviation of the prediction from observed system behavior is allowed. Since Ω and D are both strictly convex, a single global maximum exists making the solution for h_δ unique [Skilling et al., 1984].

While various alternatives for the definition of Ω exist, the principle of maximum entropy has been proven axiomatically to be a uniquely correct method for inductive inference [Shore et al., 1980]. It is the only method consistent with simple and general requirements that have been described elsewhere [Shore et al., 1980; Livesey et al., 1985]. MaxEnt deconvolution has been applied successfully to a number of problems including the calculation of drug absorption rates [Charter et al., 1987], reconstruction of images [Skilling et al., 1984; Gull et al., 1978], crystal structures [Livesey et al., 1985], structures from EM tomography [Rullgard et al., 2007] and deconvolution of mass spectrometry data [Mohammad-Djafari et al., 2002]. A systematic comparison with other deconvolution methods has been given by Madden et al. [Madden et al., 1996].

The main difficulty in applying (2-23) remains in choosing appropriate values for ε. In statistical regularization theory, it is assumed that D is a random function with approximately known probability distribution. If, for instance, the distribution of error is homoscedastic and variance is known a priori, χ^2-statistics can be used for deriving values of ε [Skilling et al., 1984]. Regarding chromatography, however, homoscedastic distribution of error is unlikely. Experimental data is typically prone to error from baseline drift, non-linearity of detectors and deviation from ideal behavior due to particle-particle interactions. In addition, error due to discretization has to be taken into account. Sound derivation of ε is hence difficult and impractible in most cases. Consequently, an empirical approach was pursued here. Firstly, the minimum distance ε_{NNLS} of the

non-negatively constrained least-squares solution (NNLS; special case for $\lambda = 0$) was calculated. Secondly, ε was set from 2 ε_{NNLS} to 6 ε_{NNLS} in the following such that a meaningful solution without oscillations was obtained.

2.7 Ion-Exchange Chromatography

The principle of ion-exchange chromatography (IEC) is based on electrostatic (coulombic) interactions between charged solutes and immobilized charge on the stationary phase. Common ligands include quaternary ammonia and diethylaminoethyl. Common ligands in cation-exchange chromatography (CIEC) are sulphonyl and carboxyl groups. Functional groups may be either coupled directly to the stationary phase or via spacers (also called tentacles) allowing for more flexibility in the binding of macromolecules. Under appropriate conditions (ionic strength and pH) solutes adsorb to the oppositely charged stationary phase and are separated from other compounds on the basis of differential retention. For macromolecules with multiple interaction sites often a very strong bond with affinity-like character can be observed. In this case, it is more favorable to operate in gradient mode. Firstly, product and a share of impurities are adsorbed to the column under conditions which maximize selectivity but also dynamic capacity - a process referred to as frontal chromatography. Secondly, desorption of the product is either achieved by displacement with an increasing concentration of salt or by gradual changes in pH reducing and eventually reversing the charge of adsorbed solutes. Comprehensive overviews on the subject have been provided by Yamamoto et al. [1988] and Choudhary and Horvarth [1996].

Since virions are polyelectrolytes IEC is almost always applicable presuming the proper choice of ion-exchanger and supporting matrix. Chromatographic purification by IEC has been described for a variety of viruses. Examples involving packed-bed chromatography comprise the purification of influenza virus [Muller et al., 1952], hepatitis A virus [Hagen, Oliver, et al., 1996], adenovirus [Konz et al., 2005; Brument et al., 2002; Kaludov et al., 2002; Green et al., 2002], adeno-associated virus [O'Riordan et al., 2000; Smith et al., 2003] and retroviral vectors [Rodrigues et al., 2006]. Ion-exchange membrane chromatography has been described for influenza virus [Goyal et al., 1980], rotavirus-like particles [Vicente et al., 2008], alphaherpesviruses [Karger et al., 1998], baculovirus [Wu et al., 2007], densonucleosis virus [Specht et al., 2004] and bacteriophage PRD1 [Walin et al., 1994]. Regarding monoliths,

examples for tomato mosaic virus [Kramberger et al., 2007] and bacteriophage T4 [Smrekar et al., 2007] can be found in literature. Besides, a patent application describing AIEC of influenza virus with different media including adsorptive membranes and monoliths has been submitted [Peterka et al., 2008].

The choice of ion-exchanger mostly depends on the net charge of virions. If pH is above the isoelectric point, virions are negatively charged and anion-exchangers are most appropriate. Otherwise cation-exchangers should be used. Although, net charge can be influenced via pH (e.g. [Specht et al., 2004]), stability of viruses often limits the pH working range. In the case of influenza virus, a pH below 5 induces conformational changes in the hemagglutinin protein [Lamb et al., 2001], resulting in a loss of infectivity [Scholtissek, 1985] and viral aggregation [Campbell et al., 2004]. The acceptable pH working range therefore always needs to be determined experimentally ahead of developing IEC operations.

The isoelectric point of virions can be determined by isoelectric focusing or isoelectric titration (i.e. measurement of ζ-potential or electrophoretic mobility as a function of pH). The latter provides additional information on the quantity of charge in addition to sign. Concerning electrophoretic methods, at least agarose gels or free-flow electrophoresis have to be used due to the size of virions. The isoelectric point of influenza virus A2/Singapore/57, for example, has been determined as 5.0 by isoelectric focusing [Zhilinskaya et al., 1972]. The isoelectric point of influenza virus PR-8 has been determined as 5.3 by isoelectric titration [Miller et al., 1944]. Theoretical calculations of isoelectric points, in contrast, are highly unreliable since the precise composition of virions is often not known; neither is the fraction of proteins, which are exposed on the viral surface. Moreover, post-translational modifications such as glycosylation can severely alter the charge of virions. A peculiarity of macromolecules and virions is that even if the net charge has been determined, patches of the opposite charge may exist. Respectively, purification of influenza virus A/PR/8/34 (H1N1) by CIEC at neutral pH has been reported even though overall virus charge would be expected to be negative [Muller et al., 1952]. Suitability of ion-exchangers therefore always remains to be confirmed experimentally.

Three applications of IEC are usually considered: In the first, virus is to be gross-purified and concentrated early in the process (referred to as capture, see e.g. [Hagen, Oliver, et al., 1996; Kalbfuss, Wolff, Geisler, et al., 2007]). During capture, the focus is set on productivity since large

volumes of feed material have to be processed. In addition, conditions upon adsorption need to be carefully optimized in order to maximize selectivity. Otherwise, a large share of the dynamic capacity would be consumed by impurities. Alternatively, virus is to separated from minor yet critical amounts of particular impurities at an intermediate or late stage of the purification process (referred to as intermediate purification or polishing, see e.g. [Konz et al., 2005; Hagen et al., 2000]). In this case, it is mainly resolution (i.e. high selectivity and column efficiency), which is the crucial feature. A third possibility is operation of AIEC in flowthrough mode particularly for the depletion of nucleic acids [Sakata et al., 2005; Knudsen et al., 2001]. This option should be considered whenever appropriate ion-exchangers for the adsorption of virus do not exist or adsorptive purification is too inefficient due to low recovery or capacity. Noteworthy, it is not necessarily electrostatic interaction alone but a combination of electrostatic and hydrophobic interaction that is involved in the binding of nucleic acids [Charlton et al., 1999].

3 Experimental

3.1 Analytical Methods

A number of analytical assays were established for the quantitation of virus and impurities. HA activity was used as the default measure for virus quantity, but had to be replaced by NA activity in some cases. The total protein and DNA concentration were determined routinely as measures for the content of impurities. An overview of assay characteristics is given in Table 3-8. Detailed descriptions of assay procedures are given in the following.

Table 3-8. Overview of Assays

Assay	Type	Unit	Dynamic Range	Precision[a]
HA Activity	Titration	HAU $(0.1\ ml)^{-1}$	100 – 1000	+16% / -14%[b]
NA Activity	Fluorogenic Substrate	NAU L^{-1}	0.07 – 5	≤5% (0.5 – 5 NAU ml^{-1}) ≤10% (0.07 – 0.5 NAU ml^{-1})
Total Protein	Colorimetric	µg ml^{-1}	5 – 45	n.a.
DNA	Fluorometric	µg ml^{-1}	0.005 – 1	n.a.

a: Intra-assay precision (or repeatability) expressed as relative standard error for default number of replicates, b: asymmetry originates from exponentiation

3.1.1 HA Activity

HA activity was determined routinely for the quantitation of influenza virus. The assay format used was derived from the description by Mahy and Kangro [1996].

For each sample, two serial 1:2 dilutions (12 x 100 µl each) were prepared in round-bottomed 96-well microtiter plates (Cat. No. 650160, Greiner Bio-One, Frickenhausen/Germany). Serial dilutions were shifted by a factor of $1:2^{0.5}$ resulting in a dilution factor of $1:2^{0.5}$ from well to well. This was achieved by starting the second row with a $1:2^{0.5}$ pre-dilution of the sample (70.7 µl sample + 29.3 µl PBS). Phosphate buffered saline (PBS; 8 g l^{-1} NaCl, 0.2 g l^{-1} KCl, 0.20 g l^{-1} KH_2PO_4, 1.15 g l^{-1} Na_2HPO_4) was used as diluent. In addition to samples, an internal standard (measured at least twice per assay run) was included. 100 µl of purified chicken erythrocytes (see below) were added to each well and plates were incubated at room temperature for at least 2 h up to over night. Afterwards, plates were scanned with a plate photometer (Rainbow Spectra, Tecan

Deutschland GmbH, Crailsheim/Germany) measuring light extinction at 700 nm. Extinction was reported in arbitrary units. If infectious samples were to be measured, the assay was pipetted in a S2 safety hood. Plates were covered with transparent lids (Cat. No. 656101, Greiner Bio-One, Frickenhausen/Germany) immediately afterwards and sealed with scotch tape or parafilm.

Extinction data were evaluated using an Excel spreadsheet template (Microsoft, Redmond/United States). Extinction was plotted over the negative logarithm of dilutions and a Boltzmann sigmoid was fitted to each data set by non-linear least squares using the Excel solver tool. The dilution at the point of inflection (one of the parameters) was defined as the end point of titration (Figure 3-10a). The inverse of the dilution was defined as the specific HA activity with units 1 HAU (0.1 ml)$^{-1}$. Activities of all samples were corrected (that is multiplied) by the average ratio of nominal to measured activity of the internal standard in order to compensate for day to day variations. Note that multiplicative correction of HA activity corresponds to an additive correction of the primary assay measure (negative logarithm of dilution at the endpoint).

Intra-assay and intermediate precision of the assay were estimated in a validation study and from data obtained under routine use. Statistics were calculated on the primary assay quantity (negative logarithm of dilution at endpoint). Average standard deviations of 0.066 under routine use and 0.027 in the validation study were estimated for single determinations (intra-assay precision). Corresponding 95% confidence intervals (CIs) obtained by t-statistics were ±0.149 and ±0.063, respectively. Confidence intervals of the primary assay quantity converted to intervals for the HA activity are given in Figure 3-10b. Due to exponentiation of negative log-dilutions, resulting CIs became asymmetric (upper and lower limits reported in the following). The average CI for HA activity determined under routine use was +41% / -29%. The average CI derived from the validation study was +15% / -13%. Intermediate precision was inferred from data obtained under routine use. For a single-determined sample and a double-determined internal standard, an SD of 0.081 can be predicted assuming the previously determined intra-assay SD of 0.066.

For full details on assay development and validation, including the preparation of erythrocyte suspensions and internal standards, readers are referred to the article by Kalbfuss et al. [2008].

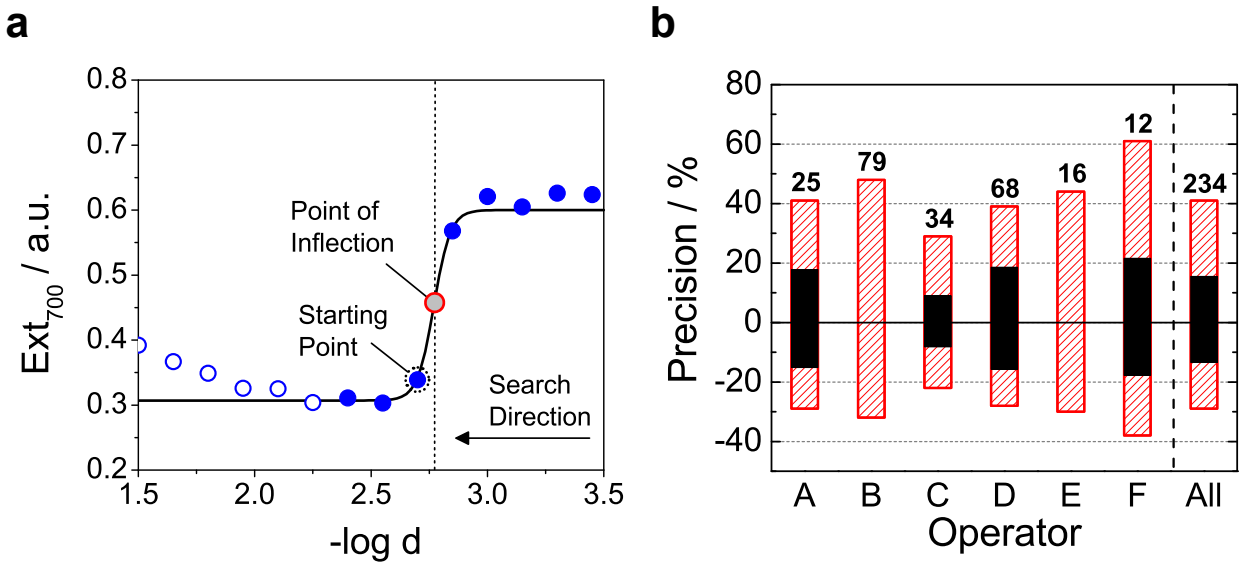

Figure 3-10. Precision of the automatically evaluated HA assay.
Sigmoidal fit to extinction data for the determination of HA activity (a). A search is started from the right-hand side for the first point below average extinction (starting point). Only data points two steps further to the left are included into regression analysis (●). The location of the starting point as well as minimum and maximum extinction values (of the whole data set) are used as initial values for fitting of a Boltzmann sigmoid (—). Its point of inflection (○) is defined as the endpoint of titration. Precision of the HA assay (b). Data from a double-determined internal standard (included in routine assay use) was collected over 1 year. Relative error (▨, 95% confidence interval) was estimated for six operators (A to F) and mean precision was calculated (All). Small numbers indicate the number of double-determinations included in the analysis. Black bars (■) indicate precision as estimated in a preliminary validation study.

3.1.2 NA Activity

NA activity was determined for the quantitation of influenza virus during selective precipitation of DNA and subsequent TFUF (see 4.3 and 4.4.3). It was further considered as a marker for the progress of viral infection (see 4.1). The assay employed is based on the method proposed by Potier et al. [1979], which relies on the enzymatic cleavage of the substrate 2'-(4-Methylumbelliferyl)-α-D-N-acetylneuraminate (4-MU-NANA) and subsequent release of fluorescent 4-Methylumbelliferone (4-MU).

10-fold stock solutions of 4-MU-NANA (Cat. No. M8639) and 4-MU (Cat. No. M1381, both Sigma-Aldrich Chemie GmbH, Taufkirchen/Germany) were prepared in reaction buffer (150 mM NaCl, 30 mM Na-MES, pH 6.5) and ethanol, respectively. Stock solutions were divided into aliquots and stored at -20 °C. Frozen aliquots were thawed and diluted with reaction buffer or

water to appropriate concentrations immediately before assay runs. For activity measurements, 10 µl of samples were dispensed into black 96-well microtiter plates (Cat. No. 3915, Corning GmbH, Kaiserslautern/Germany) after appropriate pre-dilution in reaction buffer. Except in measurements of NA activity during virus infection, reaction buffer was supplemented with 1 mg ml^{-1} BSA (Cat. No. A7906, Sigma-Aldrich Chemie GmbH, Taufkirchen/Germany). In addition to samples, a 4-MU calibration standard comprising of 8 concentrations (0...12.5 µM) was prepared. Samples and calibration standards were measured in duplicates by default. In order to compensate for spontaneous hydrolysis of 4-MU-NANA and a small fraction of 4-MU already contained in the 4-MU-NANA stock solution, a four-fold blank was included in every plate.

200 µl of reaction buffer were added to each well of the calibration standard using a multipette (Eppendorf, Hamburg/Germany) with 10 ml tip. In the next step, 200 µl of substrate dissolved at 105 µM in reaction buffer were added to sample and blank wells as fast as possible (typically in less than 4 minutes). Plates were sealed with PCR foil (Cat. No. 676001, Greiner Bio-One, Frickenhausen/Germany) and incubated at 37 °C for 60 minutes while shaking at 1000 rpm in a Thermomixer Comfort (Eppendorf, Hamburg/Germany). PCR foil was removed immediately afterwards and enzyme reactions were stopped by addition of 100 µl stop buffer (180 mM glycine, pH 10.7) in the same order as substrate had been added before. The difference in incubation time between samples was typically less than one minute. Finally, 100 µl of stop buffer were added to wells of the concentration standard. Fluorescence of 4-MU was measured (Ex: 365 nm, Em: 450 nm) using a Cary Eclipse plate fluorometer (Varian Deutschland GmbH, Darmstadt/Germany). If infectious samples were to be measured, the assay was pipetted in a S2 safety hood. Plates were re-sealed with PCR foil after addition of stop buffer and virus was heat-inactivated at 70 °C for 20 minutes. After having cooled down, liquid on the foil was spun down briefly by centrifugation (1000 g for about 1 min) and plates were scanned as described above.

Fluorescence data were evaluated using an Excel spreadsheet template (Microsoft, Redmond/United States). A second order polynomial was fitted to the data points of the calibration standard. Its parameters were estimated by weighted linear least-squares assuming that the variance is proportional to intensity squared using the Excel solver tool. The calibration function was applied to convert fluorescence intensities to concentrations and all concentrations were corrected for the average concentration of blank wells. Activities (that is reaction rates under defined assay conditions) were calculated from concentrations by zero order approximation of

Michaelis-Menten kinetics. Specific activities were expressed in units $\mu M\ min^{-1}$ or $NAU\ L^{-1}$ (according to the international unit definition).

For full details on assay development and validation, readers are referred to the article by Kalbfuss et al. [2008].

3.1.3 Total Protein

Total protein concentration was determined using the Coomassie dye-binding assay (Bradford assay). Ready-to-use Coomassie dye reagent was purchased from Biorad Laboratories (München/ Germany, Cat. No. 500-0006). The assay was conducted in transparent flat-bottomed 96-well microtiter plates (Cat. No. 655201, Greiner Bio-One, Frickenhausen/Germany). In each well, 200 µl of sample were mixed with 50 µl of dye reagent. After 5 min of incubation at room temperature while shaking at 1000 rpm in a Thermomixer comfort incubator (Eppendorf, Hamburg/Germany) microtiter plates were scanned for their extinction of light at 595 nm using a Tecan Spectra Rainbow Reader (Tecan, Crailsheim/Germany). The assay was calibrated with BSA (Sigma-Aldrich, Munich/Germany, Cat. No. A-3912) dissolved at 7 concentrations ranging from 7 to 50 $\mu g\ ml^{-1}$ in addition to a blank. All samples including the calibration standard were measured in triplicate. For compensation of matrix interference, BSA was dissolved in buffers resembling the sample matrix as closely as possible. Where necessary (e.g. after anion-echange chromatography), pH or ionic strength of samples were altered by pre-dilution in appropriate buffers and BSA was dissolved accordingly. For samples from virus culture containing medium components, it was generally necessary to pre-dilute 1:10 in PBS (8 $g\ l^{-1}$ NaCl, 0.2 $g\ l^{-1}$ KCl, 0.20 $g\ l^{-1}$ KH_2PO_4, 1.15 $g\ l^{-1}$ Na_2HPO_4) prior to measurements. The standard was similarly dissolved in fresh Ex-Cell MDCK or V-Medium diluted 1:10 in PBS. Since the soy hydrolysate in Ex-Cell MDCK medium but also the yeast peptone in V-Medium contained peptides, which were partly detected as protein, only the excess concentration of protein could be determined this way. The basal concentration contributed by hydrolysate or peptone had to be estimated separately from pure compounds (4.4 to 6.8 $\mu g\ ml^{-1}$ in the case of Ex-Cell MDCK medium and 6.2 $\mu g\ ml^{-1}$ in the case of V-Medium; equivalent concentrations in undiluted media). Extinction data were evaluated using an Excel spreadsheet template (Microsoft, Redmond/United States). Firstly, a Boltzmann sigmoid was fitted to extinction data for the concentration standard. Secondly, protein

concentrations of samples were calculated from extinction data by application of the inverted sigmoid. Concerning analysis of samples from virus culture, the basal concentration of media was added to concentrations of the BSA standard prior to calibration. Protein concentrations in samples below the basal concentration of media were estimated by extrapolation.

3.1.4 Double-Stranded DNA

Determination of DNA concentration was based on the fluorescence enhancement of PicoGreen dye upon binding of DNA. Ready-to-use dye reagent was purchased from Invitrogen (Karlsruhe/Germany, Cat. No. P-7581). The assay was conducted in black flat-bottomed 96-well microtiter plates (Corning, US, Cat. No. 3915) by mixing of 200 µl of sample with 50 µl of dye working solution prepared according to the manufacturer's instructions. After 5 min of incubation at room temperature while mixing at 1000 rpm in a Thermomixer comfort incubator (Eppendorf, Hamburg/Germany) microtiter plates were scanned for their fluorescence intensity (Ex. 480 nm, Em. 520 nm) using a Carry Eclipse fluorometer (Varian, Darmstadt/Germany). Alternatively, a Mithras LB 940 (Berthold Technologies, Bad Wildbad/Germany) reader with appropriate filters was used. The assay was calibrated with λ-DNA (Promega, Mannheim/Germany, Cat. No. D1501) dissolved at 7 concentrations ranging from 4 to 1000 ng ml^{-1} in addition to a blank. All samples including the calibration standard were measured in duplicate. For compensation of matrix interference, λ-DNA was dissolved in buffers resembling the sample matrix as closely as possible. Where necessary (e.g. after anion-echange chromatography), pH or ionic strength of samples were altered by pre-dilution in appropriate buffers and λ-DNA was dissolved accordingly. For samples from virus culture containing medium components, it was generally necessary to pre-dilute 1:10 in TE buffer (20 mM Tris-Cl, 2 mM EDTA, pH 7.5) prior to measurements. The standard was similarly dissolved in fresh Ex-Cell MDCK or V-Medium diluted 1:10 in TE buffer. Since the soy hydrolysate in Ex-Cell MDCK medium but also the yeast peptone in V-Medium contained DNA fragments, only the excess concentration of DNA could be determined this way. The basal concentration contributed by hydrolysate or peptone had to be estimated separately from pure compounds (1.0 to 2.7 µg ml^{-1} in the case of Ex-Cell MDCK medium and 1.1 µg ml^{-1} in the case of V-Medium; equivalent concentrations in undiluted media). Fluorescence data were evaluated using an Excel spreadsheet template (Microsoft, Redmond/United States). Firstly, a power law or quadratic function were fitted to fluorescence

data for the concentration standard. Secondly, DNA concentrations of samples were calculated from fluorescence data by application of inverted functions. Concerning analysis of samples from virus culture, the basal concentration of media was added to concentrations of the λ-DNA standard prior to calibration. DNA concentrations in samples below the basal concentration of media were estimated by extrapolation.

3.2 Virus Cultivation

3.2.1 Preparative Cultivations

Influenza virus was propagated in Madin-Darby canine kidney cells (MDCK) from ECACC (Salisbury/United Kingdom, Code 841211903) by a two-stage procedure. MDCK cells were grown to confluency in 850 cm^2 PET roller bottles (Greiner Bio-One, Frickenhausen/Germany, Cat. No. 680160) using a total of 250 ml medium per bottle. Cells were either cultivated in serum-free Ex-Cell MDCK medium (Sigma-Aldrich, Munich/Germany, Cat. No. 14581C) or GMEM supplemented with 10% fetal calf serum (PAN Biotech GmbH, Aidenbach/Germany, Cat. No. 3302-P250922) and 0.2% yeast peptone (Lab M, Lancashire/United Kingdom, Cat. No. MC001). GMEM itself was prepared from 13.91 g L^{-1} instant powder (Invitrogen, Paisley/United Kingdom, Cat. No. 22100-093), 4.44 g L^{-1} Na_2HCO_3 and 1.11 g L^{-1} additional glucose (Carl Roth GmbH, Karlsruhe/Germany, Cat. No. X997.3). The supplemented GMEM is referred to as Z-medium in the following.

Cells were seeded at an initial density of $9 \cdot 10^3$ cells cm^{-2} in cultivations with Ex-Cell MDCK medium. The density of cell suspensions was determined manually by counting under the microscope using a hemacytometer. Roller bottles were sealed tightly and incubated at 37 °C with 0.25 rpm. Cell growth was carried out over a period of 7 days into the stationary phase. For cultivations in Z-medium, cells were seeded at an initial density of $4.3 \cdot 10^4$ cells cm^{-2}. Cell density prior to seeding was determined automatically using a ViCell XR counting device (Beckman-Coulter, Krefeld/Germany). Cell growth was carried out at 0.66 rpm over a period of 5 days until the late exponential growth phase. Pre-cultures were derived from roller bottles in most cases. The passage count was generally kept below 20 except for some cultivations with Ex-Cell MDCK medium. Typically, 8 up to 16 roller bottles were grown in parallel plus a reference bottle which was sacrificed prior to infection for determination of the final cell density. Average cell

densities were in the range of 2.2 to 3.2 · 10^5 cells cm^{-2} depending on the medium and campaign (Table 4-20).

Samples of influenza virus were added to supernatants of confluent cell cultures for infection and virus propagation. Human influenza strains A/PR/8/34 (H1N1) and A/Wis/67/2005 (H3N2) used for infection were purchased from NIBSC (Potters Bar/United Kingdom). A sample of the strain A/PR/8/34 (H1N1) was purchased from the Robert Koch Institute (RKI; Berlin/Germany) in addition. Sources are distinguished by the tags NIBSC and RKI in the following. Samples of viruses were first propagated in static cultures. Infectious supernatant, later used for infection of roller bottles, was aliquoted and conserved at -70 °C. Infectivity of aliquots was determined by the $TCID_{50}$ assay as described by Mahy and Kangro [1996].

In cultivations with serum-containing Z-medium, medium had to be exchanged prior to infections. Old medium was disposed and bottles were rinsed with 100 ml of PBS twice. Afterwards, bottles were re-filled with 250 ml of fresh V-Medium, i.e. Z-medium without serum addition. Cultures in Ex-Cell MDCK Medium, in contrast, were infected directly. An m.o.i. of 0.025 was used for both strains. For enhancement of virus propagation, trypsin (Invitrogen, Paisley/United Kingdom, Cat. No. 27250-018) was added to supernatants at a final concentration of 10 µg ml^{-1} in cultivations with Ex-Cell MDCK medium. In cultivations with V-Medium, trypsin concentration was adjusted to a final activity of 1500 U per bottle (6 U ml^{-1}) according to lot specifications of the manufacturer. Infections were carried out for exactly 3 days under identical conditions as during cell growth. Supernatants of bottles were pooled afterwards resulting in volumes between 2 and 4 L. Pooled supernatants were clarified immediately by filtration or centrifugation (see 3.3.1 and 3.3.2) and typically inactivated by the addition of *β-PL* (see 3.4). HA activity and turbidity (extinction of light at 700 nm) were determined routinely before and after clarification. NA activity, protein and DNA concentration were measured only after inactivation. In cultivations with Ex-Cell MDCK medium, protein and DNA concentration were only measured after secondary clarification by membrane filtration.

3.2.2 Course of Infection

For optimization of preparative cultivations, time courses of infection in roller bottles were acquired for human strains A/PR/8/34 (H1N1) RKI, A/Wis/67/2005 (H3N2) and

B/Mal/2506/2005. The strain B/Mal/2506/2005 was purchased from NIBSC (Potters Bar/United Kingdom). Virus seed was prepared as described above (see 3.2.1). Courses of infections were acquired in two experiments. In the first experiment, MDCK cells were infected with A/PR/8/34 (H1N1) RKI at different m.o.i.'s (2.5, 0.025 and 0.00025). In the second experiment MDCK cells were infected with A/PR/8/34 (H1N1) RKI and A/Wis/67/2005 (H3N2) at an m.o.i. of 0.025 (same as in preparative cultivations) and B/Mal/2506/2005 at an m.o.i. of 0.001. All infections belonging to the same experiment were conducted in parallel. Two bottles were infected per condition and measured data averaged. Infections were carried out over a prolonged period of up to 115 h (only 72 h in preparative cultivations). Cell growth prior to infections were conducted under the conditions described for preprative cultivations (see 3.2.1). The same pre-culture (or pool of pre-cultures) was used for seeding of roller bottles. The combination of serum-containing Z-medium and serum-free V-Medium was used in both experimets.

Initially, bottles were sampled every 6 h until the third day. Subsequently, the sampling interval was increased to 12 h. Turbidity (extinction of light at 700 nm) of supernatants was determined immediately. The remainder of samples was clarified by centrifugation (4200 g for 20 min, Avanti J-20 XP from Beckman-Coulter with JS-4.3 rotor, Krefeld/Germany) and aliquots were conserved at -70 °C. In the first experiment, infectivity ($TCID_{50}$), HA and NA activity as well as protein and DNA concentrations were determined from frozen samples. In the second experiment, determination of infectivity, NA activity and protein concentration was skipped. Experimental data were analyzed by fitting of Gompertz' functions (see 2.1.2). Non-linear regression was conducted in Matlab (The Mathworks, Ismaning/Germany) using the function *lsqnonlin* (optimization toolbox). In order to minimize bias at early times, residuals were weighted by the square-root of measured values (weighted regression with variance ~ regressand).

3.3 Clarification

3.3.1 Normal-Flow Filtration

Crude supernatant from the campaign with serum-free Ex-Cell MDCK medium was routinely clarified by a combination of normal-flow filters. Firstly, pooled supernatant was filtered through a 0.65 µm fibrous polypropylene filter (CFAP96, GE Infrastructure, United States). Afterwards, virus in the filtrate was inactivated chemically by the addition of *β-PL* (see 3.4). After incubation,

supernatant was filtered again through a 0.45 µm polysulphone membrane filter (CMMP94, GE Infrastructure, United States) for the removal of residual fines. Both filtrations were conducted at a differential pressure of 0.5 bar. Batch volumes were between 2 to 4 L. Filter areas of CFAP96 and CMMP94 filter capsules were 743 cm^2 and 748 cm^2, respectively. Use of a single capsule was sufficient at each stage. All work was conducted under sterile conditions in an S2 safety hood. Filters and tubing were autoclaved prior to their use. Sterility controls were prepared from supernatant at each stage. HA activity and turbidity were determined from samples taken before and after filtrations. The DNA and protein concentration were determined before and after membrane filtration only. Clarified supernatant was stored at 4 °C up to four but typically less than two weeks until further processing.

3.3.2 Centrifugation

Clarification efficiency of different centrifugation systems (vessel, rotor and centrifuge) was characterized based on Sigma theory (see 2.2). For small volumes, experiments were conducted in a Biofuge Primo R table-top centrifuge with swing-bucket rotor No. 7500 7592 (both Heraeus Instruments, Osterode/Germany). For larger volumes, an Avanti J-20 XP with swing-bucket rotor JS-4.3 (both Beckman Coulter, Krefeld/Germany) was used. The Biofuge Primo R was operated with 2.2 ml Eppendorf reaction tubes having conical bottom. The Avanti J-20 XP was either operated with 15 ml Falcon centrifuge tubes (conical bottom) or 230 / 240 ml buckets from Beckman Coulter (conical / flat bottom).

Acceleration and deceleration of centrifuge / rotor combinations was characterized prior to experiments. The break was set to level 9 for the Biofuge Primo R. Maximum acceleration and break levels were used for the Avanti J-20 XP centrifuge. Rotational velocities were recorded over time. Acceleration and deceleration of rotor velocities were determined by linear regression analysis. Acceleration and deceleration of the Biofuge Primo R were $2.5 \cdot 10^{-3}$ $rpm^{-1}\,s^{-1}$ and $3.2 \cdot 10^{-3}$ $rpm^{-1}\,s^{-1}$, respectively. Values for the Avanti J-20 XP were $3.0 \cdot 10^{-3}$ $rpm^{-1}\,s^{-1}$ and $3.5 \cdot 10^{-3}$ $rpm^{-1}\,s^{-1}$, respectively. In addition, a delay of 15 s post acceleration before the counter is started was detected for the Avanti J-20 XP centrifuge and considered in calculations. Centrifugal load, considering acceleration and deceleration phases, was calculated according to (2-7). Fractions of overall centrifugation time for acceleration and deceleration phases were calculated

from correlations determined before. Characteristics of centrifugation systems and the experimentally covered range have been summarized in Table 3-9.

In experiments, supernatant pooled from several roller bottles or single microcarrier cultivations was mixed well and distributed into centrifugation vessels. If supernatant had been stored at 4 °C it was let warm up to room temperature first. Filled vessels were inverted several times right before insertion into rotors and spun under various conditions. Centrifugal load was altered by change of the relative centrifugal force (RCF) and centrifugation time. Centrifugation was either conducted at room temperature (Biofuge Primo R) or 23 °C (Avanti J-20 XP). After spinning, vessels were carefully unloaded and supernatant was decanted into fresh vessels for analysis. Clarification efficiency was calculated according to (2-5) with concentrations being determined as the extinction of light at 700 nm (referred to as turbidity). For the determination of product recovery, HA activity was analyzed from samples taken before and after centrifugation. Modified Verhulst's functions (2-8) were fitted to experimental data for the generation of trend lines. Parameters x_c and b were estimated by nonlinear regression analysis. Curve fits were conducted in Microcal Origin (Northampton/United States) using the nonlinear regression tool.

Table 3-9. Characteristics of centrifugation systems and experimentally covered range

Centrifuge / Rotor	Vessel	V^1 / ml	H^2 / mm	r_1^3 / mm	r_2^4 / mm	RCF[5]	Q / Σ^6 / m s^{-1}
Biofuge Primo R / No. 7500 7592	2.2 ml Eppendorf	2	35	52	87	97 / 1191	$5.59 \cdot 10^{-8}$ - $7.12 \cdot 10^{-6}$
Avanti J-20 XP / JS-4.3	15 ml Falcon	10	80	124	204	3000 / 4200	$3.64 \cdot 10^{-8}$ - $6.06 \cdot 10^{-7}$
	230 ml Conical	200	102	102	204	300 / 2000 / 3000 / 4200	$1.57 \cdot 10^{-8}$ - $7.04 \cdot 10^{-6}$
	240 ml Bucket	200	75	129	204	1000 / 4200	$1.11 \cdot 10^{-8}$ - $1.56 \cdot 10^{-6}$

1: liquid volume, 2: liquid height, 3: inner radius, 4: outer radius, 5: relative centrifugal force, 6: centrifugal load

In preparations, supernatant from roller bottles was clarified directly after pooling at the time of harvesting. Pooled supernatant was distributed into 230 ml vessels with conical bottom. Filled vessels were centrifuged at 4200 g for 30 min corresponding to a load of $1.57 \cdot 10^{-8}$ m s^{-1}. After spinning, supernatants were decanted carefully into a fresh vessel. All work was conducted under

sterile conditions under an S2 safety hood (except for centrifugation itself). All vessels were autoclaved prior to their use. Sterility controls were prepared from supernatant before and after the complete procedure. Turbidity and HA activity were determined from samples taken before and after centrifugation. Clarified supernatant was typically inactivated directly after centrifugation (see 3.4) or stored at 4 °C until further processing.

3.4 Inactivation

Clarified supernatant containing infectious virus was inactivated chemically by the addition of *β*-propiolactone (Cat. No. 33672.01, Serva Electrophoresis, Heidelberg/Germany). Firstly, pH was stabilized with HEPES buffer (0.5 M, pH 7.5) added to a final concentration of 25 mM in order to prevent drift upon hydrolysis of *β-PL* and degassing of CO_2. Secondly, *β*-propiolactone was added to a concentration of 3 mM except for the inactivation of A/Wis/67/2005 (H3N2). For this strain the dose was increased to 6 mM due to occasional residual infectivity after inactivation. Based on literature, a dose of 3 mM leads to a reduction in infectivity by about 6 orders of magnitude, a dose of 6 mM corresponds to a reduction by about 15 orders (see 2.3 for details). The vessel containing supernatant was mixed well by swirling and supernatant was transferred to a new vessel after brief incubation (simulated tank transfer). The inactivation reaction was carried out at 37 °C for 24 h. In the campaign with A/PR/8/34 (H1N1) NIBSC propagated in Ex-Cell MDCK medium, supernatant was filtered through a 0.45 polysulfone membrane filter immediately afterwards (see 3.3.1). All parts were autoclaved before their use and work was conducted under an S2 safety hood under sterile conditions. Inactivation was tested in confluent MDCK cultures over two passages (T75 flasks, 1 ml sample in 50 ml culture volume). HA activity was measured at the end of each passage. Only inactivated lots showing HA activity according to the dilution in the first passage and no activity after the second passage were considered successful. Inactivated supernatant was stored at 4 °C up to four but typically less than two weeks until further processing.

3.5 Selective Precipitation of DNA

3.5.1 Development of Operation

For the delineation of optimal precipitation conditions a factorial experimental design was set up and executed. As input variables the pH and ionic strength of supernatant and molecular weight of polyethylenimine (PEI) were considered. A full factorial design with two levels for each variable (Table 4-24) was chosen leading to eight different combinations. In addition, PEI concentration was varied in 8 steps from 0% to 0.45% (w/v) for each combination resulting in a total of 64 different conditions.

Experiments were conducted with supernatant from a single batch produced in roller bottles. Influenza virus A/PR/8/34 (H1N1) RKI was used for infection. V-Medium was selected for the virus propagation phase. Pooled supernatant was clarified by centrifugation (3.3.2) and inactivated chemically with *β-PL* (3.4). A number of stock solutions were prepared and used in all experiments (Table 3-10). Boric acid purchased from Merck (Cat. No. 1.00162.100, Darmstadt/Germany) was dissolved at 0.2 M and titrated to pH 7 or 9 with concentrated NaOH solution. Solutions of branched PEI (2 and 750 kDa, 50% (w/v), Cat. No. 408700 and P3143, Sigma-Aldrich, Steinheim/Germany) were diluted to 5% (w/v) and titrated to pH 7 or 9 with concentrated HCl solution. Moreover, sequential dilutions were prepared from each PEI stock solution covering the concentration range from $5 \cdot 10^{-5}$% to 5% (w/v). Reverse osmosis water was used for the preparation of all solutions. Liquids including supernatant were chilled on ice prior to their use in experiments.

Table 3-10. Overview of stock solutions

Reagent	MW	Conc.	pH
Boric Acid		0.2 M	7 9
NaCl		2 M	-
PEI, branched	750 kDa[1]	5% (w/v)	7 9
	2 kDa[1]	5% (w/v)	7 9

1: average value determined by light scattering (specified by the manufacturer)

Clarified and inactivated supernatant was divided into four equal parts. Boric acid solution at pH 7 or 9 was added to each part to a final concentration of 20 mM. In mixtures requiring high pH, pH was re-adjusted to precisely 9 by titration with 1 M NaOH solution under stirred conditions. In other mixtures, pH was left at the resulting value of 7.5. Secondly, NaCl solution was added to a final concentration of 200 mM in mixtures requiring high ionic strength. The same volume of water was added to remaining mixtures.

7 x 20 ml of conditioned supernatant from each mixture were dispensed into beakers of 50 ml volume (Cat. No. X701.1, Carl Roth AG, Karlsruhe/Germany, 38 mm inner diameter). Beakers were placed inside a tray filled with ice and put on top of a magnetic drive (Variomag Poly 15, Carl Roth AG, Karlsruhe/Germany). Magnetic stir bars were inserted into beakers (Cat. No. 2152.2, Carl Roth AG, Karlsruhe/Germany, 25 mm length, 6 mm diameter) and rotated at 400 rpm throughout the experiment. Once temperature checked in a reference beaker had reached 4 °C, 2 ml of PEI solution at the appropriate concentration were added drop by drop to each beaker ($4.5 \cdot 10^{-6}$ to 0.45% PEI final concentration). In addition, controls were prepared with water added only (referred to as 0% PEI). The general recipe of precipitation mixtures is given in Table 3-11. Beakers were sealed with parafilm to prevent drift of pH and precipitation was carried out over a period of 2 h. Temperature was checked every 30 minutes and remained between 3 to 5 °C. Mixtures were filtered through 0.45 syringe filters immediately afterwards (PES Minisart, Cat. No. 16555K, Sartorius AG, Göttingen/Germany) and filtrates were stored at 4 °C for later analysis. Filtrates were analyzed for NA activity and DNA concentration after the experiment. Besides, the intensity of scattered laser light was measured using a Horiba LB500 dynamic light scattering instrument (Horiba Europe GmbH, Oberursel/Germany).

Table 3-11. Recipe of precipitation mixtures

Reagent	***V* / ml**	**Conc.**
Supernatant	16	
Boric Acid, 0.2 M, pH 7 / 9	2	20 mM
NaCl, 2 M / H_2O	2	200 mM / -
PEI solution, up to 5%	2	$4.5 \cdot 10^{-6}$% to 0.45%

The depletion of DNA D was calculated from concentrations measured before ($c_{DNA,0}$) and after precipitation (c_{DNA}). Its dependency on PEI concentration was characterized by fitting of Hill's functions

$$D(c)=\frac{K}{1+(c/c_{50})^{p}}, \quad \text{with } D\equiv\left(1-\frac{c_{DNA}}{c_{DNA,0}}\right) \tag{3-24}$$

to calculated values. Curve fits were executed in Microcal Origin (Northampton/United States) using the nonlinear regression tool. In (3-24) the concentration of PEI is denoted by c. The maximum depletion of DNA is represented by K. The parameter c_{50} can be interpreted as the effective concentration at which precipitation occurs and was used in factorial analysis. Concerning NA activity and light scattering data, values measured for PEI concentrations of 0.045% were used in analysis. All values were normalized to their respective controls (i.e. 0% PEI). Factorial analysis was conducted with the software JMPin (Version 4.0.3, SAS Institute, http://www.jmp.com, Unites States) using a step-wise regression procedure. Polynomial models including all single input variables and their two- and three-variable interactions were considered. The probability threshold for inclusion of variables or interactions was set to $\alpha = 0.1$.

3.5.2 Preparative Precipitation

Firstly, supernatant was conditioned by the addition of sodium borate and sodium chloride solution (Table 3-12). No more than 1 L of supernatant was processed at a time. Larger batches were split and reunited after processing. All components were added while stirring with a magnetic stir bar (10 mm diameter, 60 mm length) at 400 rpm. The mixture was allowed to cool down to 4 °C in a cold room. As soon as the final temperature had been reached, pH was adjusted to 9.0 by titration with 1 M NaOH solution. Finally, PEI stock solution (2 kDa molecular weight) was added to the mixture to a final concentration of 0.045% (w/v). After 30 minutes of incubation at 4 °C, separation of precipitate was started. The first batch processed was filtered directly through PES membrane filters with 0.45 µm pores (MMP94-B, Cat. No. S04WP04700, GE Osmonic, Unites States) protected by polypropylene pre-filters (MMP92-B, Cat. No. FAPB004700, GE Osmonic, United States). Later on, supernatant was centrifuged first under conditions previously developed for the separation of cell debris (230 ml conicals, Avanti J-20 XP centrifuge with JS-4.3 rotor, 4200 g for 30 min, see 3.3.2). However, centrifugation was

conducted at 4° C in a pre-chilled centrifuge. Afterwards, supernatant was decanted and clarified by additional filtration through 0.45 µm PES membrane filters (Cat.No. 15406-47-K, Sartorius, Göttingen/Germany). In both cases, filters were packed into re-usable polypropylene filter holders (PP47, Cat. No. 501 200, Advantec MFS, Dublin/Unites States). Supernatant was pumped through filters by a peristaltic pump (Reglo Analog, Cat. No. ISM 829, Ismatec, Wertheim-Mondfeld/Germany) at a rate of approximately 3.5 L h^{-1} (average flow rate). Filters had to be exchanged about every 400 ml of filtrate volume. Samples were taken before and after precipitation. All samples were analyzed for DNA concentration, HA and NA activity. HA and NA activity were corrected for the activity found in permeates after TFUF (see 4.4.3).

Table 3-12. Preparative precipitation mix

		Stock	Final
Reagent	**pH**	**Conc.**	**Conc.**
Supernatant	~7.5	1x	0.8x
Sodium Borate	11.7	0.2 M	0.02 M
NaCl	-	2 M	0.2 M
PEI, 2 kDa	9.0	5% (w/v)	0.045% (w/v)

Note: pH was adjusted to 9 with 0.1 M NaOH after mixing of all components.

3.6 Tangential-Flow Filtration

TFUF of virus-containing supernatant was conducted with various poylsulfone hollow-fiber modules (all purchased from GE Healthcare Biosciences, Munich/Germany; see Table 3-13). Small modules with only two fibers (38 cm^2 filter area) were used in scouting experiments. Two larger modules with 225 cm^2 and 420 cm^2 filter area were used in preparative filtration runs. Of these, the larger module had shorter fibers of only 30 cm length (compared to 60 cm in all other cases).

All experiments were conducted with clarified and inactivated supernatant produced in roller bottles. Scouting experiments for the selection of hollow-fiber cut-off, determination of critical flux by the TMP method and a number of preparative concentrations were conducted with supernatant containing A/PR/8/34 (H1N1) NIBSC. In this case, the virus was propagated in Ex-

Table 3-13. Specification of hollow-fiber modules

Type	Cut-Off	# Fibers[1]	Fiber ID[2]	Fiber L[3]	Area
			mm	cm	cm^2
UFP-750-E-4MA	750 kDa	45	0.97[4]	30	420
UFP-750-E-3X2MA	750 kDa	12	0.97	60	225
UFP-750-E-H22LA	750 kDa	2	0.97	60	38
CFP-1-E-H22LA	0.1 µm	2	0.97	60	38
CFP-4-E-H22LA	0.45 µm	2	0.97	60	38

1: number of fibers, 2: fiber inner diameter, 3: length of fibers, 4: personal communication of the manufacturer

Cell MDCK medium. Supernatant was clarified by normal-flow filtration (3.3.1) and inactivation chemically (3.4) prior to filtration. Critical flux determination based on the mass balance method and concentrations followed by DF were either conducted with A/PR/8/34 (H1N1) RKI or A/Wis/67/2005 (H3N2). Both strains were propagated in V-Medium. Supernatant was clarified by centrifugation (3.3.2), inactivated chemically (3.4) and DNA was precipitated prior to experiments (3.5.1).

New modules were rinsed with water or PBS in order to remove glycerol according to manufacturer's instructions. PBS was used for equilibration of membranes prior to filtration and for rinsing afterwards. Membranes were regenerated by extended incubation in 0.5 M or 1 M NaOH up to one day. Filter resistance was checked routinely before and after filtration using PBS as test fluid. Filter resistance was determined in dead-end mode by closing the retentate outlet and forcing water completely through the membrane. Modules were either stored in 20% ethanol at 4 °C or 0.1 M NaOH at room temperature.

Standard filtration set-ups with flux control were used for the concentration and DF of influenza virus. In the small-scale setup, designed for modules of 38 cm^2 membrane area, the retentate and permeate were circulated by peristaltic pumps of type Reglo Analog (Cat. No. ISM 829, Ismatec, Wertheim-Mondfeld/Germany). Calibration of pumps was executed in-system, i.e. with the module and tubing in place. Pressures at the retentate inlet and permeate outlet were measured with disposable Medex Transtar pressure transducers (model MX950, Smiths Medical, Kirchseeon/Germany). Silicone tubing with 2 mm inner diameter was used for the connection of all parts. Hold-up of the retentate circuit was determined as 5.5 ml in a dilution experiment using acetone as tracer. Firstly, the retentate circuit was flushed with water end emptied again.

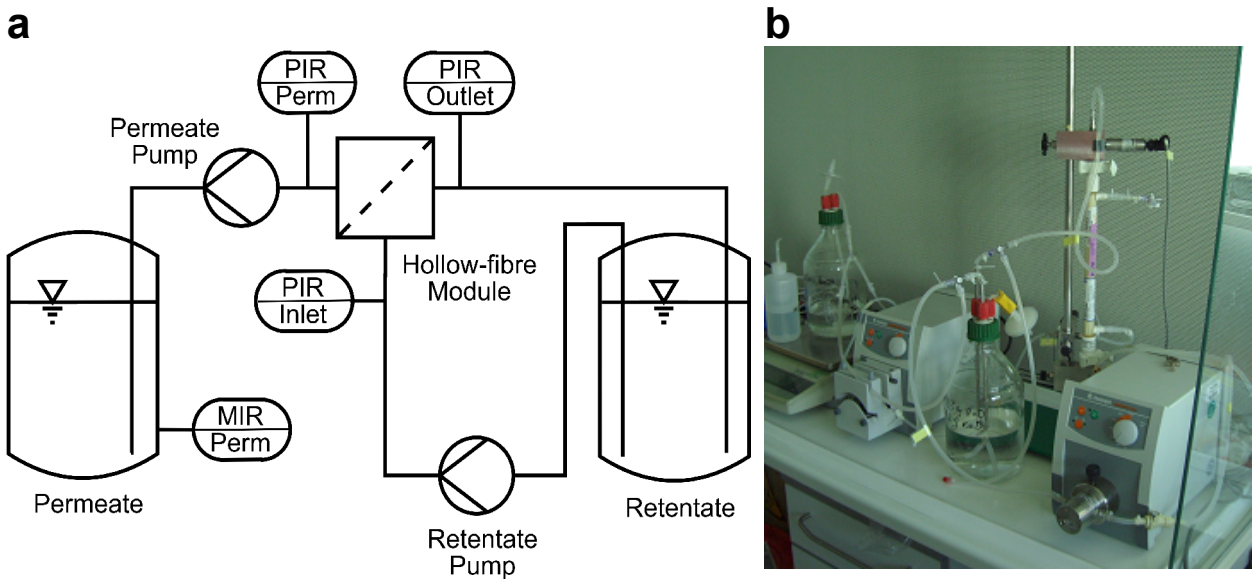

Figure 3-11. Tangential-flow filtration set-up with flux control
Flow-chart of the filtration set-up (a). The retentate was circulated by a gear pump, permeate flux was controlled by a peristaltic pump. Pressure was measured with gauges at the module inlets and outlets. Permeate mass was determined online by a balance. Data was recorded and pumps were controlled by a custom-made Labview software application. Picture of the filtration setup (b). PIR: pressure indication and recording, MIR: mass indication and recording

Secondly, a defined volume of 1% acetone solution was circulated for several minutes. Thirdly, a sample was drawn and absorbance at 280 nm was compared to the initial absorbance of the 1% acetone solution. Validity of the Beer-Lambert law up to 1% acetone had been verified before. Finally, hold-up volume was calculated based on the dilution of the tracer.

In the large-scale setup, designed for modules having 225 and 420 cm^2 membrane area (Figure 3-11), retentate was circulated by a gear pump (drive 5130 with ZP1 pump head, Schwabach/Germany). Permeate flux was controlled by a peristaltic pump (drive 5101 with SP Quick D pump head, Heidolph Instruments, Schwabach/Germany). Pressure was acquired at the retentate inlet, outlet and on the permeate side with pressure gauges (model CTE9000, SensorTechnics, Germany). Both pumps were calibrated considering their dependency on backpressure. Online pressure data was used for the correction of set points. A balance (model CP4202S, Sartorius, Göttingen/Germany) was used for measurement of total permeate mass. The precise permeate flow rate was calculated from the derivative of permeate mass assuming a fluid density of 1000 kg m^{-3}. All parts were connected with silicone tubing of 4 mm inner diameter.

Gauge data and the balance reading were recorded by a custom-made Labview 7 application (National Instruments, Munich/Germany). Hold-up of the retentate circuit was determined as 60 ml in a dilution experiment using acetone as tracer.

For constant-volume DF, a second hose was clamped into permeate pumps in reverse direction for refilling of retentate reservoirs. Small differences in the permeate and buffer flow rates due to differences in backpressure were compensated manually several times during filtration.

Initial retentate volumes prior to concentration were in the range from 30 to 100 ml when using small modules and 1 to 4 L when using large modules. The long module having 225 cm^2 membrane area was used in preparative concentrations of virus grown in Ex-Cell MDCK medium. The short module having 420 cm^2 membrane area was used for the concentration and DF of virus grown in V-Medium. A single module of each type was used in preparations. If not otherwise stated, the long module was operated at a wall shear rate of 9500 s^{-1} with permeate flux set to 28 L m^{-2} h^{-1}. The short module was operated at a wall shear rate of 3800 s^{-1} and a permeate flux of 19 L m^{-2} h^{-1}. Operating conditions were maintained during DF except for one run with A/Wis/67/2005 (H3N2) were a lower flux of only 12 L m^{-2} h^{-1} was used.

Volume concentration factors of preparative runs were approximately 20-fold for virus in Ex-Cell MDCK medium and 5-fold for virus in V-Medium. Concentrates were diafiltered at constant volume in two steps. In filtrations with A/Wis/67/2005 (H3N2), primary DF was run against four volumes of 0.20 mM Tris-Cl buffer at pH 8.7 containing 0.6 M NaCl. Secondary DF was run against four volumes of 20 mM or 15 mM Tris-Cl buffer at pH 8.7 ($N = 1$) or 7.7 ($N = 3$) containing 0.2 M ($N = 1$) or 0.15 M NaCl ($N = 2$). In one run, the high salt concentration of 0.6 M NaCl was also used during secondary DF. For DF of A/PR/8/34 (H1N1) RKI, 20 mM Hepes buffer at pH 7.3 was used instead of Tris-Cl buffer supplemented with 0.6 M NaCl for primary and 0.15 M NaCl for secondary DF. A wash fraction was collected always after the last filtration step. This was done by flushing the retentate circuit with 100 to 200 ml of PBS. Virus and impurities detected in the wash fraction were added to respective retentate fractions in material balances.

3.7 Chromatography

3.7.1 Size-Exclusion Chromatography

An ÄKTA explorer 100 chromatography system was used for SEC. Chromatography media (Sepharose CL-2B, Sepharose 4 FF and Sepharose 6 FF and Superdex 200 p.g.) were packed into XK 16/40 or Tricorn 10/30 columns (all from GE Healthcare, Uppsala/Sweden). Void volumes were determined with BSA-coated latex beads of 100 nm diameter (Postnova, Landsberg/Germany) or estimated from the virus-containing peak. The packed bed of each column was tested regularly by determination of the asymmetry and HETP with acetone (2% v/v dissolved in eluent). Columns were sanitized with 0.5 M sodium hydroxide for at least one hour before and after experiments. Columns were stored in 20% (v/v) ethanol at room temperature. Specifications of columns have been summarized in Table 3-14. SEC scouting experiments were conducted with columns one to five. Column five was used exclusively in experiments belonging to experimental set A and B used in the modeling study. Column six was used in preparations.

All experiments were conducted with influenza virus A/PR/8/34 (H1N1) NIBSC propagated in roller bottles using Ex-Cell MDCK medium. Chromatography was fed with 20-fold concentrates prepared by TFUF (3.6). Frozen concentrates stored at -70 °C were used in scouting experiments (including set A and B). Concentrates used in preparations were always processed immediately.

Table 3-14. Specifications of chromatography columns

#	Medium	Exclusion Limit[a]	H[b] cm	V_{col}[c] ml	ε[d]	HETP[e] µm	Asym.[f]
1	Sepharose CL-2B	30 nm	31.5	63.3	0.38	208	1.09
2	Sepharose 4 FF	30 MDa	23	46.2	0.36	405	1.16
3	Sepharose 6 FF	4 MDa	25	50.3	0.34	256	1.08
4	Supderdex 200 p.g.	500 kDa	23	46.2	0.41	103	1.88
5	Sepharose 4 FF	30 MDa	30	23.6	0.36	271	1.07
6	Sepharose 4 FF	30 MDa	31	62.3	0.35	193	1.05
7	Sepharose Q FF	-	15.7	3.1	-	760	1.22
8	Sepharose Q XL	-	15.7	3.1	-	956	1.04

a: hydrodynamic diameter or molecular weight of globular protein excluded from the medium; b: bed height, c: volume and d: porosity of column packing; e: height of one theoretical plate and f: asymmetry of the elution peak for acetone.

Most runs were conducted at a constant mobile phase velocity of 60 cm h^{-1} with 20 mM phosphate buffer (pH 7.3) as eluent containing up to 0.65 M NaCl[6]. Only in runs belonging to set B mobile phase velocity was varied to 30 or 120 cm h^{-1}. In these runs, 20 mM HEPES buffer, pH 7.3 supplemented with 200 mM NaCl was used as eluent. In runs belonging to experimental set B, sample was injected using a 1.5-ml capillary loop (partial injection). In all other runs, feed material was injected using a 50 or 150 ml superloop (GE Healthcare Bio-Sciences, Sweden). In preparations, complete batches were processed automatically by multiple injection-elution cycles. Injection profiles for the modeling study were acquired by injection of acetone (1% v/v in eluent) at the same volume and mobile phase velocity as in runs with virus sample. Elution of solutes was monitored online at a wavelength of 280 nm and in some cases by a static light scattering detector (Dawn EOS, Wyatt, Dernbach, Germany).

Eluates were either fractionated by a Frac-950 fraction collector (GE Healthcare, Uppsala/Sweden) or using the outlet valve of the chromatography system (preparative runs). Collected fractions were analyzed for HA activity, total protein and in some cases DNA concentration. The fraction collector and UV detector were aligned by injection of a phenol red solution (~5 mg ml^{-1}) through a bypass capillary. Collected fractions (0.2 ml per fraction into analytical microtiter plates) were scanned with a plate photometer (Rainbow Spectra, Tecan Instruments, Crailsheim/Germany) and compared to the online signal. The delay volume was chosen to minimize mismatch between profiles. Delay between the UV and light scattering detectors was determined by matching the first peak in the UV trace with the single peak detected by light scattering.

Presentation of signals over K_{av} (see eq. 2-17 in 2.6.1) instead of elution volume or retention time was preferred in scouting experiments for better comparability between chromatography media. Elution volume normalized by column volume was used in the modeling study. In general, area normalized concentrations (i.e. density distributions) instead of absolute concentrations are reported for HA activity, DNA and total protein concentrations. In the modeling study, online signals (UV absorbance and light scattering) were equally normalized to represent true density distributions. Both signals were re-sampled to a uniform grid by linear interpolation (200 data points per column volume). Offline data (HA activity and total protein) were re-sampled to the same grid by the following procedure: data were first summed up and normalized to represent true

6 0.2 M NaCl in media screen, 0.65 M in other experiments

cumulative distributions. Cumulative distributions were then interpolated using weighted splines (Matlab Spline Toolbox, The Mathworks, Aachen, Germany) and differentiated to yield density distributions. Distributions of host-cell protein were reconstructed by subtracting re-scaled distributions of HA activity from distributions of total protein. The scaling factor was determined under the assumption of pure virus in early fractions (set A: 0.34–0.42 cv; set B: 0.33–0.38 cv elution volume).

Impulse-responses for all types of signals were estimated by MaxEnt deconvolution (2.6.2) of normalized chromatograms using experimentally determined injection profiles. Chromatograms were simulated by convolution of approximated impulse-responses with experimentally determined injection profiles (set A) or rectangular pulses of variable length (set B) . Limits of the product fraction were determined from cumulative distributions of HA activity based on 0.01 and 0.91 quantiles. Windows of elution were determined from cumulative distributions of the UV signal (10^{-3} and 0.999 quantiles). A safety margin of 0.2 cv was added for calculation of the total run length. The final concentration of product, content of host-cell protein and volumetric productivity were predicted as functions of injection volume and flow velocity. Concerning productivity, a second mode of operation was considered. In this mode, flow velocity was increased to 250 cm h^{-1} after elution of product in order to wash out impurities as fast as possible (Figure 4-30). Deconvolution of chromatograms and simulations were conducted in Matlab (The Mathworks, Aachen/Germany). Further details are given in the article by Kalbfuss, Flockerzi. et al. [2008]. Matlab script files used in numerical calculations can be downloaded from http://www.mpi-magdeburg.mpg.de/research/groups/bpt/sec-modeling.

3.7.2 Ion-Exchange Chromatography

3.7.2.1 Virus Stability

Stability of HA activity was investigated by titrating inactivated supernatant to different pH using 1 M NaOH or HCl while stirring in a beaker (pH was measured with an electrode and recorded for each reaction). Titrated supernatants were incubated for 2.5, 4.5, or 23 h at room temperature and neutralized immediately afterwards. Neutralized supernatants were analyzed for HA activity. Testing the stability with respect to salt, 200 ml of phosphate buffer (10 mM, pH 7.3) containing different concentrations of NaCl were mixed with 100 ml of SEC-purified virus (150 mM NaCl,

pH 7.3) in microtiter plates. Plates were incubated for 2 h at room temperature. After incubation, 100 ml of each reaction were transferred into a sample tube and diluted 1:10 in appropriate phosphate buffer to reduce the concentration of NaCl to 150 mM. Diluted reactions were analyzed for HA activity.

3.7.2.2 Flowthrough Anion-Exchange Chromatography

An ÄKTA explorer 100 chromatography system was used for flowthrough AIEC (GE Healthcare, Uppsala/Sweden). First experiments with ion-exchangers were conducted with HiTrap screening columns. For preparative columns, AIEC media were packed into Tricorn 10/15 column housings (all from GE Healthcare, Uppsala/Sweden). The packed bed of each column was tested regularly by determination of the asymmetry and HETP with acetone (2% v/v dissolved in eluent). Columns were sanitized with 0.5 M sodium hydroxide for at least one hour before and after experiments. Columns were stored in 20% (v/v) ethanol at room temperature. Specifications of columns have been summarized in Table 3-14.

All experiments were conducted with influenza virus A/PR/8/34 (H1N1) NIBSC propagated in roller bottles using Ex-Cell MDCK medium. Chromatography was fed with SEC-purified virus conditioned to high ionic strength (3.7.1). The first two runs (batches No. 1 and 2) were conducted with frozen material stored at -70 °C. Subsequent preparations were conducted immediately after SEC.

All AIEC runs were operated at a constant flow rate of 200 cm h^{-1}. The same eluent as for SEC was used to equilibrate columns and wash out unbound feed material. Adsorbed DNA and other impurities were desorbed by a salt gradient up to 1.5 M NaCl. Columns were regenerated and sanitized afterwards by a mixture of 0.1 M HCl and 2 M NaCl followed by a mixture of 1 M NaCl and 1 M NaOH (5 cv / 23 min contact time and 7 cv / 32 min contact time, respectively). Elution of solutes was monitored online at a wavelength of 280 nm. In addition, gradients were traced by acquisition of conductivity. Eluates were fractionated into 96-fold deep well microtiter plates (Cat. No. 391-5705, VWR, Darmstadt/Germany) using a Frac-950 fraction collector (GE Healthcare, Uppsala/Sweden). The fraction collector and UV detector were aligned as described above (3.7.1). Collected fractions were analyzed for HA activity and DNA concentration. For measurement of DNA concentration, ionic strength of samples collected during gradient elution

had to be reduced by dilution to a known NaCl concentration. The initial concentration of NaCl in collected fractions was calculated from conductivity. Standard solutions for calibration of the assay were prepared accordingly. Pooled product fractions were additionally analyzed for total protein concentration.

Batch adsorption was conducted in 96-fold deep well microtiter plates (Cat. No. 391-5705, VWR, Darmstadt/Germany). Unused Sepharose Q XL resin (GE Healthcare, Uppsala/Sweden) was rinsed with water three times and adjusted to an approximate volume fraction of 62.5% in a graduated cylinder. 80 µl of resin slurry (approximately 50 ml of packed volume) were mixed with 120 ml of phosphate buffer (10 mM, pH 7.3) containing different concentrations of NaCl. In the next step, 100 ml of SEC-purified virus, dissolved in 150 mM NaCl, 20 mM phosphate buffer, pH 7.3, were added to each well resulting in a final volume of 300 ml. Plates were incubated in a Thermomixer Comfort (Eppendorf, Wesseling-Berzdorf/Germany) for 2 h at room temperature shaking with 1 000 rpm. After incubation, 100 ml of each reaction were transferred into a sample tube and diluted 1:10 in appropriate phosphate buffer to reduce the concentration of NaCl to 150 mM. Diluted samples were analyzed for HA activity and DNA concentration.

3.7.2.3 Scouting with Membrane Adsorbers

Four membrane adsorbers were tested for their ability to bind influenza virus. All membranes were bought as 96-well microtiter plate inserts. Quaternary ammonia (Q) and sulphonyl (S) ion-exchangers but also IDA metal affinity membranes were purchased from Sartorius (Göttingen/Germany). Glass fiber prefilters (AcroPrep) were purchased from Pall (Dreieich/Germany). Specifications of membrane devices are given in Table 3-15.

Table 3-15. Overview of membrane adsorbers used in screening experiments

		Q	S	GF	IDA
Cat. No.		VW96IQ02	VW96IS02	5051	VW96MC02
Manufacturer		Sartorius	Sartorius	Pall	Sartorius
Membrane Area	cm²	0.57	0.57	0.25	0.57
Bed Volume	µL	18.2	18.2	n.a.	n.a.
Pore Size	µm	3 - 5	3 - 5	1	> 3
Max. Volume	µL	800	800	1000	300

Q: quaternary ammonia, S: sulphonyl, GF: glass fiber, IDA: iminodiacetic acid

Influenza virus A/PR/8/34 (H1N1) RKI propagated in a stirred-tank microcarrier fermentation with V-Medium was used in experiments. One part of the experiments were conducted with clarified and inactivated supernatant. The other part was conducted with a diafiltrate of the same supernatant, which was produced by TFUF and DF against 20 mM Hepes buffer at pH 7.3 and 50 mM NaCl. For experiments with ion-exchangers, part of the diafiltrate was further adjusted to pH 9.0 by titration with 1 M NaOH solution.

Firstly, membranes were primed and equilibrated. The IDA membrane was further loaded with Ca^{2+} ions after priming by application of 2 x 0.2 ml of a 0.2 M $CaCl_2$ solution and was primed again. Virus-containing sample was loaded afterwards. Unbound material was removed by rinsing with equilibration buffer. Finally, bound virus was eluted under appropriate conditions. Applied buffers and volumes are specified in Table 3-16. All steps were conducted at room temperature. Liquid was spun through membranes by centrifugation in an Avanti J-20 XP centrifuge with JS-4.3 rotor (Beckman Coulter, Krefeld/Germany) either at 500 g in the case of IDA membranes or 1000 g in all other cases. Flowthroughs and eluates were collected individually and analyzed for HA activity. Each cavity was used only once.

Table 3-16. Buffers and applied volumes

Membrane		Priming	Equilibration	Wash	Load	Elution
Q	**Solution**	1 M NaaCl + 1 M NaOH	20 mM PB, pH 7.3		Supernatant / Diafiltrate	20 mM PB, pH 7.3 + 1.5 M NaCl
	V / ml	0.8	3 × 0.8	0.8	2 × 0.8	0.8
S	**Solution**	1 M NaCl + 1 M NaOH	20 mM Hepes, pH 7.3		Supernatant / Diafiltrate	20 mM Hepes, pH 7.3 + 1.5 M NaCl
	V / ml	0.8	3 × 0.8	0.8	2 × 0.8	0.8
GF	**Solution**	H_2O	20 mM Tris, pH 7.3		Diafiltrate	20 mM Tris, pH 8.6 + 2 M Urea
	V / ml	2 × 0.8	3 × 0.8	0.8	2 × 0.8	0.8
IDA-Ca^{2+}	**Solution**	1 M NaCl + 1 M NaOH	20 mM Hepes, pH 7.5 + 50 mM NaCl		Supernatant / Diafiltrate	20 mM Hepes, pH 7.3 + 50 mM NaCl + 0.5 M EDTA
	V / ml	2 × 0.2[a]	2 × 0.2	0.3	0.3	0.3

a: IDA membranes were loaded with Ca^{2+} ions after priming and were primed again.

3.7.2.4 Capture with Anion-Exchange Membrane Adsorbers

Scouting and preparative runs were conducted with Sartobind Q and D MA75 membrane adsorbers (Sartorius AG, Germany, Cat. No. Q75X and D75X). Specifications provided by the manufacturer are given in Table 3-17. Adsorbers were operated on an Äkta Explorer 100 chromatography system (GE Healthcare, Uppsala/Sweden) equipped with a Frac-950 fraction collector. A constant flow rate of 22 ml min^{-1}, corresponding to 264 cm h^{-1} or approximately 10 bed volumes per minute, was used in all experiments. The outlet stream was split by a T-valve and a minor fraction (approximately 1 to 2 ml min^{-1}) was directed through a Dawn EOS static light scattering detector (Wyatt, Santa Barbara/United States). Light scattering signals were recorded using the software Astra (Wyatt) and later imported into the software Unicorn (GE Healthcare).

The "BufferPrep" function[7] of the chromatography system was used to mix eluents in scouting experiments. Sodium chloride was used as displacer. A mixture of phosphate, formate and acetate, titrated with hydrochloric acid, was used as buffer. Adsorbers were equilibrated with low-salt buffer (50 mM NaCl, pH 7.0) before virus was loaded. Up to 300 ml of supernatant were injected for capacity estimations. 100 ml were injected in other scouting experiments. Adsorbed virus was either displaced by a linear salt gradient up to 1.5 M NaCl[8], by a multi-step salt gradient (0.3, 0.6, 0.9, 1.2 and 1.5 M) or multi-step pH gradient (5.7, 5.2, 4.7 and 4.2). In one experiment, a multi-step salt gradient was combined with a single pH step from 7.0 to 5.0. Adsorbers were cleaned with at least 50 ml of 0.5 M NaOH between runs (22 ml min^{-1}, reverse flow). The dynamic capacity for bovine serum albumin (Sigma-Aldrich, United Kingdom, Cat. No. A3912-100G; 1 mg/ml in 50 mM NaCl, 20 mM phosphate buffer, pH 7.3) was tested every third to fifth injection. Filters were rinsed with 20% ethanol prior to storage at room temperature.

Preparative capture runs were conducted exclusively with Sartobind Q MA75 adsorbers. A load until 10% breakthrough of scattered laser light was targeted. Between 7 and 15% breakthrough were achieved in all runs. Low salt-buffer (50 mM NaCl , 20 mM HEPES, pH 7.3) was used for equilibration and washing steps. High-salt buffer (1.5 M NaCl, 20 mM HEPES, pH 7.3) was used to elute the virus in a single step. Elution was followed by a two-phase regeneration step applying acidic (2 M NaCl, 0.1 M HCl) and alkaline (1 M NaCl, 1 M NaOH) cleaning solutions.

7 inline mixing from four stock solutions

8 only capacity estimations

Flowthroughs and eluates of chromatography runs were collected into 50 ml centrifuge tubes (VWR, Germany, Cat. No. 525-0159) or deep-well microtiter plates (VWR, Germany, Cat. No. 391-5705). Samples of the feed and collected fractions[9] were analyzed for HA activity. Samples from preparative capture runs with batches No. 5 and 6 were additionally analyzed for DNA and total protein content.

The influence of pH on the capacity of Sartobind Q membranes and virus recovery was investigated in Vivawell-96 Q-IEX spin plates (Sartorius AG, Germany, Cat. No. VW96IQ02). Specifications provided by the manufacturer are given in Table 3-17. Spin plates were operated in an Avanti J-20 XP centrifuge equipped with a JS-4.3 rotor (Beckman Coulter, Krefeld/Germany). All centrifugation steps were conducted at room temperature with 1000 g for 2 minutes. Wells were rinsed with 800 µl of cleaning solution (1 M NaCl, 1 M NaOH) and 3 x 800 µl equilibration buffer (50 mM NaCl, 20 mM phosphate buffer, pH 7.3) prior to their use. Aliquots of cell culture supernatant were titrated to various pH using 1 M NaOH or HCl solution and 800 µl of each aliquot were loaded onto wells. Unbound material was washed out with 800 µl of equilibration buffer and adsorbed virus was eluted in 800 µl of elution buffer (1.5 M NaCl, 20 mM phosphate buffer, pH 7.3). The flowthrough, wash and eluate fractions were collected and analyzed for HA activity in addition to samples from loaded aliquots.

Table 3-17. Specifications of Sartobind anion-exchangers.

		MA75 D	MA75 Q	Vivawell Q
Cross-sect. Area	cm^2	5	5	0.57
No. Layers	-	15	15	1
Total Area	cm^2	75	75	0.57
Bed Volume	ml	2.1	2.1	0.018
Pore Size	µm	> 3	> 3	3 – 5
Dyn. BSA Capacity	mg cm^{-2}	0.8	0.6	n.a.
Charge Density	µmol cm^{-2}	3 – 4	5 – 6	3 – 4

3.7.2.5 Polishing with Packed-Beds and Monoliths

Adsorptive AIEC of influenza virus with packed-beds and a monolithic column was applied for final polishing of virions. Packed-bed chromatography was conducted with Source Q and

9 pooled according to experimental requirements

Source S high-performance media packed into 1 ml housings (Resource Q / S, Cat. No. 17-1177-01 / 17-1180-01, GE Healthcare, Uppsala/Sweden). The monolithic CIM QA disc was purchased from BIA separations (Klagenfurt/Austria, Cat. No. 210.5113). Specifications of columns are given in Table 3-18. Columns were operated on an Äkta Basic 100 chromatography system equipped with a Frac-950 fraction collector. Elution of virus and impurities was monitored online by measurement of UV extinction at 280 nm. The feed material (i.e. virus-containing diafiltrate) was injected using a 50 ml superloop (all GE Healthcare, Uppsala/Sweden).

Table 3-18. Specifications of Source media and CIM QA.

		Source Q	Source S	CIM QA
Ligand		quaterarya mmonia	methyl sulphonate	quaternary ammonia
Dimensions (D x H)	mm x mm	6.4 x 30	6.4 x 30	12 x 3
Cross-sect. Area	cm^2	0.32	0.32	1.13
Bed Volume	ml	1	1	0.34
Bead Size	µm	15	15	-
Pore Size	nm	20 – 1000	20 – 1000	n.a.
Specific Surface	$cm^2\ g^{-1}$	70	70	n.a.
Dyn. BSA Capacity	$mg\ ml^{-2}$	45	45	≥ 21
Charge Density	$mmol\ g^{-1}$	n.a.	n.a.	2.0 ± 0.2

Experiments were conducted with a single batch of influenza virus A/PR/8/34 (H1N1) RKI propagated in roller bottles using V-medium. Supernatant was clarified by centrifugation (3.3.2) and DNA precipitated with PEI (3.5.2). Columns were loaded with approximately 5-fold concentrated virus, which had been diafiltered against four volumes of high-salt buffer followed by four volumes of low-salt buffer (20 mM Hepes buffer, pH 7.3 containing 150 mM of NaCl). The large-scale setup equipped with the shorter module was used for tangential-flow filtration (3.6).

Source columns were operated at a constant flow rate of 940 cm h^{-1} (5 ml min^{-1}). Flow rates used for the CIM QA disc varied between 133 (2.5 ml min^{-1}) and 540 cm h^{-1} (10 ml min^{-1}). However, a common flow rate of 265 cm h^{-1} (5 ml min^{-1}) was used during washing and elution. Five column volumes of 50 mM Tris-Cl, pH 7.3 containing 150 mM NaCl were used for equilibration and

washing after loading. Bound virus was eluted by linear salt gradients from 0.15 M to 1.5 M NaCl at a constant pH of 7.3. The length of gradients was varied between 10 to 40 cv.

4 Results

4.1 Virus Cultivation

4.1.1 Course of Infection

Concerning the purification of biological products, it is always desirable to enter the downstream process from a favorable starting point, i.e. high product concentration at low specific impurity. Moreover, productivity has to be maximized, which means that virus propagation should be aborted as early as possible. Early abortion further minimizes the risk of product degradation over the course of cultivation. For these reasons, two experiments were conducted for recording the course of infections in roller bottles under various conditions [Knöchlein, 2007; Eisold, 2008]. In these experiments, infection was carried out over a prolonged period of up to 115 h and supernatant was sampled in tight intervals. In addition to measures of viral concentration or activity (HA and NA activity, $TCID_{50}$), turbidity, protein and DNA concentration were acquired as measures for the content of impurities. Experimental details have been summarized in section 3.2.

Except for infectivity as determined by $TCID_{50}$ assay, all variables revealed a sigmoid profile with varying loci of inflection points and steepnesses (see Figure 4-12 for an example). The shape of profiles of HA and NA activity in the first experiment (all m.o.i.'s) were almost identical. The release of impurities, reflected by the concentrations of protein and DNA, in contrast, lagged behind the release of virus by several hours. The profile of turbidity typically took an intermediate position between profiles of variables reflecting the virus and impurities (not shown).

Since experimental data severely suffered from random error, empirical growth functions (see 2.1.2) were fitted to measured values in order to facilitate analysis. Among the considered sigmoid functions, Gompertz' function (2-1) resulted in the best fit of measured data. In particular at early times, a better representation of data was achieved than, for example, with Verhulst's function. Regarding turbidity, protein and DNA concentration, an offset $x_{-\infty}$ was admitted since initial values were different from zero and could not be neglected. This offset was restricted to positive values.

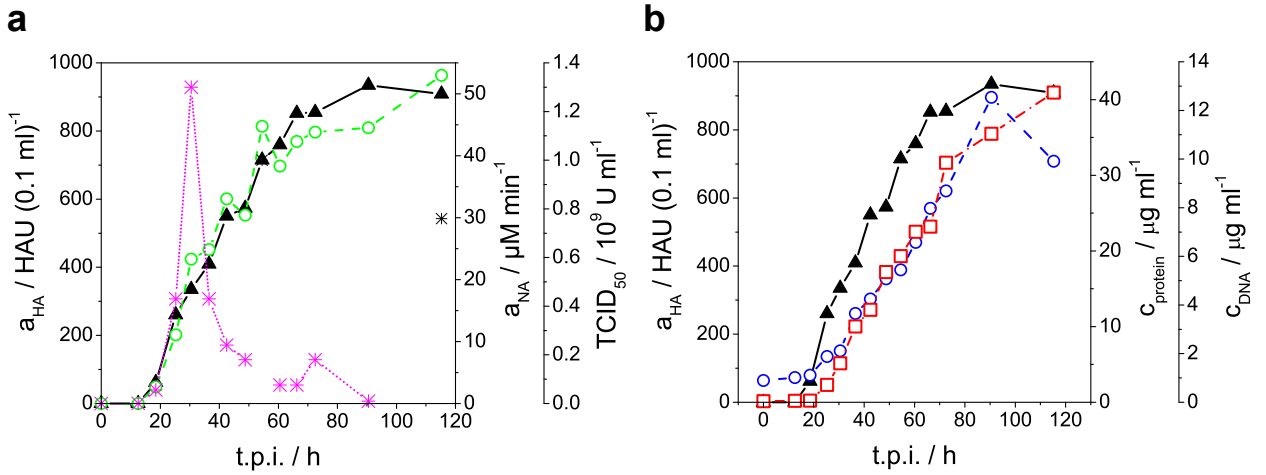

Figure 4-12. Propagation of influenza virus A/PR/8/34 (H1N1) RKI in mammalian cell culture.

Confluent roller bottle cultures of MDCK cells were infected at an m.o.i. of 0.025 and virus propagation was carried out for five days. Samples from supernatant were analyzed for HA activity (▲), NA activity (○) and infectious activity (✳) determined by $TCID_{50}$ (a). Assumed outliers at 55 h and 115 h were excluded from the profile of infectious activity. Release of total protein (○) and host-cell DNA (□) compared to HA activity (▲) (b). Average values from two runs in parallel are presented except for infectious activity. t.p.i.: time post infection

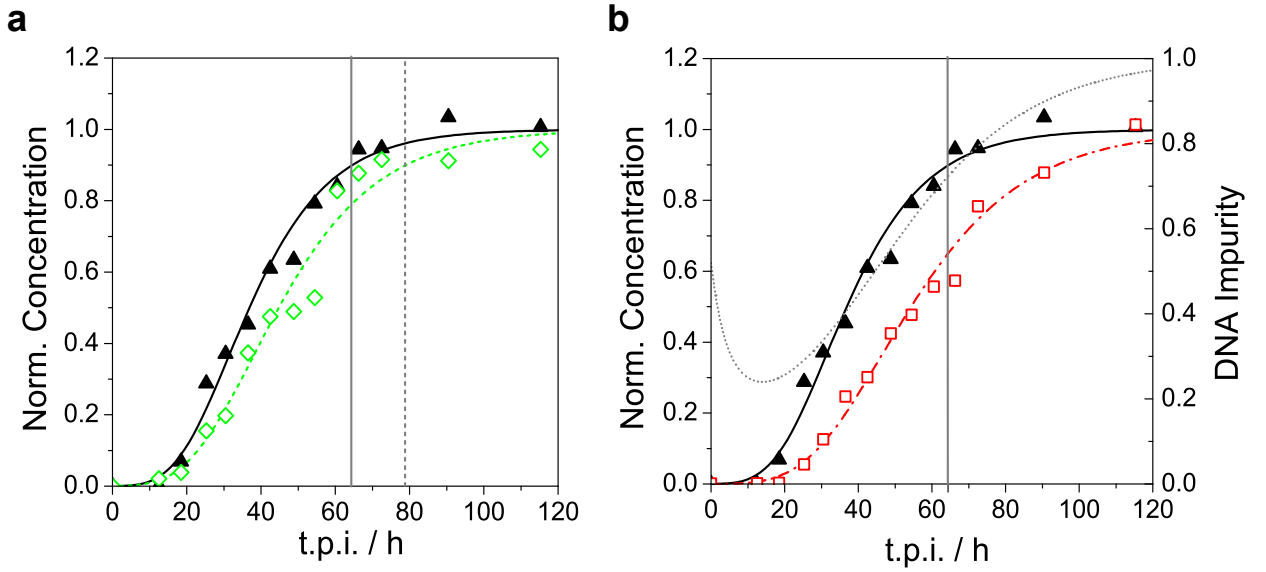

Figure 4-13. Release of virions and impurities.

HA activity (▲) and turbidity (◇) of cell culture supernatant after infection of MDCK cells with A/PR/8/34 (H1N1) RKI at an m.o.i. of 0.025 (a). HA activity (▲), host-cell DNA (□) and virus-specific DNA impurity (···) (b). Gompertz' function was fitted to experimental data. Measured values and curves were normalized to their upper asymptotic values. Virus-specific DNA impurity was calculated as the ratio of normalized Gompertz' functions (DNA concentration over HA activity). 90% quantiles are marked for the HA activity (—) and turbidity (···) by vertical lines.

Generally, HA activity was regarded the reference measure for the concentration of virus in supernatant. Infectivity, in contrast, was not further considered, partly due to its non-sigmoid profile but mostly due to the low relevance for inactivated vaccines production. Fitted curves normalized to their upper asymptotic values and experimental data for HA activity and turbidity from one condition are given in Figure 4-13a. Curves and data for the HA activity and DNA concentration are displayed in Figure 4-13b. Moreover, the normalized virus-specific content of DNA is provided. It was calculated as the quotient of profiles (DNA concentration over HA activity) with both curves normalized to their upper asymptotic values.

Apart from direct comparison of estimated parameters, Gompertz' functions can be interpreted as cumulative distributions (see 2.1.2). Consequently, statistical quantiles can be derived according to (2-2). The 10%-quantile $t_{0.1}$, e.g., can be used as marker for the end of lag-phases. The 90%-quantile $t_{0.9}$ may be considered a possible abortion criteria for the virus propagation phase or more generally interpreted as the time at which the upper asymptote is almost reached.

One important characteristic of virus propagation are the rates of compound release (virus and impurities). Due to the nature of Gompertz' function, the parameter b is independent of units and absolute values of described variables and can be used for direct comparison. For a first analysis, mean values and standard deviations were calculated over all conditions and experiments. Mean values of b for the HA and NA activity were $0.075 \pm 0.022\ h^{-1}$ ($N = 6$) and $0.063 \pm 0.022\ h^{-1}$ ($N = 3$), respectively. The release of protein and DNA was slower with $0.042 \pm 0.006\ h^{-1}$ ($N = 3$) and $0.041 \pm 0.005\ h^{-1}$ ($N = 6$), respectively. The rate of increase in turbidity, again, was similar to rates of HA and NA activity with $0.065 \pm 0.018\ h^{-1}$ ($N = 6$).

A different approach was taken for the interpretation of quantiles. Due to an expected dependency of lag-time on m.o.i, data were grouped accordingly. The mean $t_{0.1}$-quantile of HA activity at an m.o.i. of 0.025 was 19.2 ± 0.8 h ($N = 3$, A/PR/8/34 (H1N1) RKI and A/Wis/67/2005 (H3N2)). The value of 18 h at at an m.o.i. of 2.5 was practically indistinguishable ($N = 1$, A/PR/8/34 (H1N1) RKI). Regarding infections at the low m.o.i.'s of 0.00025 ($N = 1$, A/PR/8/34 (H1N1) RKI) and 0.001 ($N = 1$, B/Mal/2506/2005), values of the $t_{0.1}$-quantile were higher with 28 h and 38 h, respectively. Values of the $t_{0.9}$-quantile at an m.o.i. of 0.025 were, again, fairly homogeneous with 59.1 ± 6.6 h. Interestingly, the $t_{0.9}$-quantile (92 h) at an m.o.i. of 2.5 was significantly higher due to a lower than average release rate ($b = 0.042\ h^{-1}$). Values 72 h and 69 h of the $t_{0.9}$-quantile at the

low m.o.i.'s of 0.00025 and 0.001 were about 10 h above the average at 0.025 (59 h). The quantiles of NA activity closely reflected the quantiles of HA activity. The quantiles of protein and DNA concentration, in comparison, were always higher indicating a delayed release of impurities with respect to the release of virions.

Mean upper asymptotic values of HA activity in the first experiment were 906 ± 66 HAU $(0.1\ \text{ml})^{-1}$ ($N = 3$) indicating no dependency on m.o.i. Corresponding mean asymptotic values of NA activity were $45.9 \pm 3.7\ \mu\text{M min}^{-1}$. Upper asymptotic values of HA activity in the second experiment depended on the strain and adopted values between 450 and 750 HAU $(0.1\ \text{ml})^{-1}$. Noteworthy, the asymptotic value of A/PR/8/34 (H1N1) RKI in the second experiment was only 500 HAU $(0.1\ \text{ml})^{-1}$ and hence significantly lower than the mean value of 906 HAU $(0.1\ \text{ml})^{-1}$ in the first experiment. This was despite the fact that both experiments were run under identical conditions. Mean upper asymptotic values of the protein and DNA concentration (averaged over all conditions and experiments) were determined as $45 \pm 11.7\ \mu\text{g ml}^{-1}$ and $16.7 \pm 2.4\ \mu\text{g ml}^{-1}$ (both $N = 6$). Mean lower asymptotic values were determined as $3.5 \pm 0.9\ \mu\text{g ml}^{-1}$ and $0.5 \pm 0.4\ \mu\text{g ml}^{-1}$, respectively.

Since in general a dependency of parameters a and b on experimental conditions was observed, a reduced form of Gompertz' function (2-4) was preferred in order to achieve a more universal representation. The profile of HA activity and corresponding parameters were used as the reference for reduction. Moreover, quantiles $t_{0.1}$ and $t_{0.9}$ and the locus of the inflection point t_c were centered by corresponding values derived from HA activity. Centered quantiles and parameters are referred to as $t_{0.1}'$, $t_{0.9}'$ and t_c'. Reduced parameters and centered quantities from all conditions and experiments have been summarized in Table 4-19.

With respect to NA activity, values of $b^* = 1.04 \pm 0.12$ were equal to 1 within experimental precision. Corresponding quantiles $t_{0.1}'$ and $t_{0.9}'$ were close to 0 with 2.6 ± 0.4 h and 2.0 ± 5.6 h, respectively, when compared to the overall time-scale. Profiles of NA activity were hence indistinguishable from profiles of HA activity. Regarding protein and DNA concentrations, average values of 6.4 h (protein) and 8.4 h (DNA) for $t_{0.1}'$ quantiles indicated longer lag-phases compared to HA activity. In addition, average values of b^* were significantly lower than 1 with 0.71 (protein) and 0.59 (DNA), i.e. release rates were lower compared to HA activity. The same is reflected by the high values of $t_{0.9}'$-quantiles with 27.2 h (protein) and 39.4 h (DNA) on average.

Turbidity took an intermediate position. Its onset of increase was slightly delayed compared to HA activity and the rate of release was lower. But values of $b^* = 0.90 \pm 0.23$ and $t_{0.1}'$ and $t_{0.9}'$ quantiles of (4.1 ± 3.6) h and (9.7 ± 13.4) h, respectively, suggest profiles quite close to those of HA or NA activity.

Apart from a universal representation in the case of self-similarity, non-dimensional representations facilitate the generation of working diagrams. Such a working diagram prepared from average parameters in Table 4-19 is illustrated in Figure 4-14a. Note that the graph of NA activity was omitted due to the closeness to HA activity. For convenience, a second dimensional time axis is provided assuming reference parameters $b = 0.079\ h^{-1}$ und $a = 2.36$ h, which were calculated from infections at an m.o.i. of 0.025 ($N = 3$). In addition to reduced Gompertz' functions, reduced data points from individual experiments were plotted for the HA activity and DNA concentration. The reduction of data was executed experiment-wise using respective parameters for HA activity. Accordingly, data points of HA activity are represented quite well by the corresponding Gompertz' function. Only at values close to 0% or 100% systematic deviation from the curve is observed. Data points of the DNA concentration, in contrast, are quite well resembled in shape but not in terms of actual values. Depending on the experiment, a more rapid

Table 4-19. Statistics on reduced parameters and relative quantiles

Parameter		NA Activity	Protein	DNA	Turbidity
		(N = 3)	(N = 3)	(N = 6)	(N = 6)
Name	Unit	Mean ± Std	Mean ± Std	Mean ± Std	Mean ± Std
b*	-	1.04 ± 0.12	0.71 ± 0.11	0.59 ± 0.17	0.90 ± 0.23
a*	-	0.14 ± 0.08	0.50 ± 0.08	0.69 ± 0.12	0.39 ± 0.35
$t_{0.1}'$	h	2.6 ± 0.4	6.4 ± 1.5	8.4 ± 1.2	4.1 ± 3.6
tc'	h	2.5 ± 1.5	12.0 ± 0.3	16.8 ± 2.2	5.6 ± 5.0
$t_{0.9}'$	h	2.0 ± 5.6	27.2 ± 4.5	39.4 ± 11.0	9.7 ± 13.4

Note: Average values and standard deviations from two experiments are presented. Values for the NA activity and protein concentration are based on data from 3 roller bottle cultivations with A/PR/8/34 (H1N1) RKI at different m.o.i. (first experiment). Values for the DNA concentration and turbidity are based on data from 6 roller bottle cultivations with strains A/PR/8/34 (H1N1) RKI, A/Wis/67/2005 (H3N2) and B/Mal/2506/2005 at various m.o.i. (first and second experiment).

or slower increase than predicted by the Gompertz' function with average parameters can be noticed. Similar observations were made for the protein concentration and turbidity (not shown).

Finally, the degree of virus-specific impurity can be calculated from average profiles as a function of time. As described before (see Figure 4-13b) the degree of specific impurity was calculated as the quotient of profiles (protein concentration, DNA concentration or turbidity over HA activity). Results have been depicted in Figure 4-14b. The $t_{0.9}$' quantile of HA activity is indicated by a dashed vertical line. As can be seen in all three cases, degrees of specific impurity decrease first until they reach a minimum close to the inflection point of HA activity at $t^* = 0$. This minimum is most strongly pronounced for the content of DNA, while it is only weakly pronounced for the content of protein and specific turbidity. Beyond $t^* = 0$, specific impurities increase again and approach their asymptotic values of 1. High starting values of specific impurities are the consequence of non-zero lower asymptotes $x_{-\infty}$ of impurities (reached for $t \to -\infty$) while the lower asymptote of HA activity was forced zero. Pronounced minima near the inflection point are the result of diminishing virus release, while impurities are still being released at high rate into the

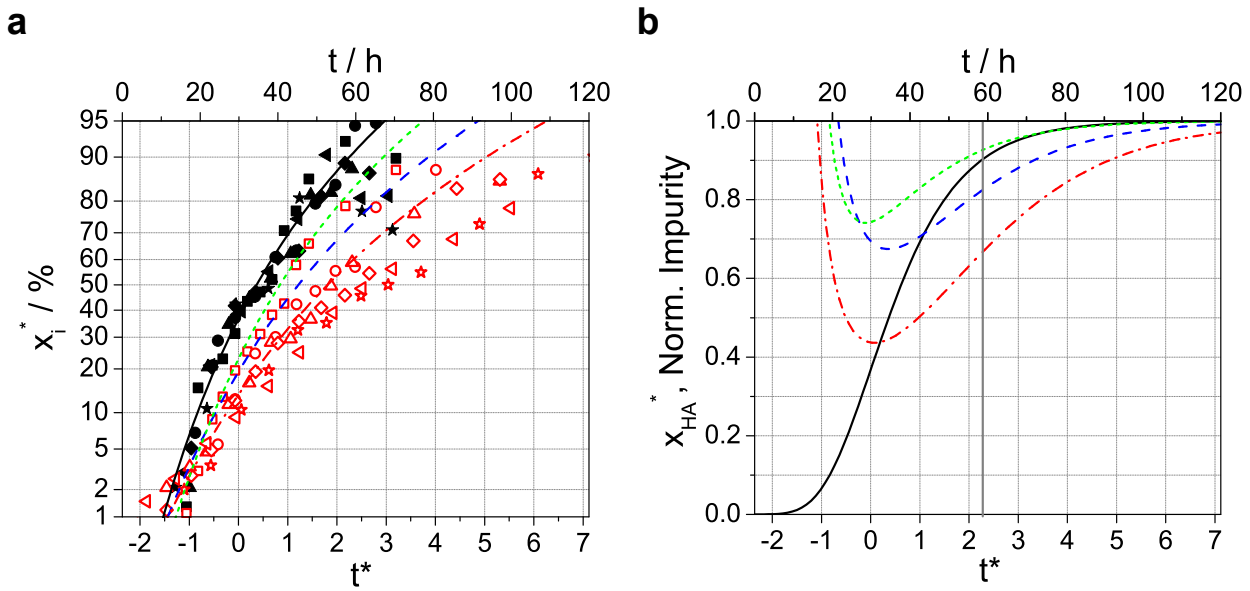

Figure 4-14. Non-dimensional characteristics of cultivation in roller bottles.
Average non-dimensional profiles of HA activity (—), protein concentration (– –), DNA concentration (·-·) and turbidity (---) (a). Individual measurements of HA activity (filled symbols) and DNA concentration (open symbols) were included for comparison. Specific content of protein (– –), DNA (·-·) and turbidity (---), calculated as the quotient of profiles over HA activity normalized by their upper asymptotic values (b). The average non-dimensional profile of HA activity (—) was included for orientation. Its 90% quantile is indicated by the vertical line. For convenience, a second time axis representative for experiments conducted at an m.o.i of 0.025 is provided in both graphs.

supernatant. At the $t_{0.9}$' quantile of HA activity, virus-specific DNA content is only at 66% of its asymptotic value while the protein content has already reached 82%.. The specific turbidity is even higher with 92% of its asymptotic value.

4.1.2 Preparative Cultivations

For the production of starting material, roller bottles were used almost exclusively. Only in a few incidences supernatant from stirred tank or wave biorecators (referred to as supernatant from microcarrier cultivations) was used in experiments. For preparative cultivations, virus strains were restricted to A/PR/8/34 (H1N1) NIBSC/RKI or A/Wis/67/2005 (H3N2), both added at an m.o.i. of 0.025. Infections were carried out for 3 days and harvested by pooling of supernatants. The harvesting time of 72 h approximately corresponds to the 95% quantile of HA activity (Figure 4-14b) and is about 12 h beyond the 90% quantile discussed before. Average values from measurements grouped by strains and culture media are summarized in Table 4-20. Different groups will be referred to as campaigns in the following.

Statistics revealed significant scatter of the cell density prior to infection but also HA activity at the time of harvest. Values displayed significant variability within single campaigns (indicated by large standard deviations), but further appeared to have different mean values from campaign to campaign. Particularly high variability was observed in the campaign with Ex-Cell MDCK medium, which was run over a long period (about one year) including almost 30 batches. Here, the relative standard deviation (RSD) of HA activity in crude harvests was as high as 59%, RSD of the cell density prior to infection was still 32%. Even turbidity of supernatants varied considerably, while it was comparatively reproducible in other campaigns.

Moreover, a strong dependency of HA activity from strains can be recognized. Highest activities were achieved with A/PR/8/34 (H1N1) RKI cultivated in V-Medium with 555 HAU $(0.1\ ml)^{-1}$ on average. Lowest activities resulted after cultivation of A/PR/8/34 (H1N1) NIBSC in V-Medium with an average value of 150 HAU $(0.1\ ml)^{-1}$. Remarkably, the average activity was much higher when the same strain was cultivated in Ex-Cell MDCK medium. The value of 394 HAU $(0.1\ ml)^{-1}$ even takes the second placing among all campaigns. HA activities after clarification were generally lower with losses up to 20% independently of the clarification method.

Table 4-20. Batch analyses of cell culture supernatants.

Medium		**V-Medium**						**Ex-Cell MDCK**	
Strain		**A/PR/8/34 (H1N1) NIBSC**		**A/PR/8/34 (H1N1) RKI**		**A/Wis/67/2005 (H3N2)**		**A/PR/8/34 (H1N1) NIBSC**	
Variable	**Unit**	**Value[7]**	**N[8]**	**Value**	**N**	**Value**	**N**	**Value**	**N**
Crude Harvest									
Cell Density[1]	10^5 cells cm^{-2}	2.57 ± 0.41	6	2.15 ± 0.31	5	3.06 ± 0.86	5	3.15 ± 1.02	11
a_{HA}[2]	HAU (0.1 ml)$^{-1}$	150 ± 50	6	555 ± 193	5	280 ± 40	5	394 ± 233	11
Ext_{700}[3]	O.D.	0.201 ± 0.020	6	0.256 ± 0.013	5	0.254 ± 0.031	5	0.454 ± 0.146	11
Clarified Harvest[9]									
a_{HA}	HAU (0.1 ml)$^{-1}$	129 ± 33	6	452 ± 160	5	230 ± 47	5	321 ± 171	11
Ext_{700}[3]	O.D.	0.025 ± 0.016	6	0.025 ± 0.023	5	0.014 ± 0.004		0.041 ± 0.023	11
a_{NA}[4]	µM min^{-1}	4.3	1	24.4 ± 14.9	4	2.0 ± 0.2	4	n.a.	
c_{prot}[5]	µg ml^{-1}	n.a.		n.a.		34.7 ± 6.1	4	62.2 ± 11.8	6
c_{DNA}[6]	µg ml^{-1}	8.9 ± 1.7	4	7.0 ± 0.7	4	7.7 ± 0.7	4	5.94 ± 0.73	6

1: cell density of the reference bottle prior to infection, 2: volumetric HA activity, 3: turbidity as extinction of light at 700 nm, 4: volumetric neuraminidase activity, 5: total protein concentration, 6: double-stranded DNA concentration, 7: average value ± standard deviation, 8: number of batches analyzed, 9: clarified either by centrifugation (V-Medium) or filtration through a 0.65 um fibrous polypropylene filter (Ex-Cell MDCK), n.a.: not available.

Values of the turbidity were consistent among campaigns run with V-Medium. Average values of infections with A/PR/8/34 (H1N1) NIBSC, however, were lower by about 20% than average values for other strains. Cultivations in Ex-Cell MDCK medium, which were conducted without medium-exchange prior to infection, resulted in much higher turbidity at the time of harvest. The average value of 0.454 was almost twice as high. Besides, a high RSD of 32% was noticeable while RSDs of other campaigns were in the range of 5% to 12%.

Final concentrations of DNA were comparable among campaigns with average values between 5.9 und 8.9 µg ml^{-1}. RSDs within campaigns were 10% to 20%. The highest concentration of

8.9 µg ml^{-1} was detected with A/PR/8/34 (H1N1) NIBSC in V-Medium. The lowest concentration was found with the same strain cultivated in Ex-Cell MDCK medium.

Data for protein is unfortunately incomplete, since it was not determined routinely after inactivation. However, the comparison between concentrations measured with A/Wis/67/2005 (H3N2) in V-Medium and A/PR/8/34 (H1N1) NIBSC in Ex-Cell MDCK medium reveals a remarkably large difference. The average value of 62.2 µg ml^{-1} in the second case is almost twice as high as the value of 34.7 µg ml^{-1} in the first case. RSDs within campaigns, however, were moderate with 18% and 19%.

Concerning microcarrier cultivations, statistically reliable data has not been acquired yet. Only supernatants from two cultivations conducted in stirred-tank bioreactors and a single cultivation conducted in a wave bioreactor were used in experiments (data not shown). But despite the low number of batches analyzed, it can already be concluded that the final content of DNA appears to be lower in microcarrier cultivation systems. Average concentrations were only 3.6 ± 1.5 µg ml^{-1} and therefore lower by a factor of 2 to 2.5 compared to roller bottle cultivations.

4.2 Clarification

4.2.1 Normal-Flow Filtration

Sequential normal-flow filtration by a combination of two filters was used for the clarification of crude supernatant in the first process (Figure 1-5) [Kalbfuss, Genzel, et al., 2007]. Supernatant originated exclusively from the campaign with serum-free Ex-Cell MDCK medium (Table 4-20). For the purpose of pre-filtration, a fibrous 0.65 µm Flotrex AP polypropylene filter medium was selected. Several other media (membrane filters, membrane filters with pre-filters and fibrous filters of various pore size) had been tested before. Fibrous filters with about 1 µm pore size, however, appeared to be the best compromise between capacity and separation efficacy (data not shown). A second filtration step employing a 0.45 µm Memtrex AP membrane filter medium was conducted after inactivation in order to remove remaining fines.

Statistics on the clarification of supernatant from up to 13 batches are given in Table 4-21. Best results with respect to virus yield were obtained if broth was filtered immediately at the time of harvesting and temperature was kept constant at 37 °C in a water bath. Storage at 4 °C prior to

depth filtration, in contrast, led to decreased virus yields that were sometimes as low as 30% (data not shown). Average product yields of pre- and membrane filtration steps were 85% and 93%, respectively. Turbidity was reduced to 9% by the fibrous filter and 25% by the membrane filter. In total, turbidities of supernatants were reduced to 2.3% of their initial values by the combination of both filters while 79% of product was preserved. Absolute initial values of the turbidity (arithmetic mean ± standard deviation) were 0.454 ± 0.146 on average (see also Table 4-20). Values after pre-filtration and membrane filtration were 0.041 ± 0.023 and 0.006 ± 0.002, respectively. Protein and DNA concentrations were not determined for the pre-filtration step but remained unaffected by membrane filtration. The initial flux of both steps was in the order of 600L m^{-2} h^{-1} at a pressure difference of 0.5 bar. Flux decline was negligible since filter capsules were oversized with respect to processed volumes. Consequently, no data on the capacity of filters can be provided.

Table 4-21. Average percentage yields of pre- and membrane filtration

	Pre-Filtration		Membrane Filtration			
Yield / %	**HA[1]**	**Turb.[2]**	**HA**	**Turb.**	**Protein**	**DNA**
Mean	85	9	93	25	91	105
Std[3]	± 15	± 5	± 14	± 15	± 16	± 13
N[4]	13	13	13	13	5	6

1: HA activity, 2: turbidity, 3: standard deviation, 4: number of batches analyzed

4.2.2 Centrifugation

Separation of cell debris by centrifugation was investigated as an alternative to normal-flow filtration in the second process (Figure 1-5) [Knöchlein, 2007; Kröber, 2007]. Due to the generally small scale of virus cultivations, experiments were exclusively conducted in laboratory-scale batch centrifuges. However, Sigma theory was employed for a scale- and device-independent description of data (see 2.2). Moreover, a modified Verhulst's function was fitted to data for the generation of trend lines. Crude supernatant was mostly derived from roller bottle cultivations. In addition, supernatants from a single wave bag (Wave5) and stirred-tank (F99) microcarrier cultivation were used in experiments. Infections were exclusively conducted with influenza strain A/PR/8/34 (H1N1) either from NIBSC or RKI. Both, V-Medium and Ex-Cell

MDCK medium were used for virus propagation. An overview of culture batches is given in Table 4-22.

Table 4-22. Overview of culture batches used in centrifugation experiments

		Virus Cultivation			Crude Supernatant		0.45 um[5]
Batch	**Medium**	**Virus[1]**	**Cell Density[2]**	**Viability[2]**	**a_{HA}[3]**	**Ext_{700}[4]**	**Ext_{700}**
			/ 10^6 cells ml^{-1}	/ %	/ HAU (0.1 ml)$^{-1}$	/ O.D.	/ O.D.
VC #A2	V-Medium	NIBSC	01.01.14	97	188	0.201	n.a.
VC #A5			0.73	87	127	0.223	0.010
VC #A8			0.79	85	142	0.210	0.009
VC #A10			0.84	95	126	0.211	0.012
VC #A14			0.86	98	90.2	0.191	0.004
F99		RKI	2.17	98	776	0.332	0.009
Wave5			3.13	99	994	0.294	0.001
VC #A1	Ex-Cell MDCK	NIBSC	0.98	73	103	0.392	n.a.
VC #A3			1.07	80	154	0.493	0.014

1: source of A/PR/8/34 (H1N1) seed virus, 2: cell density and viability prior to infection, 3: HA activity, 4: turbidity as the extinction of light at 700 nm, 5: supernatant filtered through 0.45 µm Minisart membrane filter. Note: Roller bottle cultivations are denoted by batches VC #A1 to VC #A14. Batches from a stirred tank or wave bag microcarrier cultivation are denoted as F99 and Wave5, respectively.

For a first check on the applicability of sigma theory (see 2.2), crude supernatants from microcarrier cultivations (Wave5, F99) and roller bottles (VC #A14) were clarified in vessels with conical (2 or 10 ml working volume) or flat bottom (200 ml working volume). Centrifugal load was varied by both – centrifugation time and relative centrifugal force (97 to 4200). Determined clarification efficiency (2-5) as a function of load is depicted in Figure 4-15. Since the bottom shape of vessels showed a significant influence data were grouped accordingly. Separate modified Verhulst's functions (2-8) were fitted to groups of data, respectively (see Table 4-23 for parameters). As can be seen, best clarification efficiency was achieved in vessels with conical bottom. Regarding vessels with flat bottom, comparable efficiency was only achieved at loads lower by about one order of magnitude. The scale of centrifugation systems (vessel, rotor and centrifuge) and the difference in RCF, in contrast, was successfully taken care of by Sigma theory. This is indicated by the fact that all data within one group collapse on the same trend line.

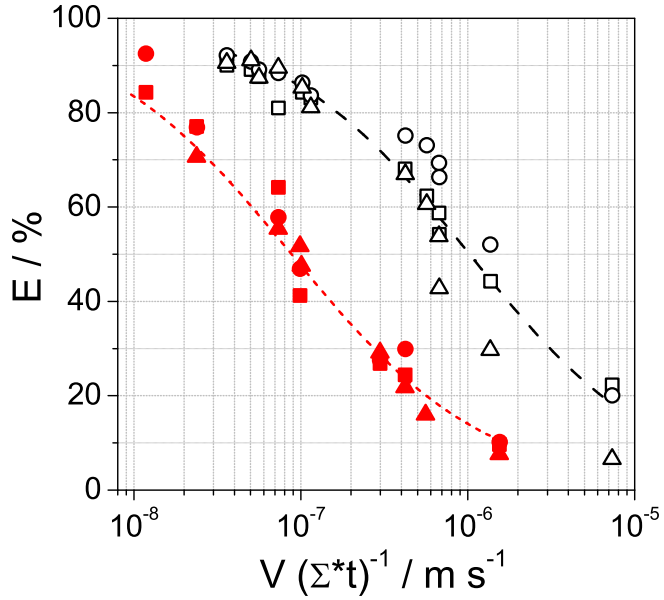

Figure 4-15. Applicability of Sigma theory to laboratory-scale batch centrifuges.

Crude supernatants derived from roller bottles (▲△) or wave bag (●○) and stirred-tank (■□) microcarrier cultivations were clarified by centrifugation in vessels with conical (filled symbols) or flat bottom (open symbols). Clarification efficiency E is plotted over centrifugal load $V(\Sigma t)^{-1}$.

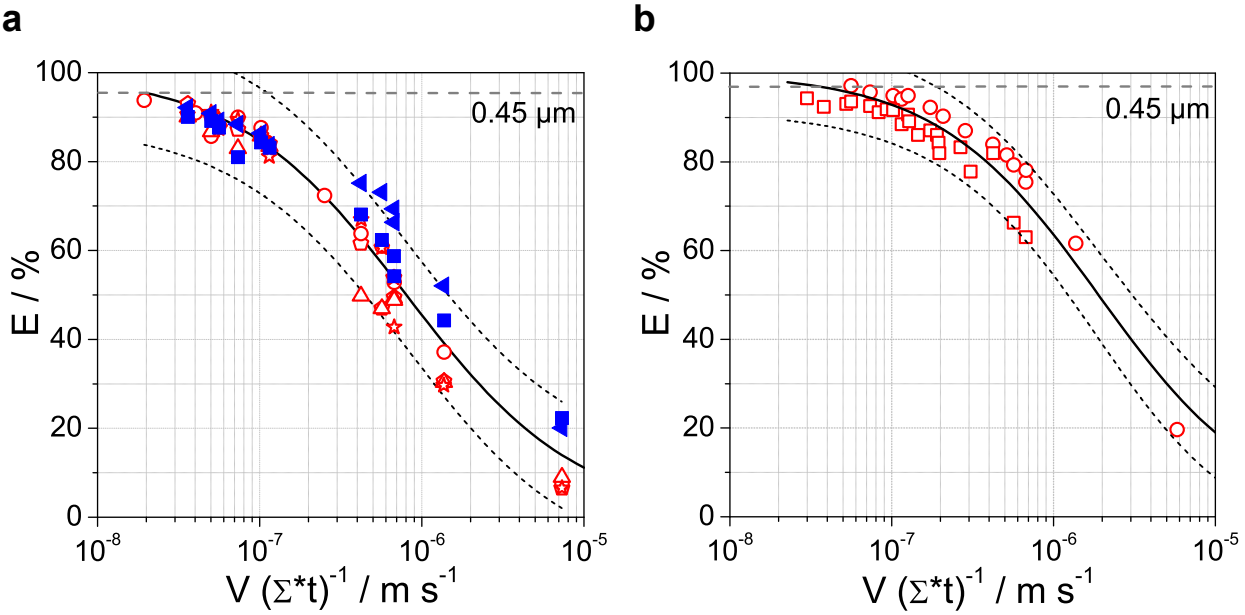

Figure 4-16. Clarification of cell culture supernatant by centrifugation.

Virus was either propagated in roller bottles (red open symbols) or microcarrier cultivation systems (blue filled symbols). V-Medium (a) or Ex-Cell MDCK medium (b) were used for propagation. Centrifugation was conducted at various scales using vessels with conical bottom. Modified Verhulst's functions (—) were fitted to experimental data with confidence bands of prediction (α = 0.05) indicated by short dashed lines (---). Clarification efficiency by filtration through a 0.45 um membrane filter is given by dashed horizontal lines (- -).

The influence of cell culture medium on clarification efficiency was investigated using vessels with conical bottom (Figure 4-16). Crude supernatants from roller bottles and microcarrier cultivations were used in the case of V-Medium. However, supernatant only from roller bottles was used with respect to Ex-Cell MDCK medium. Again, modified Verhult's functions were fitted to data with parameters summarized in Table 4-23. Filtration through 0.45 µm syringe membrane filters was conducted for comparison to normal-flow membrane filtration. The recovery of virus was determined by measurement of HA activity before and after centrifugation.

The closeness of parameter values with respect to standard errors indicate that there was no significant influence of cell culture medium on clarification efficiency. Noteworthy, this was despite the fact that cultivations with Ex-Cell MDCK resulted in turbidities about twice as high as in cultivations with V-Medium (Table 4-25). Average clarification efficiencies by filtration through 0.45 µm filters were 95.9% and 97.% for supernatant produced in V-Medium and Ex-Cell MDCK medium, respectively. In both cases, comparable clarification efficiency was achieved by centrifugation at a load of approximately $2 \cdot 10^{-8}$ m s^{-1}. Concerning the recovery of virus based on HA activity, no significant dependency on load was observed. Average recoveries scattered around 100% (data not shown).

Table 4-23. Estimated parameters of modified Verhulst's functions

Category	x_c	b	R^2
Conical Bottom	-5.989 ± 0.036	-0.569 ± 0.038	0.934
Flat Bottom	-7.056 ± 0.033	-0.583 ± 0.037	0.951
V-Medium	-6.095 ± 0.022	-0.528 ± 0.023	0.944
Ex-Cell MDCK Medium	-5.722 ± 0.046	-0.498 ± 0.031	0.914

Note: Least-squares estimates and standard errors after linearization are reported.

Crude supernatants from campaigns with A/PR/8/34 (H1N1) RKI and A/Wis/67/2005 (H3N2) produced in V-Medium were routinely clarified by centrifugation in vessels of 230 ml with conical bottom (Table 4-20). Centrifugation was conducted under conditions corresponding to a load of $1.57 \cdot 10^{-8}$ m s^{-1}. Average clarification efficiencies were 90.3% ($N = 5$) for A/PR/8/34 (H1N1) RKI and 94.5% ($N = 5$) for A/Wis/67/2005 (H3N2). Average recoveries of virus based on

HA activity were 81% and 82%, respectively. Absolute values of the turbidity before and after centrifugation (arithmetic mean ± standard deviation) were 0.256 ± 0.013 and 0.025 ± 0.023 in the campaign with A/PR/8/34 (H1N1) RKI. Values in the campaign with A/Wis/67/2005 (H3N2) were similar with 0.254 ± 0.031 and 0.014 ± 0.004, but slightly lower after centrifugation (see Table 4-20 for comparison).

4.3 Selective Precipitation of DNA

4.3.1 Development of Operation

A selective precipitation operation was added in the second process (Figure 1-5), in order to enhance depletion of host-cell DNA. For this purpose, various metal ions ($CaCl_2$, $MgCl_2$, $MgSO_4$), protamine sulphate and polythethyleneimine (PEI) were tested with respect to their suitability as selective agents for the precipitation of DNA [Knöchlein, 2007]. Among these, PEI showed the highest selectivity for DNA under tested conditions. Yet, some co-precipitation of virus occurred at PEI concentrations that were necessary to achieve the maximum reduction in DNA. An example for the precipitation of DNA from supernatant produced in roller bottles (strain A/PR/8/34 (H1N1) RKI propagated in V-Medium) is given in Figure 4-17.

In order to enhance the selectivity of the operation, a factorial design for investigating the impact of ionic strength, pH and PEI molecular weight (referred to as input variables in the following) was set-up and executed [Kröber, 2007]. A full factorial design with two levels for each input variable (Table 4-24) was chosen leading to 8 different combinations. In addition, PEI concentration was varied in 8 steps from 0% to 0.45% (w/v) resulting in a total of 64 different conditions (see 3.5.1 for details). NA activity was used as the primary measure for virus content, since HA activity could not be determined due to PEI interfering with the assay. In addition, the intensity of scattered laser light was considered as a second measure for the virus content. Both measures were normalized to respective values observed for 0% PEI controls (see 3.5.1 for details). Depletion of DNA was calculated according to (3-24) from measured concentrations. Polynomial models including all single input variables plus their two- and three-variable interactions were fitted to experimental data by step-wise regression. The probability threshold for inclusion of variables or interactions was set to $\alpha = 0.1$.

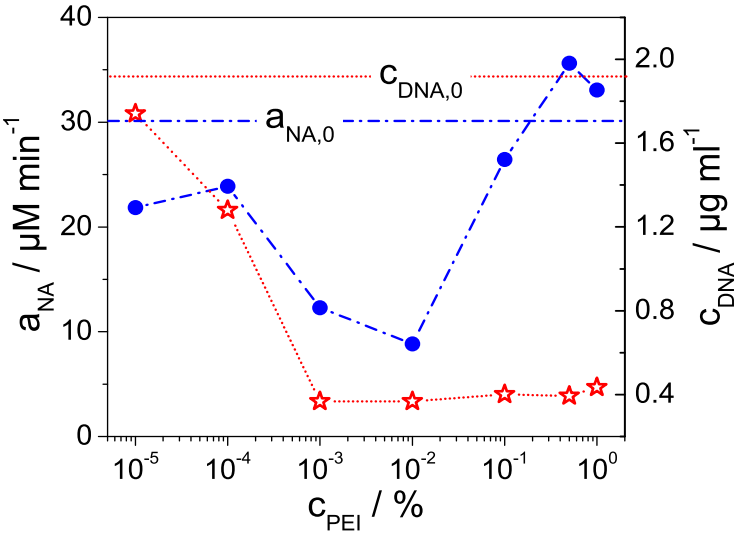

Figure 4-17. Precipitation of host-cell DNA by PEI from clarified and inactivated cell culture supernatant.

The concentration of DNA (☆) was reduced about 5-fold at PEI concentrations higher than 10^{-3}% (w/v). Influenza virions (●) quantitated by NA activity co-precipitated with DNA to a degree depending on the concentration of PEI. The pH of supernatant was approximately 7.5. Precipitation was carried out at 4 °C over a period of 2 hours. The initial DNA concentration (···) and NA activity (–·–) are indicated by horizontal lines.

Table 4-24. Levels of input variables

Parameter	**Level**	
	high (+)	**low (-)**
pH	9	~7.5[a]
Ionic Strength	+ 200 mM[b]	-
Molecular Weight	750 kDa	2 kDa

a: pH value of supernatant after addition of boric acid buffer, b: ionic strength increased by 200 mM by the addition of NaCl solution

Reduction of DNA by about 90% was achieved under all conditions for PEI concentrations ≥ $4.5 \cdot 10^{-3}$% (w/v). Precipitation of DNA occurred within a concentration range from $4.5 \cdot 10^{-5}$% to $4.5 \cdot 10^{-3}$ (w/v) depending on conditions (data not shown). Effective concentrations for precipitation as defined by fitting of Hill's function (see 3.5.1 for details) were found a function of all three input variables and the product of ionic strength and PEI molecular weight (data not shown). Overall regression, however, was non-significant with a *p*-value of 0.0663. While high pH and

high ionic strength seemed to hamper the precipitation of DNA, high PEI molecular weight led to precipitation of DNA at lower PEI concentrations already. With respect to NA activity, pH, ionic strength and the product of pH and PEI molecular weight were found significant for the prediction of final activity. The plot of actual over predicted activity is given in Figure 4-18a ($R^2 = 0.95$). Concerning the intensity of scattered laser light, the impact of pH, ionic strength and molecular weight alone were found significant. The plot of actual over predicted intensity is given in Figure 4-18b ($R^2 = 0.95$). Both regressions were considered significant with overall *p*-values of 0.0047 and 0.0051, respectively.

The impact of input variables on NA activity or scattered laser light intensity is illustrated in Figure 4-19. Whereas high pH and ionic strength were beneficial for the recovery of NA activity (a), there was no impact of molecular weight alone. Concerning scattered light intensity, all three variables correlated positively with recovery (b).

Additional experiments were conducted in order to ensure adequate operating conditions for the preparative precipitation of DNA [Kröber, 2007]. In these experiments it was confirmed, that a filter cut-off of 0.45 µm is appropriate for the separation of virus from precipitate. Virus yields after filtration through 0.45 µm membrane filters were close to 100% based on NA and HA activity. Some loss was observed for a filter cut-off of 0.2 µm but yields were not improved by using filters with 0.8 µm cut-off. Moreover, it was ruled out that virus (i.e. viral HA and NA activity) is damaged by conditioning of supernatant prior to precipitation. In time-lapse experiments, an incubation time of 30 minutes after the addition of PEI was found sufficient for the formation of precipitates. Furthermore, an impact of inactivation due to covalent modification of virions and/or DNA was excluded by comparing the precipitation of DNA from active and inactivated supernatant from the same batch.

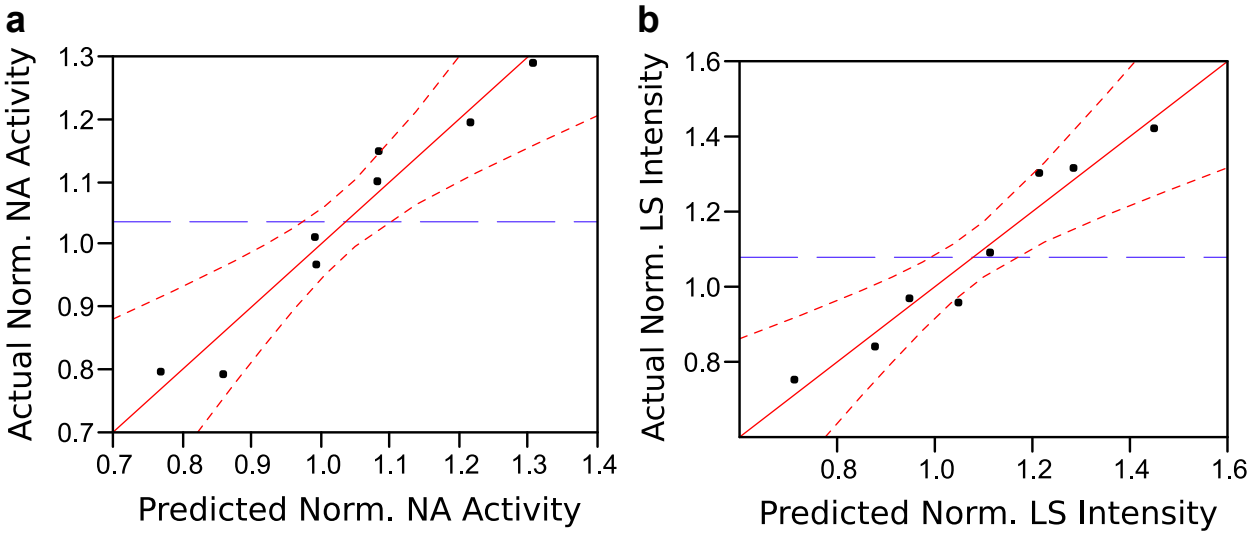

Figure 4-18. Normalized NA activity (a) and intensity of scattered laser light (b) plotted over predicted values.

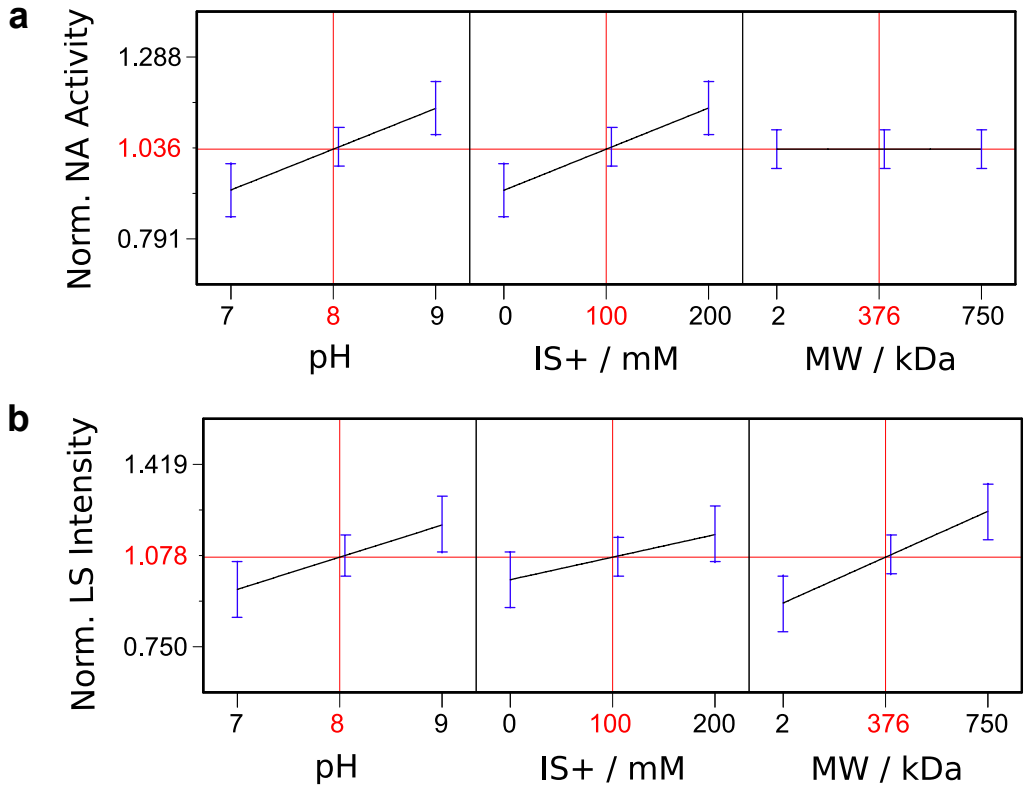

Figure 4-19. Influence of input variables on the relative concentration of virus as determined by NA activity (a) or the intensity of scattered laser light (b).

4.3.2 Preparative Precipitation

A total of five batches of supernatant produced in roller bottles was processed at larger scale [Kröber, 2007; Eisold, 2008]. Volumes of batches were between 1 and 2 L. Influenza strains A/PR/8/34 (H1N1) RKI or A/Wis/67/2005 (H3N2) were used for infection and propagated in V-Medium. Pooled supernatants were clarified by centrifugation (3.3.2) and inactivated chemically by the addition of *β-PL* (3.4). After inactivation, supernatants were stored at 4 °C until success of inactivation had been confirmed (typically one week). Preparative precipitations were conducted under conditions that had been found suitable before (pH 9, +200 mM NaCl). The smaller PEI of 2 kDa molecular weight was chosen for precipitation due to its better separability from virus by ultrafiltration. The first batch was still filtered directly through a 0.45 µm membrane filter. However due to the low filter capacity, additional centrifugation prior to filtration was introduced for processing of subsequent batches. This centrifugation step was not optimized with respect to throughput but conditions as developed for the separation of cell debris were applied.

The average percentage yield of NA activity after precipitation was 84 ± 8% ($N = 5$, arithmetic mean ± standard deviation presented in all cases). The effect of correction (see 3.5.1) was negligible due to very low activities found in permeates after ultrafiltration. The average yield of HA activity was similar with 76 ± 28%. In this case, correction proved essential due to the high pseudo-affinity caused by the presence of PEI in samples. Absolute values, in contrast, differed dramatically between the two strains (see Table 4-20 for comparison). Average concentrations of DNA before precipitation were 7.13 ± 0.62 µg ml^{-1}. Concentrations after precipitation were 0.79 ± 0.06 µg ml^{-1}. Considering dilution due to conditioning of supernatants, the content of host-cell DNA was reduced by 85.3 ± 1.2% on average, corresponding to 6.8-fold reduction. For comparison, precipitation of DNA from a single batch produced in a microcarrier stirred-tank cultivation, the reduction was only 16% (not shown). The initial concentration of DNA, however, was much lower with only 0.74 µg ml^{-1} .

4.4 Tangential-Flow Filtration

4.4.1 Development of Operation

TFUF was employed for the concentration and conditioning of virus in supernatant prior to chromatography in both processes (Figure 1-5) [Kalbfuss, Genzel, et. al., 2007; Kröber, 2008]. In

the first place, operating conditions had to be derived that allow for the concentration of virus at high yield and minimize fouling of membranes. For this purpose, a number of scouting experiments were conducted using very small hollow-fiber modules with 38 cm^2 membrane area and of 60 cm length. If not otherwise stated, influenza virus A/PR/8/34 (H1N1) NIBSC propagated in roller bottles with Ex-Cell MDCK medium was used in experiments. Virus-containing supernatant was clarified twice by normal-flow filtration (4.2.1) and inactivated chemically (3.4) prior to tangential-flow filtration.

In the first experiment, supernatant was circulated at different wall shear rates (step-wise increase from 3600 s^{-1} to 16 000 s^{-1}) and zero flux in order to test the sensitivity of virions towards shear stress. Sample was pumped through the retentate circuit for 20 theoretical cycles at each setting. The total circulation time was 2:45 h. Even at the highest wall shear rate of 16 000 s^{-1} no decrease in HA activity was observed (data not shown). Nevertheless, a lower wall shear rate of 9 500 s^{-1} was chosen in subsequent experiments for economic reasons and due to the strong pressure gradient observed between the retentate inlet and outlet at a wall shear rate of 16 000 s^{-1}.

In the next step, hollow-fibers with 750 kDa and 0.1 µm cut-off were tested for the rejection of virions. A third hollow-fiber with 0.45 µm cut-off was included in the study to assess whether the normal-flow membrane microfiltration step described in 4.2.1 could be replaced by tangential-flow microfiltration. Batches of 600 ml starting volume were concentrated about 12-fold with 750 kDa and 0.1 µm hollow-fibers. The 0.45 µm hollow-fiber was used for the clarification of 1.8 L of inactivated supernatant that had been pre-filtered only (see 3.3.1). Filtration flux was varied similarly to the experiment described below in order to get a first impression on membrane fouling (data not shown). Material balances of the three runs are reported in Table 4-25.

The 750 kDa hollow-fiber seemed to reject virions completely, whereas full permeation was observed for the 0.45 µm hollow-fiber. Both filtrations can be regarded lossless with respect to HA activity (106% for the 750 kDa and 100% for the 0.45 µm hollow-fiber). In addition, concentration with the 750 kDa hollow-fiber led to a significant reduction in total protein and DNA (12% and 39% of their initial mass). Similar to normal-flow membrane microfiltration, clarification with the 0.45 µm hollow-fiber resulted in a decrease of turbidity (3.3% of initial extinction). Regarding the 0.1 µm hollow-fiber, fractionation of virions was observed. Since only 4% of the initial HA activity was found in the permeate (data not shown) and 54% in the retentate,

Table 4-25. Material balances of hollow-fiber selection experiment.

Cut-off	Feed					Product Fraction				
	V^1	$a_{HA}{}^2$	$c_{prot}{}^3$	$c_{DNA}{}^4$	$Ext_{700}{}^5$	V	a_{HA}	c_{prot}	c_{DNA}	Ext_{700}
	ml	HAU (0.1 ml)$^{-1}$	µg ml^{-1}	µg ml^{-1}	O.D.	ml	HAU (0.1 ml)$^{-1}$	µg ml^{-1}	µg ml^{-1}	O.D.
0.45 µm	1805	200	74.0	5.58	0.030	1663	200 (100%)	72.3 (97.7%)	6.23 (112%)	0.001
0.1 µm	616	100	48.1	3.96	0.003	52.6 (1 : 12)	631 (54%)	50.6 (9%)	7.43 (16%)	0.012
750 kDa	619	100	59.0	4.81	0.003	52.2 (1 : 12)	1260 (106%)	81.3 (12%)	22.2 (39%)	0.014

1: volume, 2: volumetric HA activity, 3: total protein concentration, 4: double-stranded DNA concentration, 5: extinction of light at 700 nm

Note: Product fractions are listed on the right (retentate and wash for 750 kDa and 0.1 µm hollow-fibers, permeate for 0.45 µm hollow-fiber). Feed of clarification with 0.45 µm hollow-fiber was only pre-filtered and inactivated. Volume reduction and yields of analytes are given in brackets below.

42% of HA activity seemed to have deposited on or inside the membrane. Based on these results, the 750 kDa membrane was chosen for subsequent concentration and DF of influenza virus. Due to the higher complexity of tangential-flow filtration compared to normal-flow filtration, the clarification of cell culture supernatant with hollow-fibers was not further pursued.

In the next experiment fouling of 750 kDa hollow-fibers was investigated in more detail by the TMP method (see 2.5). In this experiment permeate flux was varied from 15 to 60 L m^{-2} h^{-1} over the course of filtration. More precisely, flux was altered step-wise applying a staircase profile and kept constant for 10 to 15 min at each setting. Fouling became evident as an increase in the TMP and overall filtration resistance calculated from pressure data according to (2-12) and following equations. Fouling was quantitated by the first derivative of filtration resistance and is referred to as fouling rate in the following. A decrease in the viscosity was observed during filtration caused by warming of the retentate from about 10 °C (cold storage) to room temperature. Filtration resistance decreased from an approximate starting value of $2 \cdot 10^{12}$ m^{-1} at 15 L m^{-2} h^{-1} to $1.5 \cdot 10^{12}$ m^{-1} with increasing flux (Figure 4-20a). This apparent reduction of the resistance was caused by a reduction of permeate backflow near the filter outlet. Here, at low flux, the pressure gradient on the retentate side led to a locally negative TMP and hence inverse flow through the membrane. With increasing flux the local TMP became positive over the whole length of the module and the resistance stabilized. Fouling seemed to be non-critical if permeate flux was kept

below about 28 L m^{-2} h^{-1}. If set higher, a sudden increase of the fouling rate could be observed being approximately proportional to filtration flux. This finding was supported by filtration runs at a constant flux of 28 L m^{-2} h^{-1}. These runs only showed a slight increase in the resistance independent of the actual concentration factor or run time (see Figure 4-23b below). However, despite the observed fouling at higher flux, layer formation and pore-blockage did not immediately lead to a change in separation behavior. In a similar experiment, samples taken from the permeate over the course of filtration resulted in nearly constant protein and DNA concentrations (Figure 4-20b).

Appropriate flux for the filtration at lower wall shear rates was determined by the mass balance method [Kröber, 2008]. Influenza virus A/PR/8/34 (H1N1) RKI propagated in roller bottles with V-Medium was used in the experiment. Supernatant was clarified by centrifugation (4.2.2) and inactivated chemically prior to TFUF. Small volumes of supernatant (30 ml) were concentrated about three to four-fold at two levels for the flux (19 and 38 L m^{-2} h^{-1}) and three levels for the wall shear rate (1700, 3400 and 4200 s^{-1}). Recovery of the virus in retentates was determined by analysis of HA and NA activity. At the higher flux of 38 L m^{-2} h^{-1}, higher wall shear rate led to improved recovery of HA activity starting from 24% at the lowest up to 71% at the highest wall shear rate. At the lower flux of 19 L m^{-2} h^{-1}, the increase was less pronounced. The highest recovery of 91% was reached at the wall shear rate of 3400 s^{-1}. At the highest wall shear rate, recovery was slightly lower again with 87%. Recoveries based on NA activity closely resembled recoveries based on HA activity.

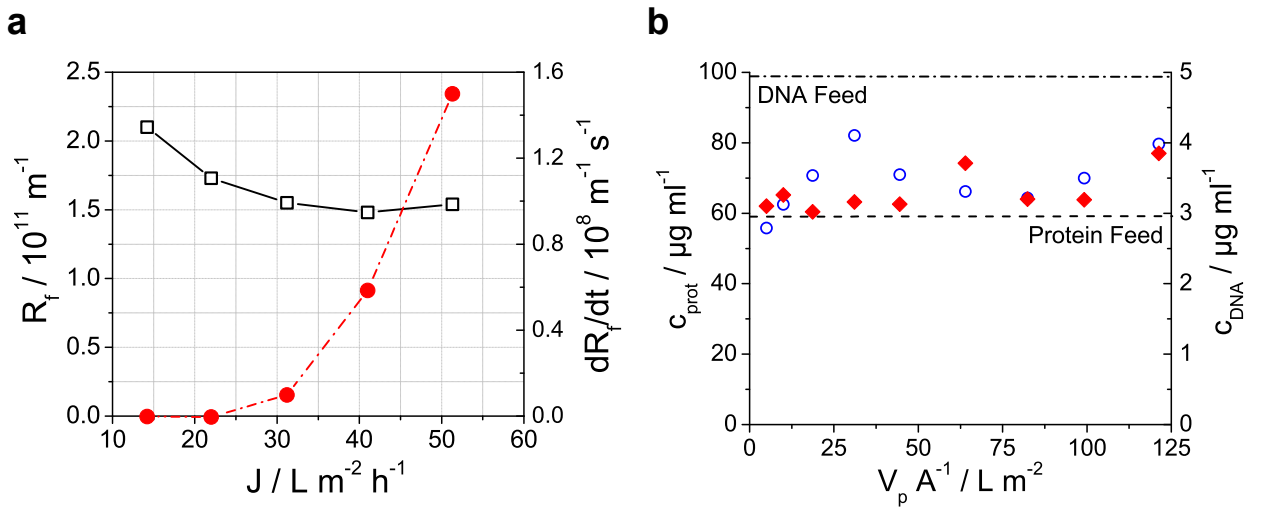

Figure 4-20. Fouling of hollow-fiber modules.

Filtration resistance (□) and fouling rate (●) as a function of flux (a). Supernatant was concentrated at a constant wall shear rate of 9 500 s^{-1} and various levels for the flux. A 750 kDa hollow-fiber module of 60 cm length was used for filtration. The fouling rate was determined as the first derivative of overall filtration resistance in time. Protein (○) and DNA (♦) concentrations in the permeate over total permeate volume normalized by the membrane area (b). Concentrations in the feed are indicated by horizontal lines.

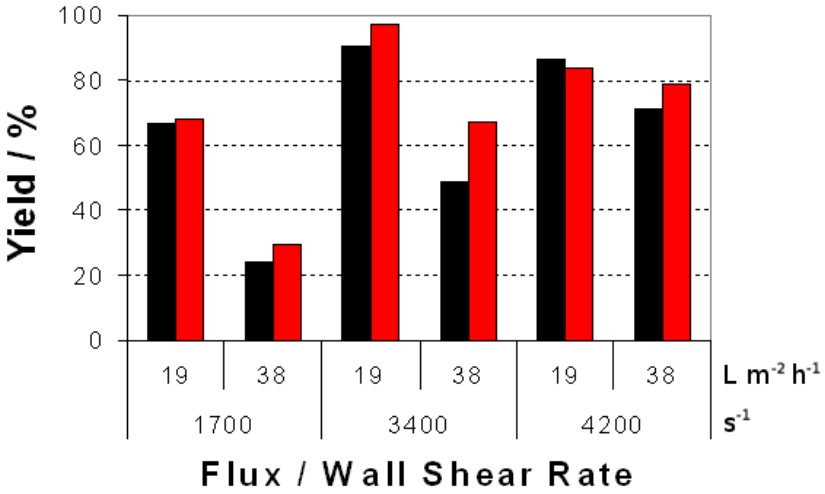

Figure 4-21. Optimization of flux by the mass balance method.

Yields of HA (■) and NA (■) activity after three to four-fold concentration of virus-containing supernatant. Filtration was conducted at different combinations for the flux and wall shear rate.

4.4.2 Preparative Concentration

In order to confirm the results from previous experiments and for the preparation of feed material for use in SEC (4.5.1), six independent concentration runs were conducted at larger scale during development of the first process [Kalbfuss, Genzel, et al., 2007]. Runs were fed with at least 1.8 L of supernatant containing influenza virus A/PR/8/34 (H1N1) NIBSC, which had been propagated in roller bottles using Ex-Cell MDCK medium. Supernatant was clarified twice by normal-flow filtration (4.2.1) and inactivated chemically prior to tangential-flow filtration. A single hollow-fiber module with 750 kDa cut-off, 225 cm^2 membrane area and of 60 cm length was used in preparations. Filtrations were conducted either at a constant flux of 42 L $m^{-2} h^{-1}$ or 28 L $m^{-2} h^{-1}$ (three runs each) and a wall shear rate of 9500 s^{-1}. Fractions from each run were analyzed for HA activity, protein and DNA concentration. Extinction of light at a wavelength of 700 nm was determined as a measure of turbidity. Material balances of individual runs and their statistics are presented in Table 4-26. Analyses of concentrates, sieving coefficients and impurity measures are given in Table 4-27. High product yields could only be achieved at the lower flux of 28 L $m^{-2} h^{-1}$ (97% compared to 44% at 42 L $m^{-2} h^{-1}$). The reduction of protein and DNA in concentrates (16% and 33% of their initial mass at 28 L $m^{-2} h^{-1}$, 11% and 19% at 42 L $m^{-2} h^{-1}$) was comparable to results obtained in the scouting experiment (12% and 39%). Concentrations conducted at a flux of 28 L $m^{-2} h^{-1}$ resulted in specific protein and DNA impurities of 4.8 ± 1.6 and 1.1 ± 0.7 µg $kHAU^{-1}$ compared to 6.9 ± 3.9 and 1.2 ± 0.9 µg $kHAU^{-1}$ for concentrations conducted at 42 L $m^{-2} h^{-1}$. Sieving coefficients for protein and DNA seemed to be slightly higher for runs at 42 L $m^{-2} h^{-1}$ (86% and 67% compared to 69% and 53% at 28 l $m^{-2} h^{-1}$). It should be noted, however, that protein concentrations in the feeds and permeates of runs 4 and 5 were close to the limit of detection. Coefficients based on these measurements possibly suffer from bias.

Table 4-26. Material balances of preparative concentrations.

		Concentrate (+ Wash)			Permeate			Total Recovery		
Run	**Flux**	**HA[1]**	**Prot.[2]**	**DNA[3]**	**HA**	**Prot.**	**DNA**	**HA**	**Prot.**	**DNA**
	L m^{-2} h^{-1}	%	%	%	%	%	%	%	%	%
1	42	51	13	26	n.d.[5]	91	64	51	104	90
2	42	49	11	12	n.d.	84	57	49	95	69
3	42	31	9	19	n.d.	85	79	31	94	98
Mean		**44**	**11**	**19**		**86**	**67**	**44**	**97**	**86**
± Std[4]		**± 11**	**± 2**	**± 7**		**± 4**	**± 11**	**± 11**	**± 5**	**± 15**
4	28	101	19[a]	34	n.d.	66[a]	51	101	85	85
5	28	114	13[a]	24	n.d.	57[a]	60	114	71	84
6	28	76	15	41	n.d.	83	50	76	98	91
Mean		**97**	**16**	**33**		**69**	**53**	**97**	**85**	**87**
± Std		**± 19**	**± 3**	**± 8**		**± 13**	**± 5**	**± 19**	**± 14**	**± 4**

1: HA activity, 2: total protein, 3: double-stranded DNA, 4: standard deviation, 5: not detectable. a: protein concentrations used in calculations were close to the limit of detection.

Note: Total recovery was defined as the total mass or activity recovered in the concentrate, wash and permeate.

Table 4-27. Analyses of concentrates, sieving coefficients and impurity measures of preparative concentrations.

		Concentrate				Sieving Coeff.		Impurity		
Run	**Flux**	**a_{HA}[1]**	**c_{prot}[2]**	**c_{DNA}[3]**	**Ext_{700}[4]**	**Prot.**	**DNA**	**Prot.**	**DNA**	**Turbidity**
	L m^{-2} h^{-1}	KHAU (0.1 ml)$^{-1}$	µg ml^{-1}	µg ml^{-1}	O.D.	%	%	µg kHAU^{-1}	µg kHAU^{-1}	O.D. 0.1 ml kHAU^{-1}
1	42	2.6	136	33	0.024	92	65	5.3	1.3	0.009
2	42	3.1	127	9	0.035	85	58	4.1	0.3	0.011
3	42	1.4	161	31	0.038	87	80	11.4	2.2	0.027
Mean		**2.4**	**141**	**24**	**0.032**	**88**	**68**	**6.9**	**1.2**	**0.016**
± Std		**± 0.9**	**± 18**	**± 13**	**± 0.007**	**± 3**	**± 12**	**± 3.9**	**± 0.9**	**± 0.010**
4	28	3.3	177	38	0.057	67[a]	51	5.4	1.2	0.017
5	28	5.6	169	20	0.060	58[a]	60	3.0	0.4	0.011
6	28	3.3	200	54	0.057	85	51	6.1	1.6	0.017
Mean		**4.1**	**182**	**37**	**0.058**	**70**	**54**	**4.8**	**1.1**	**0.015**
± Std		**± 1.3**	**± 16**	**± 17**	**± 0.002**	**± 14**	**± 5**	**± 1.6**	**± 0.7**	**± 0.004**

1: volumetric HA activity, 2: total protein concentration, 3: double-stranded DNA concentration, 4: extinction of light at 700 nm, 5: standard deviation. a: Protein concentrations were close to the limit of detection.

Note: Sieving coefficients were calculated as the ratio of permeate concentration to initial feed concentration. Impurity measures were defined as the ratios of contaminant concentration or turbidity to volumetric HA activity.

Analysis of supernatants and concentrates by non-reducing SDS-PAGE indicated the enrichment of several protein bands (Figure 4-22a, left side). Among these the hemagglutinin protein at approximately 66 kDa and the influenza virus matrix protein at approximately 26 kDa could be identified by tryptic digestion and tandem mass spectrometry (data not shown). Even though separation is based on size, the cut-off of the membrane cannot be seen since proteins and biological membranes are denatured during SDS-PAGE. Analysis of the same fractions by agarose gel electrophoresis (Figure 4-22a, right side) revealed a DNA ladder typical for apoptotic cells [Darzynkiewicz et al., 1997]. Since DNA was run under native conditions a reduction of smaller DNA fragments could be seen in concentrates due to the membrane cut-off. Moreover, individual bands of the ladder seemed to be slightly shifted. Particle volume distributions acquired by dynamic light scattering analysis gave similar results for concentrations at a flux of 28 L $m^{-2} h^{-1}$ (Figure 4-22b). Shoulders in the distributions resulted from averaging of individual measurements (six per sample). Modal values of distributions were around 100 nm, which corresponds to the average size of influenza A virions [Lamb et al., 2001]. Common to all distributions was a long tail towards larger diameters.

Aging of the hollow-fiber module was monitored routinely by measuring the filtration resistance with PBS before filtration and after regeneration (Figure 4-23a). A drop of the resistance from about $1.2 \cdot 10^{12}$ to $0.6 \cdot 10^{12}$ m^{-1} was observed over time indicating a change in the pore structure of the membrane. It became further evident, that the regeneration procedure was not sufficient to clean the membrane completely. Subsequent sanitization with sodium hydroxide over night resulted in a further reduction of filtration resistance in almost all cases (compare to the resistance before filtration of the next run). The presumable change in pore structure also became evident when looking at filtration resistance. From run 11 on strong initial fouling of the hollow-fiber module was observed (Figure 4-23b). This was in part reflected by the larger discrepancy between the initial filtration resistance and the resistance after regeneration as measured with PBS.

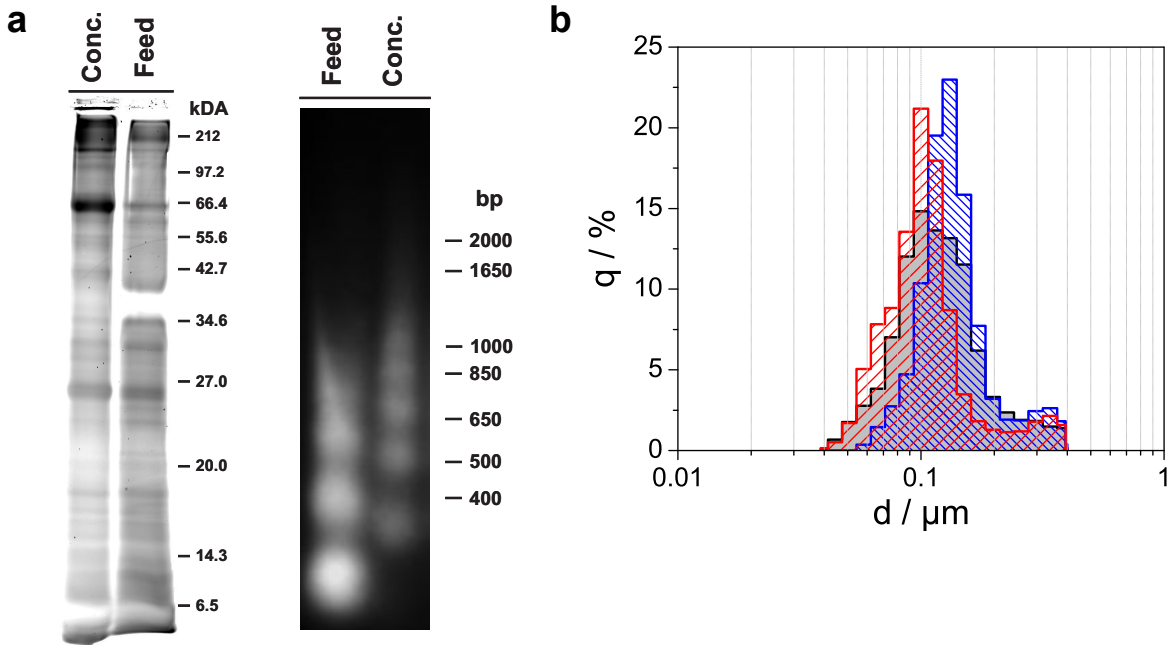

Figure 4-22. Characterization of virus concentrates.

Non-reducing SDS–PAGE and agarose gel electrophoresis of samples from the feed and concentrate of a preparative concentration run conducted at 28 L m^{-2} h^{-1} (a). Corresponding particle volume distributions of three concentrates (b). Distributions were obtained by dynamic light scattering analysis. Averages from six measurements per sample presented.

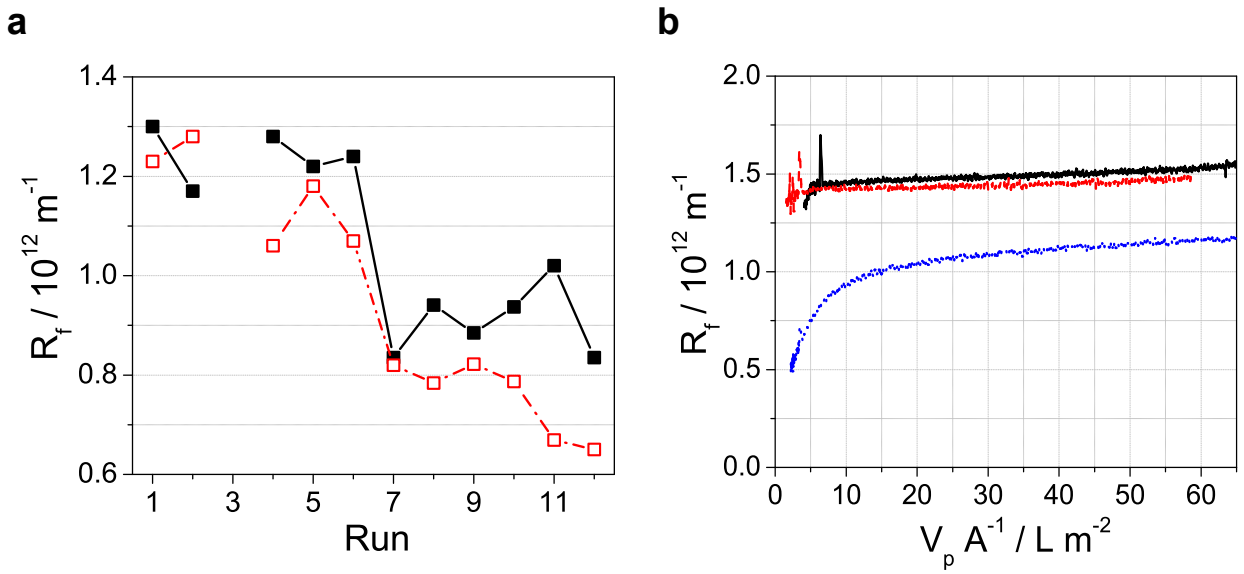

Figure 4-23. Aging of hollow-fiber modules.

Filtration resistance before filtration (□) and after regeneration (■) measured with PBS for the 225 cm^2 hollow-fiber module (a). No data were recorded for run three. Filtration resistance over filtrate volume normalized by membrane area for runs 8 (—), 9 (- - -), and 11 (· · ·) (b). All runs were conducted at a constant flux of 28 L m^{-2} h^{-1}.

4.4.3 Preparative Concentration and Diafiltration

Concentration by TFUF followed by DF was applied after selective precipitation of DNA (4.3) in the second process [Kröber, 2007; Eisold, 2007]. DF was included in order to remove residual PEI from viral concentrates. At the same time ionic strength was adjusted for subsequent adsorptive IEC (4.5.2.5). Runs were fed with at least 1.5 L of supernatant containing influenza virus A/PR/8/34 (H1N1) RKI ($N = 1$) or A/Wis/67/2005 (H3N2) ($N = 4$), which had been propagated in roller bottles using V-Medium. A single hollow-fiber module with 750 kDa cut-off, 420 cm^2 membrane area and of 30 cm length was used in preparations. Filtrations were generally operated at a wall shear rate of 3800 s^{-1} and a constant flux of 19 L m^{-2} h^{-1}. Volume concentration was approximately 5-fold. A primary DF step using buffer of high ionic strength (0.6 M NaCl) was included in order to break ionic interactions between PEI and the virus. A secondary DF step with buffer of modest ionic strength (0.15 M or 0.2 M NaCl) was performed in preparation of IEC. Each DF was run at constant volume against four exchange volumes of buffer (i.e. eight exchange volumes in total). HA and NA activity were used for quantitation of virus. Measured values for both activities were corrected by subtraction for activities in permeates. This correction is based on the assumption that overall activity is constituted not only by virions but also smaller compounds that are fully permeable. In the case of HA activity, leak activity in permeates was due to agglutination of erythrocytes by PEI [Boeckle, 2004]. The source of NA activity in permeates remains unclear but may be attributed to cellular neuraminidases.

HA and NA activities of the single batch with A/PR/8/34 (H1N1) RKI prior to filtration were 270 HAU $(0.1\ ml)^{-1}$ and 19.4 µM min^{-1}, respectively (corrected values presented). Average activities of the four batches with A/Wis/67/2005 (H3N2) were significantly lower with 92 ± 29 HAU $(0.1\ ml)^{-1}$ and 1.29 ± 0.031 µM min^{-1} (arithmetic mean ± standard deviation reported in all cases). In addition, a decay in activity was observed for these batches by more than 50% compared to activities at the time of harvest (see Table 4-20 for comparison).

Similar to results reported for A/PR/8/34 (H1N1) NIBSC propagated in Ex-Cell MDCK medium, concentration of virus was almost lossless regarding HA activity with 94 ± 28% recovered in retentates (Table 4-28). Yields of NA activity, in contrast, were lower with only 75 ± 5%. Even worse, step yields of subsequent DF steps indicated significant loss of NA activity with only 21% and 47%. Latter values are, however, only based on the single batch with A/PR/8/34 (H1N1) RKI. Yields of HA activity after DF were likewise lower with 78 ± 11% and 82 ± 13%. The difference,

however, was not as pronounced as for NA activity. Total recoveries of HA activity were between 77% and 93% in all steps. Overall yield of HA activity was 57% after the second DF step compared to only 7.3% for NA activity.

Concerning DNA, a reduction to 15 ± 0.8% of the initial amount was observed after the concentration step. The content of DNA was further reduced to 3.3 ± 4.0% and 25 ± 19% after DF, which multiplies to an overall reduction down to 0.13% of the initial amount. It should be noted, however, that values measured after the concentration step had to be extrapolated due to the calibration procedure applied for the compensation of matrix interference by cell culture medium (see 3.1.4). These values, therefore, likely suffer from bias. Accordingly, the balance of the following DF step does not close with a total recovery of 8.4 ± 4.5% only. Total recovery of the second step was 86 ± 53% and thus close to 100%, again, but results suffer from great experimental error due to very low concentrations at this stage. Since initial concentrations of DNA were consistent for all batches 7.13 ± 0.62 µg ml^{-1} before and 759 ± 9 ng ml^{-1} after

Table 4-28. Material balances for preparative concentration and diafiltration

Step	Fraction	HA[1] Yield / %			NA[2] Yield / %			DNA[3] Yield / %		Conc.[4] /
		step	corr.[5]	overall[6]	step	corr.	overall[6]	step	overall	ng ml^{-1}
Concent.[7]	**Retentate**	75 ± 17	**94 ± 28**	**94**	73 ± 7	**75 ± 5**	**75**	**15 ± 0.8**	**15**	780 ± 20
	Permeate	18 ± 17			1.2 ± 1.0			61 ± 0.7		
	Total	93 ± 26			74 ± 7			102 ± 0.6		
1st Diafilt.[8]	**Retentate**	74 ± 9	**78 ± 11**	**73**	21	**21**	**16**	**3.3 ± 4.0**	**0.50**	39 ± 31
	Permeate	4 ± 9			0.93			3.1 ± 1.4		
	Total	77 ± 12			21			8.4 ± 4.5		
2nd Diafilt.	**Retentate**[8]	82 ± 13	**82 ± 13**	**57**	46	**47**	**7.3**	**25 ± 19**	**0.13**	14 ± 15
	Permeate	0			1.8			8.3 ± 16.6		
	Total	82 ± 13			47			86 ± 53		

1: based on HA activity, 2: based on NA activity, 3: double-stranded DNA, 4: double-stranded DNA concentration, 5: yield corrected for leak activity in permeates, 6: overall yield based on corrected yields, 7: concentration step, 7: diafiltration, 8: includes activity and DNA found in membrane wash

Note: Average values (arithmetic mean ± standard deviation) from five experiments are presented except for NA activity after DF (N = 1) and DNA (N = 4).

precipitation), average concentrations were summarized in the last column of Table 4-28. The concentration of DNA remained constant after the concentration step with 780 ± 20 ng ml^{-1}. However, significant reduction of the DNA concentration was observed after the first and second DF step with 39 ± 31 ng ml^{-1} and 14 ± 15 ng ml^{-1}, respectively.

4.5 Chromatography

4.5.1 Size-Exclusion Chromatography

4.5.1.1 Empirically Established Size-Exclusion Chromatography

SEC operated in group separation mode was established for intermediate purification of influenza virus and simultaneous conditioning for subsequent flowthrough AIEC (4.5.2.2) in the first process (Figure 1-5) [Kalbfuss, Wolff, Morenweiser, et al., 2007]. Experiments were exclusively conducted with influenza virus A/PR/8/34 (H1N1) NIBSC propagated in roller bottles with Ex-Cell MDCK medium (Table 4-25). Chromatography was fed with 20-fold concentrates prepared by TFUF (4.4.2).

In scouting experiments, columns one to four (packed with Sepharose CL-2B, Sepharose 4 FF, Sepharose 6 FF and Superdex 200 p.g.; see 3.7.1) were loaded with 10% of their column volume (cv). Virus concentrate from the same batch was used in all runs. UV absorbance of the effluent at a wavelength of 280 nm was acquired online. In addition, eluates were fractionated coarsely and analyzed offline for HA activity, total protein and DNA (Figure 4-24). The UV trace of all runs showed two distinct peaks corresponding to the K_{av}'s of the void volume and small solutes (data not shown). Between those peaks the UV trace did not reach the baseline completely. According to offline-measured HA activity, partial retention of the virus population could be observed with Sepharose CL-2B (largest pore size). For all other media, the virus eluted exclusively in the void volume. Protein and DNA mostly eluted between the two peaks visible in the UV trace. A shift was observed from larger to smaller K_{av}'s with decreasing pore size of the chromatography medium. In the case of Superdex 200 p.g. (smallest pore size) almost no separation between the virus and protein or DNA was achieved.

In principle, viral and host-cell proteins are not distinguishable by the protein assay used. The correlation of HA activity and total protein in the first fractions of runs with Sepharose CL-2B and

Sepharose 4 FF, however, suggested that the assay was mainly detecting viral proteins in these fractions. Based on this assumption, best separation of the virus from impurities was achieved with Sepharose CL-2B. Nevertheless, Sepharose 4 FF was chosen for preparative runs since elution of the virus occurred exclusively in the void volume. Elution in the void volume leads to narrower peaks (absence of mass transfer, no spread due to the size-distribution of the virus population) and hence less dilution of the product. In addition, Sepharose 4 FF is more rigid than Sepharose CL-2B and therefore better to handle (easier column packing, higher flow rates).

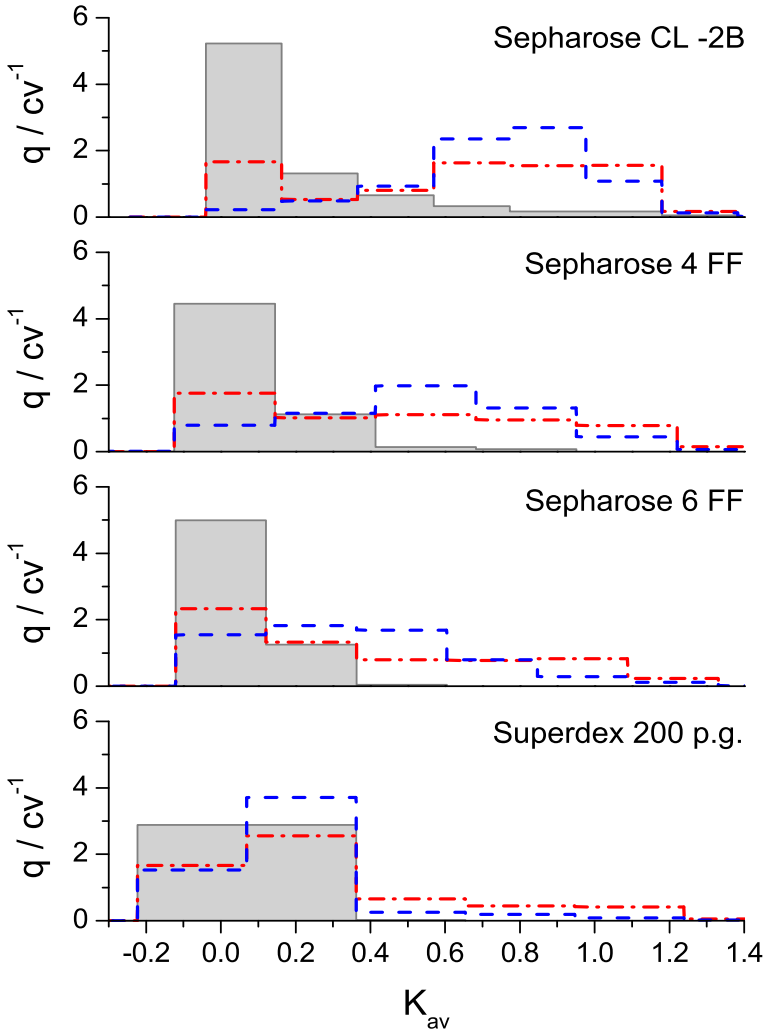

Figure 4-24. Scouting of SEC media.

Columns were loaded with 10% of their volume. Virus concentrate from the same batch was injected in all runs. Eluates were fractionated coarsely and analyzed offline for HA activity (▩), total protein (– –) and host-cell DNA (–·–). Density distributions were plotted over K_{av}. The exclusion limit of chromatography media decreases from top to bottom.

In the next step, column load was optimized for a good compromise between productivity and purity of the product. Column five was loaded with 0.07, 0.14 and 0.28 cv using virus concentrate from the same batch[10]. Again, UV absorbance of the effluent was acquired online and collected fractions were analyzed offline (Figure 4-25). Only the total protein concentration was considered for optimization since DNA can be removed more efficiently in the subsequent step. Similar to the scouting experiment with Sepharose 4 FF, HA activity seemed to correlate with total protein within first fractions. This time, due to the lower volume of collected fractions, the correlation became even more evident. However, no baseline separation between viral and host-cell proteins could be achieved even at the lowest load. In general, separation became worse with increasing volume load due to resulting peak broadening.

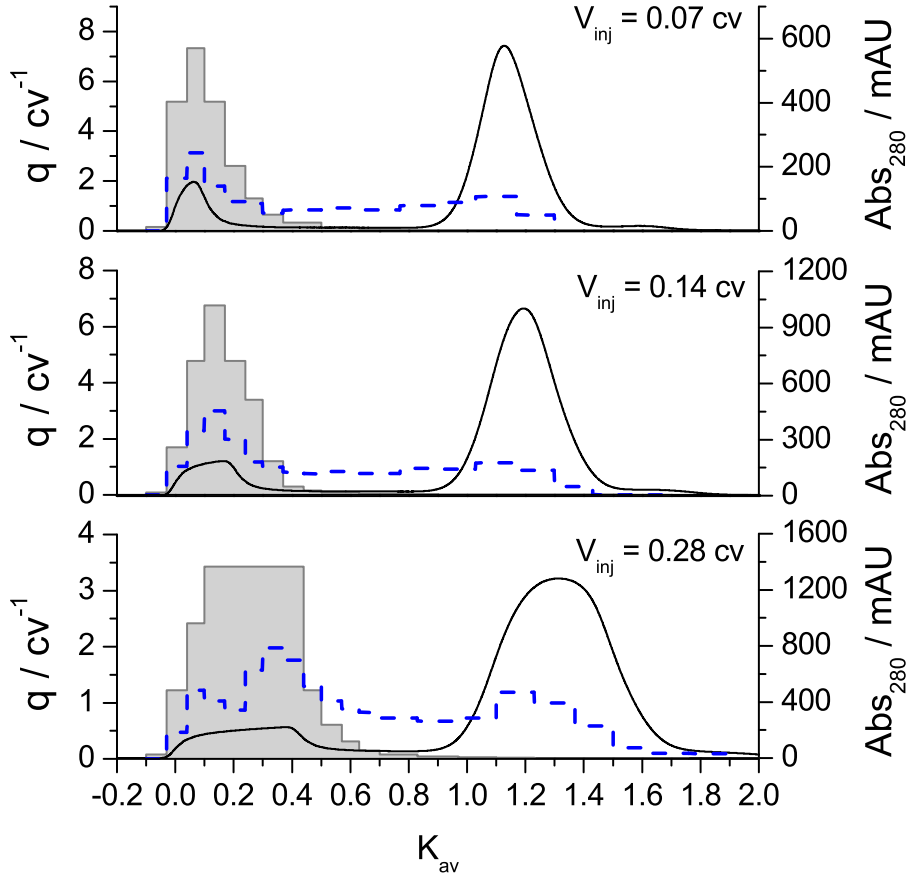

Figure 4-25. Loading study with Sepharose 4 FF.

Column five was loaded with 0.07, 0.14 and 0.28 cv. Eluates were fractionated at high resolution and analyzed offline for HA activity (▩) and total protein (– –). UV absorbance at 280 nm (—) and density distributions of HA activity and protein were plotted over K_{av}.

10 Data from this experiment is referred to as set A in the modeling study (4.5.1.2)

Fractionation limits were chosen such that approximately 95% of eluted HA activity is recovered in product fractions (Table 4-29). The left fractionation limit was set to 0.3 cv independently of load. The right fractionation limit was calculated based on injected volumes adding 0.14 cv for axial dispersion. Applying these limits, virtually pooled product fractions contained 93% of eluted HA activity on average. The amount of eluted total protein in product fractions increased from 35% for a load of 0.07 cv to 48% for a load of 0.28 cv. Productivity increased from 0.08 to 0.27 cv of feed per hour while dilution of the virus decreased from 0.32 to 0.64 (a yield of 95% was assumed for calculation). Depending on process requirements, productivity needs to be traded off vs. purity in SEC. The optimum clearly depends on product specifications. In the case of this study an arbitrary choice was made selecting a moderate load of 0.15 cv, which corresponds to a productivity of 0.15 cv of feed per hour.

Table 4-29. Yield, productivity and dilution in SEC on Sepharose 4 FF as a function of the column load

Load[a]	Prod. Fraction[b]		Yields[c]		Run Time[d]	Prod.[e]	Dilution[f]
	Start	Stop	HA	Protein			
cv	cv	cv	% (Eluate)	% (Eluate)	h	cv h^{-1}	
0.07	0.3	0.51	87	35	0.92	0.08	0.32
0.14	0.3	0.58	96	44	0.95	0.15	0.48
0.28	0.3	0.72	96	48	1.02	0.27	0.64

a: normalized feed volume injected onto column, b: normalized limits of the product fraction, c: percentage yield of eluting HA activity and total protein, d: duration of one injection-elution cycle, e: normalized feed volume processed per hour, f: dilution of the product assuming a yield of 95%.

For determination of the maximum number of injections before regeneration is required, column five was loaded 13 times with 0.15 cv of virus concentrate[11]. An overlay of UV traces is given in Figure 4-26. UV traces were almost indistinguishable. Virus-containing product fractions were collected within 0.30 to 0.58 cv elution volume. Individual runs were assigned to five groups and pooled product fractions from each group were analyzed for HA activity. There was no indication of decreasing yield. HA activities of pools were found identical within the precision of the assay.

11 equivalent of a complete batch produced in roller bottles

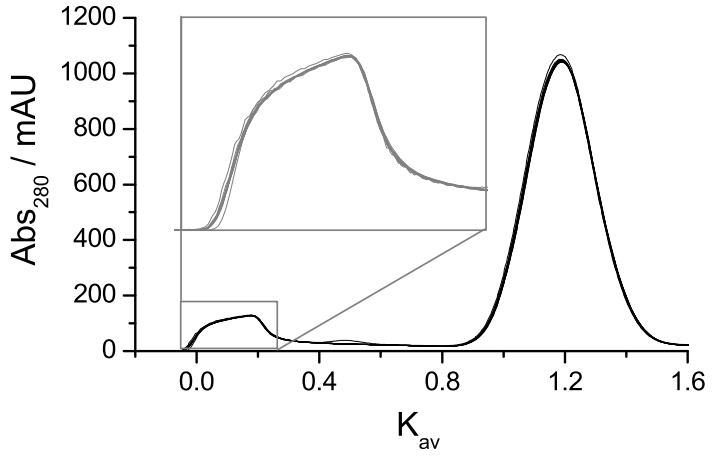

Figure 4-26. Fouling of SEC column.
Overlay of UV traces from 13 subsequent injections onto column packed with Sepharose 4 FF. Column was loaded with 0.15 cv of virus concentrate from the same batch. No change in the separation behavior was observed.

For the preparation of larger amounts of purified virus subsequently fed into flowthrough (4.5.2.2), column six had to be loaded multiple times with 0.15 cv of virus concentrate. Only two fractions were collected: a product and a waste fraction. The product fraction was collected from 0.30 to 0.58 cv elution volume, the waste fraction from 0.58 to 1.91 cv. Typically, three to five injections were necessary in order to process one batch. Volumetric HA activities, protein and DNA concentrations from four independent preparations have been summarized in Table 4-30. The product yield based on HA activity was 85% on average, corresponding to 95% of eluted HA activity. Total recoveries were slightly higher with 89% on average. About 10% of loaded HA activity was lost in chromatography. The amounts of total protein and DNA in product fractions were reduced to 35% and 34% of injected amounts, respectively. Noteworthy, material balances for protein and DNA did not close. On average, total recoveries were 69% and 136% for protein and DNA, respectively.

Table 4-30. Material balances of preparative SEC on Sepharose 4 FF

Batch	Feed				Product Eluate Fraction				N_{inj}[e]
	V[a]	a_{HA}[b]	c_{prot}[c]	c_{DNA}[d]	V	a_{HA}	c_{prot}	c_{DNA}	
	ml	KHAU (0.1 ml)$^{-1}$	µg ml^{-1}	µg ml^{-1}	ml	KHAU (0.1 ml)$^{-1}$	µg ml^{-1}	µg ml^{-1}	
1	37	3.31	185	37.1	69	1.73 (96 %)	33.1 (33 %)	6.62 (33 %)	4
2	28	4.27	167	20.2	51	1.89 (81 %)	32.5 (36 %)	4.95 (45 %)	3
3	47	2.72	200	53.9	86	1.17 (79 %)	33.0 (30 %)	7.52 (26 %)	5
4	47	3.24	146	30.5	86	1.50 (85 %)	32.3 (40 %)	5.39 (32 %)	5
Mean		3.38	174	35.4		1.57	32.7	6.12	
Std		± 0.64	± 23	± 14.1		± 0.31 (85%)	± 0.4 (35%)	± 1.17 (34%)	

a: total volume, b: volumetric HA activity, c: total protein concentration, d: DNA concentration, e: number of injections

Note: Virus concentrates from ultrafiltration were purified by SEC. Three to five injections were necessary to process one batch. Average activities and concentrations are reported for each batch. Yields of analyzed species are given in brackets below. Arithmetic means and standard deviations for all batches are provided at the bottom.

4.5.1.2 Optimization of Volume Load in a Modeling Study

The preparative SEC operation described in the previous section has been established fully empirically. Although some effort was put into maximizing purity and productivity, it is to be assumed that operating conditions were still sub-optimal. The influence of mobile phase velocity, for instance, had been totally neglected. The reason was that empirical optimization constitutes a laborious task due to the many parameters involved. The two-dimensional parameter space by injection volume and mobile phase velocity alone would require at least 10 to 20 experiments for adequate characterization. It is needless to say that such effort is unrealistic in most cases. Hence, in order to reduce the number of experiments, a modeling framework based on linear systems theory was developed for predicting the influence of volume overloading [Kalbfuss, Flockerzi, et al., 2008]. Chromatograms resulting after extended injection of virus-containing sample were simulated by convolution of impulse-responses with rectangular injection profiles. Impulse-responses characterizing system behavior were derived from experimental data by maximum

entropy deconvolution. By application of this framework, the investigated parameter space was reduced by one dimension. In addition, chromatography at three different mobile phase velocities was conducted for obtaining a first impression of its impact on separation performance.

The first experimental set A used in this study comprises three chromatography runs conducted at a constant superficial mobile phase velocity of 60 cm h^{-1} but different injection volumes (0.07, 0.14 and 0.28 cv). It was derived from data of the three chromatography runs illustrated in Figure 4-25. Global impulse-responses were determined for each signal (UV absorbance, HA activity and total protein). Values between $2\varepsilon_{NNLS}$ and $6\varepsilon_{NNLS}$ were set as the limit for misfit in MaxEnt deconvolution. All chromatograms, including impulse-responses, were normalized to represent true density distributions of elution volume. An overlay of all three responses and original data is provided in Figure 4-27 (bold lines). For clarity, the response to an injection of 0.14 cv was omitted from the plot of total protein.

UV absorbance showed two distinct peaks near the total exclusion and inclusion limits. Absorbance was low but not zero between these peaks. The impulse-response for UV absorbance was almost identical to the chromatogram obtained after the shortest injection (0.07 cv), but both peaks were narrower. Virions reflected by HA activity eluted in a single tailing peak with maximum between 0.3 and 0.55 cv. Similar to UV absorbance, the impulse-response was close to the chromatogram obtained after the shortest injection. Elution of total protein, in contrast, was spread over a wide range from 0.3 to 1.2 cv. A definite peak coinciding with the peak of eluting virions indicated that viral protein was detected in these fractions.

Impulse-responses for UV absorbance, HA activity and total protein were used to simulate original data, i.e. chromatograms were predicted for injections of 0.07, 0.14 and 0.28 cv, by convolution with experimentally determined injection profiles. Results of simulations are provided in Figure 4-27 (thin lines). A perfect match was obtained for UV absorbance – the signal of highest quality. Slight deviation was observed for HA activity but original data was well resembled. Significant mismatch was, in contrast, observed for total protein but the principle features of original data were still reflected. This mismatch was particularly evident at the highest load.

A second set B was acquired for characterizing the impact of mobile phase velocity on separation. Three chromatography runs were conducted by injection and elution of 0.05 cv at different mobile

phase velocities (30, 60 and 120 cm h^{-1}). Due to a limitation in starting material, a different batch of virus concentrate had to be used. Moreover, the eluent employed was of lower ionic strength (only 0.2 M compared to 0.65 M NaCl)[12]. In addition to UV absorbance, scattering of red laser light at an angle of 90° was acquired as an online signal. A uniform value of $5\varepsilon_{NNLS}$ was used as the limit for misfit in MaxEnt deconvolution. Based on the assumption of pure virus in early fractions an attempt was made to reconstruct the impulse-response for host-cell protein (HCP). Impulse-responses for the different mobile phase velocities are illustrated in Figure 4-28.

Results for HA activity were almost indistinguishable. If at all, peak tailing was less pronounced at higher mobile phase velocities. Significant differences were, in contrast, observed for total protein and hence HCP. In the case of total protein, a second peak at about 0.8 cv could be observed at the lowest mobile phase velocity of 30 cm h^{-1}. At 60 cm h^{-1} this peak was less pronounced and shifted towards lower elution volume (about 0.6 cv). At the highest mobile phase velocity of 120 cm h^{-1} the peak had merged almost completely with the peak of virus protein, being merely visible as a shoulder. This trend could be followed even more clearly in reconstructions for HCP. The peak previously located at 0.8 cv became wider and shifted towards lower elution volume with increasing mobile phase velocity similar to the 201 kDa PMA shown in Figure 2-9b.

Experimentally determined impulse-responses (both sets) were used to simulate the outcome of preparative SEC for the separation of virions from HCP. Firstly, maximum purity was estimated from cumulative distributions of elution volume in the limiting case of an infinitely short injection[13]. The lower limits of product fractions were set to 0 cv, the upper limits were chosen such that 90% of eluting HA activity are collected in product fractions. The content of light scattering area (only set B), UV area, total protein and HCP in product fractions was calculated accordingly. Results for all signals are summarized in Table 4-31. Good correlation of light scattering area and HA activity was observed in all cases (86 to 90%) indicating a high specificity of the light scattering detector for virions. The minimum content of total protein increased from 30% to 40% with increasing mobile phase velocity in the case of set B. Similarly the estimated

12 The high ionic strength of the eluent used in set A had only been necessary for pre-conditioning to subsequent flowthrough AIEC.

13 i.e. from integrals of impulse-responses

content of HCP increased from 0.2 to 9.3%. Prediction for total protein in the case of set A was slightly higher with 44%[14] but content of HCP was similar (5.9% and 6.4%).

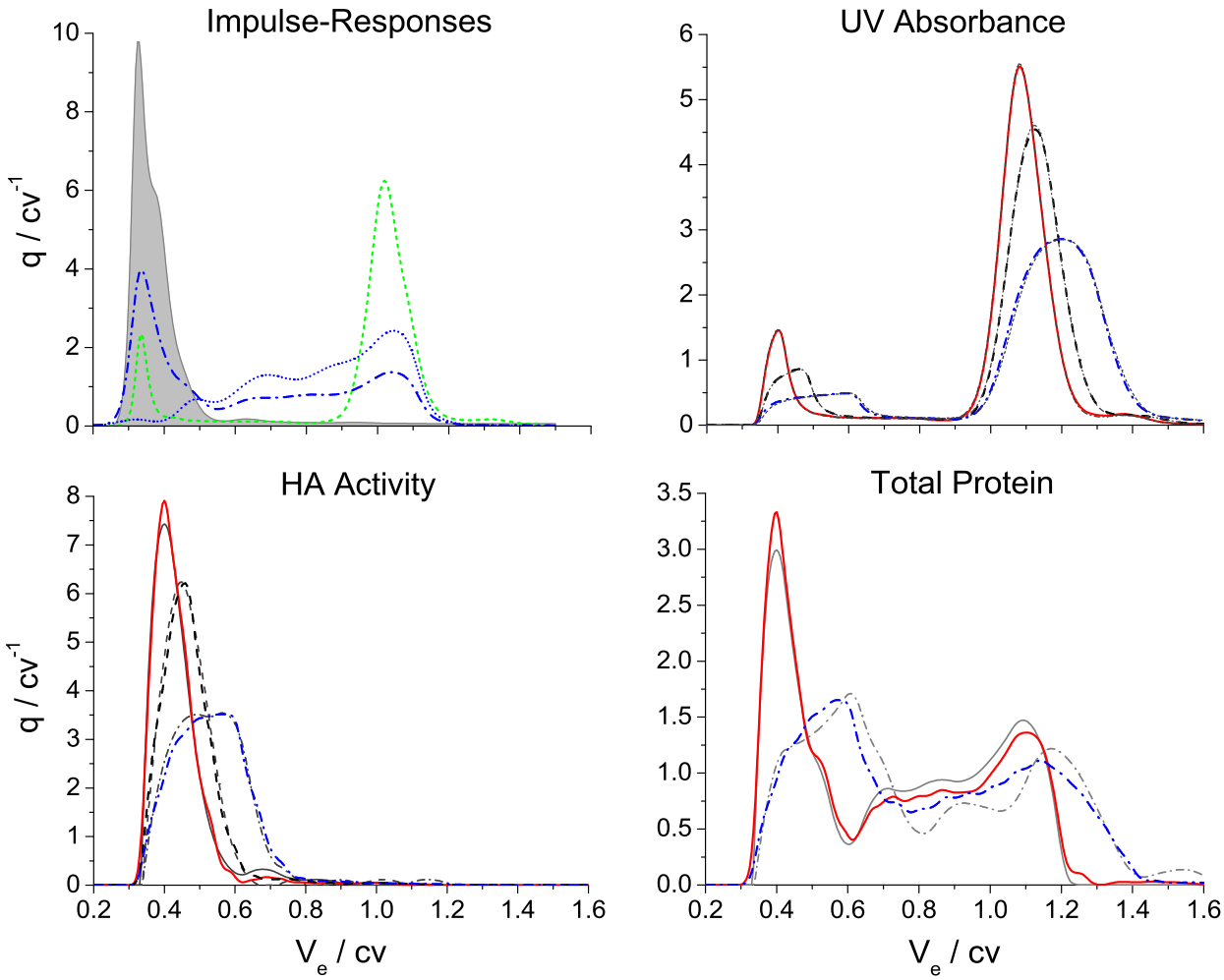

Figure 4-27. Impulse-responses and simulations at a constant superficial mobile phase velocity.

Impulse-responses for UV absorbance (---), HA activity (■), total (– –) and host-cell protein (···) at a constant superficial mobile phase velocity of 60 cm h^{-1} (upper left corner). Impulse-responses were determined from a set of three chromatograms by maximum entropy deconvolution. Distributions of UV absorbance were acquired online, distributions of HA activity and total protein were determined offline. The impulse-response for host-cell protein was reconstructed from distributions of HA activity and total protein under the assumption of pure virus in early fractions. Results were used to simulate original data. Overlays of original data (bold lines) and simulations (thin gray lines) for injections of 0.07 (—), 0.14 (---) and 0.28 cv (–·–) are provided in remaining graphs. For clarity, results for 0.14 cv were omitted from the plot of total protein.

14 compared to set B at a superficial mobile phase velocity of 60 cm h^{-1}

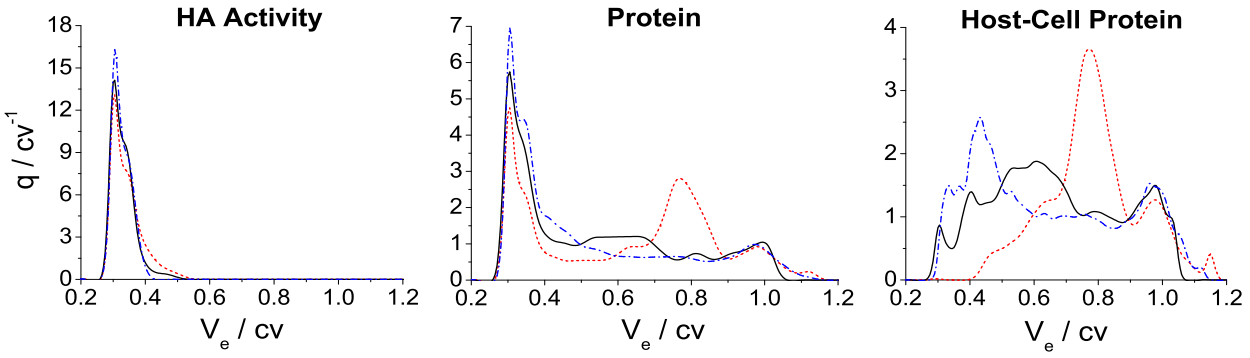

Figure 4-28. Impulse-responses for HA activity, total and host-cell protein at different superficial mobile phase velocities.

Injections of 0.05 cv were eluted at 30 (···), 60 (—) and 120 cm h^{-1} (- - -). Impulse-responses were determined by MaxEnt deconvolution. The impulse-response for host-cell protein was reconstructed from distributions of HA activity and total protein. Results for HA activity were almost indistinguishable. Impulse-responses for total protein and particularly host-cell protein showed strong a dependency on mobile phase velocity.

Table 4-31. Maximum purity at 90% yield of HA activity in the limiting case of an infinitely short injection.

			Product		Impurity		
Set	**u[a]**	**V_r[b]**	**HA[c]**	**LS[d]**	**UV[e]**	**Protein**	**HCP[f]**
	cm h^{-1}	cv	%	%	%	%	%
B	30	0.41	90	90	8.5	30	0.2
A	60	0.49	90	-	12.5	44	5.9
B	60	0.38	90	86	9.2	38	6.4
B	120	0.37	90	86	9.8	40	9.3

a: superficial mobile phase velocity, b: upper limit of product fraction, c: HA activity, d: light scattering area, e: UV area, f: host-cell protein

Secondly, finite injections with volumes ranging from 0.01 to 0.5 cv were considered (Figure 4-29). Impulse-responses determined from experimental set B were used in simulations assuming rectangular injection profiles. Lower limits of the product fraction were chosen flexibly to permit a loss of 1% of HA activity but are almost constant with values around 0.3 cv (data not shown). Upper limits of the product fraction were predicted as a function of injection volume such that 90% of HA activity are recovered (bold lines). Correlations are almost identical for all mobile phase velocities due to similar impulse-responses for HA activity.

The residual content of HCP (shaded areas) was predicted as a function of injection volume and the upper fraction limit[15]. Numbers in shaded areas denote the maximum content of HCP to be expected for a given value pair. Evidently, the degree of impurity increases with increasing injection volume and mobile phase velocity. The final content of HCP for the special case of 90% yield of HA activity can be determined along bold lines.

Similarly, the final concentration of virus normalized by the initial concentration and volumetric productivities are provided for the special case of 90% yield. Again, predicted concentrations are almost identical at different mobile phase velocities due to similar impulse-responses for HA activity. Concerning productivity, two strategies for elution were considered: In the first scenario, sample is injected and eluted at a constant mobile phase velocity. In the second scenario, mobile phase velocity is increased to 250 cm h^{-1} after virus has eluted[16] (referred to as two-step elution). A scheme of the second scenario is depicted in Figure 4-30. In both scenarios overlapping injection cycles were assumed. Naturally, productivity increases with injection volume and mobile phase velocity. A significant gain in productivity is achieved by the second elution strategy - in particular at the lowest mobile phase velocity. For higher mobile phase velocities the difference is less pronounced.

Crosshairs were included in the first diagram to give an example of how to read graphs. In this example, injection of 0.3 cv requires an upper fraction limit of 0.62 cv for 90% recovery of HA activity. The normalized concentration of HA activity after chromatography (0.9) and volumetric productivities (0.42 and 0.21 cv h^{-1}) are obtained at intersections of the vertical line with respective graphs (not shown). The maximum content of host-cell protein (5%) is indicated by the shaded area underneath.

Thirdly, injection volume was eliminated as a free parameter by setting limits for the final content of HCP. Accordingly, injection volume, the final concentration of product and productivity reduced to functions of mobile phase velocity alone. Simulation results for the two scenarios of 10% and 20% final HCP content are illustrated in Figure 4-31. As before, two strategies were considered for the calculation of productivity: a constant mobile phase velocity and two-step elution.

15 not necessarily the limit corresponding to 90% product yield

16 recommended maximum for Sepharose 4 FF

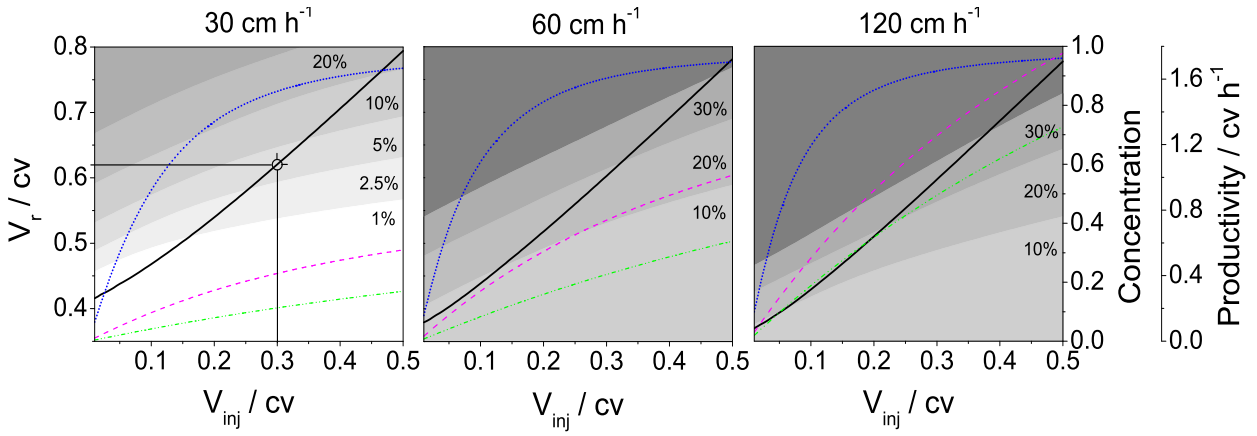

Figure 4-29. Model-based design of a preparative SEC operation for the separation of influenza virus from host-cell protein.

Upper limits of the product fraction V_r (—) were predicted as a function of injection volume V_{inj} (90% yield of HA activity). Corresponding normalized concentration of the virus (···) and volumetric productivities for a constant superficial mobile phase velocity (- · -) and two-step elution strategy (---) are provided in addition. The maximum residual content of host-cell protein is indicated by shaded areas underneath.

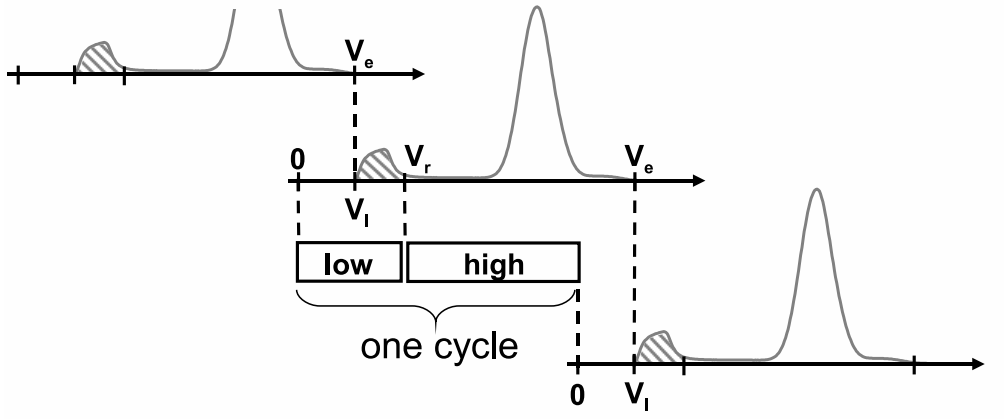

Figure 4-30. Two-step elution strategy for maximizing productivity in SEC.

Sample is injected and eluted in overlapping cycles with chromatograms of three cycles (UV trace over elution volume) being illustrated by cascaded graphs. Product (hatched area) elutes first and is to be separated from impurities (open area). Sample is injected and product eluted at low speed (respective phase marked by box "low"). The left and right limit of the product fraction are indicated by V_l and V_r. After elution of the product, resolution is no longer important and mobile phase velocity is increased to the maximum rate compatible with the chromatography medium (phase marked by box "high"). The endpoint of elution is denoted by V_e. The next cycle is started such that V_l and V_e match and there is no contamination of the product by residual impurities in the column.

Remarkably, the trend in productivity was inverse for both scenarios. For the lower limit of 10% HCP, productivity decreased with increasing mobile phase velocity. In contrast, for the higher limit of 20% a significant gain in productivity was achieved. Productivity of the two-step elution strategy was always higher than for elution at a constant mobile phase velocity. Since higher mobile phase velocities required the reduction of injection volume due to stronger band broadening, concentration of the product was likewise reduced. Higher mobile phase velocities also led to slight shortening (up to 0.27 cv) of injection-elution cycles due to a shift of HCP towards lower elution volumes (data not shown).

Finally, simulations based on impulse-responses from both sets were compared to the outcome of the preparative SEC operation that had been established before (4.5.1.1). Product yields based on HA activity and the final content of total protein (predicted and experimental) are given in Table 4-32. Predictions for the mobile phase velocities of 30 and 120 cm h^{-1} are provided for completeness. The yield of UV area was included as a precise but abstract measure. The content of HCP could not be determined in preparations due to lack of an appropriate assay. Light scattering measurements were neither available since the detector saturated for large injection volumes. Supplementary to data on yield and purity, productivities were included for both elution strategies. Note that the slight difference in productivities for set A and B at a mobile phase velocity of 60 cm h^{-1} result from differences in corresponding UV traces, which were used to determine the length of elution.

Average recovery of HA activity (95.8%) was close to the predicted value based on set B (98%). The same was true for the final content of total protein (50.2% compared to 52%). In general, both quantities were slightly overestimated by predictions based on set B and underestimated by predictions based on set A. Recovery of UV area, in contrast, was slightly underestimated by both sets (15.3% compared to 13% and 11%). Most striking was the difference in predicted HCP content (7.1% and 25%). Unfortunately, experimental data for comparison was not available here.

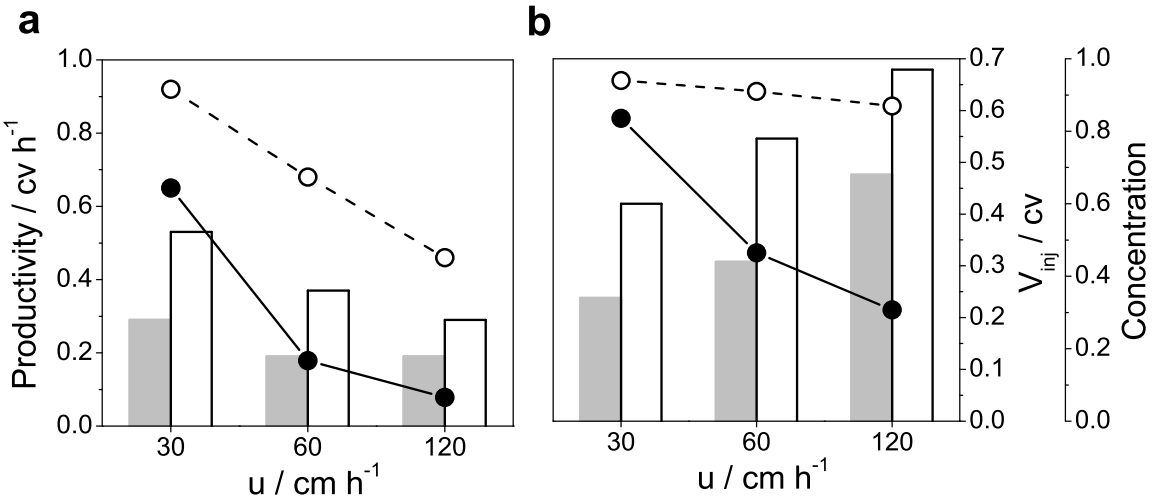

Figure 4-31. Performance of a simulated preparative SEC operation for the purification of influenza virus.

Limits of the product fraction were set to result in 90% yield of HA activity. Injection volume V_{inj} (●) was maximized under the constraint of 10% (a) or 20% (b) final content of HCP. The normalized concentration of virus (○) and productivity were predicted as functions of superficial mobile phase velocity. Productivity was calculated assuming a constant mobile phase velocity (shaded bars) or two-step elution strategy (non-shaded bars). Trends of productivity with respect to mobile phase velocity were inverse for 10% and 20% final content of host-cell protein. The two-step elution strategy yielded significant gains in productivity.

Table 4-32. Comparison of simulation results to experimental data from the previously established preparative SEC operation.

			Product		Impurities			Productivity	
Set	**u[a]**	**V_{inj}[b]**	**HA[c]**	**LS[d]**	**UV[e]**	**Protein**	**HCP[f]**	**Constant[g]**	**Two-Step[h]**
	cm h^{-1}	cv	%	%	%	%	%	cv h^{-1}	cv h^{-1}
B	30	0.15	97	95	9	35	4.1	0.11	0.25
A	60	0.15	90	-	13	45	7.1	0.21	0.37
B	60	0.15	98	97	11	52	25	0.22	0.44
B	120	0.15	98	98	14	60	37	0.49	0.72
Exp.[i]	60	0.15	95.8 ± 0.4	-	15.3 ± 1.4	50.2 ± 3.7	-		

a: superficial mobile phase velocity, b: normalized injection volume, c: HA activity, d: light scattering area, e: UV area, f: host-cell protein, g: elution at constant mobile phase velocity, h: two-step elution strategy, i: experimental data from 4 preparative runs (arithmetic mean ± standard deviation).

4.5.2 Ion-Exchange Chromatography

4.5.2.1 Virus Stability

Before chromatography, two experiments were conducted for investigating the stability of HA activity [Kalbfuss, Wolff, Morenweiser, et al., 2007]. In order to find a suitable pH working range, inactivated cell culture supernatant containing influenza virus A/PR/8/34 (H1N1) NIBSC propagated in ExCell MDCK medium was titrated to various pH and incubated at room temperature. Reactions were neutralized immediately after incubation and HA activity was analyzed (Figure 4-32a). Results revealed that HA activity was only stable within a narrow range between pH 7 and 8. At higher or lower pH degradation occurred. Under alkaline conditions the rate of degradation increased with increasing pH. Under acidic conditions maximum degradation was observed for a pH around 5. Below this maximum the rate of degradation reduced again. In contrast, elevated ionic strength beyond physiological conditions did not seem to affect HA activity. Adding up to 1.5 M of NaCl to SEC-purified virus (4.5.1) resulted in identical HA activities after incubation for 2 h at room temperature (Figure 4-32b). Ionic strength was hence chosen to control the adsorption-desorption process in AIEC.

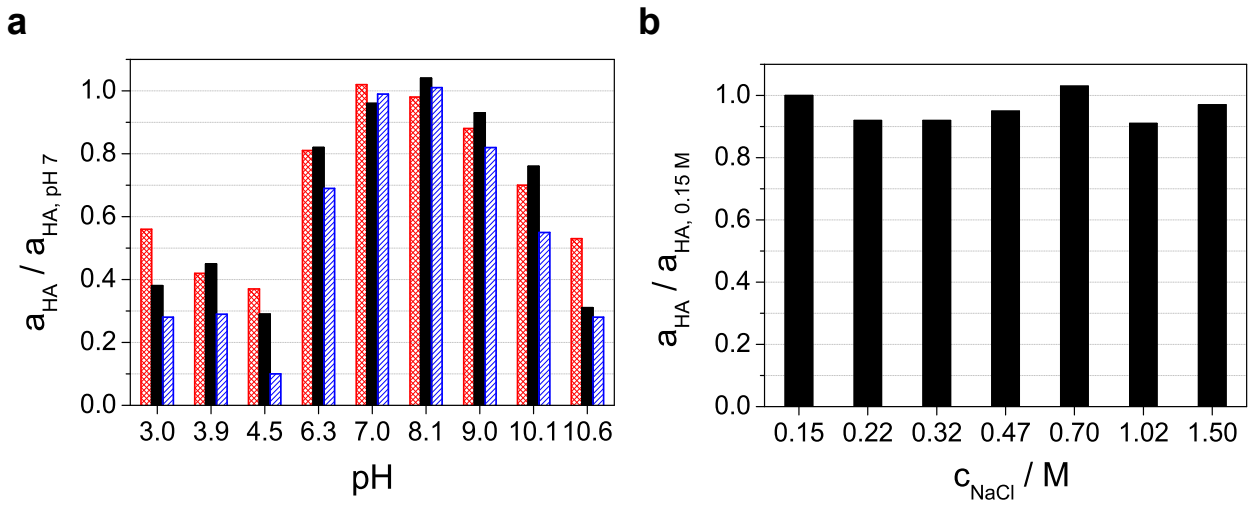

Figure 4-32. Stability of influenza virus.

Stability of HA activity with respect to pH (a). Inactivated cell culture supernatant was titrated to different pH (3.0 to 10.6). Reactions were neutralized immediately after incubation for 2.5 (▩), 4.5 (■) or 23 h (▨) at room temperature and HA activity was determined. Values normalized by the average activity at pH 7 are reported. HA activity was found stable only within a narrow range around physiological pH (7 to 8). Stability of HA activity with respect to ionic strength (b). NaCl up to 1.5 M was added to SEC-purified virus and incubated for 2 hours at room temperature. Concentration of NaCl was reduced to 150 mM immediately afterwards by dilution with appropriate buffer and HA activity was determined. Activities normalized to the initial activity considering dilution are reported.

4.5.2.2 Flowthrough Anion-Exchange Chromatography

AIEC was applied for the polishing of SEC-purified virus (4.5.1) in the first process (Figure 1-5) [Kalbfuss, Wolff, Morenweiser, et al., 2007]. In this particular context, AIEC was operated in flowthrough-mode, i.e. adsorption of virus was prevented by appropriate operating conditions while highly charged impurities, in particular DNA, were adsorbed to resins.

Two chromatography media (Sepharose Q FF and Sepharose Q XL) were considered for the separation of virus from DNA. NaCl was selected for displacement while pH was stabilized at 7.3 with phosphate buffer. Based on initial experiments with HiTrap screening columns (data not shown), feed was conditioned to a salt concentration of 0.4 M NaCl. Columns seven and eight were loaded with 1.6 cv of conditioned feed. After washing with equilibration buffer, linear gradients over 10 cv were run from 0.4 to 1.5 M NaCl. The flowthrough and eluate of each run were fractionated and analyzed offline for HA activity and DNA (Figure 4-34). In contrast to scouting experiments with screening columns, most of the virus still adsorbed to anion-

exchangers. Displacement by NaCl lead to elution of adsorbed virus over a wide range of salt concentrations. Elution of the virus from Sepharose Q XL even resulted in a split peak, indicating distinct viral populations or association of virions with DNA. With both media, DNA eluted in a sharp peak overlapping with part of the virus peak. Higher NaCl concentrations were necessary to displace DNA from Sepharose Q XL resulting in better separation from the virus. Accordingly, Sepharose Q XL was selected for subsequent experiments.

Since results from experiments with screening columns were not transferable[17], the minimum salt concentration required for preventing adsorption of virus was determined in a batch experiment. Sepharose Q XL resin was mixed with SEC-purified virus in a microtiter plate at various salt concentrations. The specific HA activity or DNA concentration in mixtures was about half the activity or concentration found in column chromatography. The ratio, however, was identical. The amount of virus added corresponded to a load of 35 kHAU per ml of resin. After incubation for 2 h at room temperature, samples were taken from supernatants and analyzed for HA activity and DNA concentration. Desorbed fractions of each analyte, i.e. fractions in supernatants, were calculated for each salt concentration as the ratio of actual activity or concentration over respective values for 1.5 M NaCl (Figure 4-35). Only at the lowest concentration of 0.15 M NaCl virus adsorbed completely to the stationary phase whereas complete adsorption of DNA was observed up to a concentration of 0.7 M NaCl. At this concentration only 10% of the virus was adsorbed to the resin.

Four preparative runs where conducted on column 8 packed with Sepharose Q XL. The column was fed with SEC-purified virus conditioned to 0.65 M NaCl. Different amounts of virus (28 to 239 kHAU per ml of resin) from four independent batches were loaded onto the column (Table 4-33). Virus was collected in flowthroughs whereas DNA (and possibly other impurities) adsorbed to the stationary phase. However, some leakage of DNA into product fractions occurred (about 100 ng ml^{-1} compared to about 6 µg ml^{-1} in the feed). Even at the highest load no breakthrough of DNA was observed. Consequently, no data on the dynamic binding capacity of the column can be provided. Adsorbed impurities were displaced by a step gradient to 1.5 M sodium chloride and two cleaning solutions[18]. The chromatogram of batch No. 4 containing offline data for HA

17 This was most likely due to lower concentrations of virus and DNA or different concentration ratios in the feed material.

18 acidic and alkaline high salt solutions

activitiy and DNA is given in Figure 4-33. The product yield of HA activity seemed to depend on the amount of virus loaded. For loads greater than 160 kHAU per ml of resin, product yields of 80% and more could be achieved similar to the result obtained in the batch adsorption experiment. The removal of DNA was efficient in all cases leading to 67-fold reduction on average. The amount of protein was reduced to 67% of the initial amount.

Table 4-33. Yields and purities after preparative flowthrough AIEC of SEC-purified influenza virus on Sepharose Q XL

Batch		Flowthrough				Impurity		
	Load[a]	V^b	$a_{HA}{}^c$	$c_{prot}{}^d$	$c_{DNA}{}^e$	$c_{HA}{}^f$	Protein	DNA
	kHAU ml^{-1}	ml	kHAU (0.1 ml)$^{-1}$	µg ml^{-1}	µg ml^{-1}	µg ml^{-1}	µg dose^{-1}	ng dose^{-1}
1	28	12.0	0.16 (63 %)	n.a.	0.02 (0.6 %)	0.53	n.a.	485
2	161	35.3	0.52 (84 %)	n.a.	0.07 (2.0 %)	1.67	n.a.	620
3	94	28.0	0.60 (58 %)	18.2 (64 %)	0.07 (1.0 %)	1.93	141	513
4	239	56.0	1.05 (80 %)	20.0 (69 %)	0.10 (2.1 %)	3.39	88	455
Mean			-	19.1	0.06		115	518
Std			-	± 1.3	± 0.04			
			-	(67%)	(1.5%)			

a: total HA activity loaded per volume of resin, b: injection volume, c: volumetric HA activity, d: total protein concentration, e: double-stranded DNA concentration, f: estimated concentration of hemagglutinin protein, n.a.: not available

Note: Yields of analyzed species are given in brackets below. Arithmetic means and standard deviations for all batches are provided at the bottom. Statistics for HA activity were omitted due to differences in the feed material. Concentrations of hemagglutinin protein were estimated from HA activities [Kalbfuss et al., 2008]. For calculation of impurities, a content of 15 µg of hemagglutinin antigen were assumed per dose.

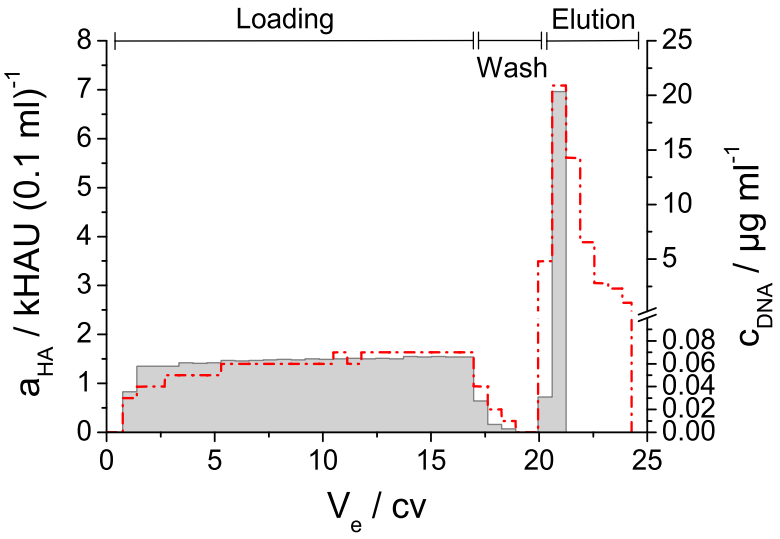

Figure 4-33. Preparative flowthrough AIEC of SEC-purified influenza virus on Sepharose Q XL.

Column eight was loaded with 16 cv of SEC-purified virus conditioned to 0.65 M NaCl (batch No. 4). Flowthrough and eluate fractions were analyzed for HA activity (■) and DNA concentration (–·–). 80% of loaded HA activity was recovered in the flowthrough while DNA almost completely adsorbed to the stationary phase. DNA was desorbed by a step gradient to 1.5 M NaCl.

4.5.2.3 Scouting with Membrane Adsorbers

In preparation of adsorptive IEC, suitability of four membrane adsorbers was tested with respect to their ability of binding influenza virus [Kröber, 2007]. Membranes included a strong cation- and anion-exchanger. Furthermore, an unmodified borosilicate glass fiber filter and an iminodiacetic acid (IDA) membrane loaded with Ca^{2+} were used in investigations. All experiments were conducted with screening devices of 96-well microtiter plate format. A single concentrate of influenza virus A/PR/8/34 (H1N1) RKI diafiltered against low-salt HEPES buffer at pH 7.3 or clarified and inactivated supernatant were loaded onto membranes. In experiments with ion-exchangers, one part of the diafiltrate was further titrated to pH 9. Collected flowthroughs, eluates and corresponding feeds were analyzed for HA activity. Total activities and derived material balances have been summarized in Table 4-34.

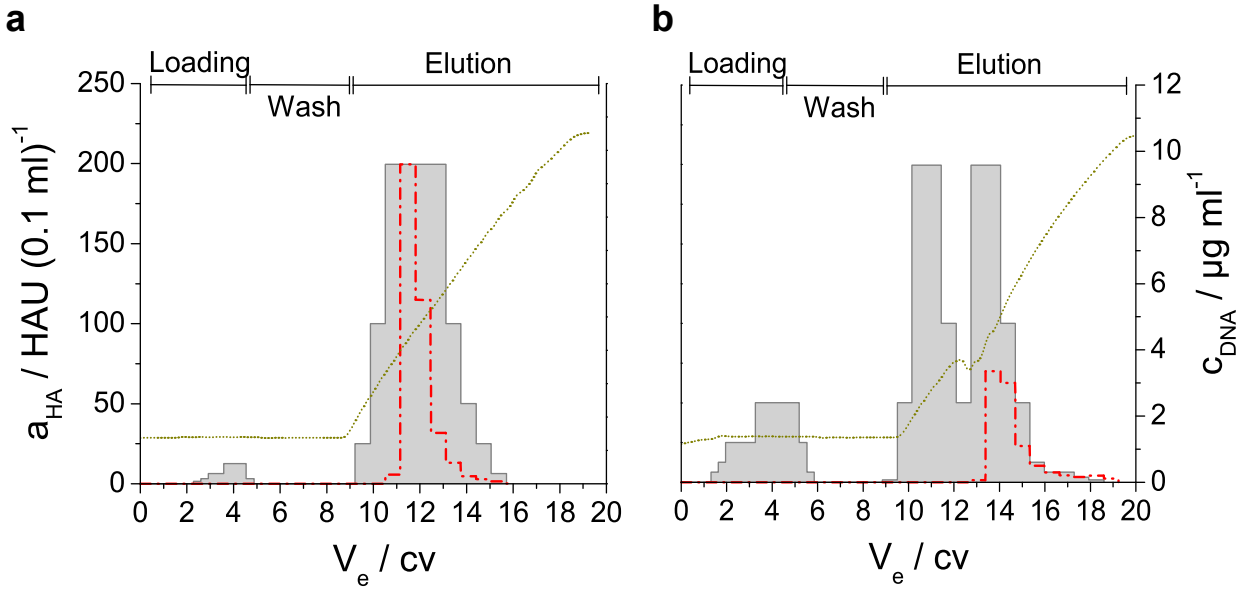

Figure 4-34. Selectivity of Sepharose Q FF (a) and Q XL (b) between virus and DNA.

Columns were loaded with 1.6 cv of SEC-purified virus conditioned to 0.4 M NaCl. Linear gradients were run from 0.4 M to 1.5 M NaCl (···). Flowthrough and eluate fractions were analyzed for HA activity (▩) and DNA (–·–). Co-elution of DNA was observed for both chromatography media. Split peak elution in the case of Q XL suggested two virus populations and possibly association of virus with DNA.

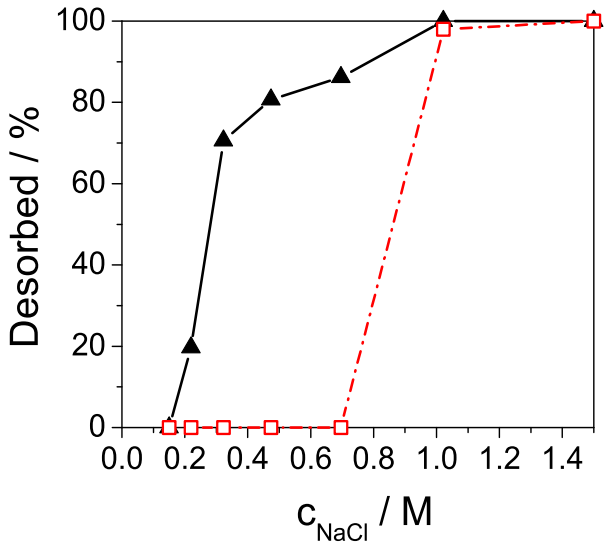

Figure 4-35. Batch adsorption of influenza virus and host-cell DNA to Sepharose Q XL.

SEC-purified virus was adjusted to various salt concentrations and incubated in the presence of Sepharose Q XL. HA activtiy (▲) and DNA (□) were measured in supernatants after incubation for 2 h at room temperature. Fractions of desorbed virus and DNA were calculated for each salt concentration. Best separation was achieved around 0.7 M NaCl were 85% of the virus was found in the supernatant while DNA was quantitatively adsorbed.

Table 4-34. Material balances of scouting experiments with membrane adsorbers

	Harvest		Diafiltrate			
	A_{HA} / kHAU		pH 7.3		pH 9.0	
Q						
Load	5.80		8.32		5.90	
FT-1	0.31	(11%)	1.06	(26%)	0.18	(6%)
FT-2	0.38	(13%)	1.09	(26%)	0.51	(17%)
Wash	n.d.	n.d.	n.d.	n.d.	n.d.	n.d.
Bound	5.11	(88%)	6.16	(74%)	5.22	(88%)
Eluate	1.40	(28%)	1.17	(19%)	0.71	(14%)
S						
Load	5.80		8.32		5.90	
FT-1	2.67	(92%)	2.23	(54%)	2.07	(70%)
FT-2	2.91	(100%)	3.03	(73%)	2.40	(81%)
Wash	0.04	(1%)	0.04	(0%)	0.03	(0%)
Bound	0.19	(3%)	3.01	(36%)	1.42	(24%)
Eluate	n.d.		0.67	(22%)	0.18	(13%)
GF						
Load	8.28					
FT-1	0.29	(7%)				
FT-2	2.59	(62%)				
Wash	0.07	(1%)				
Bound	5.33	(64%)				
Eluate	0.22	(4%)				
IDA-Ca^{2+}						
Load	1.04		1.55			
FT	0.53	(51%)	n.d.	n.d.		
Wash	0.03	(2%)	0.01	(1%)		
Bound	0.48	(46%)	1.54	(99%)		
Eluate	0.03	(5%)	0.03	(2%)		

Q: quaternary ammonia, S: sulphonyl, GF: glass fiber, IDA-Ca^{2+}: iminodiacetic acid complexed with Ca^{2+}, n.d.: not detectable, FT: flowthrough

The strong anion-exchanger (Q) was capable of binding influenza virus from all three feed solutions. Average dynamic capacities were in the range from 5.11 to 6.16 kHAU per well (8.96 to 10.8 kHAU cm^{-2}). The strong cation-exchanger (S), in contrast, only seemed to be capable of binding influenza virus from diafiltrate. Dynamic capacity at a pH of 7.3 was significantly higher with 3.01 kHAU per well (5.28 kHAU cm^{-2}) compared to 1.42 kHAU per well (2.49 kHAU cm^{-2})

at a pH of 9. The glass fiber filter (GF) provided remarkably high capacity with 5.33 kHAU per well (21.3 kHAU cm^{-2}). Capacities obtained with IDA-complexed Ca^{2+} (IDA-Ca^{2+}), however, were poor with only 0.48 kHAU per well (0.84 kHAU cm^{-2}) for virus from harvest and 1.54 kHAU per well (2.70 kHAU cm^{-2}) for virus from diafiltrate (pH 7.3). Noteworthy, dynamic capacities cannot be compared straightly, since different amounts of virus per membrane area were loaded and flow rates were only poorly controlled. Therefore, reported values only provide a rough indication of dynamic capacity. Common to all materials was the low to very low recovery of virus upon elution. Virus bound to ion-exchangers was displaced by elevated concentrations of NaCl (1.5 M). However, only 14% to 28% of bound virus could be eluted concerning the strong anion-exchanger (Q). Recoveries obtained with the strong cation-exchanger (S) were comparable with 0% to 22%. For the elution of virus from the glass fiber filter (GF) a combination of pH change and elevated concentration of urea (2 M) was used. Elution from IDA-Ca^{2+} was attempted by competitive complexation of Ca^{2+} with 0.5 M EDTA. In both cases, recoveries were in the range of only a few percent (2% to 5%).

4.5.2.4 Capture with Membrane Adsorbers

As confirmed in scouting experiments, inactivated influenza A virus in cell culture supernatant can be adsorbed directly to quaternary ammonia membrane anion-exchangers (4.5.2.3). Based on this finding, Sartobind Q and D anion-exchangers were tested for their suitability of a direct capture of influenza virus from cell culture supernatant [Kalbfuss, Wolff, Geisler, et al., 2007]. Experiments were conducted with influenza virus A/PR/8/34 (H1N1) NIBSC propagated in roller bottles. In one experiment, equine influenza virus A/NM/1/93 (H3N8) produced in a stirred-tank microcarrier cultivation was used. Either Ex-Cell MDCK medium or V-Medium were used for propagation. Virus-containing supernatant was clarified twice by normal-flow filtration (4.2.1) and inactivated chemically (3.4) prior to chromatography.

In a first step, dynamic binding capacities of Sartobind Q MA75 adsorbers were determined for four batches of influenza A virus produced in Ex-cell MDCK medium and two batches produced in V-medium (Table 4-35). In these experiments Sartobind Q adsorbers were loaded with supernatant until near-complete breakthrough (typically 300 ml). Offline-measured HA activity or the intensity of scattered laser light at an angle of 90° was used to trace the virus. HA activities or

scattering intensities of supernatants were determined separately. Dynamic capacities were expressed as the loaded volume after which 10% breakthrough of the feed activity or scattering intensity was observed in the flowthrough. A volumetric capacity of (2.23 ± 0.20) ml cm^{-2} (mean value ± standard deviation reported in all cases) was determined for influenza A virus propagated in Ex-Cell MDCK medium corresponding to an activity based capacity of (3.12 ± 0.54) kHAU cm^{-2}. The volumetric capacity for influenza A virus propagated in GMEM medium was higher with (4.72 ± 2.15) ml cm^{-2} due to a higher activity based capacity of (5.19 ± 0.16) kHAU cm^{-2} but also due to lower virus titers in these batches.

Table 4-35. Dynamic capacity of Sartobind Q anion-exchangers.

Batch	Virus	Medium	System	Method	Vol. Cap.[1] ml cm^{-2}	HA Cap.[2] kHAU cm^{-2}	N[7]
1	H1N1	Ex-Cell	RB[3]	HA[4]	2.09	3.48	1
2	H1N1	Ex-Cell	RB	HA	2.23	2.33	1
5	H1N1	Ex-Cell	RB	LS[5]	2.08	3.43	1
6	H1N1	Ex-Cell	RB	LS	2.51	3.24	1
				Mean ± Std[6]	2.23 ± 0.20	3.12 ± 0.54	
7	H1N1	V-Medium	RB	LS	3.23	5.30	1
8	H3N8	GMEM	STR[8]	LS	6.24	5.07	2
				Mean ± Std	4.72 ± 2.15	5.19 ± 0.16	

1: volumetric capacity, 2: HA activity-based capacity, 3: roller bottles, 4: HA activity-based, 5: light scattering-based, 6: standard deviation, 7: number of determinations, 8: stirred-tank reactor

Note: Sartobind Q MA75 adsorbers were loaded with supernatant until near-complete breakthrough. Dynamic capacities were expressed as the loaded volume after which 10% breakthrough of the feed activity or scattering intensity was observed in the flowthrough.

A typical chromatogram of a capacity determination followed by a linear salt gradient to 1.5 M sodium chloride is provided in Figure 4-36. The flowthrough and eluate were fractionated and analyzed for HA activity. Good agreement was observed between the intensity of scattered light and HA activity. Particularly during loading, scattered light intensity was able to indicate breakthrough of the virus as opposed to UV absorbance. Due to an abundance of UV absorbing compounds unable to bind to the anion-exchanger, the latter was immediately close to saturation - increasing only slightly during loading.

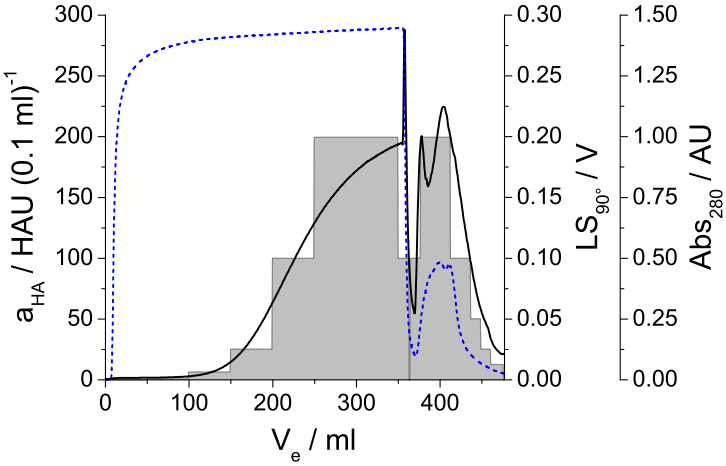

Figure 4-36. Breakthrough and elution of human influenza A virus in cell culture supernatant loaded onto a Sartobind Q MA75 adsorber.

Supernatant was loaded until near-complete breakthrough of HA activity. Adsorbed virus was eluted by a linear salt gradient to 1.5 M sodium chloride. UV absorbance at 280 nm (---), the intensity of scattered laser light (—) and HA activity (■) are plotted over total eluent volume.

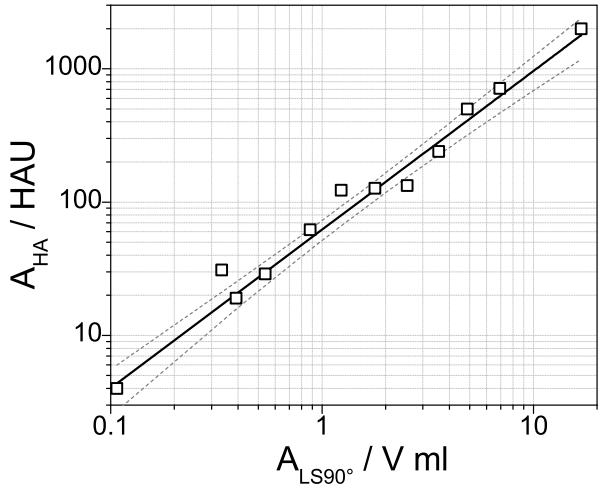

Figure 4-37. Correlation of HA activity and intensity of scattered laser light.

HA activity and areas under the light scattering signal correlated well within the same batch. A power law of type $y = ax^b$ was fitted to experimental data.

Plotting HA activity of individual fractions over corresponding areas of scattered light intensity revealed a correlation between the two quantities (Figure 4-37). A power law of type $y = ax^b$ was fitted to experimental data. The coefficients obtained by weighted least-squares analysis were $a = (62.1 \pm 4.8)$ HAU (V ml)$^{-1}$ and $b = 1.19 \pm 0.05$ ($R^2 = 0.9337$). The correlation was thus close to

linear ($b = 1$). A range of almost three orders of magnitude could be covered by the power law. More data points, however, were found outside the predicted confidence band ($\alpha = 0.05$) than would have been expected. Confidence intervals should hence be interpreted with care.

Different elution strategies were tested for their ability to recover the virus quantitatively (Table 4-36). A Sartobind Q MA75 adsorber was loaded three times with 100 ml of supernatant from the same batch. Unbound material was washed out with 150 mM sodium chloride at pH 7.0. Adsorbed virus was eluted either by a step salt gradient from 0.3 to 1.5 M sodium chloride, a step pH gradient from 5.7 to 4.2 or a step salt gradient from 0.3 to 1.5 M combined with a change in pH from 7.0 to 5.0. Eluates were fractionated and analyzed for HA activity. Eluting virions were traced by a light scattering detector. Only the step salt gradient was able to recover the virus quantitatively (113% recovery of HA activity). In the case of the step pH gradient, no virus could be detected in the eluate (neither by HA activity nor light scattering). Some virus eluted by the combination of a step salt gradient and change in pH but recovery of HA activity was low. Only traces of eluting virions could be detected by the light scattering detector.

Table 4-36. Comparison of different strategies for elution from Sartobind Q.

	Salt		pH		Salt + pH	
	A_{HA}[1] / kHAU	Y_{HA}[2]	A_{HA} / kHAU	Y_{HA}	A_{HA} / kHAU	Y_{HA}
Load	105		105		105	
Flowthrough	0	(0 %)	0	(0 %)	6	(6 %)
Elution	118	(113%)	0	(0 %)	1	(1 %)
Recovery	118	(113%)	0	(0 %)	8	(7 %)

1: HA activity, 2: Recovery of HA activity

Note: 100 ml of cell culture supernatant from the same batch were loaded onto a Sartobind Q MA75 adsorber. Adsorbed virus was eluted either by a step salt gradient (salt), a step pH gradient (pH) or a step salt gradient combined with a decrease in pH from 7.0 to 5.0 (salt + pH).

In the following, recovery of adsorbed virus by salt displacement was investigated for additional three batches using Sartobind Q and Sartobind D MA75 adsorbers (Table 4-37). Experiments were conducted as described above. Again 100 ml of supernatant were loaded corresponding to about 160 kHAU per run on average. Only negligible amounts of virus were found in

flowthroughs (typically less than 2% of loaded HA activity). Average recoveries of HA activity with Sartobind D were significantly lower compared to Sartobind Q (38% compared to 86%).

Table 4-37. Yields and recoveries of virus loaded onto Sartobind Q and D membrane adsorbers.

Sartobind Q										
Batch #	**1**		**2**		**3**		**4**		**Mean**	
	A_{HA}[1] / kHAU	Y_{HA}[2]	A_{HA} / kHAU	Y_{HA}	A_{HA} / kHAU	Y_{HA}	A_{HA} / kHAU	Y_{HA}	**A_{HA} / kHAU**	**Y_{HA}**
Load	166		105		174		182		**157**	
Flowthrough	3	(2%)	0	(0%)	2	(1%)	7	(4%)	**3**	**(2%)**
Elution	129	(78%)	118	(113%)	146	(84%)	111	(61%)	**126**	**(84%)**
Recovery	133	(80%)	118	(113%)	148	(85%)	118	(65%)	**129**	**(86%)**
Sartobind D										
Batch #			**2**		**3**		**4**		**Mean**	
			A_{HA} / kHAU	Y_{HA}	A_{HA} / kHAU	Y_{HA}	A_{HA} / kHAU	Y_{HA}	**A_{HA} / kHAU**	**Y_{HA}**
Load			105		191		174		**156**	
Flowthrough			0	(0%)	4	(2%)	4	(2%)	**2**	**(1%)**
Elution			53	(51%)	66	(34%)	45	(26%)	**55**	**(37%)**
Recovery			53	(51%)	69	(36%)	49	(28%)	**57**	**(38%)**

1: HA activity, 2: Recovery of HA activity

Note: 100 ml of cell culture supernatant from up to four batches were loaded onto Sartobind Q or D MA75 adsorbers. Adsorbed virus was eluted by a multi-step salt gradient from 0.3 M to 1.5 M sodium chloride.

Average light scattering intensities over total elution volume are illustrated in Figure 4-38a. In the case of Sartobind Q, virions eluted over the whole range of salt concentrations starting at the first step with 0.3 M sodium chloride. Onset of elution for Sartobind D was delayed occurring only after the second step with 0.6 M sodium chloride. Distinct peaks were observed for every step, however, less virions seemed to elute from Sartobind D, reflecting the lower recoveries of HA activity. The highest peak for Sartobind Q was observed at 0.9 M sodium chloride. In the case of Sartobind D, peaks at 0.9 M and 1.2 M NaCl were about equally high. Integrals of light scattering intensities and standard deviations are plotted over the salt concentration in Figure 4-38b. Total areas at 1.5 M NaCl for Sartobind D were only about one fourth of areas for Sartobind Q. Due to

the significantly higher recoveries Sartobind Q adsorbers were used exclusively in subsequent experiments.

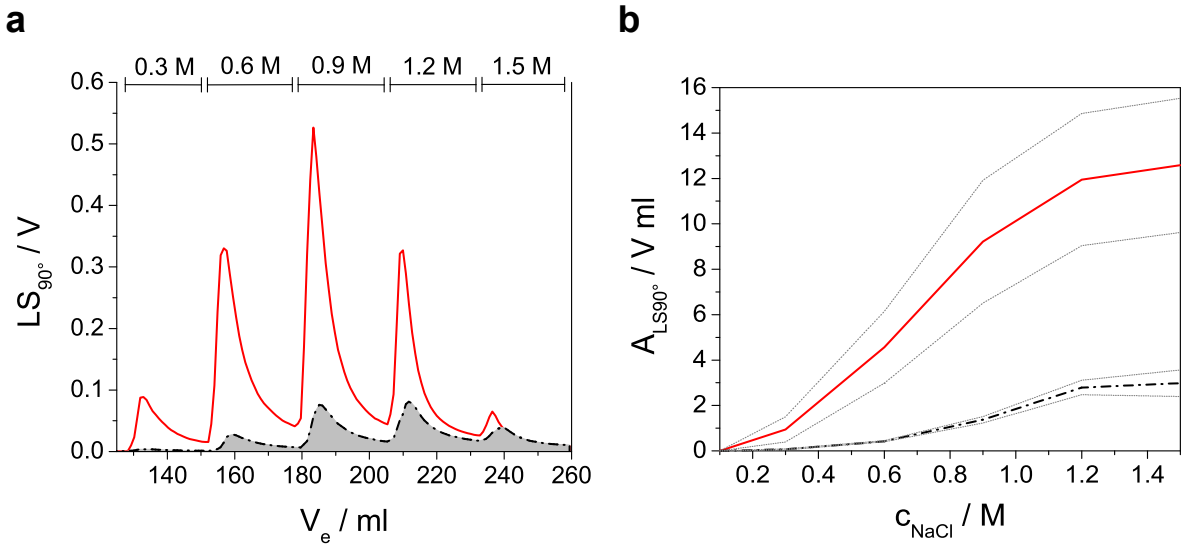

Figure 4-38. Elution of virions from Sartobind Q and D.
Elution profiles of HA activity from Sartobind Q (—) and D (■) MA75 anion-exchange adsorbers (a). Adsorbed virus was eluted by a multi-step salt gradient from 0.3 to 1.5 M sodium chloride. Average intensities of scattered laser light are presented. Intensities were integrated and plotted over the salt concentration (b). Averages from four (— Sartobind Q) and three batches (–·– Sartobind D) are presented. The standard deviation of integrals is given by dotted lines.

Next, influence of pH on the capacity of Sartobind Q and the recovery of HA activity was investigated. Supernatants from two independent batches (No. 5 and 6) were titrated to various pH ranging from 5.5 to 9.0. Wells of a Vivawell-96 Q-IEX spin plate were loaded with 0.8 ml of titrated supernatants and adsorbed virus was eluted by a single salt step to 1.5 M sodium chloride. Supernatants, flowthroughs and eluates were analyzed for HA activity. HA activity in titrated supernatants was only stable at a pH higher than 7, but no significant decay occurred in the range from 7.0 to 9.0 (Figure 4-39a). The recovery of HA activity, in contrast, showed a maximum between pH 7.0 and 7.5 (around 70% of adsorbed virus recovered). Lowest recoveries were observed at alkaline and acidic pH with about 30% to 50% at pH 9.0 and 45% at pH 5.5 (Figure 4-39b). Interestingly, the volumetric capacity remained constant over the whole pH range with about 1.6 ml of supernatant per cm^2 of membrane (Figure 4-39c). The activity based capacity, however,

showed a maximum around pH 7.5 similar to the stability of HA activity in supernatants (data not shown).

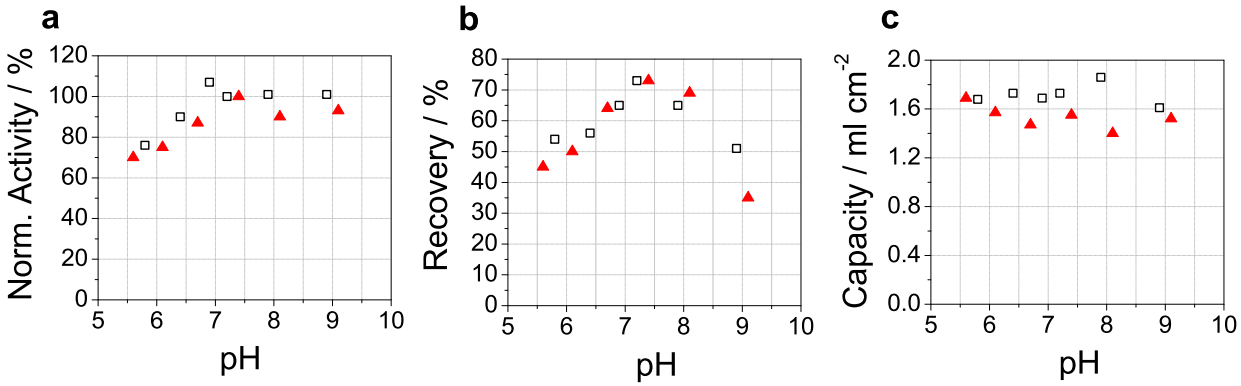

Figure 4-39. Influence of pH on the stability and recovery of HA activity and the capacity of Sartobind Q.

Cell culture supernatant was titrated to various pH and loaded onto Vivawell Q adsorbers. Adsorbed virus was eluted with 1.5 M sodium chloride. HA activity was stable between pH 7.0 and 9.0 (a). The recovery of HA activity was highest between pH 7.0 and 8.0 (b). In contrast, the volumetric capacity was independent of pH (c). Data from two independent experiments shown (□▲)

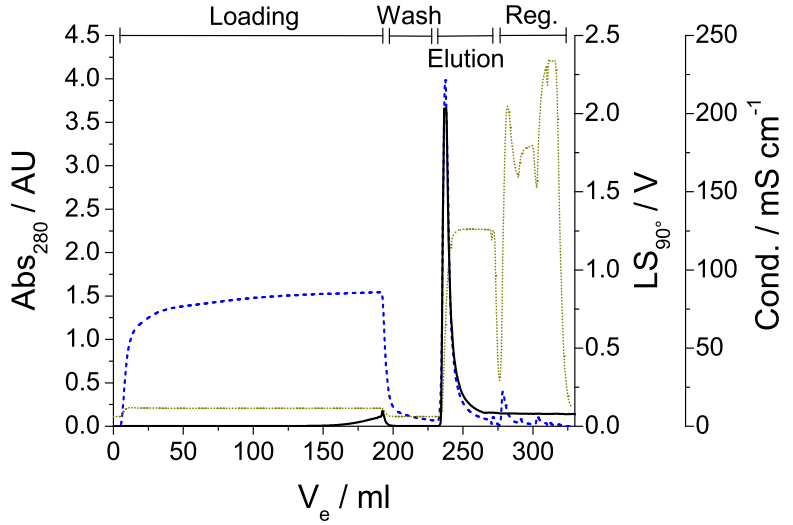

Figure 4-40. Capture of influenza A virus from cell culture supernatant using a Sartobind Q MA75 adsorber.

The adsorber was loaded with supernatant until 10% breakthrough of scattered light intensity. Adsorbed virus was eluted in a single salt step to 1.5 M NaCl. UV absorbance at 280 nm (---), the intensity of scattered laser light (—) and conductivity (···) are plotted over total eluent volume.

Finally, operating conditions for a capture operation were elucidated from scouting experiments. Supernatants from four batches (batches no. 5 to 8) were loaded onto a Sartobind Q MA75 adsorber until 7 to 15% breakthrough of scattered light intensity. Adsorbed virus was eluted in a single salt step to 1.5 M sodium chloride. A constant pH of 7.3 was maintained during all phases. Fractions were collected and analyzed for HA activity together with the feed. Total protein and DNA was quantitated for batches with Ex-Cell MDCK medium (batches no. 5 and 6). Material balances of all runs are summarized in Table 4-38. Negligible amounts of HA activity were found in flowthroughs. On average, more than 70% of HA activity were recovered in eluates, which is in good agreement with spin plate experiments (around 75% between pH 7.0 and 7.5). For batches No. 5 and 6 total protein was reduced to less than one fourth of the loaded amount. DNA, in contrast, was recovered completely in eluate fractions. The complete chromatogram for batch No. 6 including UV absorbance, scattered light intensity and conductivity is given in Figure 4-40.

Table 4-38. Yields and recoveries of preparative runs with Sartobind Q.

Batch	Load				Adsorbed		Eluate						N[5]
	V_{inj}[1]	A_{HA}[2]	m_{prot}[3]	m_{DNA}[4]	A_{HA}		A_{HA}		m_{prot}		m_{DNA}		
	ml	kHAU	mg	mg	kHAU		kHAU		mg		mg		
5	156	257	10.8	1.30	257	(100%)	187	(73%)	2.57	(24%)	1.40	(108%)	1
6	188	243	10.6	1.43	240	(99%)	180	(74%)	2.36	(22%)	1.46	(102%)	1
7	242	506	-	-	479	(95%)	414	(82%)	-	-	-	-	1
8	479	406	-	-	402	(99%)	246	(61%)	-	-	-	-	3
Mean						**(98%)**		**(72%)**		**(23%)**		**(105%)**	

1: Injection volume, 2: HA activity, 3: protein mass, 4: DNA mass, 5: number of experiments
Note: Cell culture supernatants were loaded onto a Sartobind Q M 75 adsorber until 10% breakthrough. Adsorbed virus was eluted by single step salt gradient to 1.5 M sodium chloride.

4.5.2.5 Polishing with Packed-Beds and Monoliths

Adsorptive AIEC with media adequate for the purification of nanoparticles was attempted for final polishing of virions in the second process (Figure 1-5) [Kröber, 2008; Eisold, 2008]. Previously, ion-exchangers had been found suitable for the binding of influenza virus in scouting experiments (4.5.2.3). In subsequent experiments, a scale-up to small columns was performed using packed beds of small-sized beads and a monolithic column. Both types of media were chosen in order to overcome limitations in mass-transfer, which typically pose a problem in the

chromatography of virus particles. For AIEC, the media Source Q and CIM QA were selected. For CIEC, Source S was used exclusively. Details on columns are listed in Table 3-18.

A single batch of influenza virus A/PR/8/34 (H1N1) RKI propagated in roller bottles with V-Medium was used in experiments. Chromatography runs were conducted with clarified and concentrated supernatant (4.2.2) from which DNA had been precipitated prior to concentration (4.3). Supernatant was concentrated 5-fold and diafiltered against four volumes of high-salt buffer followed by four volumes of low-salt buffer (4.4.3).

In first runs, 5 ml of diafiltrate were loaded onto anion-exchangers (Source Q and CIM QA). Adsorbed virus was eluted by linear gradients from 0.15 to 1.5 M NaCl (Chromatograms are not shown but are similar to the ones depicted in Figure 4-42). Runs were conducted twice in order to confirm reproducibility. Replicates were almost indistinguishable based on the UV trace. Due to the low volume of diafiltrate injected, no breakthrough was observed in any of the runs. Elution as followed in the UV trace showed two distinct peaks, which were almost baseline-separated in runs with Source Q but showed some overlap in runs with CIM QA. An increase in backpressure from about 0.9 MPa 1.1 MPa in the case of CIM QA and from 0.75 MPA to 0.95 MPa in the case of Source Q was detected upon injection. Backpressure reduced again during elution but not completely to initial values. CIEC with Source S, in contrast, failed to bind the virus. Unlike in scouting experiments, the virus was almost completely found in the flowthrough after injection. During elution only a minor peak was detected.

Particularly, runs with CIM QA showed an undesired overlap of eluting peaks. It was therefore attempted to find appropriate operating conditions under which better separation is achieved. Flow rate and gradient length were considered for optimization. A number of chromatography runs were conducted around the reference flow rate of 265 cm h^{-1} and gradient length of 20 cv. Either the flow rate (133 or 530 cm h^{-1}) or gradient length (10 or 40 cv) were modified in experiments resulting in 5 different conditions. A common flow rate of 265 cm h^{-1} during injection and washing of the column was maintained in all runs. 5 ml of the diafiltrate, which was also used in previous experiments, were injected and eluted. All runs were conducted in random order. Two runs were conducted per condition. Combinations of the linear flow rate and gradient length including corresponding chromatograms are depicted in Figure 4-41. Only the first run of each condition is illustrated since replicates were almost indistinguishable. Doubling the flow rate from

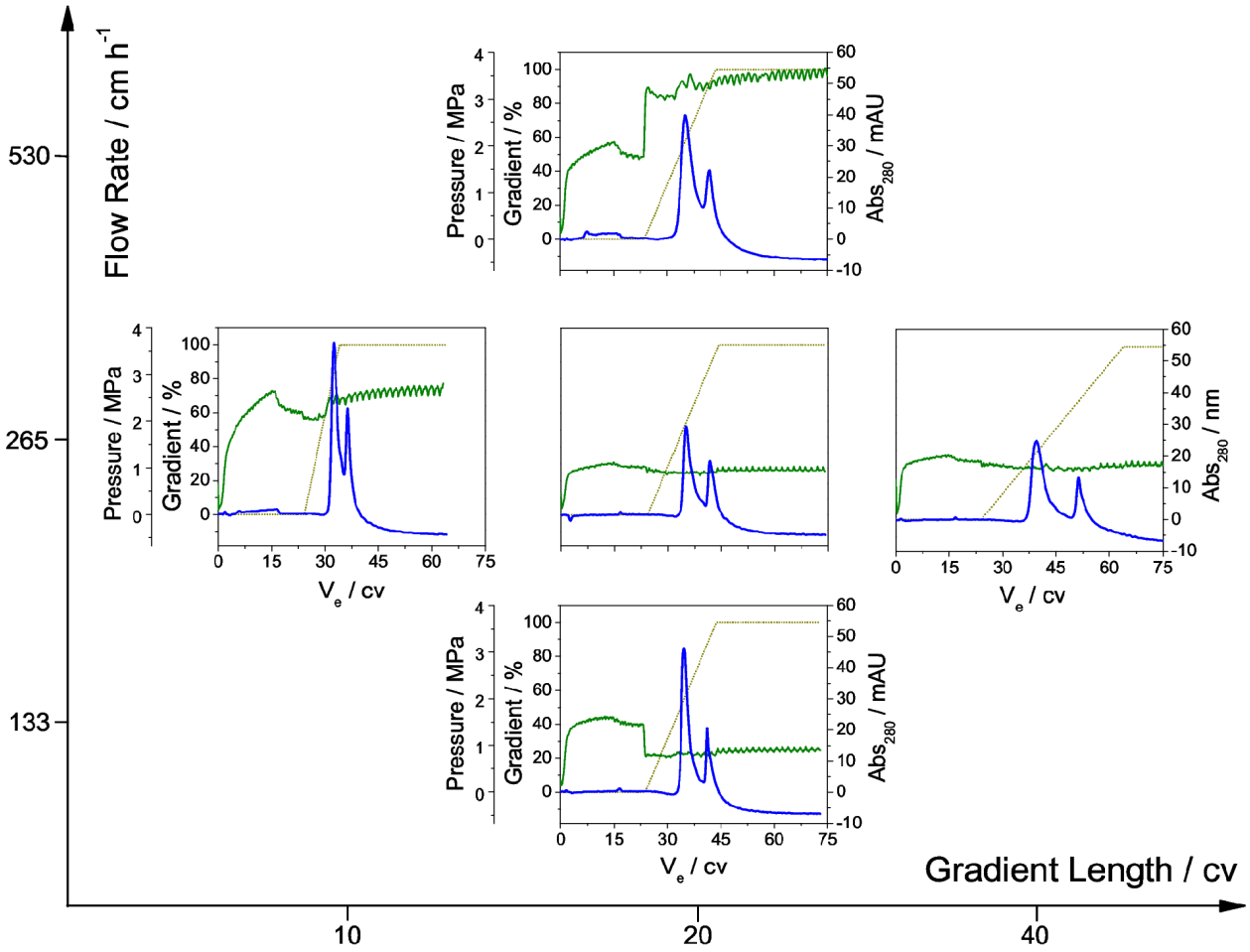

Figure 4-41. Optimization of AIEC on CIM QA.
Flow rate (133, 265 or 530 cm h^{-1}) and gradient length (10, 20 or 40 cv) were considered for maximizing resolution. 5 ml of diafiltered virus were loaded in each run. A common flow rate of 265 cm h^{-1} during loading and washing was used in all runs. Adsorbed virus and impurities were eluted by linear salt gradients (⋯) from 0.15 to 1.5 M NaCl. UV extinction at 280 nm (—) and column backpressure (—) were acquired online.

265 cm h^{-1} to 530 cm h^{-1} led to significant deterioration of resolution. A reduction to 133 cm h^{-1}, in contrast, resulted in more narrow peaks that were separated slightly better. The improvement in resolution was accompanied by an increase in concentration. The maximum height of the first peak (virions[19]) recorded at a flow rate of 265 cm h^{-1} was only 30 mAU compared to 46 mAU at the lowest flow rate of 133 cm h^{-1}. Elution by a steeper gradient likewise reduced the resolution between peaks, however, peaks were more narrow and hence more concentrated. The maximum of the first peak was as high as 55 mAU after elution within 10 cv compared to 30 mAU under reference conditions. Elution by a more shallow gradient on the other hand led to better separation

19 see below for justification

but wider peaks. Close to baseline separation was achieved by elution within 40 cv. The maximum height of the first peak was 25 mAU. Noteworthy, an increase in backpressure was observed during the experiment indicating fouling of the column. While in the beginning backpressure was about 1 MPa during loading, backpressure of up to 3.5 MPa was observed at the end of the experiment. During the last two runs, even slight breakthrough was observed in the UV trace. Only after regeneration with 1 M NaOH, the initial backpressure of 1 MPa could be restored.

For comparison, two additional runs with a shallow gradient of 40 cv were conducted on Source Q. Likewise, 5 ml of diafiltered virus were loaded onto the column. The flow rate was set to 940 cm h^{-1} as had been used before. Similar to results for CIM QA, replicates were almost indistinguishable based on the UV trace. Fractions collected from flowthroughs and eluates of both runs (CIM QA) or the first run (Source Q) were analyzed for HA activity and DNA concentration. Chromatograms including data from offline analysis are depicted in Figure 4-42. Material balances for HA activity are given in Table Table 4-39. In chromatography with both media, little or no breakthrough of HA activity was observed during loading. Total recoveries of HA activity were 45% and 106% with CIM QA and Source Q, respectively. According to offline-measured data, first peaks were constituted by influenza virions. Second peaks were identified as host-cell DNA. However, a small fraction of DNA was also found in first peaks.

Product fractions were cut virtually based on offline data such that most of the HA activity eluting before the DNA peak was recovered. Corresponding volumes and composition of fractions are provided in Table 4-40. The amount of HA antigen was estimated from HA activity as described by Kalbfuss et al. [2008]. The residual content of DNA in product fractions was calculated as 4.9 ng per dose in the case of CIM QA. The residual with Source Q was slightly higher with 15.7 ng per dose. An antigen content of 45 µg hemagglutinin protein was assumed in calculations.

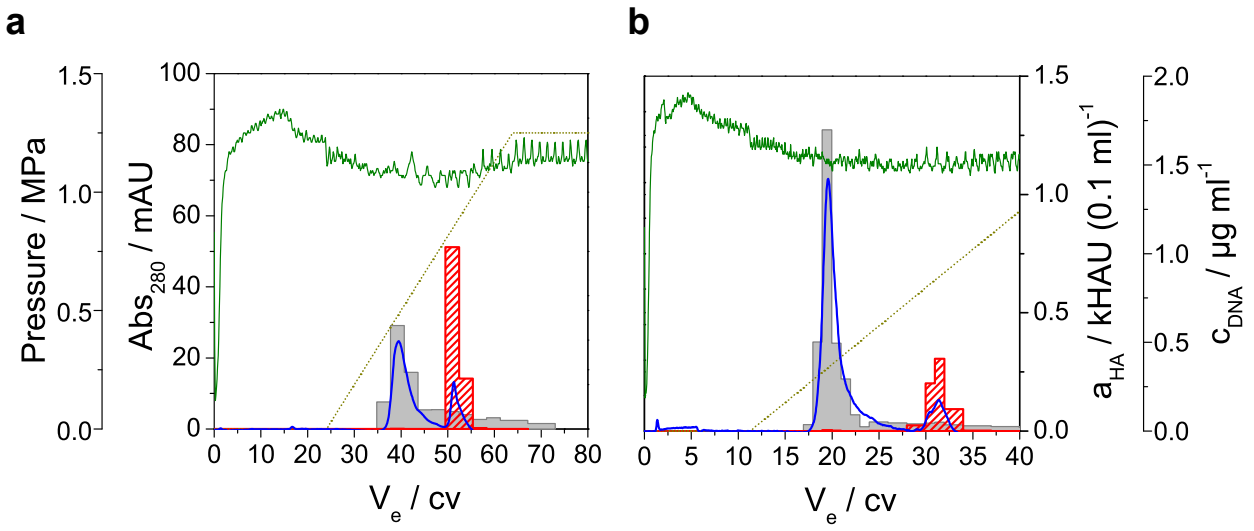

Figure 4-42. Polishing of influenza virus by AIEC on CIM QA (a) and Source Q (b).
5 ml of diafiltered virus were loaded onto columns. Adsorbed virus and impurities were eluted by linear salt gradients (⋯) from 0.15 to 1.5 M NaCl within 40 cv. UV extinction was acquired online at a wavelength of 280 nm (—). HA activity (▒) and DNA concentration (▨) were determined offline from collected fractions. Chromatography was operated at a constant flow rate of 5 ml min^{-1} corresponding to 265 cm h^{-1} in the case of CIM QA and 940 cm h^{-1} in the case of Source Q. Column backpressure (—) increased during loading and reduced again upon elution but not to initial values.

Table 4-39. Material balances of HA activity

Column	Load		Flowthrough			Eluate			Total Recovery	
	V^1 / ml	$A_{HA}{}^2$ / kHAU	V / ml	A_{HA} / kHAU	$Y_{HA}{}^3$	V / ml	A_{HA} / kHAU	Y_{HA}	A_{HA} / kHAU	Y_{HA}
CIM QA[a]	5[a]	28.8	7	n.d.	n.d.	13	13.0	(45%)	13.0	(45%)
Source Q	5	26.9	10	0.8	(3%)	27	28.6	(106%)	29.4	(109%)

1: volume, 2: HA activity, 3: Yield of HA activity, a: arithmetic means from two runs under identical conditions, n.d.: not detectable

Table 4-40. Final DNA burden

Column	V^1 / mL	$a_{HA}{}^2$ / kHAU (0.1 ml)$^{-1}$	$c_{HA}{}^3$ / µg ml^{-1}	$c_{DNA}{}^4$ / ng ml^{-1}	DNA^5 / ng per dose
CIM QA	10	0.19	0.62	0.2	4.9
Source Q	7	0.34	1.09	1.1	15.7

1: volume, 2: volumetric HA activity, 3: estimated concentration of hemagglutinin antigen, 4: DNA concentration, 5: DNA content per dose

In a third experiment, Source Q and CIM QA were tested for their dynamic capacity. About 46.5 ml of diafiltrate[20] from the same batch were injected onto columns. Injected volumes corresponded to an average HA activity of 258 kHAU. Besides, chromatography was conducted as described in the previous experiment. Chromatograms of both runs containing the UV trace and offline-measured HA activity are illustrated in Figure 4-43. Concerning chromatography on CIM QA, no breakthrough of HA activity could be detected over the whole phase of sample injection. Hence, independently of the criterion applied, dynamic capacity can be stated as > 760 kHAU per ml of resin. If the quantity of hemagglutinin antigen is estimated based on HA activity, a capacity > 246 µg per ml of resin can be stated for CIM QA. Moreover, 92% of injected HA activity was recovered in the eluate (Table 4-41). Concerning chromatography on Source Q, slight breakthrough of influenza virus – 32 HAU $(0.1\ ml)^{-1}$ compared to 537 HAU $(0.1\ ml)^{-1}$ in the feed – was observed from the very beginning. Over the course of injection, leaking activity increased up to 64 HAU $(0.1\ ml)^{-1}$ (12% of feed activity). A total of 7% of injected HA activity was found in the breakthrough. Applying the common 10% breakthrough criterion for the definition of dynamic capacity, the capacity of Source Q can be stated as approximately 250 kHAU or 85 µg of hemagglutinin antigen per ml of resin. 117% of injected activity were recovered in the eluate summing up to a total recovery of 124%.

Table 4-41. Material balances of HA activity

Column	Injection		Flowthrough			Eluate			Total Recovery	
	V^1 / ml	$A_{HA}{}^2$ / kHAU	V / ml	A_{HA} / kHAU	$Y_{HA}{}^3$	V / mL	A_{HA} / kHAU	Y_{HA}	A_{HA} / kHAU	Y_{HA}
CIM QA	46	265	46	n.d.	(0%)	8	242	(92%)	242	(92%)
Source Q	47	252	47	18.9	(7%)	17	296	(117%)	315	(124%)

1: volume, 2: HA activity, 3: yield of HA activity, n.d.: not detectable

20 46 and 47 ml, respectively

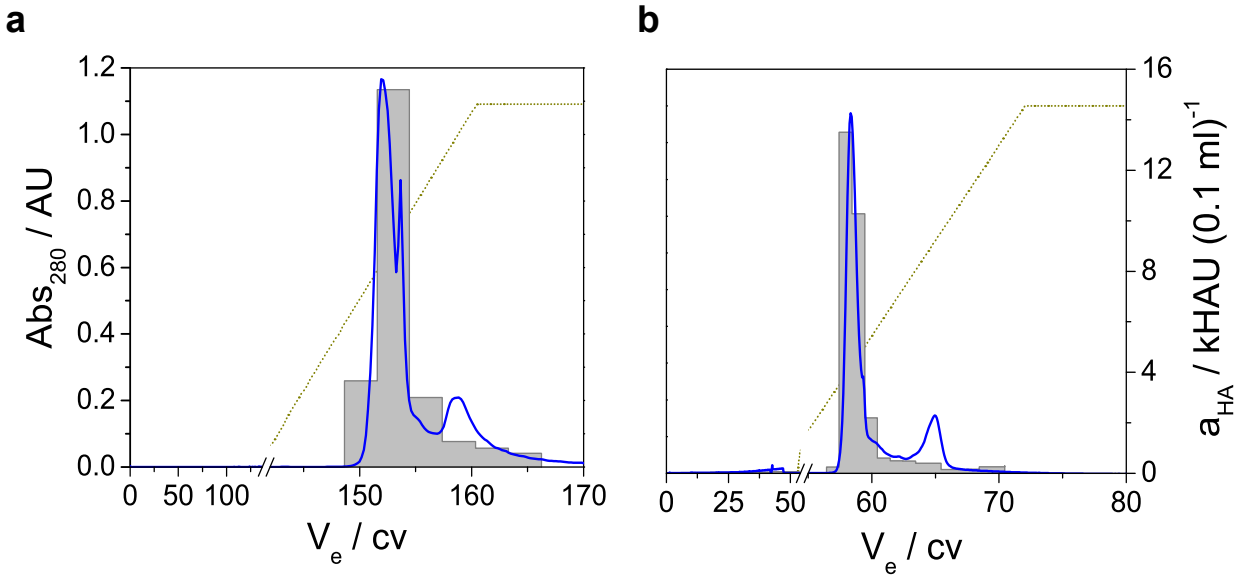

Figure 4-43. Dynamic binding capacity of CIM QA (a) and Source Q (b).

Both columns were loaded with approximately 46.5 ml of diafiltered virus corresponding to an activity of 258 kHAU. Adsorbed virus and impurities were eluted by linear salt gradients (⋯) from 0.15 to 1.5 M NaCl. UV extinction was acquired online at a wavelength of 280 nm (—). HA activity (■) was determined offline from collected fractions.

5 Discussion

5.1 Virus Cultivation

5.1.1 Course of Infection

Virus propagation in roller bottles was characterized with respect to release of virions and impurities. Overall, satisfactory description of experimental data by Gompertz' function was achieved with the exception of infectivity ($TCID_{50}$). Only at the borders systematic deviation of curves from measured values was observed. Consequently, estimates of quantiles are less precise the closer they get to 0% or 100%. But despite satisfactory fits, it shall not be concealed that application of Gompertz' function is motivated only empirically. Nevertheless, Gompertz' function can be applied for compact description of measured data (three or four parameters per variable), reducing the impact of experimental error at the same time. Moreover, profiles can be compared directly in terms of hard figures on the basis of estimated parameters. By applying the suggested non-dimensional representation (2-4), the number of parameters can be further reduced to two per variable. In addition, a universal representation is obtained if cultivations are self-similar. Indeed, data were already astonishingly well described by a set of universal (i.e. global) parameters (Figure 4-14a).

Agreement of non-dimensional parameters, however, shall not conceal the fact that original parameters, in particular the loci of the inflection points t_c and upper asymptotes $K + x_{-\infty}$, varied strongly between cultivations. Lag-phases, for example, and hence t_c appeared to be functions of m.o.i. A result which had been anticipated. Upper asymptotic values of the HA activity likewise depended on the virus strain and medium. On the other hand, upper asymptotic values of the DNA concentration should depend on cell density, or more precisely, on the total number of cells that have lyzed during the infection process. Accordingly, DNA concentrations at the time of harvest were fairly homogeneous with an average value of 16.7 ± 2.4 µg ml^{-1}. Final concentrations of protein showed somewhat larger scatter with 45 ± 11.7 µg ml^{-1}, but in principle the same assumption should be valid. Despite the fact that influenza virus is made from protein to a large extend, a simple back-of-the-envelope calculation demonstrates, that its contribution to the total protein concentration in cell culture supernatant can be neglected in most cases[21].

21 According to Kalbfuss et al. [2007], an HA activity of 1 HAU (0.1 ml)$^{-1}$ approximately corresponds to 8.83 ng ml^{-1} of viral protein. Assuming an average activity of 500 HAU (0.1 ml)$^{-1}$ at the time of harvest (see Table

If only relative profiles towards a reference are of interest non-dimensional representation is most convenient. Average parameters $b^* \approx 1$ and $a^* \approx 0$ for the NA activity (Table 4-19), for instance, indicate a profile indistinguishable from that of HA activity. Another important, but not surprising result, is that the release of impurities is delayed with respect to HA activity. It should therefore be possible, to optimize starting conditions by selecting an appropriate time of harvest. For this purpose, quantiles of the HA activity between 80% to 95% (such as the 90% quantile used in this work) appear to be appropriate for the definition of abortion criteria. If quantiles closer to 100% were chosen, prolonged cultivation times and consequently reduced space-time yields would be the result. Another issue would be that prediction of quantiles is less precise the closer they are to 100% due to systematic deviation of Gompertz' functions from experimental data near the rims (see above). In contrast, harvesting at quantiles between 80% and 95% guarantees yields close to 100%, while the burden of impurities is minimized. Besides, the risk of product damage, e.g. due to protein denaturation or aggregation, is reduced by short cultivation times.

Harvesting near the 90% quantile in roller bottles, for instance, promises a 35% reduction in DNA and 20% reduction in protein concentration in viral harvests (Figure 4-14b). Indeed, the potential of reducing product burden was confirmed in preparative cultivations (Table 4-25). Roller bottles routinely harvested near the 95%-quantile of HA activity resulted in average DNA concentrations between 5.9 and 8.9 µg ml^{-1}. These values are lower by 47% to 65% compared to the average value of 16.7 µg ml^{-1} in long-term cultivations. One may not forget, however, that DNA concentrations in preparative cultivations were only measured after inactivation or even secondary clarification. The inactivating agent β-PL is known to alkylate nucleic acids and has been reported to induce double-strand breaks in DNA [Morgeaux et al., 1993] such that the reduction may appear more drastic than it actually is. The average concentration of protein in the campaign with A/Wis/67/2005 (H3N2) was 34.7 µg ml^{-1} compared to 45.0 µg ml^{-1} in long-term cultivations. Again, the apparent reduction of 23% is even higher than predicted.

If the cultivation system is sufficiently robust, virus can be harvested according to a fixed time schedule. Working diagrams in Figure 4-14 provide the necessary information. If, however, profiles vary from cultivation to cultivation, the content of virus has to be analyzed near-online or markers for the progress of infection need to be found. Turbidity, initially acquired to monitor the content of solid matter in supernatant, has the potential of being such a marker. With the reduced

4-25 for comparison), a viral protein concentration of 4.41 µg ml^{-1} can be estimated.

parameters $b^* \approx 0.90$ und $a^* \approx 0.39$, its profile was quite similar to that of HA activity. The difference between $t_{0.9}$ quantiles was only 9.7 h on average. Moreover, turbidities at the time of harvest were fairly homogeneous among different cultivations and campaigns with an RSD of ± 14%. A fact that can be related to turbidity rather depending on cell density than the virus strain. Reliable prediction of $t_{0.9}$ quantiles during cultivations should hence be feasible. But most importantly, determination of turbidity is rapid, simple and cheap. Measurement of lysis-related turbidity has even been conducted successfully in microcarrier cultivations by letting microcarriers sediment first for about 2 min prior to measurements (data not shown). Another marker that has not been fully explored yet, is the intensity of laser light scattered by virions and other colloids remaining in the supernatant after clarification. First data indicate almost a perfect correlation with HA activity if microfilters with 0.2 µm cut-off are chosen for sample pre-treatment (data not shown).

If the characterization of virus propagation was to be taken further, quality should be taken a closer look at in addition to quantity. The size distribution of genomic DNA fragments, for example, matters with respect to separability of DNA from virions. Size distributions could be readily determined by agarose gel electrophoresis. But also properties of virions, like changes in glycosylation patterns of HA and NA proteins or colloidal stability should be investigated in more detail. Another risk is the rapid decline of viral infectivity during virus propagation. Although, infectivity is not required for the manufacture of inactivated vaccines, its loss indicates some kind of damage to the virus that might reduce the potency of inactivated vaccines, too. Finally, more data needs to be acquired including additional strains and more cell lines. Moreover, experiments should be repeated with the same strains in order to capture biological and/or experimental variability. The ultimate goal of characterization studies should be to develop simple models, ideally with universal parameters that are capable of predicting the most important process variables. If necessary, real-time adaptation should be considered by inclusion of data from easily determinable markers like the turbidity of supernatant. If models further included description of the most important mechanisms like, for example, the relation between m.o.i., lag-time and growth kinetics, optimization of virus propagation and hence a rational design of the unit operation should become feasible. Such effort will hopefully culminate in improved starting conditions for the downstream processing of influenza virions.

5.1.2 Preparative Cultivations

Concerning preparative cultivations, collected data provided an ambiguous picture with respect to measures for the product titer (Table 4-20). HA and NA activities showed remarkably high scatter even within single campaigns. In addition, there was a clear dependence of final titers on the virus strain. Comparison of final NA activities, however, is misleading, since differences in the Michaelis-Menten constants of neuraminidase enzymes may have equally contributed to differences observed between strains[22]. On the other hand, the final concentration of DNA appeared to be independent of virus strains and employed media. From a logical point of view it should rather be coupled to the cell density prior to infection, which was fairly conserved among campaigns. Consequently, a varying degree of virus-specific DNA content had to be dealt with in downstream processing, requiring large safety margins for the process. In principle, the same is to be expected for the virus-specific content of protein. The contradictory finding of significantly higher protein concentrations with Ex-Cell MDCK medium is likely related to the omitted medium-exchange prior to infection. Besides, the protein assay suffered from interference by media components which could be only partly compensated by calibration procedures (see 3.1.3 for details). Since all measurements were further close to the limit of quantitation, bias may have led to an overestimation of the true difference in protein concentrations.

In the future, it appears most important to enhance the robustness of the virus propagation process. While some process variability is inevitably caused by the nature of virus strains, batch to batch variability can certainly be reduced. One critical point appears to be the introduction of a master/working bank system for the virus seed in order to avoid genetic drift during campaigns. Furthermore, the influence of media lots should be minimized by blending of essential media components. This applies in particular for the yeast peptone in V-Medium and the trypsin added to infections. Equally important is the tight control of cultivation conditions. This includes the history of pre-cultures, the conditions of cultivations in general but also the time of harvest.

A second important point is the development of defined or at least animal compound-free media that carry a low burden of impurities. These are not only demanded by regulatory bodies but would further simplify the purification of virions. Finally, the differences between supernatant from roller bottles and microcarrier cultivations remain to be addressed. First data already

22 It is not the maximum reaction rate that is determined by the NA assay, but only the rate at a certain substrate concentration (see 3.1.2 for details).

indicated a quantitative difference in DNA concentrations at the time of harvest. A possible explanation is the anion-exchange functionality of Cytodex-1 microcarriers [GE Healthcare, 2007]. Similarly, some of the virus may be lost to the surface of carriers. Last but not least, a general demand for higher titers exists. Contemporary influenza virus cultivation processes are extremely inefficient, typically resulting in antigen concentrations of only a few milligrams per liter. By genetic alteration of host systems, direct expression of self-assembling VLPs and high-cell density cultivation formats, dramatic increases in antigen titers are to be expected. Once available, a complete re-design of purification processes will be required in order to deal with altered conditions.

5.2 Clarification

5.2.1 Normal-Flow Filtration

Clarification of cell culture supernatant by sequential normal-flow filtration resulted in reliable clarification of 13 batches from roller bottles. Compared to Nayak et al. [2005], insertion of an additional membrane filter after inactivation seemed to be justified, since a further reduction in the turbidity by 75% was achieved on average (Table 4-21). Membrane filters generally posses a narrower pore size-distribution and hence sharper cut-off than fibrous filters. Hence, particles larger than the nominal cut-off are less likely to pass. Fibrous filters, on the contrary, provide higher capacity and are less prone to pore-blockage. Therefore, the combination of both filter types was considered ideal in this work.

Yields for the virus in both steps appear to be inappreciably low (85% and 93% based on HA activity, respectively). This is particularly true, since filter cut-offs were chosen to be significantly larger than the average size of virions[23]. Since influenza virus is a budding virus, hemagglutinin is incorporated at high density into apical cell membranes after infection [Nayak et al., 2004]. Accordingly, fragments of cell membranes are likely to posses HA activity similar to influenza virions. The removal of these fragments upon filtration should lead to an apparent reduction in the product yield, which would explain the comparatively low yields in both steps.

Noteworthy, it was found important to filter roller bottle supernatants as early as possible after harvsting with respect to virus yield. If supernatants were stored at 4 °C prior to filtration,

23 0.65 µm and 0.45 µm compared to about 100 nm [Lamb et al., 2001]

significant losses of virus were observed with yields sometimes as low as 10% (data not shown). Consequently, clarification was conducted always directly at the time of harvesting. In addition, temperature of supernatants was kept at 37 °C during filtration, in order to mimic direct filtration from stirred-tanks or wave bags as closely as possible.

Despite the frequent use of normal-flow filtration for the downstream processing of viruses (see e.g. [Peixoto et al., 2007; Nayak et al., 2005; Hagen et al., 2000; Montagnon et al., 1984]), little data has been reported on the virus yield and clarification efficiency of this unit operation. In a publication by Nayak et al. [2005], filtration of influenza virus from mammalian cell culture through a fibrous filter is reported but no data is given. In another publication on the downstream processing of rotavirus-like particles produced in insect cell culture, a yield of 85% was reported after depth-filtration[24] [Peixoto et al., 2007]. In contrast, the filtration of hepatitis A virus from mammalian cell culture through a filter of unspecified cut-off was reported lossless [Hagen et al., 2000]. Neither of these reports provides any data on the clarification efficiency. But comparison is doubtful anyway, since rotavirus-like particles are self-assembling and do not bud from cell membranes. Similarly, hepatitis A virus is a naked virus, which is assembled in the cytosol.

Replacing normal-flow by tangential-flow microfiltration with a hollow-fiber module was feasible but did not show any advantages in the context of this study. However, if the cut-off of membranes was selected closer to the mean size of virions (e.g. 0.2 µm), tangential-flow microfiltration might be less prone to pore-blockage and layer formation. In this case, higher purity and product yield may be achievable and possibly compensate for the additional costs of investment and operation.

Ideally, some data on the capacity of filters would have been provided. Unfortunately, employed filter capsules were completely over-sized with respect to the scale of cultivations. No significant decline in the flux was observed in any of the filtration runs. Smaller capsules of the same type were not available. Instead, non-pleated disc filters would have had to be used. However, these filters are likely to produce different results due to altered hydrodynamics in the filter housing and near the surface of filter media. Hence, the only possibility for obtaining proper data are filtration experiments conducted at larger scale. Once significant flux decline by at least 20% to 30% is observed, approaches like the V_{max} method [Badmington et al., 1995; Zydney et al., 2002] or the

24 3 µm nominal cut-off

more sophisticated method suggested by Ho and Zydney [2000] can be used for extrapolation of flux data and prediction of filter capacity.

5.2.2 Centrifugation

In the second process (Figure 1-5), centrifugation was investigated as an alternative to normal-flow filtration for the clarification of cell culture supernatant. But although the second process can be considered an advancement of the first process, the choice of centrifugation shall not imply any preference here. Investigations were rather conducted for completeness, such that performance of both operations can be compared. Evidently, other factors like process economy, availability of equipment and the scale of operation do play a role in the decision of which operation is to be preferred. Decision can thus only be made on a per case basis.

Data from all centrifugation experiments resulted in sigmoid trajectories when plotting clarification efficiency over centrifugal load (Figure 4-15 and Figure 4-16). Moreover, data was independent of centrifugation systems, due to the application of Sigma theory. An influence of cultivation systems was not detectable. The only exception were data from experiments with vessels having flat bottom. Clarification efficiency obtained with these vessels was shifted by about one order in magnitude towards lower loads. Most likely, this can be attributed to a looser pellet at the bottom of tubes, which would have led to resuspension of some cell debris upon decanting of supernatant. A correction factor of $\mu = 1$ can be suggested for these vessels, however, since the degree of resuspension most likely depends on the operator as well, the use flat-bottomed vessels should be generally avoided.

When plotting clarification efficiency on a probability scale, a straight line is obtained, indicating log-normal distribution of sedimentation velocity. The same has been observed by Maybury et al. [2000] in the sedimentation of rigid particles, protein precipitates and yeast before. Choice of the error function would hence have been most appropriate for the description of data. However, since the error function cannot be formulated in closed form, Verhulst's function was preferred as an approximation instead. After the identification of parameters, working diagrams can be generated similar to those in Figure 4-16, which allow for the selection of a centrifugal load corresponding to the desired clarification efficiency. Identified parameters are further useful for the comparison of sedimentation characteristics of different systems. Due to the high uncertainty of

experimentally determined clarification efficiency, this would be impossible by looking at the raw data alone. For example, by comparison of parameters in Table 4-23, it can be seen that slopes of curves (b) are similar for all investigated groups or systems. The same is true for center points (x_c) with the exception of vessels having flat bottom, which has already been discussed above.

Preparative clarification of supernatant from roller bottles was conducted with conical vessels of 230 ml at a load of $1.57 \cdot 10^{-8}$ m s^{-1}. This value was chosen based on the working diagram for virus in V-Medium (Figure 4-16a). The corresponding predicted clarification efficiency of 97% matches the clarification efficiency obtained by membrane microfiltration (0.45 µm cut-off), which was conducted in parallel. More importantly, this clarification efficiency is practically identical to the overall efficiency of 98% achieved by sequential normal-flow filtration (4.2.1). Actually achieved clarification efficiencies, however, were significantly lower with 90.3% and 94.5% (see end of 4.2.2). On the one hand, this may be ascribed to a misfit of Verhulst's function near the extremes[25], leading to faulty prediction. Likewise, the grouping of data from all vessels may not have been appropriate. Clarification efficiency achievable in conical vessels of 230 ml may actually be lower compared to test tubes. On the other hand, differences in handling procedures could be made responsible. This is particularly true for the decanting of supernatant after centrifugation. Noteworthy, vessels for the preparative centrifugation of several liters sometimes even had to be re-used without intermediate cleaning.

In order to achieve a similar clarification efficiency as after membrane microfiltration, centrifugal load would have to be further reduced. But apart from economical considerations that may speak against this, membrane microfiltration would still be required for the the protection of chromatography columns [Kempken et al., 1995; Berthold et al., 1994]. For this reason, a membrane microfiltration step was incorporated into the second process scheme, immediately after the selective precipitation of DNA. Centrifugation hence only needs to replace the pre-filtration step implemented in the first process. Accordingly, requirements on clarification efficiency are somewhat relaxed. Clarification efficiencies of 90.3% and 94.5% after preparations already resembled those of the pre-filtration step (91%, see Table 4-21). Average virus yields of 81% and 82% were somewhat lower but still comparable (85% after pre-filtration). The reason for apparent yields being significantly lower than 100% should be the same as discussed before (see 5.2.1).

25 i.e. near 0 and 100%

Despite the use of Sigma theory, it remains to be confirmed that results are transferable to manufacturing-scale continuous centrifuges. While successful scale-up from laboratory to continuous centrifuges has been demonstrated for rigid particles [Maybury et al., 2000; Boychyn et al., 2000], shear stress at the inlet of continuous centrifuges regularly affects the size distribution of shear-sensitive matter. Resulting decrease in the average particle diameter, in turn, causes a reduction in the clarification efficiency [Maybury et al., 2000; Boychyn et al., 2000; Hutchinson et al., 2006]. It was estimated by computational fluid dynamics that maximum energy dissipation of a multi-chamber bowl centrifuge occurs at the inlet with rates being as high as $6 \cdot 10^5$ W kg^{-1} (fully flooded inlet) [Boychyn et al., 2001]. But lysis of mammalian cells already occurs at much lower energy dissipation rates [Hutchinson et al., 2006]. Similar studies on a tubular bowl centrifuge predicted shear rates up to 25 000 s^{-1} near the inlet close to the deflector plate [Jain et al., 2005]. Again, disintegration of mammalian cells has been observed during cross-flow filtration for shear rates > 3 000 s^{-1} [Maiorella et al., 1991].

A simple yet effective approach to simulate these conditions is by pre-treating samples in a shear-device mimicking the high energy dissipation rates at centrifuge inlets [Boychyn et al., 2001]. By doing so, fairly accurate prediction of centrifugal performance has been achieved for yeast protein, plasma precipitate [Boychyn et al., 2004] and mammalian cells [Hutchinson et al., 2006]. In the latter study, a clarification efficiency of 98.5% was achieved for a load of 2 x 10^{-8} m s^{-1} in experiments with a laboratory test-tube centrifuge. A mammalian cell suspension at the late culture phase was used in experiments[26]. Pretreatment of the suspension in a shear device led to up to five-fold increase in the remaining solid content, depending on the maximum energy dissipation rate. A somewhat lower ratio may be expected for cells after virus infection, due to cell lysis during the infection phase. Still, some increase in the remaining solid content should be anticipated. Execution of similar experiments with virus-containing supernatant from cell culture is therefore recommendable.

5.3 Selective Precipitation

Selective precipitation of DNA was implemented as an additional DNA-clearance step in the second process scheme. Among the considered agents, PEI was found most suitable with respect to selectivity between DNA and virions. Residual concentrations of DNA were routinely reduced

26 antibody-producing myeloma cell line, 10% viability

to levels of 0.79 ± 0.06 µg ml^{-1} after processing of supernatants from roller bottles, which corresponds to a reduction by $85.3 \pm 1.2\%$. However, these values need to be interpreted with caution. Since DNA concentrations after precipitation were below the basal concentration contributed by the cell culture medium, values had to be extrapolated in the assay (see 3.1.4 for details). True DNA concentrations may hence have been even lower, explaining the somewhat suspicious uniform values obtained after precipitation, independent of the initial concentration. This hypothesis is supported by the much lower concentrations of DNA obtained after DF. While DNA was still enriched in TFUF without preceding precipitation (Table 4-27), it appeared to be fully permeable during DF after precipitation (Table 4-28). One explanation could be that the content of DNA prior to TFUF (i.e. after precipitation) was overestimated and true values were determined only after DF in the absence of matrix effects. However, an equally likely explanation would be that particularly large fragments similar in size to virions, but at least larger than the membrane cut-off, were removed by precipitation. A distinction cannot be made before improved analytical methods have become available.

Co-precipitation of virions under certain conditions was successfully addressed by execution of a factorial design. Subsequent addition of 0.2 M NaCl to precipitation reactions and adjustment of pH to 9 resulted in satisfactory virus yields of $(84 \pm 8)\%$[27]. Since influenza virions have been reported to possess an acidic isoelectric point, they are negatively charged at physiological pH and above [Zhilinskaya et al., 1972; Miller et al., 1944]. Co-precipitation by the poly-cation PEI was therefore not unexpected within the investigated pH range from 7 to 9. Conducting precipitation at pH values below the pI of virions appears to be logical on the first glance. This approach, however, is prohibitive due to a molecular mechanism that irreversibly alters the structure of HA protein on the surface of virions. (see 5.5.2.1 for a detailed discussion). Reduced precipitation of virions at elevated ionic strength can be explained by the screening of electrostatic attraction due to free ions [Pelta et al., 1996; Raspaud et al., 1998]. The lower degree of co-precipitation at a pH of 9 is likely due to a reduction in the net charge of PEI and hence weakening of interactions with virions. Despite its name, PEI is a polyamine with pK_a's of individual amino groups presumably in the range from 9 to 11. Prediction of net charge as a function of pH, however, is difficult due to the high density of amino groups and resulting electrostatic interactions. In addition, an impact of ionic strength is to be expected. The precipitation of DNA, in contrast, was effected to a lesser

27 based on NA activity

extent by modified conditions. Albeit, higher concentrations of PEI were required for complete precipitation. The reason that DNA was still able to form stable complexes under these conditions is almost certainly related to the much higher charge density.

For comparison, experiments performed by Hoopes and McClure [1981] showed that the concentration of spermine necessary for the precipitation of DNA increased with ionic strength. More recently, dependency of the stability of DNA-polycation complexes on salt concentration was investigated by DeRouchey et al. [2005]. By addition of salt, a discontinuous phase transition was found from compact to loose bundles and finally to an isotropic network phase in which all electrostatic interactions were shielded. The critical salt concentration above which the phase transition occurred was determined to be 0.5 M for complexes of DNA with branched PEI (25 kDa). Atkinson and Jack [1973] showed that an increased ionic strength is beneficial for product recovery. After precipitation of microbial extracts with PEI, 70% of bacterial enzymes were recovered in the supernatant while more than 90% of DNA was removed. In most cases, precipitation of enzymes decreased by increasing the ionic strength while the removal of DNA was not affected.

An interesting phenomenon is the re-dissolution of virions at high concentrations of PEI that can bee seen in Figure 4-17. Similar behavior has been observed for DNA [Pelta et al., 1996; Raspaud et al., 1998], although not in this study. The existence of a critical concentration of precipitating agent, beyond which re-dissolution occurs, was explained by charge-reversal of DNA molecules. Above this critical concentration, DNA strands are highly decorated with PEI molecules, resulting in the exposure of positive charge on the surface. Negative charge in turn leads to repulsion and colloidal stabilization. Possibly, the phenomenon of re-dissolution could be exploited for enhancing selectivity of the operation. The clear disadvantage would, however, be the resulting high concentration of PEI after precipitation. Control of the operation by adjustment of ionic strength and pH is therefore to be preferred.

The molecular weight of PEI appeared to have no effect on both, DNA reduction and NA recovery. The low molecular weight PEI of 2 kDa was hence chosen, since it can easily be eliminated by subsequent DF. In addition, it is less viscous and allows for the better handling of stock solutions. Because of its in vivo toxicity [Chollet et al.; Regnström et al., 2003; Moghimi et al., 2005], the removal of residual PEI after precipitation is of essential importance. For this

purpose, an additional salt-wash was introduced during DF (4.4.3), intended to break ionic interactions and allow for the wash out of PEI. Absence of pseudo HA activity in permeates after the second DF step, indeed, indicated that complete wash-out of PEI occurred. In addition, PEI should be recovered in flowthroughs during adsorptive AIEC (4.5.2.5), resulting in a further reduction. Experimental evidence, however, is still outstanding.

Besides the efficient clearance of DNA, there are further arguments that speak in favor of an early precipitation step with PEI. Firstly, PEI is a synthetic polymer available at large quantities and low cost. Secondly, once established, precipitation is a simple operation that can be scaled almost unlimitedly. Thirdly, the continuous centrifuge used for the purpose of clarification in the second process scheme (Figure 1-5b) can be reused for the separation of precipitates. The cost of investment thus remains low. The clear disadvantage of using PEI in precipitations is the inherent *in vivo* toxicity. It may be speculated that alternative compounds exist that are less toxic but as potent with respect to the precipitation of DNA. However, since molecular properties of PEI, in both respects, are mostly determined by its poly-cationic nature, a search for alternatives would be likely in vain. The focus should hence rather be set on removing PEI efficiently in follow-up operations. For this purpose, development of a sensitive assay would be required. Alternatively, the chromatographic use of PEI could be considered. A technique that has been applied by Sakata et al. [2005]. In principle, however, this is equivalent to flowthrough AIEC described in 4.5.2.2, except for the use of a different ligand.

5.4 Tangential-Flow Filtration

5.4.1 Concentration

Shearing of virions in hollow-fibers appeared to be non-critical with respect to HA activity. Circulation of cell culture supernatant at wall shear rates up to 16 000 s^{-1} did not lead to a reduction in HA activity. In contrast, recovery of retrovirus concentrated with similar hollow-fiber modules (1 mm ID, 30 cm length) was reported to dependend on the inlet pressure[28] [Paul et al., 1993]. Only at a low input pressure of 2.5 psi (0.17 bar), recoveries of up to 86% based on infectivity were achieved. At a higher input pressure of 5 psi (0.33 bar), recoveries were in the range of only 10%. An increase in viral transcriptase activity, however, indicated that virus

28 The inlet pressure is related to the retentate flow and hence wall shear rate. Corresponding flow or wall shear rates were not specified in the publication.

particles had been concentrated but were not infectious any more. Similarly, partial disintegration of influenza virus cannot be ruled out even if HA activity remains unchanged. Depending on the degree of disintegration, the separation behavior in follow-up operations might be well affected.

Hollow-fiber modules with 750 kDa cut-off appeared to be best for the concentration of influenza virus. Whereas virions were completely rejected by the membrane, most of the protein and part of the DNA was withdrawn with the permeate. Consequently, virions were not only concentrated but the amount of impurities was simultaneously reduced. Yet, the cut-off of 750 kDa should not be taken literal, as it depends on the rating procedure used by the manufacturer. In a different study, permeation of influenza virus was already observed at a cut-off of 300 kDa with modules from a different manufacturer [Wickramasinghe et al., 2005].

Remarkably, TFUF with hollow-fibers showed critical flux behavior (Figure 4-20a). Above a flux of approximately 28 L m^{-2} h^{-1}, the module started to foul, when operated at a wall shear rate of 9500 s^{-1}. Filtrations conducted at a flux of 42 L m^{-2} h^{-1} resulted in low product yields of only 44%, most likely due to virus depositing on the surface or inside the membrane. These observations resemble at least qualitatively the results by Wu et al. [1999] obtained with model colloids. In their study, HT50 silica particles[29] started to deposit on a 50 kDa flat sheet membrane at a flux around 50 L m^{-2} h^{-1} for Re = 373 and at about 75 L m^{-2} h^{-1} for Re = 580. At lower flux no increase in the TMP was observed. Due to the differences in particle size distributions and the type of modules used, however, direct comparison is impossible. While fouling at the wall shear-rate of 9500 $s^{-1}$was investigated by the TMP-method, maximum flux permissible at lower wall shear rates was determined by the mass balance method (Figure 4-21). Again, it was found that almost lossless concentration can be achieved under appropriate flux settings. Moreover, it was demonstrated that yields based on NA activity paralleled those of HA activity.

About 20-fold volume reduction was achieved in preparations using the long module of 60 cm length and 225 cm^2 membrane area. The concentration factor was only limited by the hold-up volume of the filtration set-up. When run at a constant flux of 28 L m^{-2} h^{-1} and a wall shear rate of 9500 s^{-1}, 97% of the virus based on HA activity were recovered. In the second process, a shorter module of only 30 cm length was used in preparations. Long fibers had been found sub-optimal, due to inverse flow through the membrane at low flux, caused by a strong pressure gradient on the retentate side. In addition, the wall shear rate was lowered for reducing requirements on the

29 bimodal size distribution with modal values at 70 nm and 140 nm

retentate pump. Filtration runs (only concentrating step) conducted at a constant flux of 19 L m^{-2} h^{-1} and a wall shear rate of 3800 s^{-1}, similarly resulted in high yields for HA activity of 94% on average (Table 4-26). Yields based on NA activity, in contrast, were somewhat lower than expected. In principle, however, results obtained by the mass-balance method were confirmed. Since little is known about the stability of neuraminidase enzyme, its loss was not necessarily related to TFUF.

In both cases, yields compare well to the yield of 100% reported for the concentration of equine influenza virus [Nayak et al., 2005]. It has been further stated that up to 86% of infectious retrovirus from packaging cell lines can be recovered using similar hollow-fiber modules [Paul et al., 1993]. For the concentration of HIV-1 core and virus-like-particles, a similar yield of 87% was achieved [Cruz et al., 2000].

SDS-PAGE of cell culture supernatant and virus concentrate qualitatively visualized the enrichment of viral proteins (Figure 4-22a). In particular the low-weight components originating from the soy hydrolysate in Ex-Cell MDCK medium were removed efficiently. The maximum achievable reduction in host-cell protein, however, is difficult to determine, since virions contribute to the amount of total protein. Discrimination between viral and the host-cell protein would be the prerequisite for precise quantitation. According to the permeability for total protein, maximum depletion should be at least 70% (Table 4-26) in the case of infinite concentration or DF. In comparison to protein, DNA fragments appeared to be much larger. Only fragments running below 200 bp in a 2% agarose gel could be removed in the concentration step. According to mass balances, however, this fraction made up for about half of the DNA population (Table 4-26).

Particle volume distributions obtained by dynamic light scattering analysis showed good agreement between the concentrates from different runs (Figure 4-22b). Modal values were close to the average size of influenza virions. This finding suggests that the majority of particles being concentrated indeed are virions. The obvious idea of comparing volume distributions in cell culture supernatants with those in concentrates could not be realized due to the low concentrations in the first. Besides, the variability of measurements was rather high. It has to be doubted that minor changes in volume distributions can be tracked reliably by the method. Still, it was interesting to see that all concentrates contained a small fraction of larger particles up to 400 nm

in size. The limit of 400 nm actually fits nicely with the 0.45 µm cut-off of the microfiltration membrane, supporting the validity of measurements. Up to now, the nature of these particles remains unclear. They could equally likely originate from the aggregation of virions or incomplete removal of cell debris during microfiltration.

5.4.2 Diafiltration

Diafiltration in the second process was intended to replace SEC used in the first process. Since in both cases, separation is based on size, similar results should be obtainable at least in theory. The advantage of using DF is the saving of a costly chromatography operation. In addition, virions are not diluted during constant-volume DF, which relaxes the requirements concerning concentration of virions in follow-up operations.

The major concern about DF is the comparatively low yields achieved in this work. In addition to the 6% loss of HA activity during concentration, another 22% and 18% were lost in subsequent DF steps, multiplying to an overall yield of only 60% (Table 4-28). For comparison, virus yields close to 100% were reported for the concentration and DF of two influenza viruses [Valeri et al., 1977]. In this study, a PSVP membrane with 1 MDa cut-off was used and DF was conducted against 0.l M phosphate buffer at pH 7.3. Similarly, the DF of parvovirus-like particles resulted in a yield of 88% [Maranga et al., 2002].

Low yields for the HA activity were obtained despite the fact that operating conditions had been optimized with respect to flux and wall shear rate before (see 4.4.1). Since, however, colloidal surface interactions may play a role in the filtration of nanoparticles, it is possible that the altered sample environment during DF led to a reduction in the critical flux [Bacchin et al., 2006]. Critical flux as a function of wall shear rate should hence be re-investigated under conditions met upon DF. Moreover, the use of different membrane materials and addition of blocking agents could be considered. The latter were found essential for the concentration of viruses from ground water at high yield [Winona et al., 2001; Divizia et al., 1989; Jansons et al., 1986].

The loss in NA activity was even more strongly pronounced. While yields for the HA and NA activity still paralleled after concentration (Figure 4-21), an over-proportional loss of NA activity was observed after DF. This may be attributed to the dependency of neuraminidase enzyme on Ca^{2+}-ions as a co-factor [Carroll et al., 1982; Baker et al., 1976; Dimmock, 1971]. By

crystallography, it was shown that every subunit of the NA protein tetramer has a high-affinity binding site for Ca^{2+}-ions close to the active center [Burmeister et al., 1994]. The loss in NA activity after DF may therefore be attributed to the removal of calcium ions, which were absent in DF buffers. Addition of Ca^{2+}-ions at concentrations in the order of 1 mM should therefore be considered, not only to buffers used in DF but also chromatography.

A particularly important task during DF was the removal of excessive PEI, remaining after selective precipitation. For this purpose, additional DF against high-salt buffer was conducted for breakage of ionic interactions. Indeed, as is indicated by the absence of pseudo HA activity in permeates after the second DF step, washout of PEI below the limit of detection occurred (Table 4-28). Under ideal conditions, DF against eight volumes of buffer is equivalent to a 3000-fold reduction in fully permeable substances (2-10). The residual concentration of PEI would hence be expected to be below 150 ppb. Confirmation by respective analytical methods, however, is still outstanding. In particular, there is a risk of virions being decorated by PEI, which would alter separation characteristics in subsequent IEC and could result in the release of PEI after vaccination *in vivo*.

Besides PEI, DNA was reduced more than 55-fold during TFUF including DF (Table 4-28). Residual DNA concentrations of 0.78 ± 0.02 µg ml^{-1} after the concentrating step were almost two orders of magnitude lower than the concentrations of 37 ±17 µg ml^{-1} after TFUF without preceding precipitation (Table 4-27). After DF, residual concentrations of 14 ± 15 ng ml^{-1} were even close to the limit of quantitation of the assay. Overall reduction of DNA after DF was 500-fold compared to 3-fold after TFUF in the first scheme. Although this reduction does not suffice for fulfillment of EP requirements, it is an improvement compared to the first process and provides a good starting point for final polishing by chromatography. As mentioned before, material balances for DNA did not close after the first DF step. Since the concentration after precipitation and in concentrates had to be determined by extrapolation, it can be speculated that true concentrations were overestimated. Consequently, depletion of DNA by selective precipitation would have been higher than the 6.8-fold reduction stated before (see 3.5.2). Additional reduction by TFUF, on the other hand, would have been lower.

Analysis of protein content was inferred by the presence of PEI. Measurement only became possible again after the second DF step. In principle, determination of the joint reduction by

selective precipitation and TFUF including DF would have been possible. Since the focus during investigation of the second process was mainly set on DNA, however, no data have been generated yet. Respective measurements remain to be conducted.

5.5 Chromatography

5.5.1 Size-Exclusion Chromatography

5.5.1.1 Empirically Established Size-Exclusion Chromatography

SEC was employed for the separation of small solutes and colloids from virions. Elution from all four chromatography media led to a characteristic double peak pattern in the UV trace similar to the profiles presented for Sepharose 4 FF (Figure 4-25). Virus was eluted in the first peak (void fraction) whereas the second peak resulted from the elution of small solutes (total inclusion; most likely amino acids, nucleotides, etc.) Similar elution profiles have been reported for human influenza virus from chicken egg [Heyward et al., 1977], equine influenza virus from mammlian cell culture [Nayak et al., 2005] and turkey corona virus (TCoV) propagated in turkey embryo [Loa et al., 2002], despite the use of different chromatography media and feed material. In contrast, in SEC of vesicular stomatitis virus (VSV-G) produced by packaging cell lines, three peaks were observed upon elution from Sepharose CL-4B [Transfiguracion et al., 2003]. In all studies, virions were concentrated prior to injection.

Noteworthy, strong tailing of the virus was observed upon elution from Sepharose CL-2B. This finding suggests that part of the virus population was able to enter a fraction of the pores. In addition, mass transfer effects, due to the large size of influenza virions, may have enhanced tailing of the elution peak. A phenomenum which has been described by Li et al. [1998] on the basis of a general rate model (see 5.5.1.2 for discussion on the example of DNA).

As can be seen in Figure 4-25, the UV trace was completely misleading with respect to the elution of protein and DNA. Both eluted mostly between the two peaks, solely indicated by a slight absorbance above zero. Absorbance levels between the two peaks in elugrams of egg-derived human influenza virus [Heyward et al., 1977] and TCoV [Loa et al., 2002] suggest a similar situation there.

DNA appeared to be larger and consequently eluted earlier than host-cell protein, if one assumes that total protein correlating with HA activity is virus protein. Agarose gel electrophoresis of samples taken from the product fractions of preparative SEC runs revealed an average DNA fragment length of 1 kB with some fragments ranging up to 2 kB (Figure 1-4b). According to the correlation published by Potschka [1991], the fragment size of 1 kB translates into a characteristic radius of 42 nm, which is about the average radius of influenza virions [Lamb et al., 2001]. Complete separation of virions from DNA, thus, cannot be achieved by size-based fractionation alone, as has already been discussed in the introduction (1.6).

Due to the separation principle, volume overloading in SEC causes peak broadening and has to be limited. In addition, operation is restricted to relatively low flow rates (typically less than 60 cm h^{-1}) in order to maintain mass-transfer limitations at an acceptable level. SEC operations hence often pose a bottleneck in downstream processes. In this study, a high load of 0.15 cv was applied to a relatively short column (30 cm) operated at a rather high superficial mobile phase velocity (60 cm h^{-1}). The resulting volumetric productivity of 0.15 cv h^{-1} was 6-fold higher than the productivity estimated for [Heyward et al., 1977] and more than 8-fold higher than the productivity estimated for [Nayak et al., 2005]. An overview including more examples is given in Table 5-42. Still, an overall 19-fold reduction in total protein was achieved after SEC (see below). Significant savings due to the lower amount of chromatography media required (short column of 30 cm length only) and due to faster processing can be expected.

Since chromatograms after up to 13 injections were indistinguishable based on the UV-trace, the unit operation was considered non-critical with respect to column cleaning. In addition, there was no indication of decreasing yield after repeated injection. With respect to process hygiene, however, intermediate sanitization may be advisable in particular if the feed cannot be guaranteed to be sterile.

Viral preparations under conditions deduced from the loading study constantly resulted in yields ≥ 80% (Table 4-30). On average, 96% of eluted HA activity, corresponding to 85% of loaded activity, could be recovered in the product fraction, which is in very good agreement with the 95% originally targeted. The loss of 10% of loaded HA activity can be explained by denaturation, aggregation or non-specific adsorption of virions to the stationary phase. A similar product yield of 80%[30] was reported by Heyward *et al.* [1977] for the purification of influenza virus on

30 based on HA activity and infectious activity

controlled pore glass (Table 5-42). In contrast, the yield obtained by Nayak *et al*. [2005] was much lower (only 38%) using Sepharose CL-2B which was most likely the result of strong tailing of the virus peak. But also total recovery was lower with 70% compared to 89% in this study. Yields for vesicular stomatitis virus and moloney murine leukemia virus purified on Sepharose CL-4B were both lower with 70% and 53%, respectively. However, these yields were based on infectivity, which is considered less stable than HA activity.

On average, total protein was reduced to 35% of the amount loaded. Overall reduction was 19-fold after SEC (Table 5-43). A bias in this result, however, cannot be ruled out. Total recovery of protein was only 69% on average, which can be ascribed to matrix interference in the assay. Components of the cell culture medium had been found to interfere with the protein assay before. For samples from supernatants or concentrates this was compensated by preparation of standard solutions in cell culture medium (see 3.1.3 for details). However, such compensation was not applicable to SEC eluate fractions, since their composition is undefined. Underestimation of the protein concentration is therefore likely upon co-elution with interfering substances, leading to a total recovery of less than 100%. If interfering substances were assumed to be small, correct estimation of the total protein concentration would be expected in virus eluate fractions but underestimation in waste fractions. The situation for DNA was different. Here, a total recovery of 136% was found on average. A contribution from non-specific background fluorescence was ruled out by measurement of appropriate blanks[31]. In contrast, repeated measurement of concentrates at various dilutions resulted in slightly higher DNA concentrations at higher dilution. It was thus concluded that interference by the cell culture medium was not compensated completely by the calibration procedure. As a consequence, underestimation of the DNA concentration in virus concentrates occurred and led to a total recovery of more than 100%. Hence, the estimation of DNA concentrations in virus eluate fractions would have been correct but the degree of DNA depletion underestimated.

31 sample without dye

Table 5-42. Overview of SEC protocols reported in the literature

Virus	Medium	H[a]	V_{col}[b]	V_{inj}[c]	u[d]	Dur.[e]	Prod.[f]	Yield[g]	Reference
		cm	ml	cv	cm h^{-1}	h	cv h^{-1}	%	
X174	CPG	100	79	0.10	153	1.22	0.084	n.a.[h]	Gschwender, 1969
TCoV	Sephacryl S-1000	95	466	n.a.	6	5.94	0.002	n.a.	Loa, 2002
VSV-G	Sepharose CL-4B	40	80	0.01 2	12	n.a.	n.a.	70	Transfiguracion, 2003
MoMLV	Sepharose CL-4B	53	106	0.07	15	6.4	0.011	53	Segura, 2005
Influenza	CPG	100	64	0.05	94	1.9	0.025	80	Heyward, 1977
Influenza	Sepharose CL-2B	95	191	0.10	30	5.9	0.018	38	Nayak, 2005
Influenza	Sepharose 4 FF	31	62	0.15	60	1.0	0.15	85	Non-Overlapping
							0.21		Overlapping
							0.37		Overlapping, Two-Step

a: bed height, b: volume of column packing, c: injection volume, d: superficial mobile phase velocity, e: duration of single run, f: productivity, g: product yield, h: not available

Note: Productivities were estimated from column dimensions, injection volumes and flow rates reported. One run was assumed to last for the elution of 1.76 cv in addition to the injected volume.

5.5.1.2 Optimization of Volume Load in a Modeling Study

Various approaches have been suggested in the past for the prediction of chromatographic outcome. What is common to all of them is that the composition of the feed stream has to be known a priori and individual components need to be characterized in order to come up with valid predictions. Moreover, predicting the effect of volume overloading is not straight forward, although usually feasible. The potential of treating SEC as an LTI system is that it does not rely on any such information but is an inverse method. The effect of volume overloading can be described after a single experiment used to determine the system impulse-response. It can further deal with abstract signals like UV absorbance or total protein concentration without having to decompose them into their individual contributions. It has to be noted, however, that the effect of mobile phase velocity or column length cannot be predicted as opposed to other methods, but has to be determined experimentally. Still, by treating SEC as an LTI system, the parameter space spanned by injection volume, mobile phase velocity and column length is efficiently reduced by one dimension.

Successful prediction of chromatograms from three runs by means of a single impulse-response (one for each type of signal) underlines applicability of linear systems theory in the case of

complex feed streams (Figure 4-27). Prediction was particularly accurate for UV absorbance, the signal of highest quality. A good match between simulation and experiment was also obtained for HA activity. The poor match for total protein can be related to low concentrations in some fractions close to the limit of quantitation (about 5 µg/ml). In addition, matrix interference has been observed for this particular assay due to media components leading to unclosed material balances (typically around 60%). Results for total protein therefore do not invalidate the general approach but only reflect the poor quality of the signal.

Chromatography at different mobile phase velocities produced uniform impulse-responses for the HA activity (Figure 4-28). A result which confirms that virions are totally excluded from the resin. In the absence of mass transfer, solutes are only subject to moving zone dispersion. Moving zone dispersion, again, is characterized by the Peclet number, which is only a weak function of mobile phase velocity [Li et al., 1998].

Reconstructed impulse-responses for HCP, on the contrary, strongly depended on mobile phase velocity. Increased broadening and a shift of the distribution towards lower elution volume was observed at high mobile phase velocities (120 and 60 cm h^{-1} compared to 30 cm h^{-1}). Similar to the 201 kDa PMA marker (Figure 2-9b), these changes can be interpreted as the result of limiting mass-transfer. As derived by Li et al. [1998], broad and skewed peaks are the result of low η number, which again is caused by high mobile phase velocities. If the accessible pore fraction ε_a and effective diffusivity D_p are further low, which is the case for almost excluded solutes, very low numbers for η are the result and broad asymmetric peaks are to be expected. In terms of the stochastic model [Dondi et al., 2002], limitation in mass-transfer is represented by low values of α – the relative magnitude of the size-exclusion effect for the egress process m_p with respect to the total size-exclusion effect (ingress and egress). Low α means domination of the ingress process which occurs due to lower residence time in the column at high mobile phase velocities and the hence reduced mean values of the ingress step number $\bar{\eta}_p$. According to theory, low α leads to low effective plate heights (i.e. broad) and skewed peaks. Again, the effect is predicted to be strongest for solutes close to the exclusion limit ($K_{SEC} \to 0$).

Interestingly, impulse-responses for HCP derived from experimental sets A and B deviate significantly (Figure 4-27 and Figure 4-28). A much higher content of HCP eluting at low elution volume was seen in the response derived from set B. To some extend this may be related to the

fact that HCP was reconstructed and not measured. But qualitative differences in reconstructed distributions suggest that real differences exist. Whether these have to be attributed to batch-to-batch variability, inappropriate storage of sample or different eluents cannot be decided at this point. More experiments would have to be conducted using different lots of virus in order to collect statistical data.

Predicted minimum content of UV area, total protein and HCP were consistent in the sense that values increased with increasing mobile phase velocity due to stronger band broadening. Besides, values for the mobile phase velocity of 60 cm h^{-1} derived from both sets compared well. Obviously, the low value of 0.2% for HCP at a mobile phase velocity of 30 cm h^{-1} should not be overstressed. Reconstructions for HCP are certainly only of modest accuracy and predicted proportions will be particularly inaccurate for values close to zero. Nevertheless, it can be concluded that although complete separation from HCP does not seem to be feasible, a final content below about 10% should be achievable.

Comparison of simulation results to experimental data resulted in good agreement for the yield of product based on HA activity (Table 4-31). As expected, yields of light scattering area resembled that of HA activity quite well, confirming that light scattering can be used as an online signal for the quantitation of virions (see also 5.5.2.4). Noteworthy, simulations and experimental results were both close to a yield of 95%, the value originally targeted when designing the operation.

A good match was also observed for the final content of UV area and total protein. The value of such a comparison, however, is questionable since neither of these signals is particular specific for the product or impurities. Changes in product yield or purity are therefore less reflected by changes in material balances of these signals. This becomes immediately evident by looking at predictions for the final content of HCP. Despite similar predictions for the content of total protein (45% and 52%), a large discrepancy occurred with respect to HCP (7.1% and 25%), a result owed to the clear difference between estimated impulse-responses.

Productivity of the empirically established SEC operation[32] was calculated to be 0.15 cv h^{-1} (Table 5-42). By admitting overlapping injection-elution cycles (including a 0.2 cv safety margin) a significant gain to 0.21 or 0.22 cv h^{-1} (set A or B, respectively) can be achieved. Applying the

32 non-overlapping injection-elution cycles, 0.15 cv injection volume, 60 cm h^{-1} superficial mobile phase velocity, 1.91 cv run length

two-step elution strategy described in Figure 4-30, productivity even rises to 0.37 or 0.44 cv h^{-1}, respectively. Since, however, the high content of HCP predicted by set B is less desirable, operation at a mobile phase velocity lower than 60 cm h^{-1} should be considered. The predicted content of HCP at 30 cm h^{-1} was again below 10% but higher purity would be achieved at the cost of reduced productivity. A compromise could be to reduce the target product yield slightly to about 90% (instead of 95%), which would allow for injection of at least 0.3 cv at 30 cm h^{-1} according to predictions in Figure 4-31. In doing so, productivity would be approximately restored to previous values while the final content of HCP should remain below 10%.

In general, it can be concluded that SEC may be treated as an LTI system and that the effect of volume overloading is correctly predicted by convolution of impulse-responses with desired injection profiles. With respect to chromatography of biological feed streams, offline analytics can be identified as the major bottleneck. No online signals were available for the specific detection of virions and protein but elution profiles had to be determined by offline analysis. Consequently, impulse-responses could not be approximated from chromatograms after short injections. On the one hand, feed solutions used in experiments were fairly dilute such that the limit of quantitation would have been undercut for total protein. On the other hand, offline measurements would not have resolved the narrow elution peak of virions sufficiently. While, for example, online light scattering appears to be an acceptable replacement for HA activity in the case of influenza virus, no such alternative exists for total protein or HCP. But only after such online signals have become available, determination of impulse-responses at many flow velocities or studies on batch-to-batch variability of feed streams can be conducted efficiently. Development of appropriate online detectors is therefore mandatory before the suggested method will become truly useful.

Concerning the method itself, a combination of linear systems theory with mechanistic models should be considered in the future, in order to incorporate the effects of flow velocity and column length. Ideally, inverse methods would be developed that allowed to gain sufficient information on the composition of feed streams and properties of the principal components in a limited number of experiments. Impulse-responses could then be predicted by a rate or statistical model and volume overloading subsequently simulated by convolution with the desired injection profile.

5.5.2 Ion-Exchange Chromatography

5.5.2.1 Virus Stability

Sensitivity of HA activity to acidic and alkaline pH was revealed in experiments on virus stability. Interestingly, degradation occurred fastest around a pH of 5 and slowed down towards lower pH. It was therefore concluded that degradation in this range is not unspecific[33], but due to a molecular mechanism known to be responsible for endosomal membrane fusion after infection [Lamb et al., 2001]. This mechanism has been reported to involve an irreversible change in the conformation of hemagglutinin protein, triggered by a decrease of pH in endosomes. A similar finding for low pH was reported by Scholtissek [1985]. In his experiments, infection of chicken embryo cells by infectious allantoic fluid was impaired, if allantoic fluids were treated at low pH for one hour before. The threshold pH investigated for 34 subtypes was in the range from 5 to 6. In contrast, high concentrations of NaCl did not show any effect on HA activity despite the dramatic change in osmotic pressure. This can possibly be explained by stabilization of the envelope by viral matrix protein.

5.5.2.2 Flowthrough Anion-Exchange Chromatography

Tested AIEC media displayed differences in selectivity between influenza virions and host-cell DNA. Concerning Sepharose Q FF, virions and DNA did not seem to be separable at concentrations present in the feed (Figure 4-34). Possibly, separation could have been achieved using a different displacer (e.g. NO^{3-}, HPO_4^{2-}, etc.) but not with NaCl. Since displacement is a competitive effect, it is reasonable to assume that different displacers may yield different selectivity, depending on their affinity to the resin and mobility. Under highly saturated conditions, DNA may even displace the virus itself, since its charge density should be much higher than that of influenza virions. At the laboratory scale, however, such conditions could not be achieved with the amount of feed available. The effect of flow rate (i.e. mass-transfer effects) on selectivity, in contrast, should be negligible since both types of colloids, DNA and virions, are similar in size (Figure 1-4).

Opposed to results for Sepharose Q FF, partial separation was achieved with Sepharose Q XL. However, split-peak elution of virions and co-elution of the second peak with DNA indicated the

33 unfoalding, hydrolysis, etc.

presence of two distinct virus populations. Batch adsorption experiments resulted in a similar observation of two distinct populations (Figure 4-35). Conditioning of feed to 0.65 M NaCl resulted in the expected flowthrough of virions. Recoveries ≥80% were achieved with Sepharose Q XL at loads ≥160 kHAU per ml of resin, which was in good agreement with the batch adsorption experiment (86% at 0.7 M NaCl). Reduced yields at lower loads were most likely the result of residual binding capacity of the stationary phase. After saturation, most of the virus can be recovered in the flowthrough, leading to high yields at high loads.

On average, DNA was reduced to 1.5% of the amount loaded. Overall reduction was more than 500-fold (2.7 orders of magnitude) after AIEC. Overall yield of HA activity averaged at 53% (Table 5-43). Interestingly, the residual amount of DNA per dose did not depend on the virus yield. The virus yield after AIEC, however, was a strong function of load. In addition to split-peak elution and results of the batch adsorption experiment, this is another indicator that part of the DNA was associated to virions and hence co-purified during chromatography. A similar situation has been reported by Konz et al. [2005] regarding the purification of adenovirus. It was shown that DNA in virus-containing lysates was only completely digestable by DNase after treatment with detergent and high salt buffer. They further reported, that the addition of detergent to chromatography buffer was necessary to prevent aggregation of virions. In this work, particles in the range of 400 nm were detected by dynamic light scattering measurements after SEC and AIEC, potentially representing virus-DNA aggregates (data not shown). It can be speculated that disruption or prevention of these presumable aggregates would lead to higher purity and higher product yields as well.

Surprisingly, the amount of total protein was reduced in AIEC, too, despite the high salt concentration in feeds. This loss can be explained by a loss in viral protein in the case of batch No. 3 (Table 4-33). In the case of batch No. 4, however, the reduction in total protein was higher than the loss in HA activity. Analysis by SDS-PAGE revealed that a small protein <14 kDa was removed during AIEC that was not separated in SEC (data not shown). The separation behavior of this protein either suggests some kind of DNA-association or a highly negative charge. In the first case, histones would be a likely candidate, as they are an essential component of genomic DNA.

For determination of volumetric productivity, knowledge of the dynamic capacity of the column for DNA would have been required. Still, a rough estimate of productivity can be derived. In the

area of plasmid purification, capacities around 1 mg per ml of resin have been reported for various anion-exchangers [Ferreira et al., 2000]. Assuming a DNA concentration of 6 µg ml^{-1} in feeds, the estimated capacity of the column would be equivalent to 170 cv of injected feed. Maintaining a constant flow rate of 200 cm h^{-1} and adding 1.7 h for equilibration, desorption and cleaning, a productivity of 11.2 cv of feed per hour can be predicted.

Table 5-43. Step and overall yields of the first investigated process

Operation	HA / %		Turbid.[a] / %		Protein / %		DNA / %		N[b]
	Step	Over.[c]	Step	Over.	Step	Over.	Step	Over.	
Cultivation	-	100	-	100	-	-	-	-	
NFF-1	85	85	8.7	8.7	-	100	-	100	13
NFF-2	93	79	24	2.1	93	93	105	105	13/13/6/6
TFUF	97	77	-	-	16	15	33	35	3
SEC	85	65	-	-	35	5.2	34	12	4
AIEC	82	53	-	-	68	3.5	1.6	0.19	2/2/4

a: turbidity as the extinction of light at 700 nm, b: number of processed batches, c: overall yield after unit operation, NFF-1: normal-flow filtration through 0.65 µm fibrous pre-filter, NFF-2: normal-flow filtration through 0.45 µm membrane filter.

5.5.2.3 Scouting with Membrane Adsorbers

Scouting experiments with membrane adsorbers were conducted for obtaining a first impression on the suitability of several chromatographic techniques with respect to adsorptive purification of influenza virions. Membrane adsorbers were selected due to availability of 96-well plate formats, which are convenient for the purpose of screening. Besides, membrane chromatography is generally believed to be suitable far nanoparticle purification and superior over conventional chromatography resins [Pedro et al., 2008].

Since scouting experiments were conducted with a single influenza virus strain, results should not be considered more than a first indication. Different results may be obtained for other strains and in particular for other subtypes. Respective experiments remain to be conducted. Another drawback of the screening approach in 96-well plates was the general low recovery. Even in the case of Sartobind Q, where 70% to 80% recovery were later obtained in preparative chromatography with a MA75 device (Table 4-37 and Table 4-38), recoveries were only in the

range from 14 to 28% (Table 4-34). Thus, no conclusion with respect to recovery after scale-up can be drawn from these small-scale studies.

In the following, results for the different membranes are interpreted and discussed in the context of previous reports. It should be noted, however, that none of the publications cited were conducted with influenza virus from mammalian cell culture but virus propagated in chicken eggs. Moreover, virions were generally purified in their active state without preceding chemical inactivation, which may cause alterations in the surface of virions. Direct comparison may therefore be illegitimate and lead to contradictory conclusions.

Best results for the adsorption of influenza virions were achieved with Sartobind Q. This was not unexpected since isoelectric points of influenza virions have been reported to be around pH 5[34]. The net charge of virions is hence negative at physiological pH and above. In addition, adsorption of virions to Sepharose Q and Q XL had been observed before (see 4.5.2.2). Adsorption was independent of the matrix and pH. Capacities were similar for all three conditions (between 9.0 to 10.8 kHAU cm^{-2}). As mentioned before, recoveries were generally low but still highest when compared to other adsorbers.

Concerning Sartobind S, a significant dependency on the sample matrix was observed. While virions in supernatant did not bind to Sartobind S, some capacity was observed for virions in diafiltrates (2.5 to 5.4 kHAU cm^{-2}). Adsorption at the lower pH of 7.3 was favorable, which is in agreement with the decreasing negative net charge of virions and hence reduced repulsion from the negatively charged resin towards acidic pH. Results thus confirm an early report on the adsorption of influenza PR-8 virus to an Amberlite cation-exchange resin [Muller et al., 1952].

The attempt of purifying influenza virions by adsorption to glassfibre filters was based on the reports by Bresler et al. [1975, 1977]. In these studies, it was shown that several influenza strains adsorb to the surface of porous borosilicate glass. Elution was achieved either by a change in pH, increase in ionic strength and optional addition of urea for breakage of hydrophilic interactions. In agreement with these studies, influenza virions in supernatant were adsorbed successfully to a glassfibre filter, yielding a capacity even higher than that of Sartobind Q (21.3 compared to 9.0 kHAU cm^{-2}). Recovery, in contrast, was very low (only 4%), indicating that conditions upon elution (pH 8.6 and 2 M urea) were insufficient for the breakage of bonds. Generally, the

34 pH 5.0 for A2/Singapore/57 [Zhilinskaya et al., 1972] and 5.3 for PR-8 [Miller et al., 1944]

chromatography on glass has been reported as fairly unspecific [Mizutani, 1985; Schnabel et al., 1991]. It is therefore questionable whether reasonable purification can be achieved by this technique.

Testing of a metal-chelate membrane (Sartobind IDA) charged with Ca^{2+} was based on the presence of two Ca^{2+} binding sites in neuraminidase enzyme [Burmeister et al., 1994]. Besides, adsorption of influenza virions to insoluble $Ca_3(PO_4)_2$ has been reported [Pepper, 1967; Salk, 1945]. Indeed, some affinity of virions towards the Ca^{2+}-charged membrane was found in experiments. Capacities, however, were low in comparison to Sartobind Q. Noteworthy, the capacity for virions in diafiltrate was about three times higher than for virions in supernatant (2.7 compared to 0.84 kHAU cm^{-2}). This can be explained by the presence of free Ca^{2+} in cell culture supernatant, which competes with immobilized Ca^{2+} ions and hence reduces the capacity. But after all, it cannot be ruled out that interaction was rather unspecific and that the Ca^{2+}-charged membrane merely acted as an anion-exchanger. It can neither be ruled out that IDA residues interacted directly with virions and Ca^{2+} was not involved in the adsorption process. The latter hypothesis is supported by the low recoveries achieved upon elution with 0.5 M EDTA (5% and 2%). Hence, the suitability of Ca^{2+}-charged chromatography media as an alternative to ion-exchangers has to be questioned.

5.5.2.4 Capture with Membrane Adsorbers

Experimental results clearly demonstrate that a direct capture of influenza A virus from cell culture supernatant with Sartobind Q is feasible. Activity-based capacities determined for the Sartobind Q membrane were consistent within batches produced with Ex-Cell MDCK medium (3.12 ± 0.54 kHAU cm^{-2}) or V-Medium medium (5.19 ± 0.16 kHAU cm^{-2}). The impact of cell culture media, i.e. the environment of the virus upon adsorption, can be readily explained by a shift in the adsorption equilibrium, possibly due to a difference in ionic strength or competitors present in the media. In contrast, neither the virus strain nor the cultivation system showed a significant influence on capacity. More experiments would have been required, however, to rule out a dependency on the virus strain and confirm robustness of the operation.

Within the same batch, HA activity correlated well with areas under the light scattering signal. Measurement of scattered light intensity enables thus to quantitate virions online after calibration

of the detector. Due to an almost linear correlation[35], an approximate relative quantitation can be achieved even without calibration by comparing areas under the light scattering signal. Light scattering was therefore employed to characterize elution from Sartobind Q and D adsorbers and for the detection of virus breakthrough in capacity determinations. It should be noted, however, that light scattering is not selective for virions per se but large particles in general[36]. Fragments of host-cell DNA, present in cell culture supernatants, have been shown to reach dimensions similar to those of influenza virions (Figure 1-4). Significant bias due to scattering of DNA should therefore be expected.

Lowering pH below the presumable pI of influenza virions did not cause elution from Sartobind Q as would have been expected. The absence of a light scattering signal suggested that not only the activity of the hemagglutinin protein was lost but also that virus particles remained on the membrane. In contrast, displacement with sodium chloride resulted in almost complete elution from Sartobind Q (typically around 80%, see Table 4-37). Campbell et al. [2004] demonstrated by light scattering studies that a drop in pH from 7.3 to 5.0 led to an instantaneous expansion of PR-8 and X-31 influenza virions by about 100 Å. The expansion was ascribed to a conformational change in the hemagglutinin protein, which covers the envelope of influenza virus. On a time scale of several minutes with kinetics depending on the concentration of virions, the conformational change was followed by self-aggregation of virus particles. Generally, it is assumed that a conformational change of the hemagglutinin protein, triggered by a drop in pH in endosomes (pH 5.5-5.0), is the key event for a number of steps leading to membrane fusion and release of the viral genome from endosomes [Colman et al., 2003; Nayak et al., 2004]. If triggered outside of endosomes, virions are left with a hydrophobic shell which is likely to induce the kind of aggregation observed by Campbell et al. [2004]. Likewise, lowering the pH for elution from Sartobind Q may have resulted in massive aggregation of adsorbed virions, possibly forming a film layer within the membrane. Also, hydrophobic interaction with the membrane itself may have had a similar effect.

Total recoveries below 100% can be explained by incomplete elution but also an overall reduction in HA activity caused by disruption of virions, denaturation of hemagglutinin protein and aggregation of virions. Elution over a wide range of salt concentrations (Figure 4-38) can be

35 B = 1.19 compared to 1 in the linear case

36 The scattering intensity at a certain angle is proportional to the mass concentration times molecular weight.

explained by distributed properties of the viral population. Due to the complexity of the budding process [Nayak et al., 2004] some variability has to be expected with respect to the size of virions and their composition. As a result, different modes of interaction between virions and membrane adsorbers are likely to exist.

Compared to Sartobind Q, displacement from Sartobind D resulted in significantly lower recoveries (typically around 40%, see Table 4-37). Since not only HA activity was reduced but also the intensity of scattered light, it can be concluded that elution of virions was incomplete (Figure 4-38). In addition, the onset of elution was delayed, i.e. occurred at higher salt concentrations. This difference can be interpreted as the result of a stronger interaction of virions with Sartobind D, which is probably due to the higher charge density (5-6 μmol cm^{-2}) compared to Sartobind Q (3-4 μmol cm^{-2}). It is likely that multiple interactions of virions with the stationary phase led to cooperative binding. Only if all interactions are displaced simultaneously, a virion is desorbed and carried away with the bulk liquid. Increasing the number of binding sites should thus result in an overproportional increase of the equilibrium constant K_D [1992]. This was indeed the case when Jayaraman et al. [1993] investigated the use of dextran-based polyelectrolytes as high affinity displacers in the context of the steric mass action law formalism. Highly charged dextrans (DEAE and sulfate-modified) with characteristic charges $\nu_D = 64$ and 31 per molecule had equilibrium constants $K_D = 5.45 \cdot 10^{44}$ and $3.61 \cdot 10^{28}$, respectively. These were many orders of magnitude higher than the equilibrium constants of five proteins ($\nu_D = 4.8$ to 7.5), which ranged from $5.44 \cdot 10^{-3}$ to $1.84 \cdot 10^{-1}$. Isotherms of dextran displacers at a given salt concentration almost equaled step functions in comparison to those of proteins. Sartobind Q and D are cast from the same base matrix[37]. Therefore, it is likely that the higher charge density of Sartobind D does not only result in a higher capacity, as would have been in the case of small colloids, but also in an increase in the number of interacting sites and hence binding strength of virions to the stationary phase (Figure 5-44). Assuming a charge density of 190 μmol ml^{-1} (average value for Sartobind D), an average volume of $8.74 \cdot 10^{-15}$ m^3 would be occupied by each charge. If charge were arranged in a lattice, the mean distance between charged sites would be 94 nm. Of course, the real distance has to be much shorter, since charge is arranged on a surface and only a fraction of the filter volume is occupied by the stationary phase. But this simple back-of-the-envelope calculation

37 regenerated cellulose, identical membrane structure

already demonstrates that the distance between interaction sites is lower than colloidal dimensions and that the scenario for large colloids is likely true for influenza virions.

No major influence of pH on the capacity of Sartobind Q was detected in spin plate experiments (Figure 4-39). Control of pH, however, proved important with respect to recovery. Losses in HA activity occurred under acidic pH < 7.0. Such losses had been reported earlier for egg-derived PR-8 virus at pH values below 5 [Goyal et al., 1980]. Similarly, lower recoveries were observed at alkaline pH > 8.0. This reduction, however, cannot be explained by the stability data for HA activity in cell culture supernatant. In fact, it is the concentration of virus particles that seems to make the difference. Looking at the stability data for HA activity in 20-fold concentrates it can be seen that a reduction in HA activity already occurs at pH > 8 (Figure 4-32).

In a study with Zeta Plus filters, Goyal et al. [1980] found that adsorption of PR-8 virus was dependent on the pH of the feed. Maximum capacity was observed at pH 6.0 with a strong decline towards acidic pH (50% of maximum capacity at pH 5) and a less pronounced decline towards more alkaline pH (75% of maximum capacity at pH 7). Interestingly, full recovery of the virus based on HA activity was achieved with a number of alkaline eluents (e.g. 0.5 M NaCl at pH 9 or saline at pH 11). Eluates were, however, immediately neutralized after elution thus reducing the possible effects of degradation. In some cases, infectivity of the virus (egg-infective dose) was measured, too. The authors claim that infectivity data ”paralleled” HA activity but no data is shown. Complete recovery based on infectivity (plaque forming units) was also reported for the purification of three alphaherpesviruses on Sartobind S MA100 cation-exchangers [Karger et al., 1998]. Depending on the strain, virus eluted between 0.4 to 0.6 M potassium chloride at pH 6.2. No detailed information on the capacity is provided but more than $1.7 \cdot 10^8$ pfu cm^{-2} were adsorbed in one experiment.

Preparative runs under final operating conditions revealed that selectivity of Sartobind Q remains the key issue. On the one hand, significant reduction was achieved with respect to total protein (about 75%). In fact, part of the remaining protein may be ascribed to the virus itself but also DNA-associated protein such as histones. Clearance of host-cell protein can hence be considered even higher. Host-cell DNA, on the other hand, was recovered completely in product fractions (Table 4-38). Due to elution of virions over a wide range of salt concentrations, it seems unlikely that separation of virions from DNA can be enhanced by gradient optimization. Consequently,

early elimination of DNA, e.g. by selective precipitation (3.5.2) or DNAse treatment, appears to be recommendable. Alternatively, it could be attempted to alter the selectivity of membranes either by varying charge density or using a ligand more specific for influenza virions. At the same time, the strength of bonds should be weakened allowing for milder elution conditions.

Enrichment of the product was also sub-optimal. According to the elution peak detected by the light scattering detector, eluting virions could have been collected in a volume of approximately 25 ml. With respect to batches No. 5 and 6, a volume concentration factor of 6.3 and 7.5, respectively, would have been achieved under optimal fractionation conditions. Assuming a product yield of 70%, which is slightly lower than the total recovery, HA activity would have been enriched by a factor of 4.4 and 5.3, respectively. Two causes can be made responsible for the low enrichment: On the one hand, wide and tailing elution peaks can be caused by slow desorption kinetics of the virus. On the other hand, back-mixing and uneven flow distribution may lead to a similar result. Reducing the flow rate upon elution or even incubating the virus in desorption buffer should help to overcome the first problem and may even enhance recoveries. Increasing the number of layers should help to improve concentration factors in both cases. However, both measures would lead to a reduction in productivity as well.

Regarding productivity, the performance of Sartobind Q MA75 adsorbers was remarkable. About 20 min were required for a complete cycle consisting of equilibration, loading, washing, elution and quick regeneration[38]. Assuming a volumetric capacity of 2.23 ml cm^{-2} (roller bottles with Ex-Cell MDCK medium, see Table 4-35) a volumetric productivity of 67 L $m^{-2} h^{-1}$ is achieved. In comparison to TFUF (4.4.2), this productivity is more than twice the critical flux. Even if two modules had to be stacked or the flow rate upon elution had to be reduced, productivity should remain superior. Noteworthy, the flow rate used in experiments was only limited by backpressure generated in the chromatography system. Using specialized valves and appropriate tubing, productivity may be increased even further.

38 operated at 22 ml min^{-1}, which corresponds to a superficial mobile phase velocity of 264 cm h^{-1} or 10 bed volumes per minute.

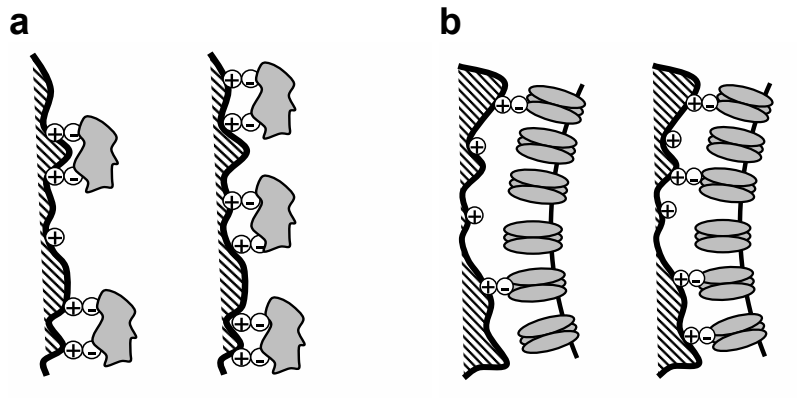

Figure 5-44. Effect of colloidal dimensions on adsorption.
Adsorption of small colloids to a stationary ion-exchange phase (a). Increasing charge density mainly leads to an increase in capacity. This is true if the distance between interaction sites is larger than colloidal dimensions. The characteristic charge (average number of interaction sites) is altered to a minor extend. In contrast, for large colloids increased charge density mainly leads to higher characteristic charge and stronger interaction (b). The increase in capacity is less pronounced due to steric hindrance among colloids.

5.5.2.5 Polishing with Packed-Beds and Monoliths

An adsorptive chromatography step for final polishing was favored in the second process scheme. Compared to flowthrough AIEC (4.5.2.2), adsorptive AIEC combines the advantage of enhanced purity with the simultaneous concentration of virions. In addition, not only highly-negatively charged molecules like DNA but also non-adsorbing impurities (i.e. weakly and positively charged molecules) can be separated from virions. The latter aspect becomes particularly important if DNA has been precipitated by poly-cationic substances at an earlier stage of the process. These substances need to be removed again, since they typically show in vivo toxicity.

Separation of virions from host-cell DNA was successful with both anion-exchangers (CIM QA and Source Q). Whereas chromatography on Source Q, conducted according to the manufacturer's instructions, immediately resulted in close-to-baseline separation, some optimization was required for CIM QA. A fact that is certainly owed to the low bed height of the CIM QA disc (only 3 mm compared to 30 mm regarding Source Q) and not to the medium itself. A second point is the low volume of the disc device (only 0.34 ml compared to 1 ml regarding Source Q) such that extra-column zone broadening probably played a role. After adaption of the mobile phase velocity and gradient length, however, comparable resolution was achieved. Results thus re-confirm that

influenza virions (i.e. at least those of certain strains) adsorb to anion-exchangers due to their negative net charge at physiological and alkaline pH (see also 4.5.2.3 and 4.5.2.4).

The dynamic capacity of Source Q (about 250 kHAU or 85 µg of hemagglutinin antigen per ml of resin) was comparable to the dynamic capacity of Sartobind Q[39]. Recoveries of HA activity were slightly above 100% in both runs (Table 4-39 and Table 4-41). The dynamic capacity of CIM QA could not be determined due the absence of virus breakthrough, but appeared to be significantly higher. Recovery in the preparative run with 46.5 ml of diafiltrate was almost complete with 92%. In contrast, recovery in the run with 5 ml of diafiltrate was significantly lower with only 45%. Since in this run, the capacity of CIM QA was barely exploited, it is likely that the loss only occurred due to unspecific adsorption, which had also been observed fore Sepharose Q XL before (Table 4-33). With both media, the estimated residual DNA content was close to the limit of 10 ng per dose (Table 4-40), which is demanded by regulatory bodies (Table 1-2). However, derived values are only rough estimates based on HA activity. For more reliable data, quantitation of the hemagglutinin antigen content by SRID assay is still outstanding. In addition, the concentration of DNA should be verified by an alternative assay (e.g. qPCR or hybridization) in order to rule out bias in measurements.

Opposed to anion-exchangers, adsorption to Source S failed completely. On the one hand, this was expected due to the acidic pI of influenza virions. On the other hand, some adsorption had been observed in scouting experiments with Sartobind S before (3.7.2.3). Failure of adsorption to Source S is also contradictory to an early report on the adsorption of influenza PR-8 virus to an Amberlite cation-exchange resin [Muller et al., 1952]. Possibly, in these cases of successful adsorption, interaction was mediated by poly-ionic impurities, which acted as a glue. Furthermore, differences in the distribution of charged residues on resins have to be taken into account. Overall net charge of virions should be negative at physiological pH, such that only patches of positive charge can be expected to exist. Hence, the supporting matrix, distribution of charge and type of immobilization matters. Another explanation could simply be that interaction was not exclusively ionic. Thus, although results with Source S in this study were negative, feasibility of an adsorptive cation-exchange step for final polishing should not be ruled out in general. It has to be doubted,

39 about 220 kHAU per ml of membrane, calculated from the capacity for A/PR/8/31 (H1N1) cultivated in V-Medium, see Table 4-35

however, that such an operation would be sufficiently robust for annual large-scale purification of influenza virions.

Albeit results for influenza virus A/PR/8/34 (H1N1) RKI with anion-exchangers were promising, a prove of general applicability is still outstanding. First experiments with influenza virus A/Wis/67/2005 (H3N2), for example, revealed a very low affinity of virions to Source Q, resulting in little or no dynamic capacity [Eisold, 2008]. Affinity to CIM QA appeared somewhat higher, but recovery was low and the increase in backpressure even stronger than observed before. Since however, there was a general issue with the stability of A/Wis/67/2005 (H3N2), failure was not necessarily related to chromatography but may have have been caused by unknown factors. In any case, more experiments with different virus strains need to be conducted before a final conclusion can be drawn.

An equally serious problem is the fouling of chromatography columns. In all cases, an increase in backpressure was observed during loading (Figure 4-42). In the case of CIM QA, this increase was so strong that injection volume had to be limited. Applicability of CIM monoliths thus has to be questioned at least for the process scheme investigated here. Although, backpressure reduced again upon elution, a permanent increase persisted until columns were regenerated with NaOH solution. It may be speculated, that this increase in backpressure can be prevented or at least mildened by an additional microfiltration step just before chromatography. According to experience with membrane microfiltration (4.2.1), however, some loss of virions would have to be expected. This would particularly be true, if part of the virus population was present in the form of microaggregates. The latter pose a general problem in the downstream processing of virions and have to be avoided under all circumstances. Still, the mechanisms leading to aggregation are yet poorly understood and require further investigation.

6 Conclusion and Outlook

In summary, results for the first process scheme demonstrate that fairly pure virions can already be obtained by a comparatively simple strategy. Material balances further indicate that all of the investigated unit operations can be realized at high product yield. Key for the development of this process was the improvement of assay formats, in particular the HA assay, which allowed for a more precise characterization of individual steps [Kalbfuss et al., 2008].

However, when visualizing the extreme depletion factor required for DNA (>20 000, see Table 1-3), it becomes clear that such a reduction by a single dedicated step (flowthrough AIEC, see 4.5.2.2) is unrealistic. Only slight backmixing or leakage during such an operation will inevitable lead to failure of specifications. Consequently, a second dedicated step (selective precipitation, see 3.5.1) was introduced in the second scheme. Admittedly, this unit operation is equally based on ionic interactions and therefore not fully orthogonal to AIEC. Still, selective precipitation resulted in a significant additional reduction that became particularly evident after TFUF (500-fold compared to 3-fold after TFUF in the first scheme).

Moreover, it can be speculated that early depletion of DNA (i.e. before the concentration of virions) aids in preventing the formation of mixed aggregates between virions and DNA. The existence of such aggregates was suspected when interpreting the results of chromatography on Sepharose Q XL (Figure 4-34) or the respective batch adsorption experiment (Figure 4-35). In both cases, an inseparable fraction of DNA was observed that could only be recovered together with virions. In addition, an increasing population of particles with diameter around 400 nm has been observed over the process by dynamic light scattering analysis (data not shown). However, more work needs to be conducted for confirmation of aggregates and analytical methods remain to be refined.

An important aspect that has not been addressed yet is the residual content of PEI remaining in the final product bulk. Development of respective analytical methods and subsequent experimental investigation are still outstanding. But also the maximum admissible amount in the final product bulk remains to be determined. The European Pharmacopoeia (EP) does not seem to contain any specifications with respect to PEI or related substances. Therefore, if not available from literature, the maximum admissible dose, will have to be determined in animal experiments and safety of vaccines confirmed in clinical studies.

Another crucial issue, concerning the second process scheme, is the fairly high loss of virions during DF. Currently, it is unclear whether this loss is due to unspecific adsorption to the membrane or excessive flux enforced during filtration. Concerning adsorption, membranes cast from different polymers (e.g. regenerated cellulose or polyethersulfone) could be tested as an alternative. Importantly, several strains should be used in these experiments, since adsorptive properties can be expected to depend on virus strains to some extend. Addition of blocking agents, which has been suggested in analytical applications [Winona et al., 2001; Divizia et al., 1989; Jansons et al., 1986], on the contrary, should be avoided. These substances would have to be removed again later in the process and are almost guaranteed to cause troubles with regulatory bodies. Concerning flux, the wall shear rate should be increased instead of decreasing flux, in order not to reduce productivity of the operation. This can be readily achieved by a reduction of the inner diameter of fibers. With respect to the hollow-fiber modules used in this work, this would simultaneously require the reduction of cut-off to 500 kDa, since 750 kDa fibers of lower diameter are not available. At least in theory, this would cause a somewhat higher impurity after TFUF. Practically however, the difference may be negligible. Finally, the use of SEC as a replacement for DF should be re-considered. According to results from the first scheme (4.5.1), SEC can be expected to work out-of-the-box and should even result in higher purity. Model-based optimization of volume load has further reduced the risk of SEC becoming a bottleneck. The drawback, of course, would be an additional unit operation in the process.

Feasibility of adsorptive polishing of influenza virions has successfully been demonstrated at least in the case of influenza virus A/PR/8/34 (H1N1) RKI. Albeit results with anion-exchangers were promising, a prove of general applicability is still outstanding. In the end, polishing of different strains may not be feasible with a single chromatography medium. In such a scenario, adsorptive chromatography may still be applicable as long as the process engineer is given sufficient alternatives at hand. Modern chromatography systems are capable of screening numerous chromatography media within reasonable time. It is thus imaginable that chromatography is re-adjusted every time vaccine strains have changed and a best fit is selected. Obviously, such a screen would not be restricted to anion-exchangers, but cation-exchangers or completely different media, like e.g. hdydrophobic interaction resins (see for [Eisold, 2008] an example), could be considered in addition. The hydrophobic interaction medium Source ISO, for example, was capable of binding A/Wis/67/2005 (H3N2) at high quantity in a preliminary study (dynamic

capacity > 160 kHAU or 55 µg of hemagglutinin antigen per ml of resin). The recovery was about 80% (data not shown). Whether complete separation from DNA can be achieved, however, remains to be confirmed.

Up to now, most of the developmental work has been driven fully empirically due to the overwhelming complexity of the process. Obviously, more rational approaches, allowing to save time and experiments, would be desirable in several respects. First steps towards that direction have been undertaken by use of a factorial design in the setup of the selective precipitation operation (4.3.1) and development of a modeling framework for predicting the effect of volume-overloading in SEC (4.5.1.2). Although the development of such frameworks is time-consuming and complex, they can be re-used afterwards. Once established, they allow for the optimization of unit operations based on a minimum set of experimental data. Beyond, the model-based approach typically results in a degree of optimization that is unmatched by purely empirical methods. In addition to refinement of the existing framework for SEC, polishing of virions by adsorptive chromatography poses another attractive target for model-based optimization. Since this last step mainly aims at the separation of DNA from virions, it can be approximately treated as a binary mixture separation problem. Hence, classical modeling approaches should be applicable. The steric mass action formalism appears particularly suitable in this respect [Brooks et al., 1992]. It considers steric effects in a simple manner and has been successfully applied for the description of membrane chromatography of rotavirus-like particles [Vicente et al., 2008].

Besides the above-mentioned problems and prospects, robustness of all unit operations with respect to batch-to-batch variability and sensitivity towards virus strains and cultivation systems remains to be confirmed. Firstly, the detailed characterization of roller bottle haversts should be extended to other cultivation systems. Secondly, the impact of cultivation outcome on downstream processing should be investigated. First comparison of supernatants from roller bottles and two stirred-tank microcarrier cultivations, for example, revealed a significantly lower initial DNA content in the latter. Thirdly, the use of more strains in experiments, but at least one strain for subtypes H1N1, H3N2, H5N1 and one influenza B virus, is highly recommendable. In particular with respect to adsorptive operations, differences in the adsorption of virions (isotherms, kinetics, reversibility etc.) are likely to occur. But also the stability of virions and changes in titers pose a challenge to every downstream process. Finally, the potency of inactivated and purified virions should be tested in animals. Although, correlation of SRID assay with

potency is generally assumed, it may not hold for a whole-virion vaccine purified by a new method. But even if the correlation holds, different amounts of antigen may be required. In the end, it is only the ability to induce protective immune response (without causing adverse reactions) that matters.

Figures

Tables

Bibliography

Abraham A, Sivanadan V, Newman JA, Maheswaran SK. 1984. Rapid purification of avian influenza virus for use in enzyme-linked immunosorbent assay. *American Journal of Veterinary Research*, **45**: 959—962.

Ada G. 2005. Overview of Vaccines and vaccination. *Molecular Biotechnology*, **29**: 255—271.

Ambler CM. 1959. The theory of scaling up laboratory data for the sedimentation type centrifuge. *Journal of Biochemical and Microbiological Technology and Engineering*, **1**: 185—205.

Amosenko FA, Svitkin YV, Popova VD, Terletskaya EN, Timofeev AV, Elbert LB, Lashkevich VA, Drozdov SG. 1991. Use of protamine sulfate for elimination of substrate DNA in poliovaccines produced on continuous cell lines. *Vaccine*, **9**: 207—209.

Armstrong EP. 2007. Economic benefits and costs associated with target vaccinations. *Journal Of Managed Care Pharmacy*, **13**: S12—S15.

Armstrong ME, Giesa PA, Davide JP, Redner F, Waterbury JA, Rhoad AE, Keys RD, Provost PJ, Lewis JA. 1993. Development of the formalin-inactivated hepatitis A vaccine, VAQTA from the live attenuated virus strain CR326F. *Journal of Hepatology*, **18**: S20—S26.

Atkinson A, Jack GW. 1973. Precipitation of nucleic acids with polyethyleneimine and the chromatography of nucleic acids and proteins on immobilised polyethyleneimine. *Biochimica et Biophysica Acta*, **308**: 41—52.

Babu GJ, Rajamanickam C. 1998. An improved method for the isolation of supercoiled plasmid DNA. *Current Science*, **74**: 572—573.

Bacchin P, Aimar P, Field RW. 2006. Critical and sustainable fluxes: Theory, experiments and applications. *Journal of Membrane Science*, **281**: 42—69.

Bacchin P, Si-Hassen D, Starov V, Clifton MJ, Aimar P. 2002. A unifying model for concentration polarization, gel-layer formation and particle deposition in cross-flow membrane filtration of colloidal suspensions. *Chemical Engineering Sciences*, **57**: 77—91.

Backman G. 1938. Three growth functions (Verhulst's, Gompertz', Backman's). *Wilhelm Roux Archiv Fur Entwicklungsmechanik Der Organismen*, **138**: 37—58.

Badmington F, Wilkins R, Payne M, Honig ES. 1995. Vmax testing for practical microfiltration train scale-up in biopharmaceutical processing. *Biopharm - The Technology & Business of Biopharmaceuticals*, **8**: 46.

Bahnemann HG. 1990. Inactivation of viral antigens for vaccine preparation with particular reference to the application of the application of binary ethyleneimine. *Vaccine*, **8**: 299—303.

Baker JP, Katz SL. 2004. Childhood vaccine development: An overview. *Pediatric Research*, **55**: 347—356.

Baker NJ, Gandhi SS. 1976. Effect of Ca++ on the stability of influenza virus neuraminidase. *Archives of Virology*, **52**: 7—18.

Bardiya N, Bae JH. 2005. Influenza vaccines: recent advances in production technologies. *Applied Microbiology and Biotechnology*, **67**: 299—305.

Bartlett PD, Small G. 1950. Beta-propiolactone. IX. The kinetics of attack by nucleophilic reagents upon the alcoholic carbon of beta-propiolactone. *Journal of the American Chemical Society*, **72**: 4867—4869.

Baruah GL, Venkiteshwaran A, Belfort G. 2005. Global model for optimizing crossflow microfiltration and ultrafiltration processes: A new predictive and design tool. *Biotechnology Progress*, **21**: 1013—1025.

Beck E, Strohmaier K. 1987. Subtyping of European foot-and-mouth disease virus strains by nucleotide sequence determination. *Journal of Virology*, **61**: 1621—1629.

Belfort G, Davis RH, Zydney AL. 1994. The behavior of suspensions and macromolecular solutions in cross-flow microfiltration. *Journal of Membrane Science*, **96**: 1—58.

Belsey MJ, de Lima B, Pavlou AK, Savopoulos JW. 2006. Influenza vaccines. *Nature Reviews Drug Discovery*, **5**: 183—184.

Benedictis PD, Beato MS, Capua I. 2007. Inactivation of avian influenza viruses by chemical agents and physical conditions: a review. *Zoonoses Public Health*, **54**: 51—68.

Berthold W, Kempken R. 1994. Interaction of cell-culture with downstream purification - a case study. *Cytotechnology*, **15**: 229—242.

Boeckle. 2004. Purification of polyethylenimine polyplexes highlights the role of free polycations in gene transfer. *Journal of Gene Medicine*, **6**: 1102—1111.

Bott S. 1983. Polydispersity analysis of QELS data by a smoothed inverse laplace transform. In: Dahneke B. (ed). *Measurement of suspended particles by quasi-elastic light scattering*. New York: Wiley.

Boutwell RK, Colburn NH, C.C M. 1969. In vivo reactions of beta-propiolactone. *Annals of the New York Academy of Sciences*, **163**: 751—763.

Boychyn M, Doyle W, Bulmer M, More J, Hoare M. 2000. Laboratory Scaledown of Protein Purification Processes Involving Fractional Precipitation and Centrifugal Recovery. *Biotechnology and Bioengineering*, **69**: 1—10.

Boychyn M, Yim SS, Bulmer M, More J, Bracewell DG, Hoare M. 2004. Performance prediction of industrial centrifuges using scale-down models. *Bioprocess Biosystems Engineering*, **26**: 385—391.

Braas G, Searle PF, Slater NK, Lyddiatt A. 1996. Strategies for the isolation and purification of retroviral vectors for gene therapy. *Bioseparation*, **6**: 211—228.

Brands R, Visser J, Medema J, Palache AM, Scharrenburg GJ. 1999. InfluvacTC: A safe Madin Darby canine kidney (MDCK) cell culture-based influenza vaccine. *Developments in Biological Standardization*, **98**: 93—100.

Bresler S et al. 1975. Immunogenicity of inactivated influenza vaccine purified by adsorption chromatography on porous glass. *Med Biol*, **53**: 456—461.

Bresler SE, Katushkina NV, Kolikov VM, Potokin JL, Vinogradskaya GN. 1977. Adsorption chromatography of viruses. *Journal of Chromatography*, **130**: 275—280.

Brooks CA, Cramer SM. 1992. Steric mass-action ion-exchange: displacement profiles and induced salt gradients. *AIChE Journal*, **38**: 1969—1978.

Brown F. 2002. Inactivation of viruses by aziridines. *Vaccine*, **20**: 322—327.

Brument N et al. 2002. A versatile and scalable two-step ion-exchange chromatography process for the purification of recombinant adeno-associated virus serotypes-2 and-5. *Molecular Therapy*, **6**: 678—686.

Brusick DJ. 1977. Genetic properties of beta-propiolactone. *Mutat Res*, **39**: 241—256.

Budowsky EI, Bresler SE, Friedman EA, Zheleznova NV. 1981. Principles of selective inactivation of viral genome. I. UV-induced inactivation of influenza virus. *Archives of Virology*, **68**: 239—47.

Budowsky EI, Friedman EA, Zheleznova N, Noskov F. 1991. Principles of selective inactivation of viral genome. VI. Inactivation of the infectivity of the influenza virus by the action of beta-propiolactone. *Vaccine*, **9**: 398—402.

Budowsky EI, Smirnov YA, Shenderovich SF. 1993. Principles of selective inactivation of viral genome. VIII. The influence of beta-propiolactone on immunogenic and protective activities of influenza virus. *Vaccine*, **11**: 343—348.

Budowsky EI, Zalesskaya MA. 1991. Principles of selective inactivation of viral genome. V. Rational selection of conditions for inactivation of the viral suspension infectivity to a given extent by the action of beta-propiolactone. *Vaccine*, **9**: 319—325.

Budowsky EI. 1991. Problems and prospects for preparation of killed antiviral vaccines. *Advances in Virus Research*, **39**: 255—290.

Burmeister WP, Cusack S, Ruigrok RW. 1994. Calcium is needed for the thermostability of influenza B virus neuraminidase. *Journal of General Virology*, **75 (Pt 2)**: 381—388.

Campbell JN, Epand RM, Russo PS. 2004. Structural changes and aggregation of human influenza virus. *Biomacromolecules*, **5**: 1728—1735.

Carroll SM, Paulson JC. 1982. Complete metal ion requirement of influenza virus N1 neuraminidases. Brief report. *Archives of Virology*, **71**: 273—277.

CDC. 1995. Pneumonia and Influenza Death Rates -- United States, 1979-1994. *MMWR Weekly*, **44**: 535—537.

CDC. 2008. Seasonal Flu. *Centers for Disease Control and Prevention*. http://www.cdc.gov/flu/ (Accessed August 12, 2008).

CDC. 2008. Update: Influenza Activity --- United States, September 30, 2007--February 9, 2008. *MMWR Weekly*, **57**: 1—5.

Chabot I, Goetghebeur MM, Gregoire JP. 2004. The societal value of universal childhood vaccination. *Vaccine*, **22**: 1992—2005.

Chackerian B. 2007. Virus-like particles-flexible platforms for vaccine development. *Expert Review of Vaccines*, **6**: 381—390.

Charlton HR, Relton JM, Slater NKH. 1999. Characterisation of a generic monoclonal antibody harvesting

system for adsorption of DNA by depth filters and various membranes. *Bioseparation*, **8**: 281—291.

Charter MK, Gull SF. 1987. Maximum-entropy and its application to the calculation of drug absorption rates. *Journal of Pharmacokinetics and Biopharmaceuticals*, **15**: 645—655.

Chen R, Mieyal JJ, Goldthwait DA. 1981. The reaction of beta-propiolactone with derivatives of adenine and with DNA. *Carcinogenesis*, **2**: 73—80.

Chen V, Li H, Fane AG. 2004. Non-invasive observation of synthetic membrane processes - a review of methods. *Journal of Membrane Science*, **241**: 23—44.

Choe WS, Middelberg APJ. 2001. Selective precipitation of DNA by spermine during the chemical extraction of insoluble cytoplasmic protein. *Biotechnology Progress*, **17**: 1107—1113.

Chollet P, Favrot MC, Hurbin A, Coll J. Side-effects of a systemic injection of linear polyethylenimine-DNA complexes. *Journal of Gene Medicine*, **4**: 84—91.

Choudhary G, Horvath C. 1996. Ion-exchange chromatography. In: *Methods in Enzymology*. San Diego: Academic Press; 47—82.

Cinatl J, Michaelis M, Doerr HW. 2007. The threat of avian influenza A (H5N1). Part I: Epidemiologic concerns and virulence determinants. *Medical Microbiology and Immunology*, **196**: 181-90.

Colman PM, Lawrence MC. 2003. The structural biology of type I viral membrane fusion. *Nature Reviews Molecular Cell Biology*, **4**: 309—319.

Cordes RM, Sims WB, Glatz CE. 1990. Precipitation of nucleic acids with poly(ethyleneimine). *Biotechnology Progress*, **6**: 283—285.

Coulson J, Richardson J. 1991. Chapter 20: Membrane separation processes. In: *Chemical Engineering (Volume 1)*. Oxford: Butterworth-Heinemann.

Coulson J, Richardson J. 1997. Chapter 3: Flow in pipes and channels. In: *Chemical Engineering (Volume 1)*. Oxford: Butterworth-Heinemann.

Cox HR, Vanderscheer J, Aiston S, Bohnel E. 1946. The purification and concentration of influenza virus by means of alcohol precipitation. *Public Health Rep*, **61**: 1682—1683.

Crooks AJ, Lee JM, Dowsett AB, Stephenson JR. 1990. Purification and analysis of infectious virions and native nonstructural antigens from cells infected with tick-borne encephalitis-virus. *Journal of Chromatography*, **502**: 59—68.

Cruz PE, Peixoto CC, Devos K, Moreira JL, Saman E, Carrondo MJT. 2000. Characterization and downstream processing of HIV-1 core and virus-like-particles produced in serum free medium. *Enzyme and Microbial Technology*, **26**: 61—70.

Darzynkiewicz Z, Juan G, Gorczyca W, Murakami T, Traganos F. 1997. Cytometry in cell necrobiology: analysis of apoptosis and accidental cell death (necrosis). *Cytometry*, **27**: 1—20.

Davis RH. 1992. Modeling of fouling of cross-flow microfiltration membranes. *Separation and purification methods*, **21**: 75—126.

de Frutos M, Raspaud E, Leforestier A, Livolant F. 2001. Aggregation of nucleosomes by divalent cations.

Biophysics Journal, **81**: 1127—1132.

Deng JS, Beutner EH. 1974. Effect of formaldehyde, glutaraldehyde and sucrose on tissue antigenicity. *International Archives of Allergy and Applied Immunology*, **47**: 562—569.

DeRouchey. 2005. Structural investigations of DNA-polycation complexes. *European Physical Journal E*, **16**: 17-28.

DeWalt BW, Murphy JC, Fox GE, Willson RC. 2003. Compaction agent clarification of microbial lysates. *Protein Expression and Purification*, **28**: 220—223.

Dickens F, Jones HE. 1961. Carcinogenic activity of a series of reactive lactones and related substances. *British Journal of Cancer*, **15**: 85.

Dimmock NJ. 1971. Dependence of the activity of an influenza virus neuraminidase upon Ca^{2+}. *Journal of General Virology*, **13**: 481—3.

Divizia M, Santi AL, Pana A. 1989. Ultrafiltration: An efficient second step for hepatitis A virus and poliovirus concentration. *Journal of Virological Methods*, **23**: 55—62.

Dondi F, Cavazzini A, Remelli M, Felinger A, Martin M. 2002. Stochastic theory of size exclusion chromatography by the characteristic function approach. *Journal of Chromatography A*, **943**: 185—207.

Drummond M, Chevat C, Lothgren M. 2007. Do we fully understand the economic value of vaccines? *Vaccine*, **25**: 5945—5957.

Eickbush TH, Moudrianakis EN. 1978. Compaction of DNA helices into either continuous supercoils or folded fiber rods and toroids. *Cell*, **13**: 295—306.

Eickmann M. 2006. Image:Flu und legende color c.jpg. *Wikimedia Commons in Wikipedia*. http://en.wikipedia.org/wiki/Image:Flu_und_legende_color_c.jpg (Accessed August 11, 2008).

Eisold K. 2008. Diploma thesis: *Reinigung von humanem Influenzavirus aus Säugerzellkultur*. University of Applied Sciences Jena, Faculty of Medicinal and Biotechnology.

Enquist LW, Krug RM, Racaniello VR, Skalka AM, Flint SJ. 1999. *Principles of Virology: Molecular Biology, Pathogenesis, and Control*. 1. ed. American Society Microbiology.

Epstein J, Rosenthal RW, ESS RJ. 1955. Use of gamma-(4-nitrobenzyl)pyridine as analytical reagent for ethylenimines and alkylating agents. *Analytical Chemistry*, **27**: 1435—1439.

Eriksson KO. 2002. Gel filtration. In: Vijayalakshmi MA. (ed). *Biochromatography - Theory and Practice*. Taylor and Francis; 9—23.

Espinasse B, Bacchin P, Aimar P. 2002. On an experimental method to measure critical flux in ultrafiltration. *Desalination*, **146**: 91—96.

European Pharmacopoeia Commission. 2005. Influenza vaccine (whole virion, inactivated). In: *European Pharmacopoeia*. Council of Europe; 3406—3407.

European Pharmacopoeia Commission. 2007. Influenza vaccine (whole-virion, inactivated, prepared in cell cultures). In: *European Pharmacopoeia*. Council of Europe; 810—812.

Ferreira GNM, Cabral JMS, Prazeres DMF. 2000. Studies on the batch adsorption of plasmid DNA onto anion-exchange chromatographic supports. *Biotechnology Progress*, **16**: 416—424.

Field RW, Wu D, Howell JA, Gupta BB. 1995. Critical flux concept for microfiltration fouling. *Journal of Membrane Science*, **100**: 259—272.

Frazatti-Gallina NM, Mourao-Fuches RM, Paoli RL, Silva MLN, Miyaki C, Valentini EJG, Raw I, Higashi HG. 2004. Vero-cell rabies vaccine produced using serum-free medium. *Vaccine*, **23**: 511-517.

Freitas SS, Santos JAL, Prazeres DMF. 2006. Optimization of isopropanol and ammonium sulfate precipitation steps in the purification of plasmid DNA. *Biotechnology Progress*, **22**: 1179—1186.

Fukuda K, Levandowski RA, Bridges CB, Cox NJ. 2004. Inactivated Influenza Vaccines. In: Plotkin SA, Orenstein WA. (eds). *Vaccines*. Phildadelphia: Saunders; 339—370.

Gajic Z. 2003. *Linear dynamic systems and signals*. New Jersey: Upper Saddle River.

Gaush CR, Smith TF. 1968. Replication and plaque assay of influenza virus in an established line of canine kidney cells. *Applied Microbiology*, **16**: 588—94.

GE Healthcare. 2007. *Microcarrier Cell Culture Handbook*. Uppsala: GE Healthcare Life Sciences http:// www.gelifesciences.com.

Genzel Y, Behrendt I, Konig S, Sann H, Reichl U. 2004. Metabolism of MDCK cells during cell growth and influenza virus production in large-scale microcarrier culture. *Vaccine*, **22**: 2202—2208.

Genzel Y, Fischer M, Reichl U. 2006. Serum-free influenza virus production avoiding washing steps and medium exchange in large-scale microcarrier culture. *Vaccine*, **24**: 3261—3272.

Genzel Y, Olmer RM, Schäfer B, Reichl U. 2006. Wave microcarrier cultivation of MDCK cells for influenza virus production in serum containing and serum-free media. *Vaccine*, **24**: 6074—87.

Gerdil C. 2003. The annual production cycle for influenza vaccine. *Vaccine*, **21**: 1776—1779.

Giddings JC, Mallik KL. 1966. Theory of gel filtration (permeation) chromatography. *Analytical Chemistry*, **38**: 997—1000.

Goerke A, To B, Lee A, Sagar S, Konz J. 2005. Development of a novel adenovirus purification process utilizing selective precipitation of cellular DNA. *Biotechnology and Bioengineering*, **91**: 12—21.

Goyal SM, Hanssen H, Gerba CP. 1980. Simple method for the concentration of influenza-virus from allantoic fluid on microporous filters. *Applied and Environmental Microbioloy*, **39**: 500—504.

Green AP, Huang JJ, Scott MO, Kierstead TD, Beaupre I, Gao GP, Wilson JM. 2002. A new scalable method for the purification of recombinant adenovirus vectors. *Human Gene Therapy*, **13**: 1921—1934.

Gschwender HH, Haller W, Hofschneider PH. 1969. Large-scale preparation of viruses by steric chromatography on columns of controlled pore glass. *Biochimica et Biophysica Acta*, **190**: 460—469.

Gull SF, Daniell GJ. 1978. Image-Reconstruction From Incomplete And Noisy Data. *Nature*, **272**: 686—690.

Gustincich S, Manfioletti G, G D, Schneider C, Carninci P. 1991. A fast method for high-quality genomic

DNA extraction from whole human blood. *BioTechniques*, **11**: 298.

Hagen A et al. 2000. Development, preparation, and testing of VAQTA (R), a highly purified hepatitis A vaccine. *Bioprocess Engineering*, **23**: 439—449.

Hagen AJ, Aboud RA, DePhillips PA, Oliver CN, Orella CJ, Sitrin RD. 1996. Use of a nuclease enzyme in the purification of VAQTA(R), a hepatitis A vaccine. *Biotechnology and Applied Biochemistry*, **23**: 209—215.

Hagen AJ, Oliver CN, Sitrin RD. 1996. Optimization of poly(ethylene glycol) precipitation of hepatitis a virus used to prepare VAQTA, a highly purified inactivated vaccine. *Biotechnology Progress*, **12**: 406—412.

Haller W. 1965. Chromatography on glass of controlled pore size. *Nature*, **206**: 693—696.

Haller W. 1965. Rearrangement kinetics of liquid-liquid immiscible microphases in alkali borosilicate melts. *J Chem Phys*, **42**: 686—693.

Harmant P, Aimar P. 1998. Coagulation of colloids in a boundary layer during cross-flow filtration. *Colloids and Surfaces A - Physicochemical and Engineering Aspects*, **138**: 217—230.

Hay AJ. 1998. Section 2: Virus structure and replication. In: *Textbook of Influenza*. Oxford: Blackwell Science.

Heyward JT, Klimas RA, Stapp MD, Obijeski JF. 1977. Rapid concentration and purification of influenza virus from allantoic fluid. *Archives of Virology*, **55**: 107—119.

Hilfenhaus J, Köhler R, Behrens F. 1976. Large-scale purification of animal viruses in the RK-model zonal ultracentrifuge. II. Influenza, mumps and Newcastle disease viruses. *Journal of Biological Standardization*, **4**: 273-83.

Ho CC, Zydney AL. 2000. A combined pore blockage and cake filtration model for protein fouling during microfiltration. *Journal of Colloid and Inerface Science*, **232**: 389—399.

Hong SP, Yoo WD, Putnak R, Srivastava AK, Eckels KH, Chung YJ, Rho HM, Kim SO. 2001. Preparation of a purified, inactivated Japanese encephalitis (JE) virus vaccine in Vero cells. *Biotechnology Letters*, **23**: 1565—1573.

Hoopes BC, McClure WR. 1981. Studies on the selectivity of DNA precipitation by spermine. *Nucleic Acids Research*, **9**: 5493—5504.

Hulskotte EGJ, Dings MEM, Norley SG, Osterhaus ADME. 1997. Chemical inactivation of recombinant vaccinia viruses and the effects on antigenicity and immunogenicity of recombinant simian immunodeficiency virus envelope glycoproteins. *Vaccine*, **15**: 1839—1845.

Hutchinson N, Bingham N, Murrell N, Farid S, Hoare M. 2006. Shear stress analysis of mammalian cell suspensions for prediction of industrial centrifugation and its verification. *Biotechnology and Bioengineering*, **95**: 483—491.

Jain M, Paranandi MR, Roush D, Goklen K, Kelly WJ. 2005. Using CFD to understand how flow patterns affect retention of cell-sized particles in a tubular bowl centrifuge. *Industrial & Engineering Chemistry Research*, **44**: 7876—7884.

Janca J. (ed). 1983. *Steric exclusion liquid chromatography of polymers*. New York: Marcel Dekker Ltd.

Jansons J, Bucens MR. 1986. Virus detection in water by ultrafiltration. *Water Research*, **20**: 1603—1606.

Jayaraman G, Gadam SD, Cramer SM. 1993. Ion-exchange displacement chromatography of proteins - Dextran-based polyectrolytes as high affinity displacers. *Journal of Chromatography*, **630**: 53—68.

Jendrisak J. 1987. The use of polyethyleneimine in protein purification. In: Burgess R. (ed). *Protein purification: micro to macro*. New York: Alan R. Liss; 75—97.

Johnson NPAS, Mueller J. 2002. Updating the accounts: global mortality of the 1918-1920 "Spanish" influenza pandemic. *Bulletin of the History of Medicine*, **76**: 105-15.

Kalbfuss B, Flockerzi D, Seidel-Morgenstern A, Reichl U. 2008. Size-exclusion chromatography as a linear transfer system - Exemplified for the purification of human influenza virus. *Journal of Chromatography B*, **873**: 102—112

Kalbfuss B, Knöchlein A, Kröber T, Reichl U. 2008. Monitoring influenza virus content in vaccine production: precise assays for the quantitation of hemagglutination and neuraminidase activity. *Biologicals*, **36**: 145—61.

Kalbfuss B, Wolff M, Geisler L, Tappe A, Wickramasinghe R, Thom V, Reichl U. 2007. Direct capture of influenza A virus from cell culture supernatant with Sartobind anion-exchange membrane adsorbers. *Journal of Membrane Science*, **299**: 251—260.

Kalbfuss B, Wolff M, Morenweiser R, Reichl U. 2007. Purification of cell culture-derived human influenza a virus by size-exclusion and anion-exchange chromatography. *Biotechnology and Bioengineering*, **96**: 932—944.

Kaludov N, Handelman B, Chiorini JA. 2002. Scalable purification of adeno-associated virus type 2, 4, or 5 using ion-exchange chromatography. *Human Gene Therapy*, **13**: 1235—1243.

Kanarek AD, Tribe MGW. 1967. Concentration of certain myxoviruses with polyethylene glycol. *Nature*, **214**: 927.

Karger A, Bettin B, Granzow H, Mettenleiter TC. 1998. Simple and rapid purification of alphaherpesviruses by chromatography on a cation exchange membrane. *Journal of Virological Methods*, **70**: 219—224.

Keitel WA, Atmar RL. 2007. Preparing for a possible pandemic: influenza A/H5N1 vaccine development. *Current Opinion in Pharmacology*, **7**: 484—490.

Kempken R, Preissmann A, Berthold W. 1995. Assessment of a disc stack centrifuge for use in mammalian cell separation. *Biotechnology and Bioengineering*, **46**: 132—138.

Kendal A. 1997. Cold-adapted live attenuated influenza vaccines developed in Russia: Can they contribute to meeting the needs for influenza control in other countries? *European Journal of Epidemiology*, **13**: 591—609.

Kilbourne ED. 2006. Influenza pandemics of the 20th century. *Emerging Infect. Dis*, **12**: 9-14.

Kim HS, Chung YJ, Jeon YJ, Lee SH. 1999. Large-scale culture of hepatitis A virus in human diploid

MRC-5 cells and partial purification of the viral antigen for use as a vaccine. *Journal of Microbiology and Biotechnology*, **9**: 386—392.

King AM, Underwood BO, McCahon D, Newman JW, Brown F. 1981. Biochemical identification of viruses causing the 1981 outbreaks of foot and mouth disease in the UK. *Nature*, **293**: 479—480.

King DJ. 1991. Evaluation of different methods of inactivation of Newcastle disease virus and avian influenza virus in egg fluids and serum. *Avian Dis*, **35**: 505—514.

Kistner O, Barrett PN, Mundt W, Reiter M, Schober-Bendixen S, Dorner F. 1998. Development of a mammalian cell (Vero) derived candidate influenza virus vaccine. *Vaccine*, **16**: 960—968.

Knipe DM, Howley PM. (eds). 2001. *Fields Virology*. 4. ed. Philadelphia: Lippincott Williams & Wilkins.

Knöchlein A. 2007. Master thesis: *Ernte von Influenza Virus aus tierischer Zellkultur: Kulturverlauf, zentrifugale Klärung, Fällung verunreinigender DNA*. University of Applied Sciences Hamburg, Faculty of Life Sciences.

Knudsen HL, Fahrner RL, Xu Y, Norling LA, Blank GS. 2001. Membrane ion-exchange chromatography for process-scale antibody purification. *Journal of Chromatography A*, **907**: 145—154.

Konz JO, Lee AL, Lewis JA, Sagar SL. 2005. Development of a purification process for adenovirus: Controlling virus aggregation to improve the clearance of host cell DNA. *Biotechnology Progress*, **21**: 466—472.

Kramberger P, Peterka M, Boben J, Ravnikar M, Strancar A. 2007. Short monolithic columns - A breakthrough in purification and fast quantification of tomato mosaic virus. *Journal of Chromatography A*, **1144**: 143—149.

Kröber T. 2008. Diploma thesis: *Ernte und Reinigung von humanem Influenzavirus aus Säugerzellkultur.* Martin Luther University Halle-Wittenberg, Faculty of Mathematics, Natural Sciences and Engineering.

Kumar AAP, Rao YUB, Joseph ALW, Mani KR, Swaminathan K. 2002. Process standardization for optimal virus recovery and removal of substrate DNA and bovine serum proteins in Vero cell-derived rabies vaccine. *J of Bioscience and Bioengineering*, **94**: 375—383.

Kwon DY, Vigneswaran S, Fane AG, Ben Aim R. 2000. Experimental determination of critical flux in cross-flow microfiltration. *Separation and Purification Technology*, **19**: 169—181.

Lamb RA, Krug RM. 2001. Orthomyxoviridae: The viruses and their replication. In: Knipe DM, Howley PM. (eds). *Fields Virology*. Philadelphia: Lippincott Williams & Wilkins; 1487—1531.

Larghi OP, Nebel AE. 1980. Rabies virus inactivation by binary ethylenimine: new method for inactivated vaccine production. *Journal of Clinical Microbiology*, **11**: 120—122.

Lauffer MA, Wheatley M. 1949. Destruction of influenza A virus infectivity by formaldehyde. *Archives of Biochemistry*, **23**: 262—270.

Li H, Fane AG, Coster HGL, Vigneswaran S. 1998. Direct observation of particle deposition on the membrane surface during crossflow microfiltration. *Journal of Membrane Science*, **149**: 83—97.

Li ZG, Gu YS, Gu TY. 1998. Mathematical modeling and scale-up of size-exclusion chromatography.

Biochemical Engineering Journal, **2**: 145—155.

Lis JT. 1980. Fractionation of DNA fragments by polyethylene glycol induced precipitation. In: Grossman L, Moldave K. (eds). *Nucleic Acids Part I*. New York: Academic Press; 347—353.

Livesey AK, Skilling J. 1985. Maximum-Entropy Theory. *Acta Crystallographica Section A*, **41**: 113—122.

Loa CC, Lin TL, Wu CC, Bryan TA, Thacker HL, Hooper T, Schrader D. 2002. Purification of turkey coronavirus by Sephacryl size-exclusion chromatography. *Journal of Virological Methods*, **104**: 187—194.

Lombard M, Pastoret PP, Moulin AM. 2007. A brief history of vaccines and vaccination. *Rev. sci. tech. Off. int. Epiz.*, **26**: 29—49.

Lucas D, Rabiller-Baudry M, Michel F, Chaufer B. 1998. Role of the physico-chemical environment on ultrafiltration of lysozyme with modified inorganic membrane. *Colloids and Surfaces A - Physicochemical and Engineering Aspects*, **136**: 109—122.

Lycke. 1958. Studies of the inactivation of poliomyelitis virus by formaldehyde. *Archives of Virology*, **8**: 267—284.

Madden FN, Godfrey KR, Chappell MJ, Hovorka R, Bates RA. 1996. A comparison of six deconvolution techniques. *Journal of Pharmacokinetics and Biopharmaceuticals*, **24**: 283—299.

Mahy BW, Kangro HO. (eds). 1996. *Virology Methods Manual*. Academic Press.

Maiorella B, Dorin G, Carion A, Harano D. 1991. Cross-flow microfiltration of animal cells. *Biotechnology and Bioengineering*, **37**: 121—126.

Maranga L, Rueda P, Antonis AFG, Vela C, Langeveld JPM, Casal JI, Carrondo MJT. 2002. Large scale production and downstream processing of a recombinant porcine parvovirus vaccine. *Applied Microbiology and Biotechnology*, **59**: 45—50.

Maybury JP, Hoare M, Dunnill P. 2000. The use of laboratory centrifugation studies to predict performance of industrial machines: Studies of shear-insensitive and shear-sensitive materials. *Biotechnology and Bioengineering*, **67**: 265—273.

Maybury JP, Mannweiler K, Titchener-Hooker NJ, Hoare M, Dunnill P. 1998. The performance of a scaled down industrial disc stack centrifuge with a reduced feed material requirement. *Bioprocess Engineering*, **18**: 191—199.

McCullers JA. 2007. Evolution, benefits, and shortcomings of vaccine management. *Journal of Managed Care Pharmacy*, **13**: S2—S6.

Merten O. 2002. Development of serum-free media for cell growth and production of viruses/viral vaccines – safety issues of animal products used in serum-free media. *Developmental Biology*, **111**: 233-257.

Miller GL, Lauffer MA, Stanley WM. 1944. Electrophoretic studies on PR8 influenza virus. *Journal of Experimental Medicine*, **80**: 549—559.

Mizutani T. 1985. Adsorption chromatography of biopolymers on porous glass. *Journal of Liquid Chromatography*, **8**: 925—983.

Moghimi SM, Symonds P, Murray JC, Hunter AC, Debska G, Szewczyk A. 2005. A two-stage poly(ethylenimine)-mediated cytotoxicity: implications for gene transfer/therapy. *Molecular Therapy*, **11**: 990—995.

Mohammad-Djafari A, Giovannelli J, Demoment G, Idier J. 2002. Regularization, maximum entropy and probabilistic methods in mass spectrometry data processing problems. *International Journal of Mass spectrometry*, **215**: 175—193.

Möhler L, Bock A, Reichl U. 2008. Segregated mathematical model for growth of anchorage-dependent MDCK cells in microcarrier culture. *Biotechnology Progress*, **24**: 110—119.

Möhler L, Flockerzi D, Sann H, Reichl U. 2005. Mathematical model of influenza A virus production in large-scale microcarrier culture. *Biotechnology and Bioengineering*, **90**: 46—58.

Montagnon BJ, Fanget B, Vincent-Falquet JC. 1984. Industrial-scale production of inactivated poliovirus vaccine prepared by culture of vero cells on microcarrier. *Rev Infect Dis*, **6**: S341—S344.

Montagnon BJ, Fanget BJ. 1985. Process for the large-scale production of a vaccine against poliomyelitis and the resulting vaccine. *US Patent No. 4525349.*

Moore D, Dowhan D. 2007. Manipulation of DNA. In: Ausubel FM, Brent R, Kingston RE, Moore DD, Seidman JG, Smith JA, Struhl K. (eds). *Current Protocols in Molecular Biology.* Wiley; Supplement 59.

Morenweiser R. 2005. Downstream processing of viral vectors and vaccines. *Gene Therapy*, **12**: S103—S110.

Morgeaux S, Tordo N, Gontier C, Perrin P. 1993. Beta-propiolactone treatment impairs the biological activity of residual DNA from BHK-21 cells infected with rabies virus. *Vaccine*, **11**: 82—90.

Mori S, Barth HG. 1999. *Size Exclusion Chromatography*. Berlin: Springer.

Muller RH, Rose HM. 1952. Concentration of influenza virus (PR-8 strain) by a cation-exchange resin. *Proc Soc Exp Biol Med*, **80**: 27—29.

Murphy F. 2005. Image:Influenza virus.png. *Wikimedia Commons in Wikipedia*. http://en.wikipedia.org/wiki/Image:Influenza_virus.png (Accessed August 11, 2008).

Murphy JC, Wibbenmeyer JA, Fox GE, Willson RC. 1999. Purification of plasmid DNA using selective precipitation by compaction agents - A scaleable method for the liquid-phase separation of plasmid DNA from RNA. *Nature Biotechnology*, **17**: 822—823.

Nagano H, Yagyu K, Ohta S. 1989. Purification of infectious bronchitis coronavirus by sephacryl S-1000 gel chromatography. *Veterany Microbiology*, **21**: 115—123.

Nayak DP, Hui EKW, Barman S. 2004. Assembly and budding of influenza virus. *Virus Research*, **106**: 147—165.

Nayak DP, Lehmann S, Reichl U. 2005. Downstream processing of MDCK cell-derived equine influenza virus. *Journal of Chromatography B*, **823**: 75—81.

NCBI. 2008. Taxonomy browser (Orthomyxoviridae). *National Center for Biotechnology Information*. http://www.ncbi.nlm.nih.gov/Taxonomy/Browser/wwwtax.cgi?id=11308 (Accessed August 27, 2008).

Nicholson KG. 1998. Section 8: Vaccines and vaccine development. In: *Textbook of Influenza*. Oxford: Blackwell Science.

Nicoletti VG, Condorelli DF. 1993. Optimized PEG method for rapid plasmid DNA purification - High yield from midi-prep. *BioTechniques*, **14**: 532.

Novartis Behring. 2008. Pressemitteilung: Neuer Zellkultur-Grippeimpfstoff jetzt saisonal zugelassen. http://www.impfserviceplus.de/impfservice/presse/index.html?msg-id=00458 (Accessed August 21, 2008).

O'Riordan CR, Lachapelle AL, Vincent KA, Wadsworth SC. 2000. Scaleable chromatographic purification process for recombinant adeno-associated virus (rAAV). *Journal of Gene Medicine*, **2**: 444—454.

Opitz L, Salaklang J, Buttner H, Reichl U, Wolff MW. 2007. Lectin-affinity chromatography for downstream processing of MDCK cell culture derived human influenza A viruses. *Vaccine*, **25**: 939—947.

Pau MG, Ophorst C, Koldijk MH, Schouten G, Mehtali M, Uytdehaag F. 2001. The human cell line PER.C6 provides a new manufacturing system for the production of influenza vaccines. *Vaccine*, **19**: 2716—2721.

Paul RW, Morris D, Hess BW, Dunn J, Overell RW. 1993. Increased viral titer through concentration of viral harvests from retroviral packaging lines. *Human Gene Therapy*, **4**: 609—615.

Pedro L, Soares SS, Ferreira GNM. 2008. Purification of Bionanoparticles. *Chemical Engineering & Technology*, **31**: 815—825.

Peixoto C, Sousa MFQ, Silva AC, Carrondo MJT, Alves PM. 2007. Downstream processing of triple layered rotavirus like particles. *Journal of Biotechnology*, **127**: 452—461.

Pelta J, Livolant F, Sikorav JL. 1996. DNA aggregation induced by polyamines and cobalthexamine. *Journal of Biological Chemistry*, **271**: 5656—5662.

Pepper DS. 1967. A chromatographic procedure for the purification of influenza virus. *Journal of Genetic Virology*, **1**: 49—55.

Perrin P, Morgeaux S. 1995. Inactivation of DNA by beta-propiolactone. *Biologicals*, **23**: 207—211.

Peterka M, Strancar A, Banjac M, Kramberger P, Maurer E, Muster T. 2008. Method for influenza virus purification. *International Patent No. WO/2008/006780 A1*.

Plotkin SA. 2005. Vaccines: past, present and future. *Nature Medicine*, **11**: S5—S11.

Polson A. 1974. Purification and aggregation of influenza virus by precipitation with polyethylene-glycol. *Preparative Biochemistry*, **4**: 435—456.

Polson A. 1993. A theory for the displacement of proteins and viruses with polyethylene-glycol (reprinted from Preparative Biochemistry, Vol. 7, Pg. 129, 1977). *Preparative Biochemistry*, **23**: 31—50.

Porath J, Flodin P. 1959. Gel filtration: a method for desalting and group separation. *Nature*, **183**:

1657—1659.

Porter MC. 1972. Concentration polarization with membrane ultrafiltration. *Industrial and Engineering Chemistry Product Research and Development*, **11**: 234.

Potier M, Mameli L, Bélisle M, Dallaire L, Melançon SB. 1979. Fluorometric assay of neuraminidase with a sodium (4-methylumbelliferyl-alpha-D-N-acetylneuraminate) substrate. *Analytical Biochemistry*, **94**: 287—296.

Potschka M. 1991. Size exclusion chromatography of DNA and viruses: properties of spherical and asymmetric molecules in porous networks. *Macromolecules*, **24**: 5023—5039.

Potter CW. 1998. Chronicle of influenza pandemics. In: *Textbook of Influenza*. Oxford: Blackwell Science; 3—18.

Rabiller-Baudry M, Chaufer B, Aimar P, Bariou B, Lucas D. 2000. Application of a convection-diffusion-electrophoretic migration model to ultrafiltration of lysozyme at different pH values and ionic strengths. *Journal of Membrane Science*, **179**: 163—174.

Race E, Stein CA, Wigg MD, Baksh A, Addawe M, Frezza P, Oxford JS. 1995. A multistep procedure for the chemical inactivation of human immunodeficiency virus for use as an experimental vaccine. *Vaccine*, **13**: 1567—1575.

Ramqvist T, Andreasson K, Dalianis T. 2007. Vaccination, immune and gene therapy based on virus-like particles against viral infections and cancer. *Expert Opinion on Biological Therapy*, **7**: 997—1007.

Raspaud E, Chaperon I, Leforestier A, Livolant F. 1999. Spermine-induced aggregation of DNA, nucleosome, and chromatin. *Biophysics Journal*, **77**: 1547—1555.

Raspaud E, de la Cruz MO, Sikorav JL, Livolant F. 1998. Precipitation of DNA by polyamines: A polyelectrolyte behavior. *Biophysics Journal*, **74**: 381—393.

Regnström K, Ragnarsson EGE, Köping-Höggård M, Torstensson E, Nyblom H, Artursson P. 2003. PEI - a potent, but not harmless, mucosal immuno-stimulator of mixed T-helper cell response and FasL-mediated cell death in mice. *Gene Therapy*, **10**: 1575—1083.

Reimer CB, Baker RS, Newlin TE, Havens ML, van Frank RM, Storvick WO, Miller RP. 1966. Comparison of techniques for influenza virus purification. *Journal of Bacteriology*, **92**: 1271—1272.

Reimer CB, Baker RS, Newlin TE, Havens ML. 1966. Influenza virus purification with the zonal ultracentrifuge. *Science*, **152**: 1379—1381.

RKI. 2008. RKI-Ratgeber Infektionskrankheiten - Merkblätter für Ärzte: Influenza. *Robert-Koch-Institut*. http://www.rki.de/cln_091/nn_200120/DE/Content/Infekt/EpidBull/Merkblaetter/Ratgeber__Mbl__Influenza.html#doc200212bodyText8 (Accessed August 12, 2008).

Roberts JJ, Warwick GP. 1963. Reaction of beta-propiolactone with guanosine, deoxyguanylic acid and RNA. *Biochemical Pharmacology*, **12**: 1441.

Rodrigues T, Carvalho A, Roldao A, Carrondo MJT, Alves PM, Cruz PE. 2006. Screening anion-exchange chromatographic matrices for isolation of onco-retroviral vectors. *Journal of Chromatography B*, **837**: 59—68.

Rullgard H, Oktem O, Skoglund U. 2007. A componentwise iterated relative entropy regularization method with updated prior and regularization parameter. *Inverse Problems*, **23**: 2121-2139.

Sakata M, Nakayama M, Fujisaki T, Morimura S, Kunitake M, Hirayama C. 2005. Chromatographic removal of host cell DNA from cellular products using columns packed with cationic copolymer beads. *Chromatographia*, **62**: 465—470.

Salk JE. 1945. The immunzing effect of calcium phosphate adsorbed influenza virus. *Science*, **101**: 122—124.

Salt DE, Hay S, Thomas OR, Hoare M, Dunnill P. 1995. Selective flocculation of cellular contaminants from soluble proteins using polyethyleneimine - A study of several organisms and polymer molecular-weights. *Enzyme and Microbial Technology*, **17**: 107—113.

Schnabel R, Langer P. 1991. Controlled-pore glass as a stationary phase in chromatography. *Journal of Chromatography*, **544**: 137—146.

Scholtissek C. 1985. Stability of infectious influenza A viruses at low pH and at elevated temperature. *Vaccine*, **3**: 215—218.

Schu P, Mitra G. 2001. Ultrafiltration membranes in the vaccine industry. In: Wang WK. (ed). *Membrane Separations in Biotechnology*. New York: Marcel Dekker, Inc.; 225—241.

Schulze-Horsel J, Genzel Y, Reichl U. 2008. Flow cytometric monitoring of influenza A virus infection in MDCK cells during vaccine production. *BMC Biotechnology*, **8**: 45.

Schwinge J, Neal PR, Wiley DE, Fletcher DF, Fane AG. 2004. Spiral wound modules and spacers - Review and analysis. *Journal of Membrane Science*, **242**: 129—153.

Segura MD, Kamen A, Garnier A. 2006. Downstream processing of oncoretroviral and lentiviral gene therapy vectors. *Biotechnology Advances*, **24**: 321—337.

Segura MD, Kamen A, Trudel P, Garnier A. 2005. A novel purification strategy for retrovirus gene therapy vectors using heparin affinity chromatography. *Biotechnology and Bioengineering*, **90**: 391—404.

Shapiro JT, Leng M, Felsenfeld G. 1969. Deoxyribonucleic acid-polylysine complexes - Structure and nucleotide specificity. *Biochemistry*, **8**: 3219.

Shore JE, Johnson RW. 1980. Axiomatic derivation of the principle of maximum-entropy and the principle of minimum cross-Entropy. *IEEE Transactions on Information Theory*, **26**: 26—37.

Sidorenko Y, Reichl U. 2004. Structured model of influenza virus replication in MDCK cells. *Biotechnology and Bioengineering*, **88**: 1—14.

Sidorenko Y, Schulze-Horsel J, Voigt A, Reichl U, Kienle A. 2008. Stochastic population balance modeling of influenza virus replication in vaccine production processes. *Chemical Engineering Science*, **63**: 157—169.

Skilling J, Bryan RK. 1984. Maximum-entropy image-reconstruction: A general algorithm. *Monthly Notices of the Royal Astronomical Society*, **211**: 111.

Smith RH, Ding CT, Kotin RM. 2003. Serum-free production and column purification of adeno-associated

virus type 5. *Journal of Virological Methods*, **114**: 115—124.

Smrekar F, Ciringer M, Peterka M, Podgornik A, Strancar S. 2007. Purification and concentration of bacteriophage T4 using Q1 monolithic chromatographic supports. *Journal of Chromatography B*.

Specht R, Han BB, Wickramasinghe SR, Carlson JO, Czermak P, Wolf A, Reif OW. 2004. Densonucleosis virus purification by ion exchange membranes. *Biotechnology and Bioengineering*, **88**: 465—473.

Srivastava AK et al. 2001. A purified inactivated Japanese encephalitis virus vaccine made in vero cells. *Vaccine*, **19**: 4557—4565.

Stegeman G, Kraak JC, Poppe H, Tijssen R. 1993. Hydrodynamic chromatography of polymers in packed columns. *Journal of Chromatography A*, **657**: 283—303.

Stegeman G, Kraak JC, Poppe H. 1993. Dispersion in packed-column hydrodynamic chromatography. *Journal of Chromatography*, **634**: 149—159.

Storhas W. 1994. *Bioreaktoren und periphere Einrichtungen*. Braunschweig/Wiesbaden: Vieweg.

Sugawara K et al. 2002. Development of Vero cell-derived inactivated Japanese encephalitis vaccine. *Biologicals*, **30**: 303—14.

Sweet C, Stephen J, Smith H. 1974. Purification of influenza viruses using disulphide-linked immunosorbents derived from rabbit antibody. *Immunochemistry*, **11**: 295—304.

Times Y. 2007. Image:Virus Replication.svg. *Wikimedia Commons in Wikipedia*. http://en.wikipedia.org/wiki/Image:Virus_Replication.svg (Accessed August 11, 2008).

Timm EA, McLean IW, Kupsky CH, Hook AE. 1956. The nature of the formalin inactivation of poliomyelitis virus. *Journal of Immunology*, **77**: 444—452.

Transfiguracion J, Jaalouk DE, Ghani K, Galipeau J, Kamen A. 2003. Size-exclusion chromatography purification of high-titer vesicular stomatitis virus G glycoprotein-pseudotyped retrovectors for cell and gene therapy applications. *Human Gene Therapy*, **14**: 1139—1153.

Transfiguracion J, Jorio H, Meghrous J, Jacob D, Kamen A. 2007. High yield purification of functional baculovirus vectors by size exclusion chromatography. *Journal of Virological Methods*, **142**: 21—28.

Tree JA, Richardson C, Fooks AR, Clegg JC, Looby D. 2001. Comparison of large-scale mammalian cell culture systems with egg culture for the production of influenza virus A vaccine strains. *Vaccine*, **19**: 3444—3450.

Trettin DR, Doshi MR. 1980. Limiting flux in ultrafiltration of macromolecular solutions. *Chemical Engineering Communications*, **4**: 507—522.

Trudel M, Marchessault F, Payment P. 1981. Purification of infectious rubella virus by gel filtration on Sepharose 2B compared to gradient centrifugation in sucrose, sodium metrizoate and metrizamide. *Journal of Virological Methods*, **2**: 141—148.

Trudel M, Trepanier P, Payment P. 1983. Concentration and analysis of labile viruses by hollow fiber ultrafiltration and ultracentrifugation. *Process Biochemistry*, **18**: 2—9.

Tsvetkova EA, Nepomnyaschaya NM. 2001. Principles of selective inactivation of a viral genome -

Comparative kinetic study of modification of the viral RNA and model protein with oligoaziridines. *Biochemistry Moscow*, **66**: 875—884.

Valeri A, Gazzei G, Botti R, Pellegrini V, Corradeschi A, Soldateschi D. 1981. One-day purification of influenza A and B vaccines using molecular filtration and other physical methods. *Microbiologica*, **4**: 403—412.

Valeri A, Gazzei G, Morandi M, Pende B, Neri P. 1977. Large-scale purification of inactivated influenza vaccine using membrane molecular filtration. *Experientia*, **33**: 1402—1403.

van Reis R, Leonard LC, HSU CC, Builder SE. 1991. Industrial-scale harvest of proteins from mammalian cell culture by tangential flow filtration. *Biotechnology and Bioengineering*, **38**: 413—422.

Vicente T, Sousa MF, Peixoto C, Mota JP, Alvesa PM, Carrondo MJ. 2008. Anion exchange membrane chromatography for purification of rotavirus-like particles. *Journal of Membrane Science*.

Vickers T. 2007. Image:InfluenzaNomenclatureDiagram.svg. *Wikimedia Commons in Wikipedia*. http://en.wikipedia.org/wiki/Image:InfluenzaNomenclatureDiagram.svg (Accessed August 11, 2008).

Voeten JTM, Brands R, Palache AM, van Scharrenburg GJM, Rimmelzwaan GF, Osterhaus ADME, Claas ECJ. 1999. Characterization of high-growth reassortant influenza A viruses generated in MDCK cells cultured in serum-free medium. *Vaccine*, **17**: 1942—1950.

Vollhardt KP, Schore NE. 1999. Heterocyclen. In: *Organische Chemie*. Wiley-VCH.

Vollhardt KP, Schore NE. 1999. Reaktionen von Oxacyclopropanen. In: *Organische Chemie*. Wiley-VCH.

Wahlund PO, Gustavsson PE, Izumrudov VA, Larsson PO, Galaev IY. 2004. Precipitation by polycation as capture step in purification of plasmid DNA from a clarified lysate. *Biotechnology and Bioengineering*, **87**: 675—684.

Walin L, Tuma R, Thomas GJ, Bamford DH. 1994. Purification of viruses and macromolecular assemblies for structural investigations using a novel ion-exchange method. *Virology*, **201**: 1—7.

Wang CH, Tschen SY, Flehmig B. 1995. Antigenicity of hepatitis A virus after ultra-violet inactivation. *Vaccine*, **13**: 835—840.

Wareing M, Tannock G. 2001. Live attenuated vaccines against influenza; an historical review. *Vaccine*, **19**: 3320-3330.

Webster RG. 1998. Section 3: Evolution and ecology of influenza viruses. In: *Textbook of Influenza*. Oxford: Blackwell Science.

WHO Technical Report Series. 1998. *Requirements for the use of animal cells as in vitro substrates for the production of biologicals*.

WHO Technical Report Series. 2005. *Recommendations for the production and control of influenza vaccine (inactivated)*.

WHO. 1995. Cell culture as a substrate for the production of influenza vaccines: Memorandum from WHO meeting. *Bull World Health Organ*, **73**: 431—435.

WHO. 2008. Epidemic and pandemic alert response: influenza.

http://www.who.int/csr/disease/influenza/en/index.html (Accessed August 20, 2008).

WHO. 2008. WHO Global Influenza Surveillance Network. *World Health Organization*. http://www.who.int/csr/disease/influenza/surveillance/en/index.html (Accessed August 27, 2008).

Wickramasinghe SR, Kalbfuss B, Zimmermann A, Thom V, Reichl U. 2005. Tangential flow microfiltration and ultrafiltration for human influenza A virus concentration and purification. *Biotechnology and Bioengineering*, **92**: 199—208.

Widom J, Baldwin RL. 1980. Cation-induced toroidal condensation of DNA studies with Co3+(NH3)6. *Journal of Molecular Biology*, **144**: 431—453.

Wiktor TJ, Fanget BJ, Fournier P, Montagnon BJ. 1987. Process for the large-scale production of rabies vaccine. *US Patent No. 4664912*.

Wilschut J, McElhaney JE. 2005. Antigenic drift and shift: epidemic and pandemic Influenza. In: *Influenza*. London: Mosby; 45— 67.

Wilschut J, McElhaney JE. 2005. *Influenza*. London: Mosby.

Wilschut J, McElhaney JE. 2005. Pathogenesis, clinical features and diagnosis. In: *Influenza*. London: Mosby; 45— 67.

Wilschut J, McElhaney JE. 2005. The influenza virus: structure and replication. In: *Influenza*. London: Mosby; 45— 67.

Wilschut J, McElhaney JE. 2005. Vaccination: corner stone of influenza control. In: *Influenza*. London: Mosby; 45— 67.

Winona LJ, Ommani AW, Olszewski J, Nuzzo JB, Oshima KH. 2001. Efficient and predictable recovery of viruses from water by small scale ultrafiltration systems. *Canadian Journal of Microbiology*, **47**: 1033—1041.

Wolf B, Berman S, Hanlon S. 1977. Structural transitions of calf thymus DNA in concentrated LiCl solutions. *Biochemistry*, **16**: 3655—3662.

Wu CX, Soh KY, Wang S. 2007. Ion-exchange membrane chromatography method for rapid and efficient purification of recombinant baculovirus and baculovirus gp64 protein. *Human Gene Therapy*, **18**: 665—672.

Wu DX, Howell JA, Field RW. 1999. Critical flux measurement for model colloids. *Journal of Membrane Science*, **152**: 89—98.

Yamamoto S, Nakanishi K, Matsuno R. 1988. *Ion-Exchange Chromatography of Proteins*. New York: Marcel Dekker.

Yamamoto S, Nomura M, Sano Y. 1990. Predicting the performance of gel filtration chromatography of proteins. *Journal of Chromatography*, **512**: 77—87.

Youil R et al. 2004. Comparative study of influenza virus replication in Vero and MDCK cell lines. *Journal of Virological Methods*, **120**: 23—31.

Zelic B, Nesek B. 2006. Mathematical modeling of size exclusion chromatography. *Engineering in Life*

Sciences, **6**: 163—169.

Zhilinskaya IN, Sokolov NN, Golubev DB, Ivanova NA, Elsaed LH. 1972. Isolation of A2/Singapore/57 influenza virus V and S antigens by isoelectric focusing. *Acta Virologica*, **16**: 436.

Zydney AL, Ho CC. 2002. Scale-up of microfiltration systems: fouling phenomena and V-max analysis. *Desalination*, **146**: 75—81.